HOKKAIDO UNIVERSITY

Title	Study of a High-Precision Analysis Method about EMI Noise for Motor Drive Systems in Inverter Air Conditioners
Author(s)	唐, 一展弋
Degree Grantor	北海道大学
Degree Name	博士(工学)
Dissertation Number	甲第11978号
Issue Date	2015-09-25
DOI	https://doi.org/10.14943/doctoral.k11978
Doc URL	https://hdl.handle.net/2115/59981
Type	doctoral thesis
File Information	Yizhanyi_Tang.pdf

Hokkaido University Collection of Scholarly and Academic Papers : HUSCAP

SSI-DT79125210

Doctor Thesis

Study of a High-Precision Analysis Method about EMI Noise for Motor Drive Systems in Inverter Air Conditioners

Yizhanyi Tang

June 2015

System Science and Informatics

Graduate School of Information Science and Technology

Hokkaido University

Sapporo, Hokkaido, Japan

Presented in Partial Fulfillment of the Requirements for the Degree of Doctor of Engineering at Hokkaido University

Yizhanyi Tang

Judging Committee: Chief Chairman Satoshi Ogasawara Professor
Deputy Chairman Hajime Igarashi Professor
Masatsugu Takemoto Associate Professor

STUDY OF A HIGH-PRECISION ANALYSIS METHOD ABOUT EMI NOISE FOR MOTOR DIRVE SYSTEMS IN INVERTER AIR CONDITIONERS

By
Yizhanyi Tang

ABSTRACT

In order to save energy and improve the efficiency of the power supply system, inverters, which are consists of power semiconductor devices, has gained wide acceptance as an important part in the power system design. When the power semiconductor devices do high-speed switching, the high-frequency leakage current will occur. This kind of leakage current backtracks to the utility power source through the ground path and leads to the conducted electromagnetic interference (EMI) noise. In addition, common-mode (CM) noise is the main ingredient of the conducted EMI noise. Furthermore, the accurate modeling of the EMI noise equivalent circuit will be beneficial to the design of effective noise suppression system. This dissertation presents an equivalent circuit containing non-linear component for inverter-fed drive air conditioner system.

By comparing the amplitude of leakage current when the air conditioner is working in different modes, the main effect factors of the CM EMI noise are indentified. Though the analysis of interference conduction mechanism and the waveform of leakage current in inverter-fed drive system, an accurate equivalent circuit with non-linear resistance is proposed for the first time.

Afterward, according to the waveform of the leakage current in the ground path when only one phase of inverter is switching, the parameters of the equivalent circuit are calculated. And the accuracy of this equivalent circuit is verified again, by comparing the result of simulation with the waveform when two phases of inverter are switching at the same time. Further, the equivalent circuit is indentified again through an optimize software modeFRONTIER to correct the errors during the subjective calculation before. A linear model and a non-linear model are separately discussed. With the results of these two models, the necessity and effectiveness of the introduction of the non-linear resistance about the common-mode equivalent circuit are confirmed. By analyzing the relationship between the current i and the magnetic flux Ψ in high consonance frequency circuit, this conclusion is verified again. In the end, this thesis proposes a method to estimate the parasitic capacitance when the motor is running and the permittivity of oil and refrigerant mixture in the air conditioner compressor for the first time. A design procedure for EMI problem is proposed. The EMI noise can be predicted and the EMI filter can be designed from after assembling to before assembling. The effectiveness of the proposed equivalent circuit is verified, by comparing the simulation result with the experiment waveform.

Keywords: Non-Linear, Equivalent Circuit, Common-Mode, Electromagnetic Interference (EMI), Inverter, Motor, Refrigerant, Lubrication Oil, Permittivity, Compressor.

TABLES OF CONTENTS

Chapter 1 Introduction 1

1.1 Research Background 1
1.2 Research Trends 3
1.3 Thesis Objective 5
1.4 Thesis Outline 6

Chapter 2 Equivalent Circuit of Inverter-Fed Motor Drive System 7

2.1 Constitution of Inverter-Fed Motor Drive System 7
2.1.1 Source of Interference 7
2.1.2 Route of Transmission 9
2.2 Measure of CM Leakage Current 10
2.2.1 Connection of equipments 10
2.2.2 Impact on Leakage Current in Different Running Mode of Air Conditioner 12
2.3 Construction of Equivalent Circuit 22
2.4 Summary 24

Chapter 3 Introduction of Non-Linear Element 25

3.1 Rationality of Non-Linear Equivalent Circuit 25
3.1.1 CM Leakage Current Measure 25
3.1.2 Resonance Frequency Calculation and FFT Transformation 26
3.1.2 Rationality of Non-Linear 27
3.2 Calculation of Equivalent Circuit 28
3.2.1 Calculation method 28
3.2.2 Calculation of CM High-Frequency Equivalent Circuit 31
3.3 PSIM Model and Simulation Result 37
3.4.1 Linear equivalent circuit 39
3.4.2 Reconfirmation of Non-Linear Equivalent Circuit 42
3.4 Necessity of Non-Linear Resistance about CM Equivalent Circuit 44
3.6 Summary 45

Chapter 4 Identification of Non-Liner Common-Mode Equivalent Circuit 46

4.1 Identification Errors in Calculating the Parameters of Equivalent Circuit and Computer-Aided Optimization Software 46

4.1.1 Speculation Errors in Calculating the Parameters of Equivalent Circuit 46
4.1.2 Computer-Aided Optimization Software 47
4.2 modeFRONTIER Simulation 52
4.2.1 Linear and Non-Linear Models 52
4.2.2 modeFRONTIER Model 55
4.2.3 modeFRONTIER Simulation Result 59
4.3 Identification of Linear Common-Mode Equivalent Circuit 68
4.3.1 New MATLAB Model for Simulation 68
4.3.2 Simulation Result of Leakage Current 70
4.3.3 Consideration of Proposed CM Equivalent Circuit 72
4.3.4 Limitation of Proposed Equivalent Circuit 74
4.4 Identification of Non-Liner Common-Mode Equivalent Circuit 75
4.4.1 Phase Switching Time Lag 75
4.4.2 Non-Linear CM Equivalent Circuit 78
4.5 Effect of Non-Linear Resistance about Common-Mode Equivalent Circuit for Inverter Drive System 83
4.5.1 Simulation for Verifying Non-Linear 83
4.5.2 Experiment for Verifying Non-Linear 85
4.5.3 Physical Meaning of Non-Linear 91
4.6 Summary 95

Chapter 5 Estimation of Stray Capacitance and Permittivity between Compressor Motor Windings and Stator in Operation 97

5.1 Development of Refrigerant 97
5.2 Air Conditioner 98
5.2.1 Structure of Air Conditioner 98
5.2.2 Compressor of Air Conditioner 99
5.3 Predict about Permittivity 102
5.4 Summary 107

Chapter 6 Research and Design System for EMI Problem 108

6.1 Novel EMI Design System and Experiment Equipment 108
6.1.1 Novel EMI Design System 108
6.1.2 Experiment Equipment 110
6.1.3 Connection of Equipment 110
6.2 Effect of EMI Filters 113
6.2.1 Outdoor Part of Air Conditioner 114

6.2.2 Outdoor Leakage Current of Air Conditioner 116
6.2.3 Indoor Part of Air Conditioner 119
6.2.4 Noise Sources of Air Conditioner System 123
6.3 Equivalent Circuit of Every Part According to the Impedance Characterstics 125
6.3.1 Structure of Air Conditioner System 125
6.3.2 Equivalent Circuit of Every Part 126
6.4 Equivalent Circuit of Air Conditioner System 134
6.4.1 Simulation Result without EMI Filters 134
4.4.2 Simulation Result with EMI Filters 136
6.5 Summary 142

Chapter 6 Conclusions and Future Work 144

6.1 Conclusions 144
6.2 Future Work 146
6.2.1 Physical Meaning of Non-Linear 146
6.2.2 CM Equivalent Circuit in Frequency Domain 146
6.2.3 EMI Suppression Method 146

REFERENCES 148

RESEARCH ACHIEVEMENTS 153

ACKNOWLEDGEMENT 154

LIST OF ILLUTRATIONS

Fig. 2.1 Constitution of PWM Inverter-Fed Motor Drive System 7
Fig. 2.2 Interference Analysis of PWM Inverter-Fed Motor Drive System 8
Fig. 2.3 Connection Diagram of Experiment 11
Fig. 2.4 Connection of Equipments 11
Fig. 2.5 Leakage Current in Warm Mode 451W 13
Fig. 2.6 Leakage Current in Warm Mode 450W 13
Fig. 2.7 RMS Value of Leakage Current in Worm Mode 14
Fig. 2.8 RMS Value of Leakage Current in Cool Mode 15
Fig. 2.9 Current FFT Transformation in Warm Mode 15
Fig. 2.10 Current FFT Transformation in Warm Mode 16
Fig. 2.11 Leakage Current in Warm Mode Just Running 17
Fig. 2.12 Leakage Current in Warm Mode after Running 1 Hour 17
Fig. 2.13 Leakage Current in Cool Mode Just Running 18
Fig. 2.14 Leakage Current in Warm Mode after Running 1 Hour 18
Fig. 2.15 Leakage Current in PWM Inverter Working Status 1 20
Fig. 2.16 Leakage Current in PWM Inverter Working Status 2 20
Fig. 2.17 Leakage Current in PWM Inverter Working Status 3 21
Fig. 2.18 Equivalent Circuit of PWM Inverter-Fed Motor Drive System 23
Fig. 3.1 Leakage Current Waveform of One Phase Switching 25
Fig. 3.2 Result of FFT Transform 26
Fig. 3.3 Equivalent Circuit with Non-Linear Resistance 27
Fig. 3.4 LCR Series Circuit 29
Fig. 3.5 Decreasing Current of LCR Series Circuit 29
Fig. 3.6 CM Equivalent Circuit 31
Fig. 3.7 Deformed CM Equivalent Circuit 32
Fig. 3.8 Calculation of Leakage Current 33
Fig. 3.9 Leakage Current Deformation 35
Fig. 3.10 PSIM Model with One Phase Switching First 37
Fig. 3.11 Simulation Result with One Phase Switching First 37
Fig. 3.12 PSIM Model with Two Phases Switching First 38
Fig. 3.13 Simulation Result of Two Phases Switching First 38
Fig. 3.14 Linear Equivalent Circuit Model 39
Fig. 3.15 Simulation Result in One Phase Switching 40
Fig. 3.16 Simulation Result in Two Phases Switching 41
Fig. 3.17 Reconfirmed Equivalent Circuit with Non-Linear Resistance 42
Fig. 3.18 Simulation Result in One Phase Switching Mode 42

Fig. 3.19 Simulation Result in Two Phases Switching Mode 43
Fig. 4.1 Decreasing Current of LCR Series Circuit 47
Fig. 4.2 Concept behind modeFRONTIER 48
Fig. 4.3 Working Flow of modeFRONTIER 49
Fig. 4.4 CM Noise Equivalent Circuit of PWM Inverter-Fed Drive System 49
Fig. 4.5 Deformation of Equivalent Circuit 50
Fig. 4.6 Parallel Connection Equivalent Circuit 50
Fig. 4.7 LCR Series Circuit 53
Fig. 4.8 MATLAB Model of LCR Series Circuit with Non-Linear Resistance 53
Fig. 4.9 MATLAB Model of Equivalent Circuit for PWM Inverter-Fed Drive System with Non-Linear Resistance 54
Fig. 4.10 MATLAB Model of Equivalent Circuit for PWM Inverter-Fed Drive System without Non-Linear Resistance 55
Fig. 4.11 MATLAB Model of Equivalent Circuit for PWM Inverter-Fed Drive System in modeFRONTIER 56
Fig. 4.12 modeFRONTIER Model in One Phase Switching 57
Fig. 4.13 modeFRONTIER Simulation Result 58
Fig. 4.14 Non-Linear PSIM Model in One Phase Switching with modeFRONTIER Optimization Parameters 59
Fig. 4.15 Non-Linear Simulation Result in One Phase Switching with modeFRONTIER Optimization Parameters 60
Fig. 4.16 Non-Linear Simulation Result in Two Phases Switching with modeFRONTIER Optimization One Phase Parameters 60
Fig. 4.17 Non-Linear PSIM Model in Two Phases Switching with modeFRONTIER Optimization Parameters 61
Fig. 4.18 Non-Linear Simulation Result in Two Phases Switching with modeFRONTIER Optimization Parameters 62
Fig. 4.19 Non-Linear Simulation Result in one Phase Switching with modeFRONTIER Optimization Two Phases Parameters 62
Fig. 4.20 Linear PSIM Model in One Phase Switching with modeFRONTIER Optimization Parameters 63
Fig. 4.21 Linear Simulation Result in One Phase Switching with modeFRONTIER Optimization Parameters 64
Fig. 4.22 Linear Simulation Result in Two Phases Switching with modeFRONTIER Optimization One Phase Parameters 64
Fig. 4.23 Linear PSIM Model in Two Phases Switching with modeFRONTIER Optimization Parameters 65
Fig. 4.24 Linear Simulation Result in Two Phases Switching with modeFRONTIER Optimization Parameters 66

Fig. 4.25 Linear Simulation Result in one Phase Switching with modeFRONTIER Optimization Two Phases Parameters 66
Fig. 4.26 Linear modeFRONTIER Simulation Model in One Phase Switching 69
Fig. 4.27 Linear MATLAB Model for modeFRONTIER 70
Fig. 4.28 Linear Model of One Phase Switching 71
Fig. 4.29 PSIM Linear Simulation Result of One Phase Switching 71
Fig. 4.30 Impedance Testing Connection 72
Fig. 4.31 Impedance Characteristic 73
Fig. 4.32 Step (2-level) Component in PSIM 76
Fig. 4.33 Modeling with no Time Lag 76
Fig. 4.34 Leakage Current with Time Lag 0 77
Fig. 4.35 Leakage Current with Time Lag 81ns 77
Fig. 4.36 Time Lag of Experiment Data 77
Fig. 4.37 Leakage Current with Time Lag 25.4ns 78
Fig. 4.39 Non-Linear modeFRONTIER Model for Both Cases 79
Fig. 4.40 Non-Linear Equivalent Circuit of Inverter-Fed Motor Drive System 80
Fig. 4.41 Simulation Result of One Phase Switching 80
Fig. 4.42 Simulation Result of Two Phases Switching 81
Fig. 4.43 modeFRONTIER Result of Linear Equivalent Circuit When Comparing to Experiment Waveform in Two Situations 82
Fig. 4.44 Circuit with Non-Linear Resistance 83
Fig. 4.45 MATLAB Model of Circuit 84
Fig. 4.46 Waveform of Voltage, Current and Magnetic Flux 85
Fig. 4.47 i-Ψ Curve of Simulation 86
Fig. 4.48 Connection Diagram of Experiment 86
Fig. 4.49 Input Voltage at 60Vpp 86
Fig. 4.50 Input Voltage at 130Vpp 87
Fig. 4.51 Equivalent Circuit of Experiment 87
Fig. 4.52 Equipment Connection for Parasitic Capacitance Testing 88
Fig. 4.53 Parasitic Capacitance in Different Frequency 89
Fig. 4.54 i-Ψ Curve of Experiment 90
Fig. 4.55 Connection of Experiment for Verifying Non-Linear Physical Meaning 91
Fig. 4.56 Waveform for Verifying Non-Linear Physical Meaning 92
Fig. 4.57 i-Ψ Curves in Different Loop Currents 93
Fig. 4.58 Logarithm Relationship between Current i and Area of i-Ψ Curve 93
Fig. 5.1 Air Conditioner System g 98
Fig. 5.2 Section Plan of Compressor 99
Fig. 5.3 Measurement Method One 100
Fig. 5.4 Measurement Method Two 101

Fig. 5.5 High-Frequency CM Equivalent Circuit 102
Fig. 5.6 Impedance Test of Compressor Motor without Refrigerant and Lubricant Oil 103
Fig. 5.7 Capacitance of Compressor without Refrigerant and Lubricant Oil 103
Fig. 5.8 Compressor with Refrigerant and Lubricating Oil in Operation 104
Fig. 5.9 Leakage Current Waveform of One Phase Switching at Compressor Just Running 105
Fig. 5.10 Parasitic Capacitance between Compressor Motor Windings and Stator as Time Going on 106
Fig. 6.1 Improvement of EMI Design Flow 109
Fig. 6.2 Research Flow Chart 109
Fig. 6.3 Connection Diagram of Experiment for EMI Noise Level 111
Fig. 6.4 Air Conditioner Picture for Experiment 112
Fig. 6.5 Equivalent Circuit of LISN 112
Fig. 6.6 E Noise Level of Every Running mode 113
Fig. 6.7 EMI Filter Of Outdoor Part 114
Fig. 6.8 Noise Level of Every Running mode 115
Fig. 6.9 Noise Level about Outdoor Fan Ferrite Core 116
Fig. 6.10 Leakage Current of Warming Mode 117
Fig. 6.11 Leakage Current of Blowing Mode 117
Fig. 6.12 MATLAB Model for modeFRONTIER 118
Fig. 6.13 Outdoor modeFRONTIER Model o 118
Fig. 6.14 EMI Filter Of Indoor Part 119
Fig. 6.15 Effect of Indoor CM Choke 120
Fig. 6.16 Effect of Indoor Y Capacitance 121
Fig. 6.17 Effect of Indoor Ferrite Core on Power Cables 121
Fig. 6.18 Effect of Indoor Ferrite Core on Fan Cables 122
Fig. 6.19 Effect of Indoor Ferrite Core on Control Signal Cables 122
Fig. 6.20 Different Noise Sources of Air Conditioner System 123
Fig. 6.21 Structure of Air Conditioner System 126
Fig. 6.22 Connection of Compressor Impedance Measurement 127
Fig. 6.23 Impedance Calculation of Compressor Motor 128
Fig. 6.24 Equivalent Circuit of Compressor Motor 128
Fig. 6.25 Impedance Calculation of Outdoor Fan 129
Fig. 6.26 Equivalent Circuit of Outdoor Fan 129
Fig. 6.27 Impedance Calculation of Indoor Fan 130
Fig. 6.28 Equivalent Circuit of Indoor Fan 130
Fig. 6.29 Equivalent Circuit of Pipe Part 131
Fig. 6.30 Equivalent Connection of Pipe Part 132

Fig. 6.31 Impedance of Pipe Part in the Case of Open 132
Fig. 6.32 Impedance of Pipe Part in the Case of Short 133
Fig. 6.33 Equivalent Circuit of Pipe Part in the Case of Short 133
Fig. 6.34 CM Model of Air Conditioner 134
Fig. 6.35 Equivalent Circuit without EMI Filters 135
Fig. 6.36 Simulation Result without EMI filters 135
Fig. 6.37 Impedance Measurement of Common-Mode Choke 136
Fig. 6.38 Impedance of Outdoor Common-Mode Choke 137
Fig. 6.39 Equivalent of Outdoor Common-Mode Choke 137
Fig. 6.40 Impedance of Indoor Common-Mode Choke 138
Fig. 6.41 Equivalent of Indoor Common-Mode Choke 138
Fig. 6.42 Impedance of Outdoor Y Capacitance 139
Fig. 6.43 Equivalent of Outdoor Y Capacitance 139
Fig. 6.44 Impedance of Indoor Y Capacitance 140
Fig. 6.45 Equivalent of Indoor Y Capacitance 140
Fig. 6.46 Equivalent Circuit with EMI Filters 141
Fig. 6.47 Simulation Result with EMI Filters 141
Fig. 7.1 Current Mirror Circuit 147

LIST OF TABLES

Table 2-1 List of Equipments.....9
Table 2-2 RMS Value of Leakage Current In Warm Mode.....14
Table 4-1 Standard Deviations between Simulation and Experiment 81
Table 4-2 List of Experiment for Effectiveness of Non-Linear 85
Table 4-3 List of Equipments for Parasitic Capacitance.....89
Table 4-4 List of Equipments for Verifying Non-Linear Physical Meaning of Refrigerant 92
Table 6-1 List of Equipments.....110
Table 6-2 Accuracy of LCR Hi-Tester 125

Chapter 1 Introduction

1.1 Research Background

Following the development of electronic science and technology, more and more power electronic devices are widely applied in almost all fields. But at the same time, when these devices are working as on-off switching, they also produce serious electromagnetic noises, and these noises will impact the other electronic products through some path just like parasitic capacitance and inductance. How to solve this kind of problem results in a new discipline called electromagnetic compatibility (EMC) [1][2].

In recent years, as people are increasingly concerned with saving energy, power electronic devices such as converters and inverters are more and more widely applied to household appliances and industrial areas, e.g., an uninterruptible power supply (UPS) uses batteries and inverters to supply alternating current (AC) power when the power supply is not available. And with high-voltage direct current (HVDC), AC power is converted to direct current (DC) power and the high voltage DC power is transmitted to another location, at the receiving location, an inverter is the key component and converts the power back to AC. Especially, the motor drive system has been changed from the industrial power direct drive to pulse width modulation (PWM) drive, i.e., PWM inverter-fed motor drive systems.

But the inverters are mainly made up of power semiconductor devices, just like insulated gate bipolar transistors (IGBTs) and metal-oxide-semiconductor field-effect

transistors (MOSFETs), etc. When these power semiconductor devices do high-speed switching, because of the switching time is quite short, *dv/dt* and *di/dt* become considerable [3][4]. It means the high-amplitude and high-frequency leakage current will occur. This kind of leakage current goes through the parasitic capacitance which exit between the devices and ground, and then it backtracks to the power supply system. This kind of noise will affect the other products in the same power system. It is called conducted electromagnetic interference (EMI) noise. Especially, the development of the modern power inverter system towards to high frequency, high efficiency, and small size, so EMI noise becomes serious.

Modern motor drive system as a kind power converter system mainly applies PWM drive method. This kind of PWM inverter-fed drive system will inevitably generate the conduced EMI problems [5]-[8]. The conduced EMI includes common-mode (CM) interference and differential mode (DM) interference. At present, there are a lot of researches and literatures about the analysis of the harmonic components of DM voltage and research on the hazards of *dv/dt* [9]-[17]. And the studies have shown that the filter capacitance and inductance can inhibit the high-frequency DM interference well. However, the parasitic capacitance exists between the semiconductor devices and heat-sinks, as well as exists between the devices and the ground such as the parasitic capacitance between the motor and ground [18][19]. Because of the parasitic capacitance, high-frequency CM noise can easily go back to the power system. CM interference is the principal part of conducted EMI and main inhibition object [20]-[25]. Furthermore, the conduction mechanism analysis and mathematical models are the basis of EMI research. Accurate and efficient model is not only beneficial to the prediction of EMI, but also beneficial to the design of filter. Therefore, in order to solve the problem of EMI, to analyze the interference mechanism and build the circuit model is a necessary step.

1.2 Research Trends

In recent years, the research of EMI caused by inverter-fed drive system has been performed comprehensively. e.g., the authors of [26] did research on the conduction mechanism analysis of the PWM inverter-fed motor drive system. The authors of [20][21][27]-[33] did research on the equivalent circuit of conducted EMI, and get progress. These equivalent circuits can well describe the characteristics of CM equipment circuit.

But all the equivalent circuits proposed before, are too complex. These complex equivalent circuits can well describe the characteristic of CM noise circuit, but the time of predicting the interference in the PWM inverter-fed drive motor system will greatly increase, and the cost of interference suppression will substantially increase too. Therefore, more simple, easy to understand and effective equivalent circuit model will greatly improve efficiency of interference suppression. This thesis will focus on the research about the simple and effective CM equivalent circuit in PWM inverter-fed motor drive system.

Following the development of the computer science, computer-aided design and simulation tools have been widely applied in industry design and research. In this paper, a kind of computer-aided optimization software “modeFRONTIER” is introduced to decide the element of CM equivalent circuit objectively and improve the accuracy. This paper focuses on a simple equivalent circuit for inverter-fed motor drive systems to describe the main characteristics of systems. And this paper proposed a kind of π type CM equivalent circuit for inverter-fed motor drive system. By analyzing the leakage current on the ground path of the system, it shows that the simulation result of simplified equivalent circuit can meet well with the experiment data. At the same time, the possibility of non-linear phenomenon is discussed in inverter-fed motor drive systems. The accuracy of the simple equivalent circuit will be improved by introducing the non-linear element.

In order to protect the environment, the new refrigerants HC and HFC are widely applied to replace the CFC and HCFC [34]-[37]. HC and HFC will lead to high

permittivity [38]-[41], high parasitic capacitance. And high parasitic capacitance will lead to high leakage current, high EMI noise [37][42]. Therefore the research about the permittivity of oil and refrigerant mixture becomes important. In order to estimate the permittivity, first it must know the parasitic capacitance when there is no oil-refrigerant mixture is in the compressor. It is the capacitance of the air. The capacitance can be measured by LCR hi-tester. And then, it must know the capacitance when the motor is running. In the past, it is almost difficult to measure the parasitic capacitance between the coil and frame of motor in operation. But base on this equivalent circuit, when the motor is running, the capacitance can be confirmed. Therefore, the permittivity of mixture is estimated. To estimate the permittivity of the lubrication oil and refrigerant mixture becomes possible for the first time.

In the past, the designer designs the product, the product is assembled, then measure the EMI noise. If the test result could not meet the demands of EMI standard, the product will be design again. This kind of design flow will waste long time and lead to high cost. This research will improve the design process like this. After the design, the EMI noise can be simulated through the computer-aided software. According to the experiment test result to built the equivalent circuit and calculate the parameters through some method. The complex model can represent the circuit well, but it will increase the simulation time. How to get the appropriate model is important. And the Power electronics devices have many parts. In order to predict the EMI noise, it must be known the model of every part. So it is need to build a parts library. According to the system connection diagram, the separate parts models can be connected to a system equivalent circuit. Then according to this system equivalent circuit it can be got the simulation result to predict the EMI noise level. this research will focus on these two points, how to build the optimized equivalent circuit and calculate the parameters by computer-aided software and how to connect parts models together as a system equivalent circuit.

1.3 Thesis Objective

The research before [43] has confirmed the structure of PWM inverter-fed motor drive system of an air conditioning and main CM interference sources. The non-linear is also confirmed in the system. And the simulation result and experiment result have proved the efficiency of the equivalent circuit with non-linear resistant.

The main objectives of this thesis are to:

i). Accurately and comprehensively analyze the influencing factors of the CM interference and construct a new equivalent circuit model.

ii). Improve the pervious algorithm, decrease the errors and calculate the parameter of equivalent circuit again, with non-linear element, parallel results without non-linear element. More convincingly end-confirm the necessity of non-linear element introduction, and improve the accuracy of the equivalent circuit.

iii). Simulate objectively the parameter of equivalent circuit by using the optimization software modeFRONTIER, further to eliminate the subjective errors in the calculation. Identify the necessity of non-linear element introduction once again. Verify the effectiveness of the non-linear element introduction, by analyzing the relationship between the magnetic flux Ψ and current i in the CM noise conduction circuit from two aspects of simulation and experiment.

iv). Determine the parasitic capacitance when the inverter-fed drive motor is running, further speculate the permittivity of mixture of lubricating oil and refrigerant in air conditioner compressor for the first time, according to this accurate equivalent circuit model.

v). Propose a novel design process from after assembling to before assembling by instruct the equivalent circuit of system according to the impedance characteristics of every part and the structure of system.

1.4 Thesis Outline

The contents of the thesis are as follows:

In Chapter 2 the structure of PWM inverter-fed motor drive system of an air conditioning is described and the CM interference sources are explained. The main conduction path is proposed. The influencing factors of the CM interference are confirmed and an equivalent circuit model with non-linear resistance is proposed.

In Chapter 3 the parameters of equivalent circuit with non-linear element, parallel results without non-linear element are separately calculated. The necessity and effectiveness of non-linear element introduction are confirmed by comparing two kinds of equivalent circuits.

In Chapter 4 the equivalent circuit with non-linear element is objectively simulated by using the optimization software to eliminate the subjective errors in the calculation. Identify the necessity and effectiveness of non-linear element introduction once again. The equivalent circuit is finalized.

In Chapter 5, according to the final equivalent circuit model in Chapter 4, speculate the parasitic capacitance when the motor is running, further speculate the permittivity of mixture of lubricating oil and refrigerant in air conditioner compressor, which could not be speculated before.

In chapter 6, according to the impedance characteristics of every part and the structure of system, an equivalent circuit in frequency domain is proposed to estimate the EMI noise level and help to design the EMI filters.

In Chapter 7 a summary of the thesis is given. Conclusions and contributions of this thesis are discussed. Suggestions for future work in this area are also suggested.

Chapter 2 Equivalent Circuit of Inverter-Fed Motor Drive System

2.1 Constitution of Inverter-Fed Motor Drive System

A PWM inverter-fed motor drive system is shown as Fig. 2.1. At first the utility AC power supply is converted to DC power through the bridge rectifier circuit. And then the DC power is converted back to AC power by the PWM inverter to drive the AC motor.

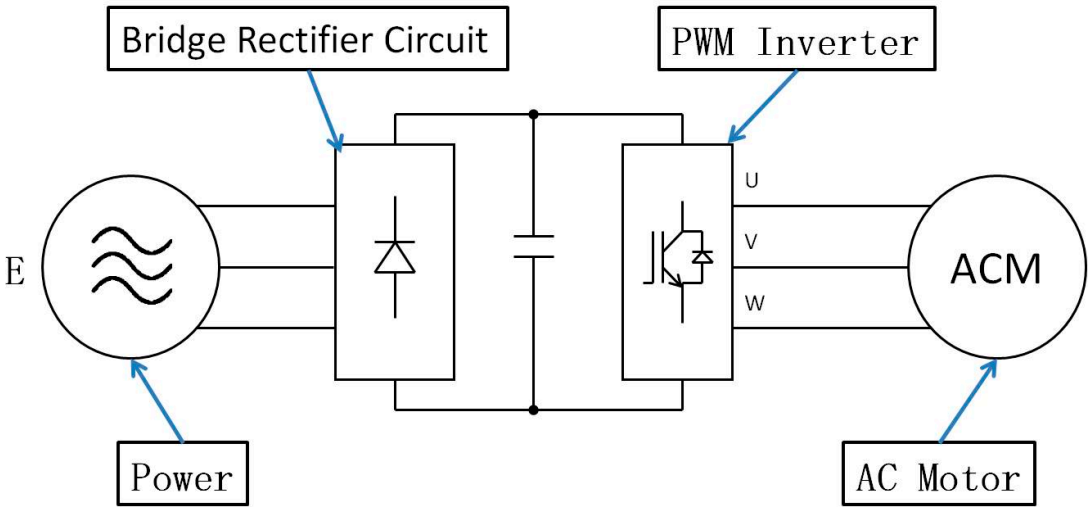


Fig. 2.1 Constitution of PWM Inverter-Fed Motor Drive System

2.1.1 Source of Interference

In order to prevent receiving and electric shock, the shell of AC motor is usually connected to ground. The parasitic capacitance exists between the coil and the shell,

i.e., between the coil and the frame of the motor which is connected to the shell. Moreover, the bridge rectifier circuit and the PWM inverter are made up by the power semiconductor devices. When the power semiconductor devices are switching, because the switching time is not zero, it will result in energy consumption on these devices. These energies will be transformed to heat, and the heat will accumulate in these power semiconductor devices. Long-term accumulation of heat may damage the power semiconductor devices. For avoiding this kind of thermal damage, the power semiconductor components are often connected to the heat sink. But after the long term running, the heat sinks will accumulate a lot of electric charge. When the conductor is close to these heat sinks, the discharge will happen. This kind of discharge is dangerous to the human and the equipment itself. So the heat sink is always connected to ground. It will result in the parasitic capacitances exists between the semiconductor devices and the heat sinks. The other parasitic capacitances of the circuit will also be sensed, but they are generally smaller than the parasitic capacitances between the coil and the motor frame, and between the power semiconductor devices and the heat sinks, so the effect of them can be ignored. The main parasitic capacitances are shown in Fig. 2.2.

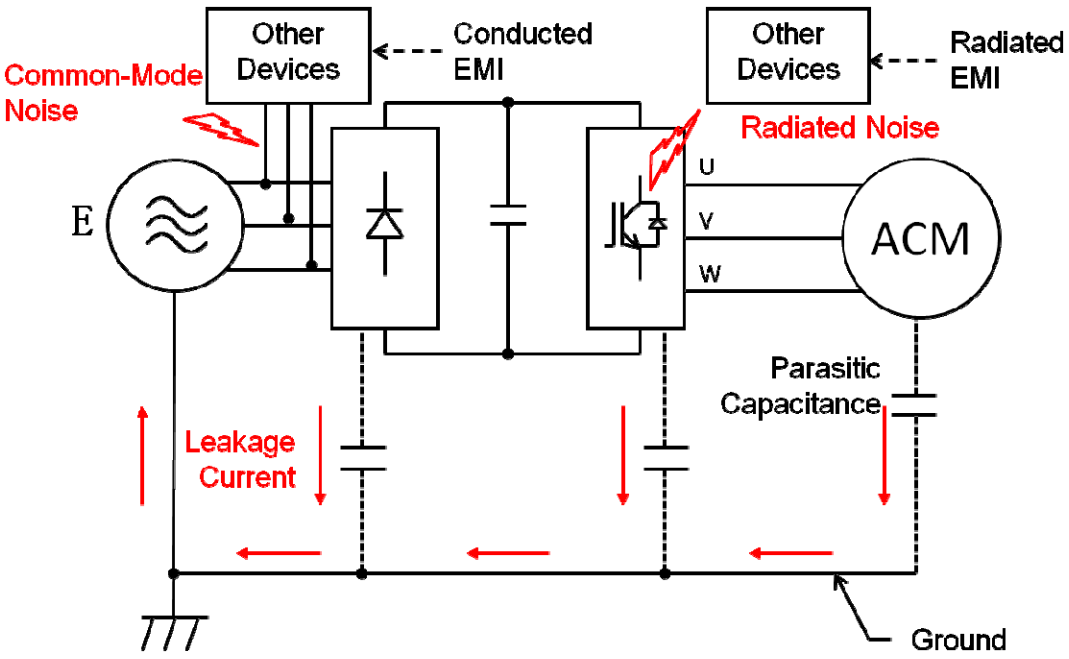


Fig. 2.2 Interference Analysis of PWM Inverter-Fed Motor Drive System

2.1.2 Route of Transmission

Whenever the power semiconductors do high speed switching, because of the rising time of switch voltage is quite short, *dv/dt* will be considerable. According to the Fourier transform, the considerable *dv/dt* will produce high frequency leakage currents. These leakage currents will go in the ground through the parasitic capacitances in the system, and then backtrack to the utility power supply system. This kind of leakage current will affect the other equipments in the same power system. And this kind interference is called conducted EMI. Meanwhile, when the power semiconductor devices do high speed switching, it will also generate the radiated noise. These electromagnetic waves will radiant energy through the wires and the other parts of the system because of antenna theory. This kind of radiated noise will affect the other equipments nearby. This kind of interference is called radiated EMI. As shown as Fig. 2.2.

2.2 Measure of CM Leakage Current

Toshiba air conditioner RAS-281A and the oscilloscope with high accuracy are adopted to analyze the CM leakage current. The list of experiment equipments are shown as Table 2-1.

Table 2-1 List of Equipments

Name	Brand	Model
Air Conditioner	Toshiba	RAS-281A
Oscilloscope	Tektronix	MSO4034
Current Probe	Tektronix	TCP0150
Voltage Probe	Tektronix	P5205
Digital Power Meter	YOKOGAWA	WT130

2.2.1 Connection of equipments

The air conditioner is composed by indoor section and outdoor section. The indoor section is connected to the power supply in the laboratory. An oscilloscope (Tektronix MSO4034) is adopted to measure the CM leakage current in the ground line of the system. In order to measure the leakage current of the ground, a copper line is connected to the metallic case of the air conditioner. The current on this line can be measured with the current probe (Tektronix TCP0150). And the phase voltage of the inverter can be measured with the voltage probe (Tektronix P5205). The working power of the air conditioner can be well known by series connecting the digital power meter between the air conditioning and power supply. In order to analyze the leakage current clearly, the EMI filters are taken away. The connection of experimental equipment including an inverter air conditioner is shown as Fig. 2.3. The connection picture of experiment equipments is shown as Fig. 2.4.

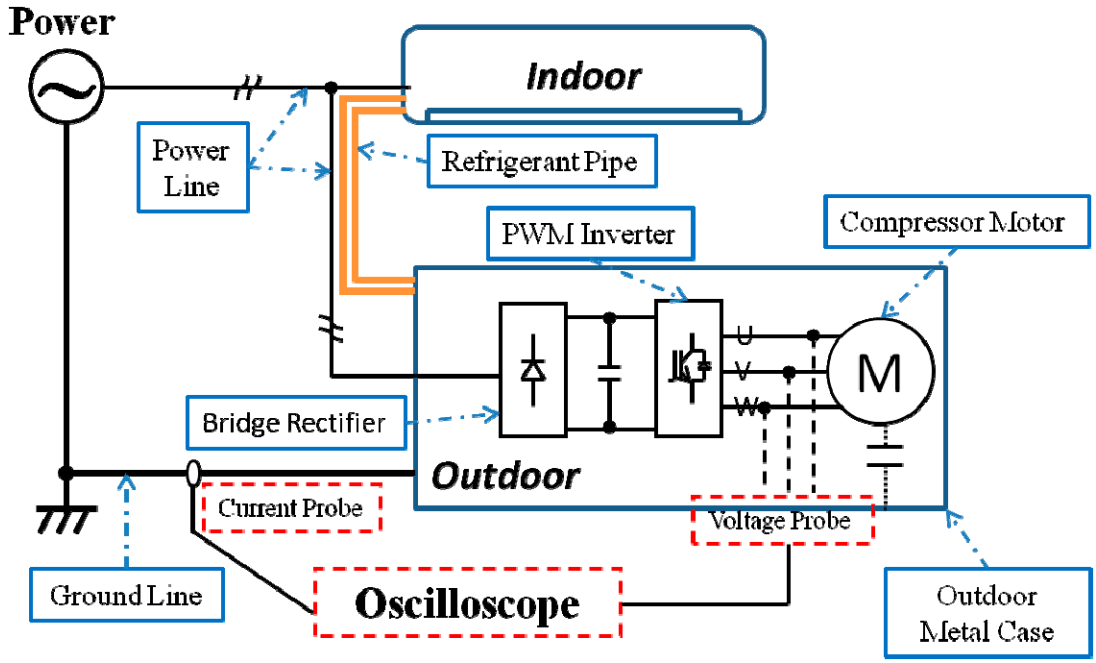


Fig. 2.3 Connection Diagram of Experiment

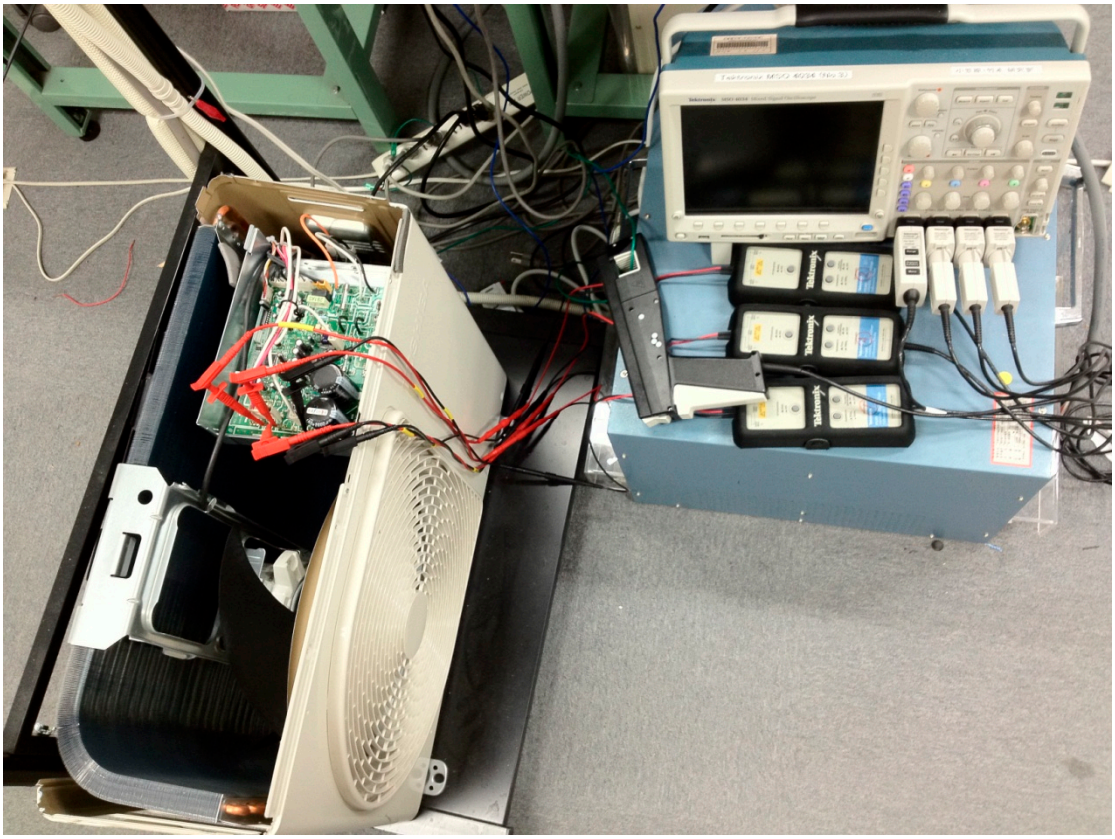


Fig. 2.4 Connection Picture of Experiment Equipments

2.2.2 Impact on Leakage Current in Different Running Mode of Ari Conditioner

This air conditioner can mainly run as three modes, cooling mode, warming mode and blowing mode. But in the blowing mode, the compressor is not running. It means the motor is not running. So the research of leakage current in the blowing mode is unnecessary. Consequently, the leakage current should be discussed when the air conditioner works with different working power. And the leakage currents will be measured in two situations, i.e. when the air conditioning is just running and after running above 1 hour. Further when the PWM inverter is working, there will be a variety of combination of the three phase voltages. So the impact which comes from PWM inverter working status should be discussed. In order to ensure the accuracy of the experiment, the temperature of air conditioner is set to the lowest in cooling mode, and set to the highest in warming mode and the running speed of the fan is set to the fastest.

The green lines of Fig. 2.5 and 2.6 show the waveform of leakage current when the air conditioning is running in warming mode and the power is about 450 W. Table 2-2 shows the root-mean-square (RMS) values of the leakage current. In the situation with the same running mode (warming mode) and the same working power, the RMS values are almost the same. Therefore, it is shown that the leakage current is almost independent of the running mode. And 1.4 mA can be considered within a reasonable range of error.

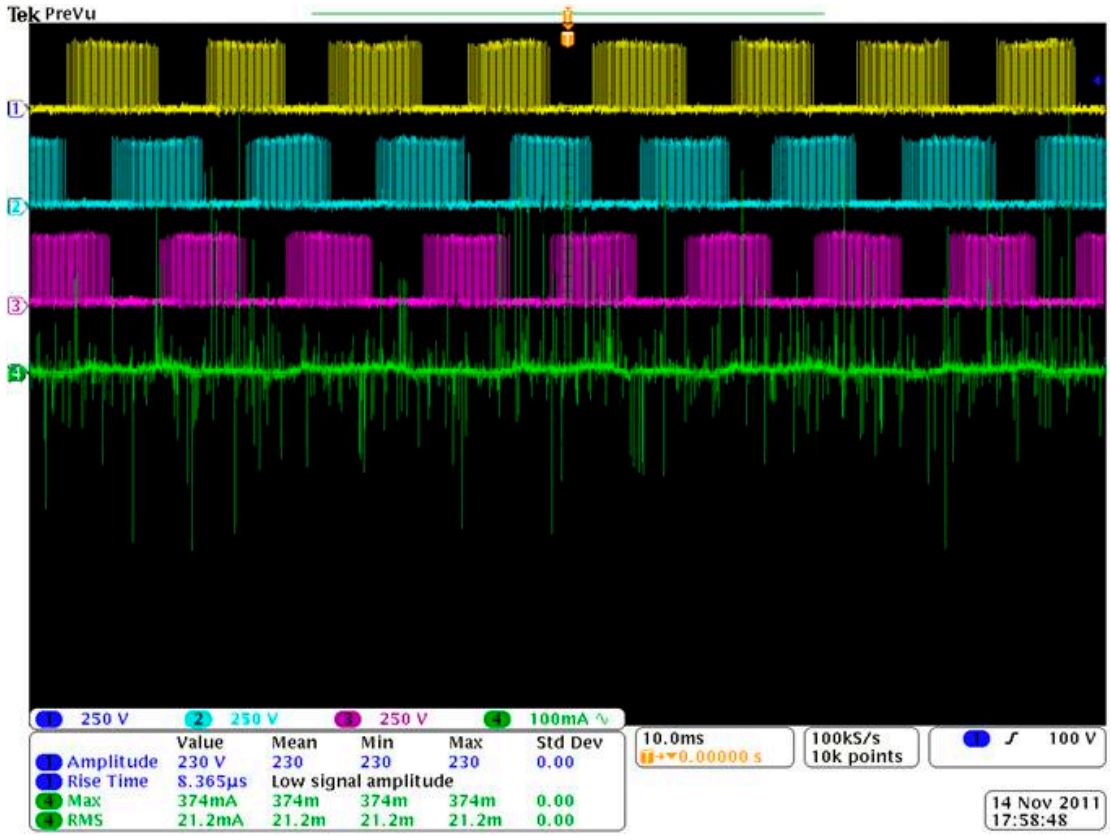


Fig. 2.5 Leakage Current in Warming Mode 451W

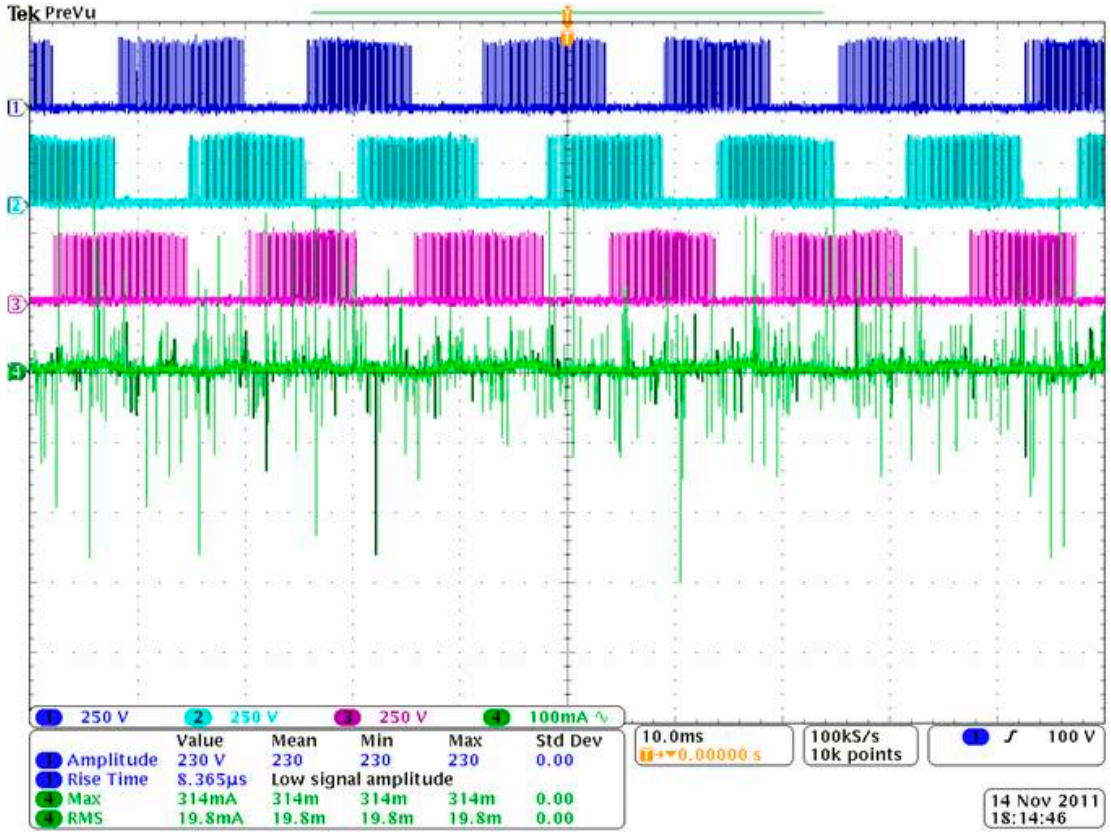


Fig. 2.6 Leakage Current in Warming Mode 450W

Table 2-2 RMS Value of Leakage Current In Warm Mode

Warm Mode 1		Warm Mode 2	
Power	RMS Value of Current	Power	RMS Value of Current
450W	19.8mA	451W	21.2mA

In the following experiments, the RMS values of the leakage current are measured in different running mode and different working power. Fig. 2.7 shows the worming mode RMS values of leakage current in different power. And Fig. 2.8 shows the cooling mode RMS values. The running mode and working power will impact the leakage current lightly. The following experiment can be trusted worthy.

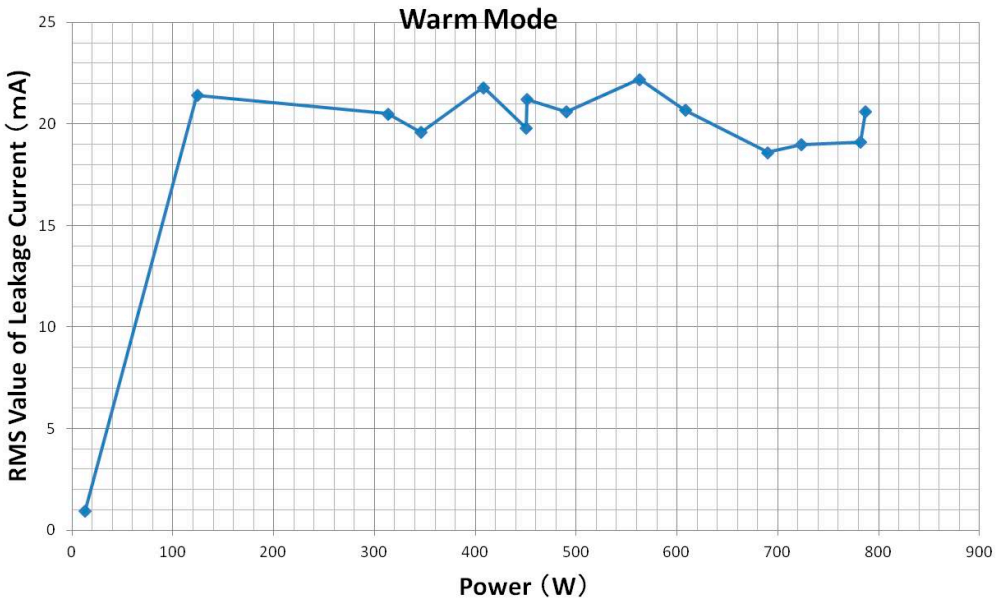


Fig. 2.7 RMS Value of Leakage Current in Worming Mode

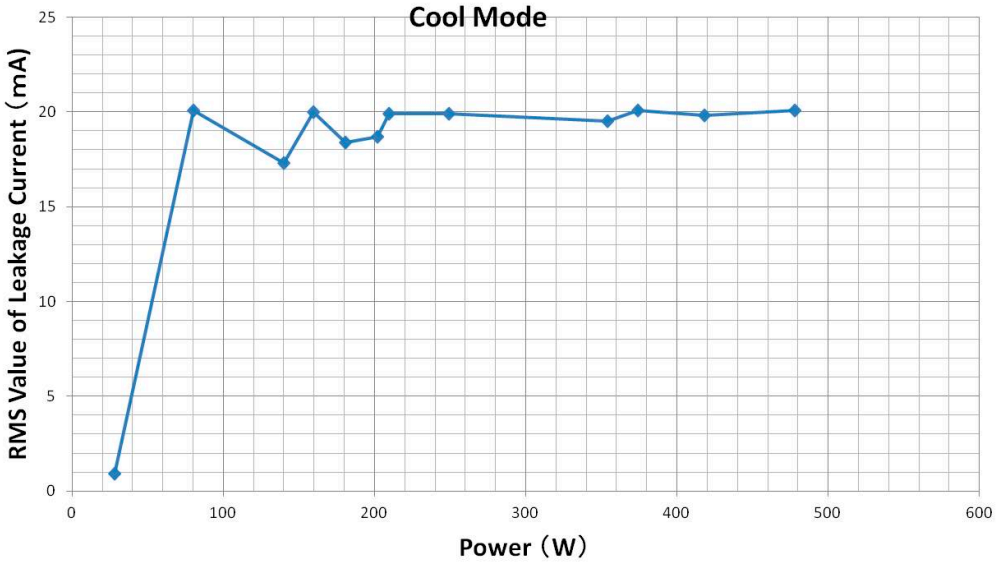


Fig. 2.8 RMS Value of Leakage Current in Cooling Mode

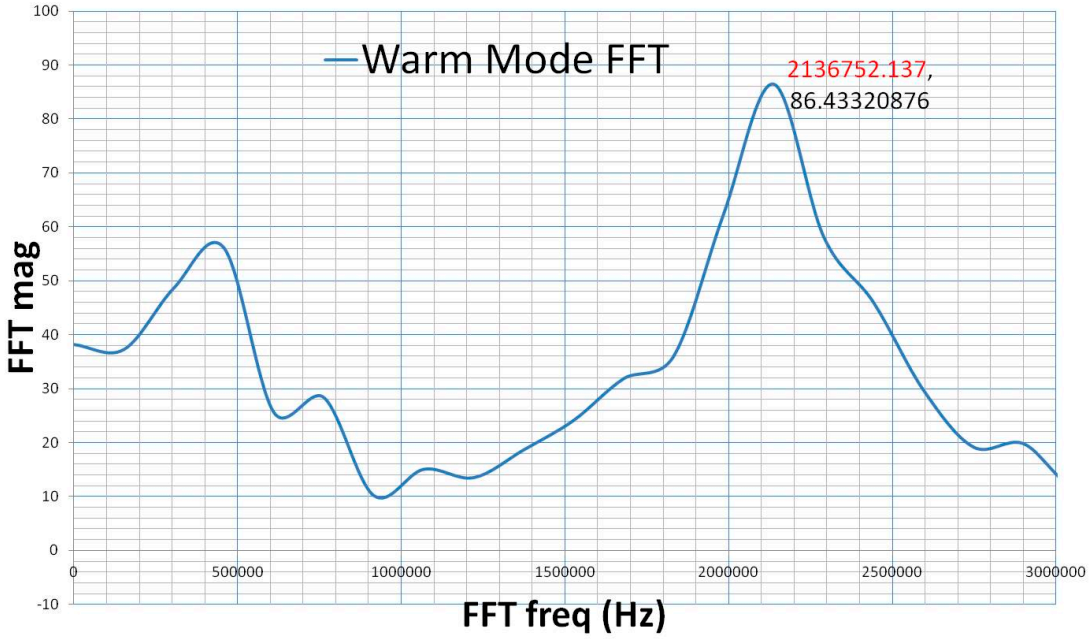


Fig. 2.9 Current FFT Transformation in Warming Mode

In order to further confirm the impact on leakage current in the different running mode, the waveform is resolved with FFT transform. The result of FFT transform shows the resonance frequencies in the system. And the same resonant frequency means the same impedance characteristic in the system. In other words, if the impedance characteristic is the same, it means that the running mode will not affect

the leakage current. Fig. 2.9 and Fig. 2.10 show the leakage current FFT transform results when the air conditioner is working in warming mode and cooling mode. The results show that running mode will not impact the leakage current.

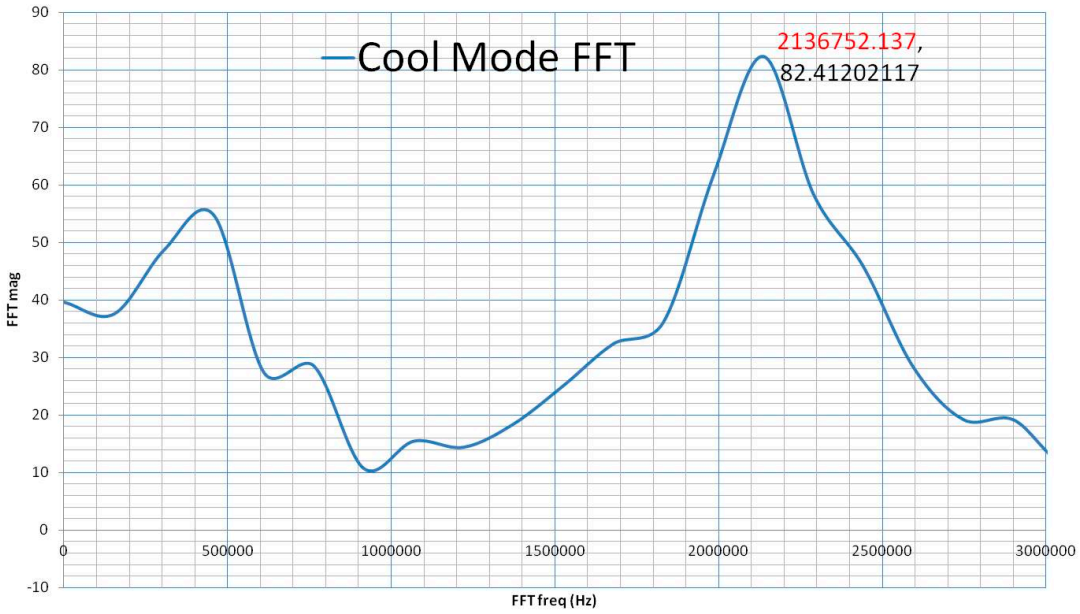


Fig. 2.10 Current FFT Transformation in Warming Mode

The leakage currents are separately measured when the air conditioning is just running, and after running 1 hour. The green line is the leakage current and the other lines are the phase voltage of PWM inverter. Fig. 2.11 shows the leakage current in warming mode when the air conditioning is just running. Fig. 2.12 shows the leakage current in warming mode after the air conditioning is running 1 hour. Fig. 2.13 shows the leakage current in cooling mode when the air conditioning is just running. Fig. 2.14 shows the leakage current in cooling mode after the air conditioning is running 1 hour.

These results show that the peak values of leakage currents in different running mode and different operating time are almost the same, about 610 mA. It means that the running mode and operating time will not affect the leakage current

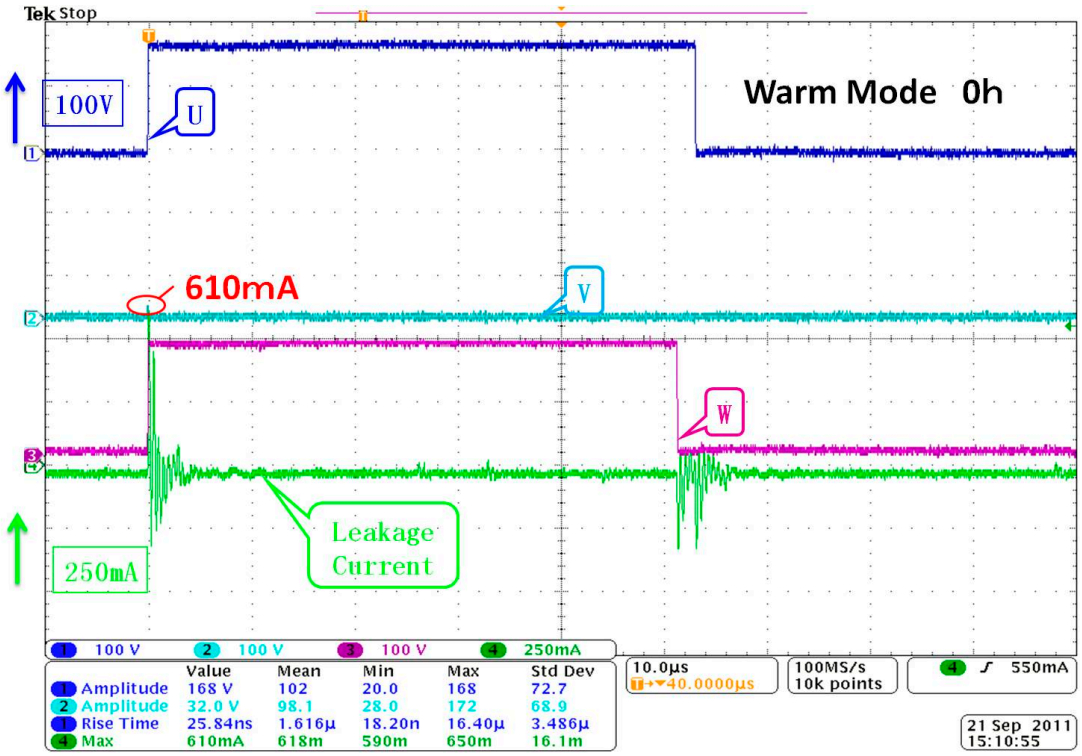


Fig. 2.11 Leakage Current in Warming Mode Just Running

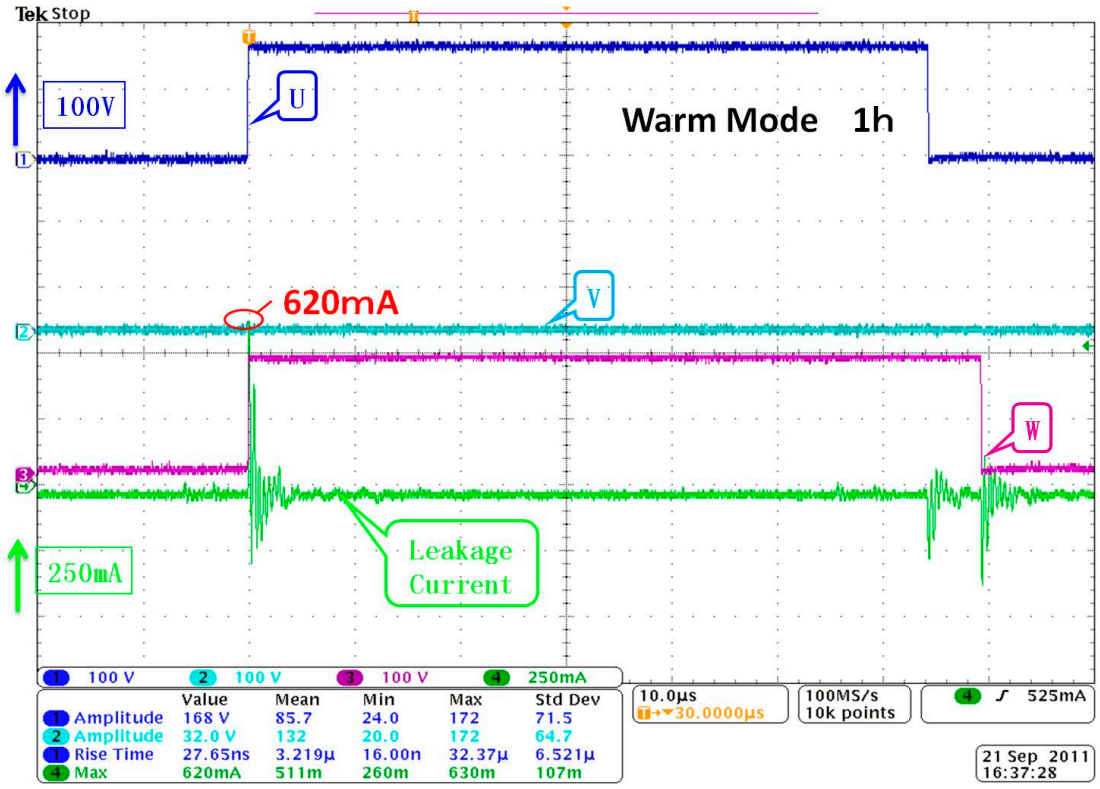


Fig. 2.12 Leakage Current in Warming Mode after Running 1 Hour

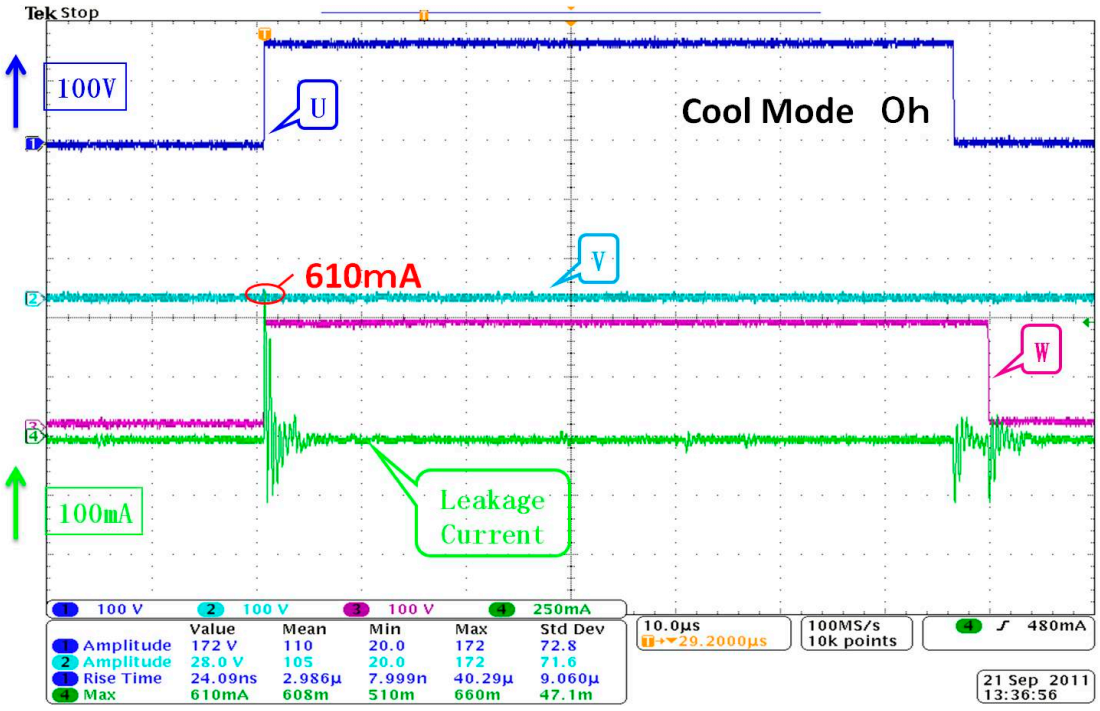


Fig. 2.13 Leakage Current in Cooling Mode Just Running

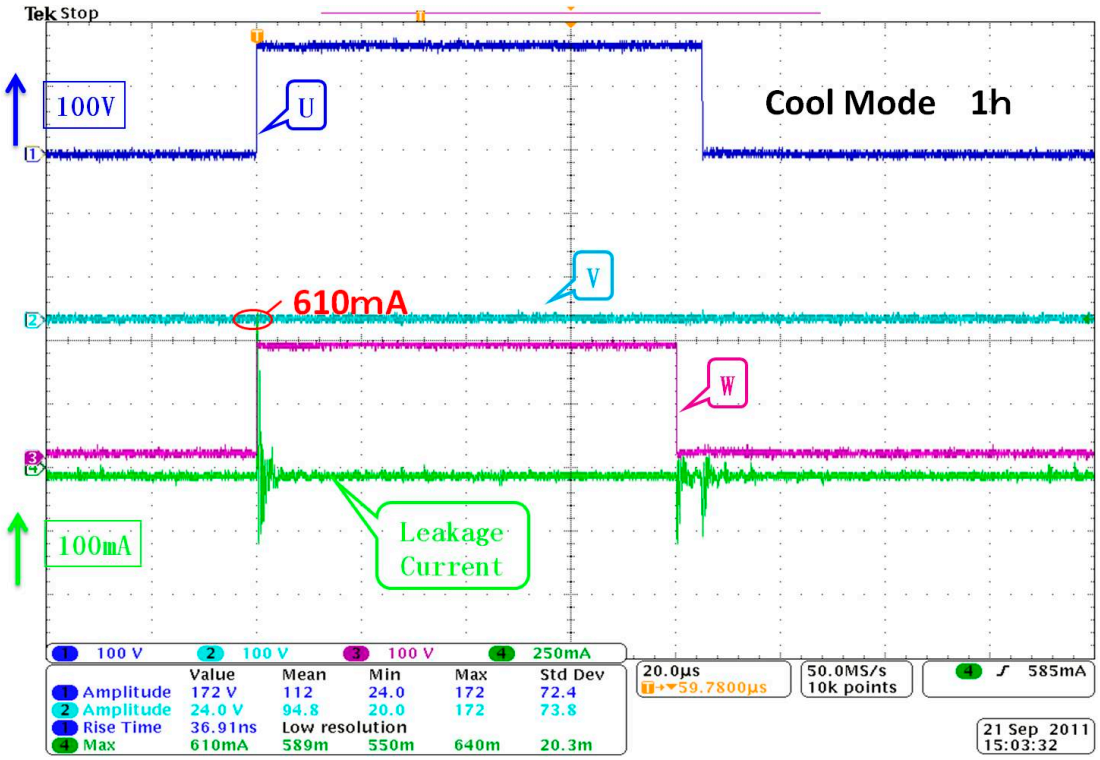


Fig. 2.14 Leakage Current in Warming Mode after Running 1 Hour

In the end, the impact is confirmed, which comes from PWM inverter working status of the combination of the three phase voltages. The green lines of Fig. 2.15, Fig.

2.16 and Fig. 2.17 show the leakage current when the PWM inverter is working on different status. Fig. 2.15 shows the leakage current when two phases of PWM inverter is switching at the same time. At this moment, the leakage current comes to the maximum. Fig. 2.16 also shows the leakage current when two phases of PWM inverter is switching at the same time. But at this moment the rising time of V phase switching is a little longer. So the leakage current is smaller. It means that short rising time of the phase switching results in large leakage current. Fig. 2.17 shows the typical leakage current when only one phase of PWM inverter is switching. The leakage current is quite smaller then Fig. 2.15 and Fig. 2.16. It can be confirmed that the PWM inverter working mode (different combination of the three phase voltages) will impact the leakage current obviously.

In most cases, CM equivalent circuit can be modeled by only linear elements. In this system, non-linearity slightly appears as mentioned in the following subsection. Fig. 2.15 shows the leakage current when two phases of PWM inverter are switching at the same time. At this moment, the leakage current comes to the maximum. Comparing this leakage current with the one in Fig. 2.17, if the equivalent circuit of leakage current is linear, when two phases are switching at the same time, the leakage current should be two times of the current when only one phase is switching. But the leakage current in two phases switching mode 668 mA is smaller than two times of the one in one phase switching mode 740 mA, though the resonant frequencies are identical. Therefore, it can be supposed that there is non-linear effect in this system depending on the amplitude of the leakage current. In order to simulate these phenomena, the author introduces a non-linear resistance that becomes higher as the amplitude of the leakage current increased. To simplify the simulation, a non-linear resistor is chosen, the resistance of which is function of the square of the current.

The following research and calculation are based on this status. And then by using the leakage current when two phases of PWM inverter is switching at the same time to double confirm.

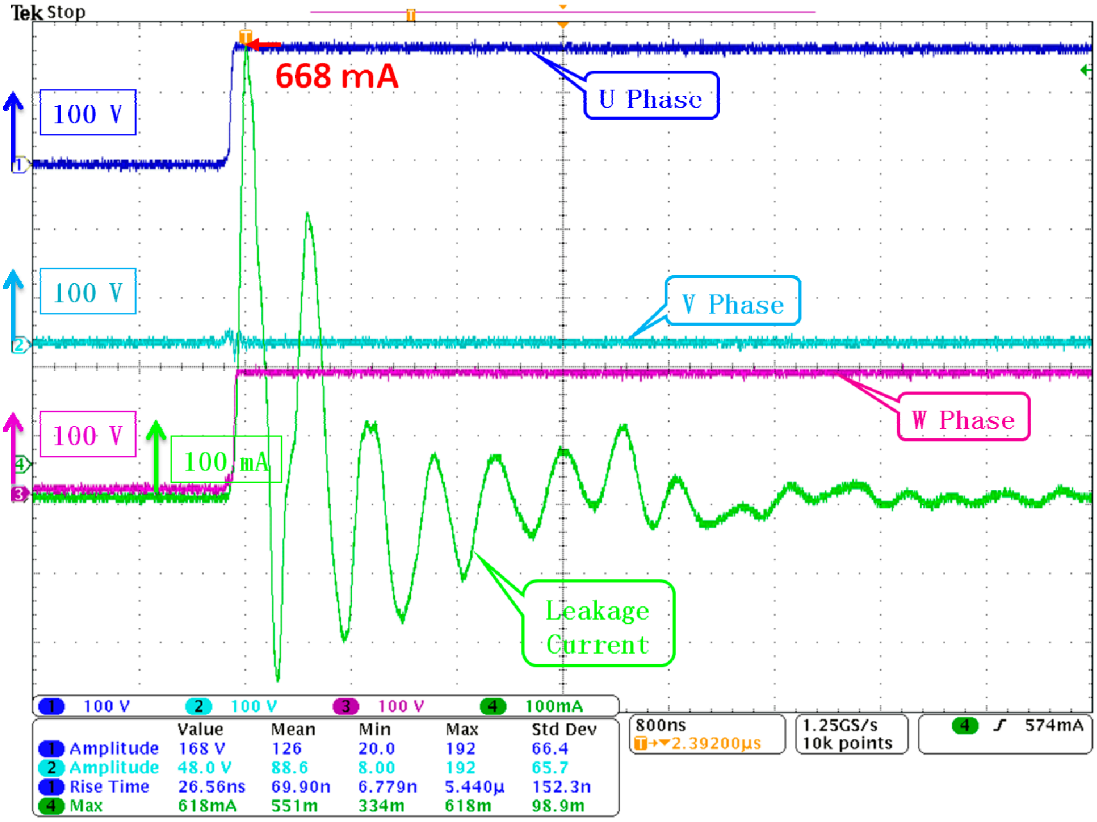


Fig. 2.15 Leakage Current in PWM Inverter Working Status 1

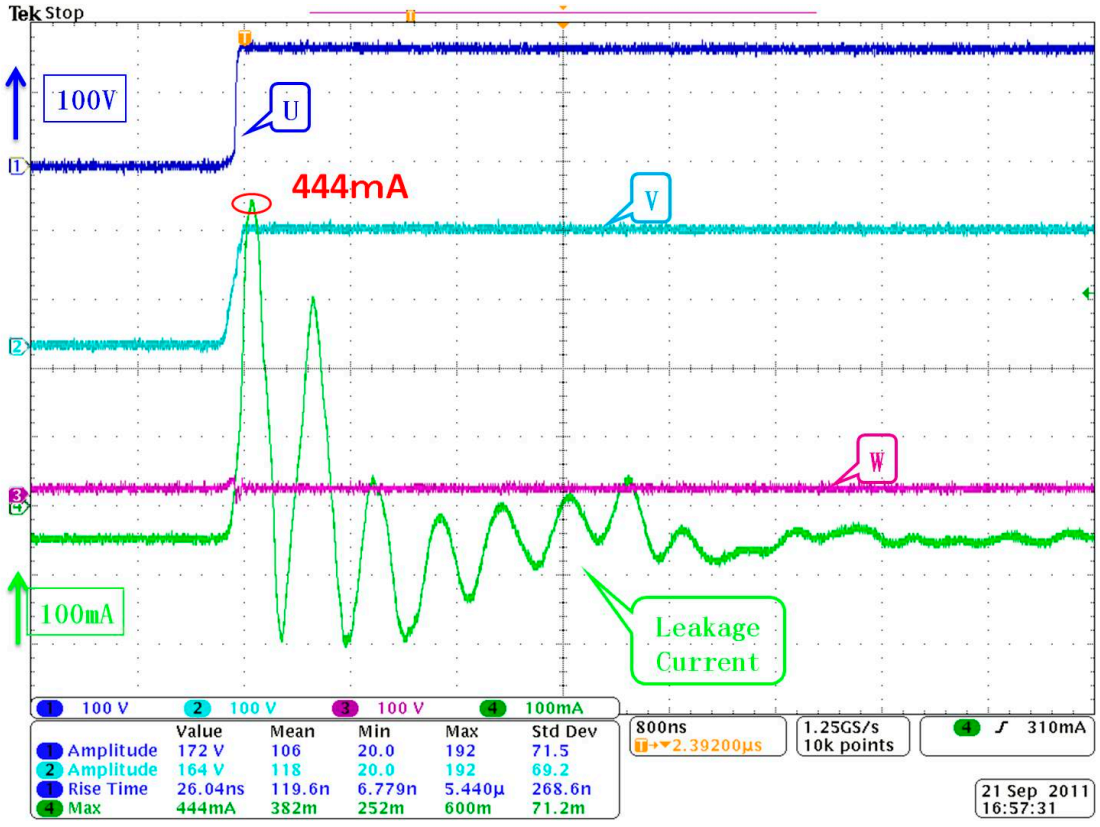


Fig. 2.16 Leakage Current in PWM Inverter Working Status 2

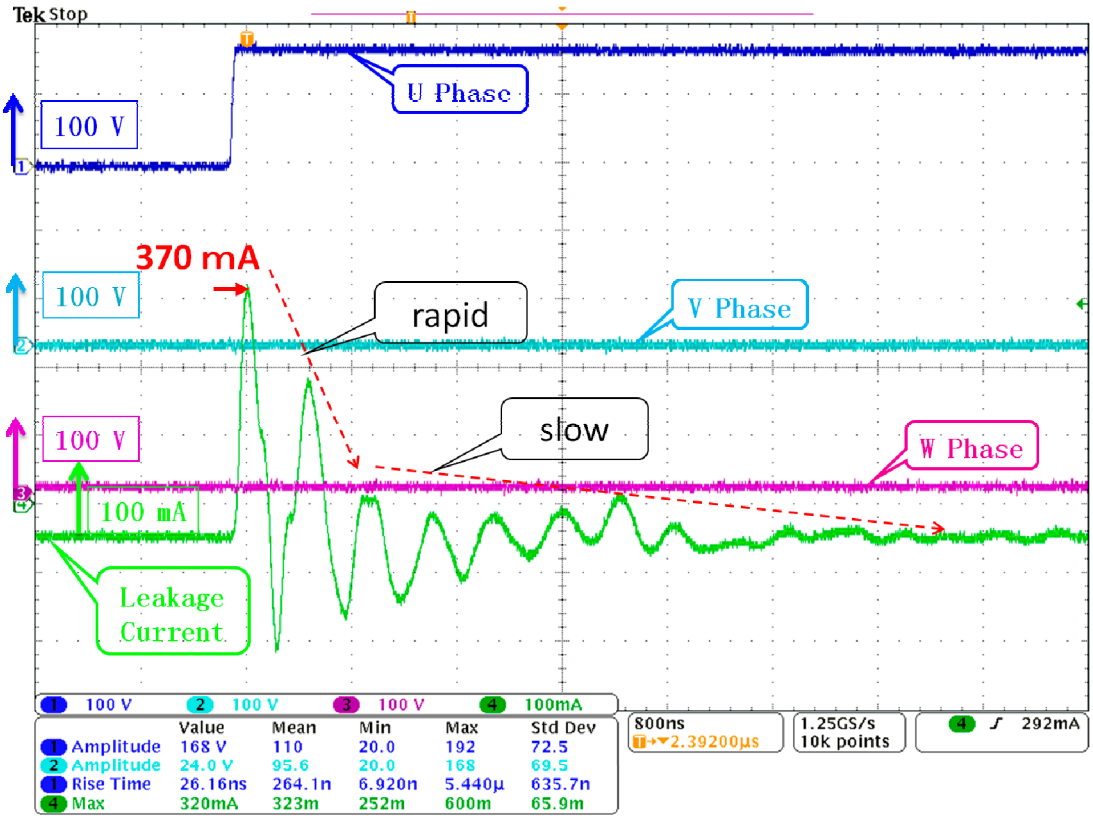


Fig. 2.17 Leakage Current in PWM Inverter Working Status 3

2.3 Construction of Equivalent Circuit

In recent years, several equivalent circuit of PWM inverter-fed motor drive system about the conducted interference was discussed [17][18][24]-[27]. These equivalent circuits can simulate well with the reality equipment results. But the equivalent circuits are too complex. The excellent equivalent circuit can help the application developer to predict the EMI noise level of the production, and also can contribute to design the EMI filter. But these complex equivalent circuits could not be easy to understand the physical meaning of every part. Therefore, the simple and easy understanding equivalent circuit with enough accuracy is the most useful tool to the developer.

According to the analysis of conduction mechanism of CM interference, the leakage current will mainly backtrack to the power supply system through the parasitic capacitances in the system. There are a large number of parasitic capacitances dispersing in the PWM inverter-fed motor drive system. Compared with the parasitic capacitance between the coil and the frame of AC motor, the other parasitic capacitances are negligible. Consequently, the leakage current mainly backtrack to the power supply system though the parasitic capacitance between the coil and the frame of AC motor. And in order to observe the coil of the AC motor, no matter from the beginning of the coil or the end of the coil, the characteristic of the coil is the same. So the π style equivalent circuit can well perform the characteristics of AC motor. By comparing the bridge rectifier with the PWM inverter, the frequency of bridge rectifier circuit switching is quite slow and almost could be negligible. So the main interference source comes from the PWM inverter. Therefore, the PSIM equivalent circuit of PWM inverter-fed motor drive system can be shown as Fig. 2.18.

For easily verifying the effect of the equivalent circuits, the interference source, i.e., the PWM inverter can be performed by a step voltage source. Not only the amplitude of switching voltage, when the power semiconductor devices are switching, but the rising time can also be well performed. There are inductances presenting on the wires. The π style equivalent circuit of AC motor is shown in the blue block. The

parasitic capacitances on the beginning of the AC motor coil and the parasitic capacitances on the end are the same. The inductance of AC motor is shown as the inductance L_{32}. The introducing of non-linear resistance will be detailed in Chapter 3 and Chapter4. By adding a current monitor, the leakage current can be easily measured. The correctness of this equivalent circuit will be confirmed by comparing the simulation leakage current with the experiment leakage current.

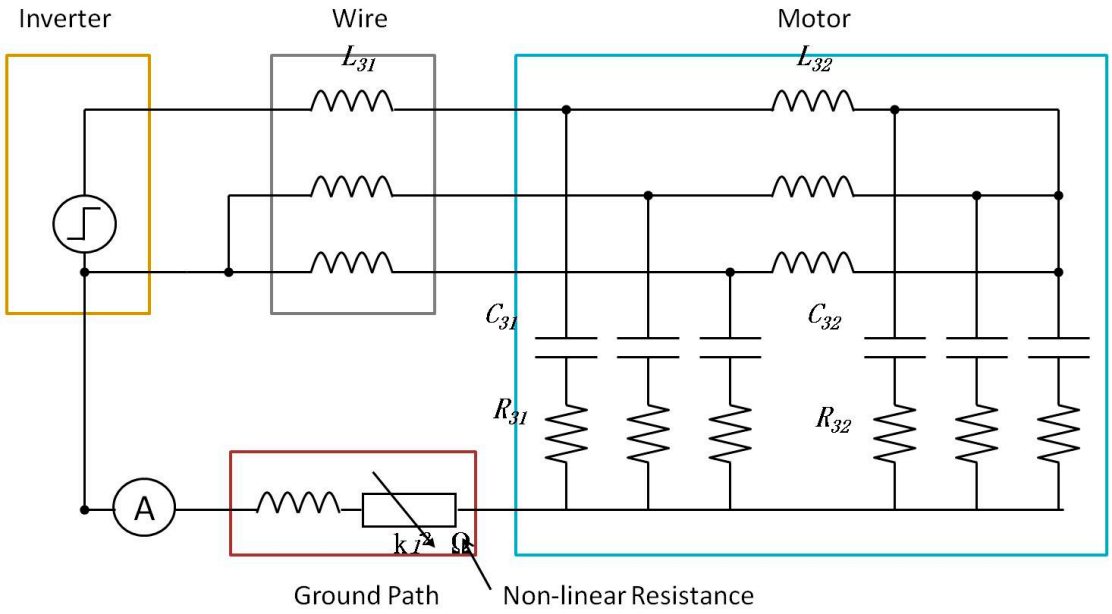


Fig. 2.18 Equivalent Circuit of PWM Inverter-Fed Motor Drive System

2.4 Summary

In this chapter, the structure of PWM inverter-fed motor drive system is described. Then the effect on the leakage current is discussed, when air conditioner is working in the different running mode, with the different working power and after the different working time. These factors do not affect the leakage current and the differences in these situations can be neglected.

And then the impact which comes from PWM inverter working status is confirmed. When two phases of PWM inverter is switching at the same time, the leakage current reaches to the maximum. And short rising time of the PWM inverter phase switching results in large leakage current. The following calculation will base on the leakage current when only one phase of PWM inverter is switching, and the result will be introduced to the status when two phases of PWM inverter is switching at the same time to double confirm.

Finally, a simple equivalent circuit of PWM inverter-fed motor drive system is discussed. A non-linear element is introduced and the implication will be verified in Chapter 3 and Chapter 4. This simple equivalent circuit is easy to understand, and the accuracy is enough to analyze conducted interference and design efficiency EMI filter. And the correctness of this equivalent circuit will be confirmed by comparing the simulation leakage current with the experiment leakage current in the following chapters.

Chapter 3 Introduction of Non-Linear Element

3.1 Rationality of Non-Linear Equivalent Circuit

3.1.1 CM Leakage Current Measure

The green line in Fig. 3.1 shows the leakage current waveform on the ground path. And the other color lines show the three phase voltages of PWM inverter.

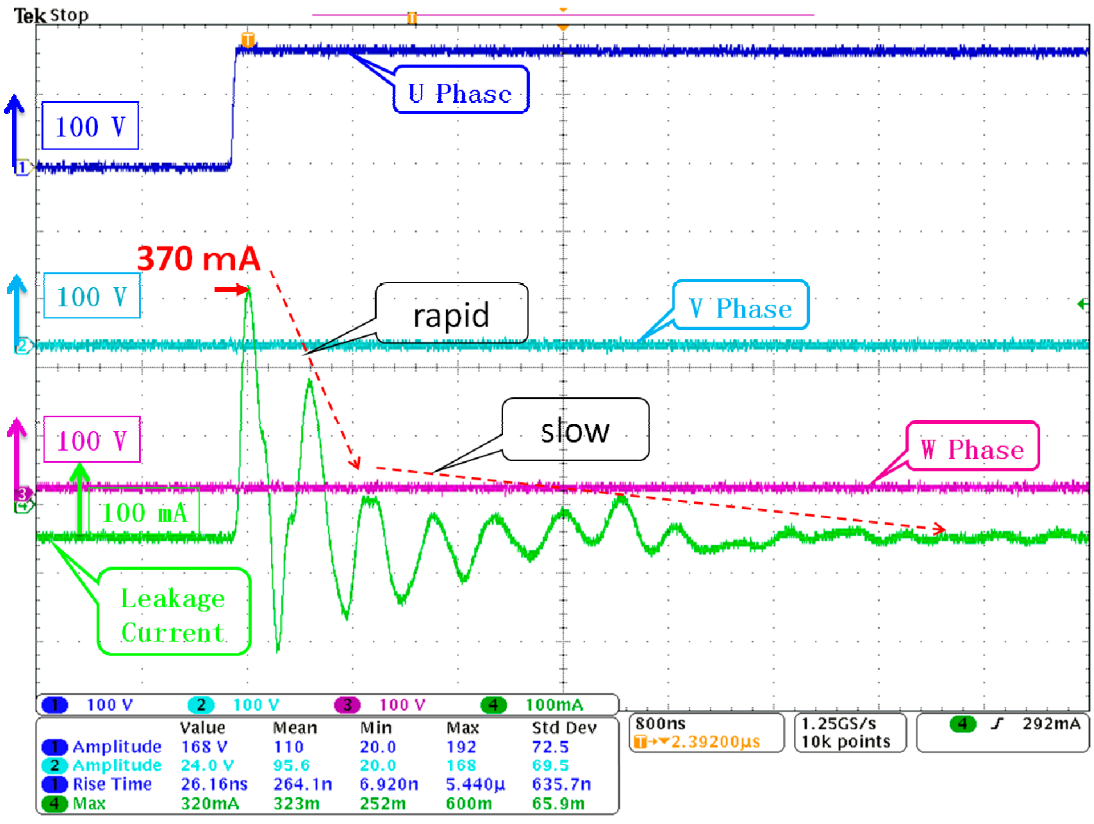


Fig. 3.1 Leakage Current Waveform of One Phase Switching

3.1.2 Resonance Frequency Calculation and FFT Transformation

Waveforms of leakage current plotted in Excel, show the amplitude (Y-axis) versus time (X-axis). Knowing the period T of the waveform, the frequency can be calculated. This frequency is the resonance frequency. FFT transform result of leakage current shows as Fig. 3.2.

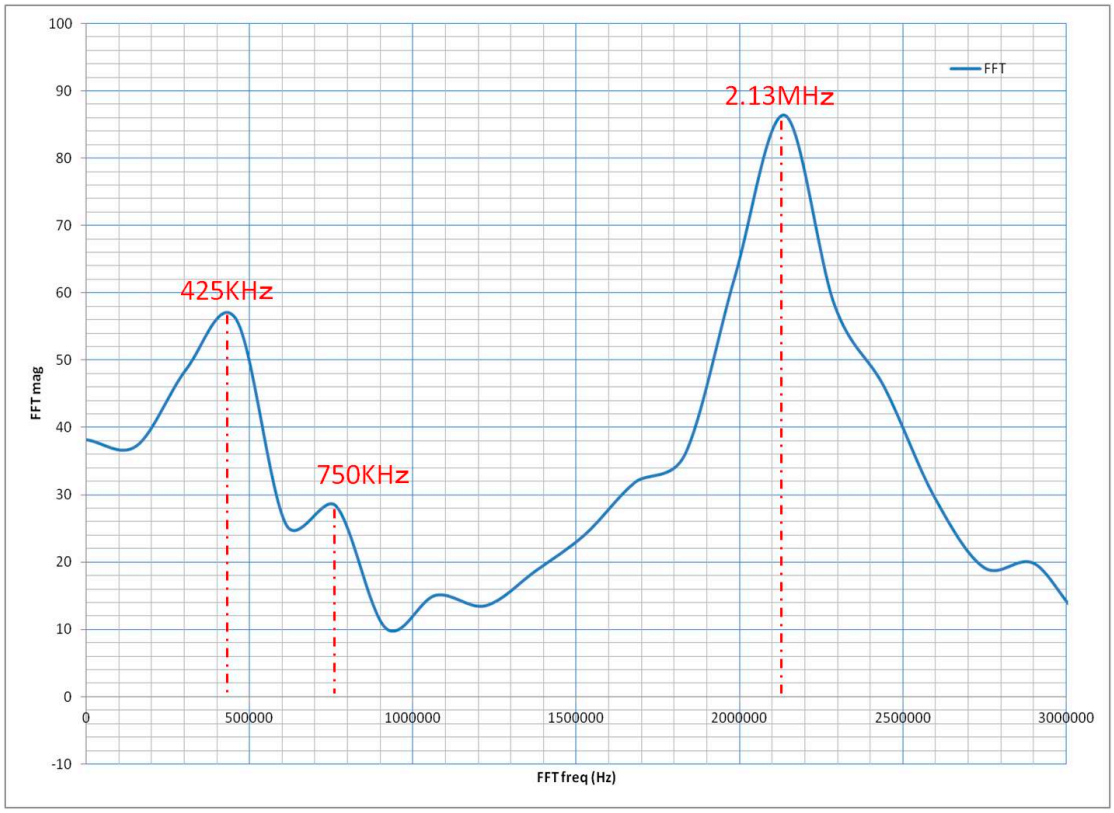


Fig. 3.2 Result of FFT Transform

Based on this result, there are two resonance frequencies in PWM inverter-fed motor drive system, 425 KHz and 2.13 MHz. Compared with the resonance frequencies 425 KHz and 2.13 MHZ, the frequency 750 KHz is negligible. This result is in line with the equivalent circuit proposed before. There are two main LCR circuit in the system, and the resonance frequencies are 425 KHz and 2.13 MHz.

3.1.3 Rationality of Non-Linear

The waveform of leakage current shown in Fig. 3.1 should be divided into two parts. It can be found that in the initial stage when the leakage current is high, the current decreases rapidly, and in the following stage when the leakage current is low, the current decreases slowly. If the system is linear, the decreasing speed of the current will not change. Therefore the non-linear impedance may exist in the PWM inverter-fed motor drive system. And the non-linear impedance should be an element associated with leakage current.

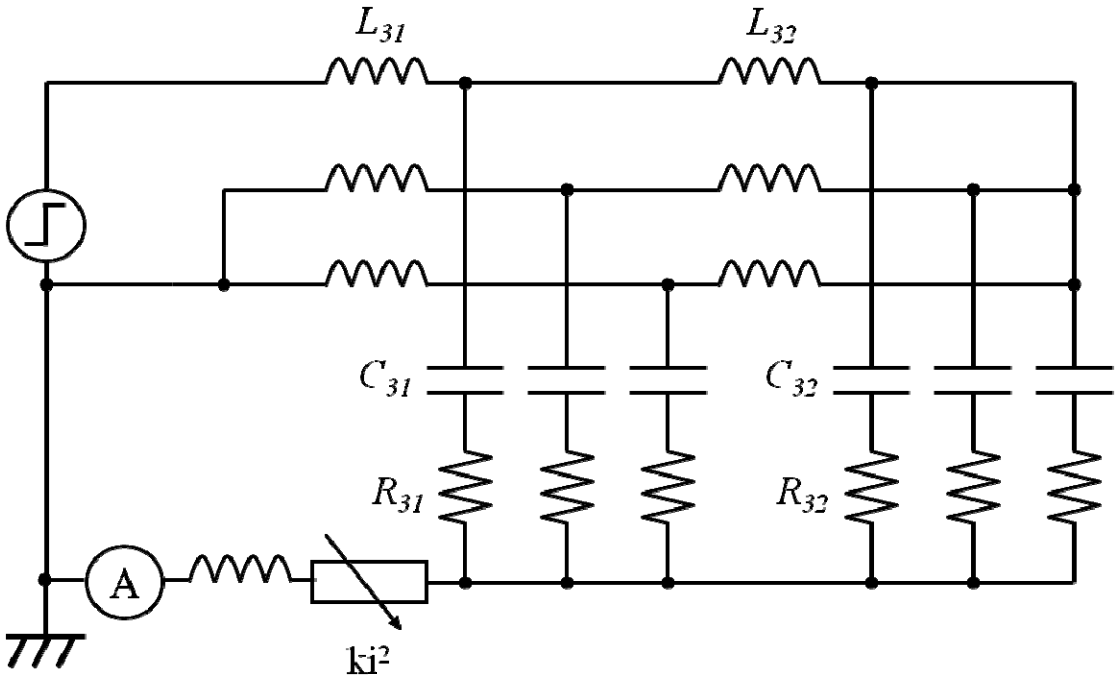


Fig. 3.3 Equivalent Circuit with Non-Linear Resistance

Fig. 3.3 shows structure of the proposed equivalent circuit. Since stator windings of a motor are embedded into slots of a stator cores, there is relatively large stray capacitance between a stator winding and the motor frame rather than between the other windings. Although, an equivalent circuit for a motor winding considering stray capacitance is expressed by a distributive circuit, π-type equivalent circuits are introduced as motor windings, in the proposed equivalent circuit, to simplify the

distributive circuits. Of course the parasitic capacitances are also existed between the semiconductor devices and heat sinks, but the parasitic capacitance of motor is much higher. So these capacitances are negligible in this modeling to make sure the clear equivalent circuit. Moreover, each of power cables and a grounding wire is modeled as an inductance. A non-linear element is connected in series to the grounding inductance. To express the non-linearity mentioned above, the non-linear element is a resistor, the value of which varies in proportion to square of the current.

3.2 Calculation of Equivalent Circuit

3.2.1 Calculation method

Fig. 3.4 shows an LCR series circuit. If the input source is a step voltage, the decreasing current shows as Fig. 3.5.

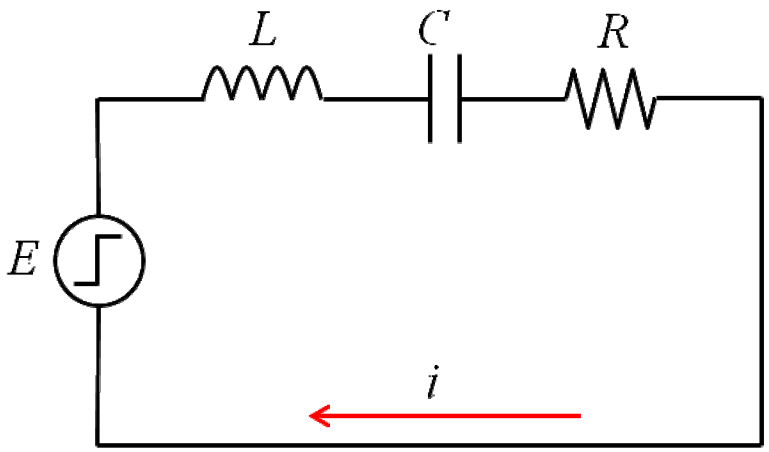


Fig. 3.4 LCR Series Circuit

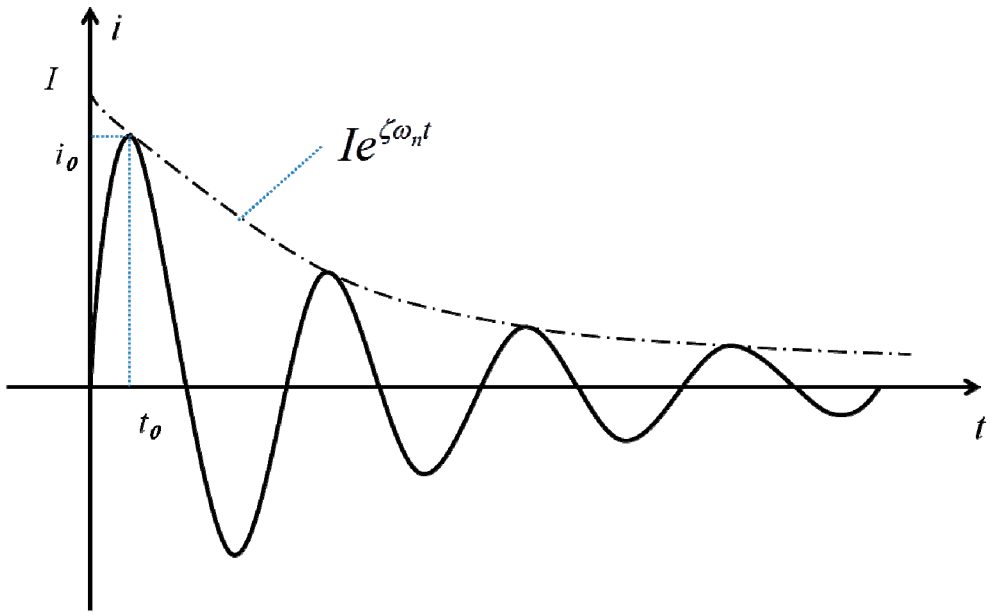


Fig. 3.5 Decreasing Current of LCR Series Circuit

The amplitude of input step source is *E*, the resonance frequency is ω_n, the characteristic impedance is Z_0, and the attenuation factor is ζ. The following formula can represent the relationship of the current.

$$\mathrm{i(t)} \cong \frac{\mathrm{E}}{\mathrm{Z_0}} \mathrm{e}^{-\zeta\omega_\mathrm{n}\mathrm{t}} \mathrm{sin}\omega_\mathrm{n}\mathrm{t} \tag{3.1}$$

where,

$$\omega_n = \frac{1}{\sqrt{LC}} \tag{3.2}$$

$$Z_0 = \sqrt{\frac{L}{C}} \tag{3.3}$$

$$\zeta = \frac{R}{2Z_0} \tag{3.4}$$

If the step voltage is known, the amplitude i_0 can be shown as follows.

$$i_0 = \frac{E}{Z_0} e^{-\zeta\omega_n t_0} \tag{3.5}$$

And then, the characteristic impedance can be shown as

$$Z_0 = \frac{E}{i_0} e^{-\zeta\omega_n t_0} \tag{3.6}$$

Further,

$$I = \frac{i_0}{e^{-\zeta\omega_n t_0}} \tag{3.7}$$

$$Z_0 = \frac{E}{I} \tag{3.8}$$

The characteristic impedance can be calculated by the amplitude *E* and the current *I*. Finally, the inductance *L* and the capacitance *C* can be shown as follows.

$$L = \frac{Z_0}{\omega_n} \tag{3.9}$$

$$C = \frac{1}{\omega_n Z_0} \tag{3.10}$$

According to the waveform of leakage current, I and i_0 can be estimated. The voltage E can be measured by the voltage probe. And the resonance frequency ω_n can be measured by solving the leakage current waveform be measured with the current probe, with the method of FFT transform. Thus all the parameters can be calculated.

3.2.2 Calculation of CM High-Frequency Equivalent Circuit

According to FFT result and the waveforms of the leakage current, which got form the experiment, the circuit parameters in the equivalent circuit can be calculated. There are two resonance frequencies in the system according to the FFT result.

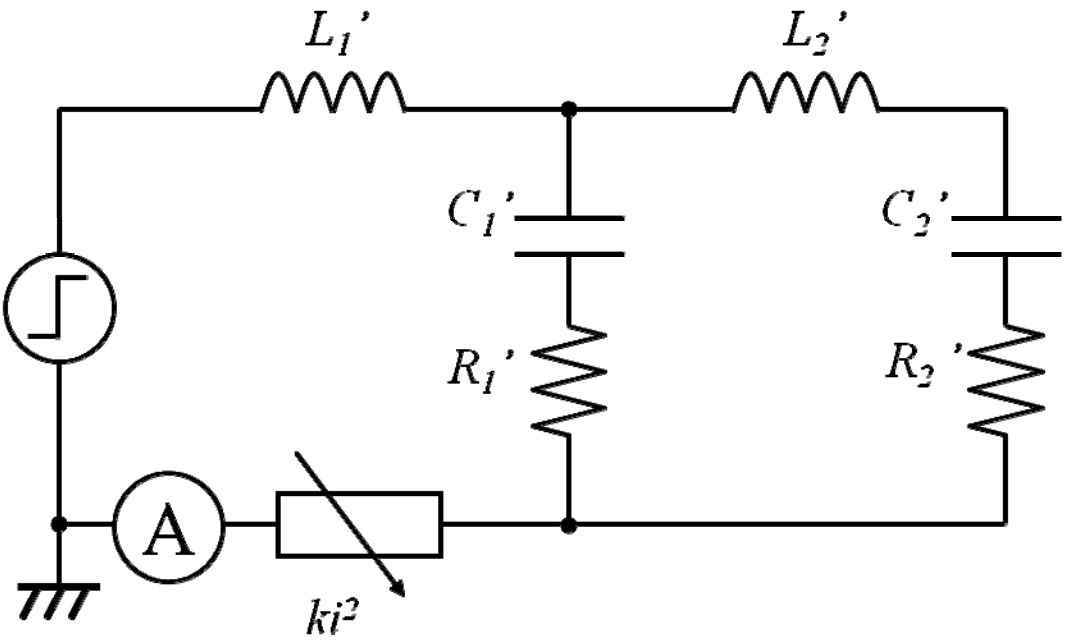


Fig. 3.6 CM Equivalent Circuit

Fig.3.6 shows the CM equivalent circuit obtained from Fig. 5. Because L_1 is

much smaller than the inductance L_2, the equivalent circuit Fig. 3.6 can be deformed into Fig. 3.7.

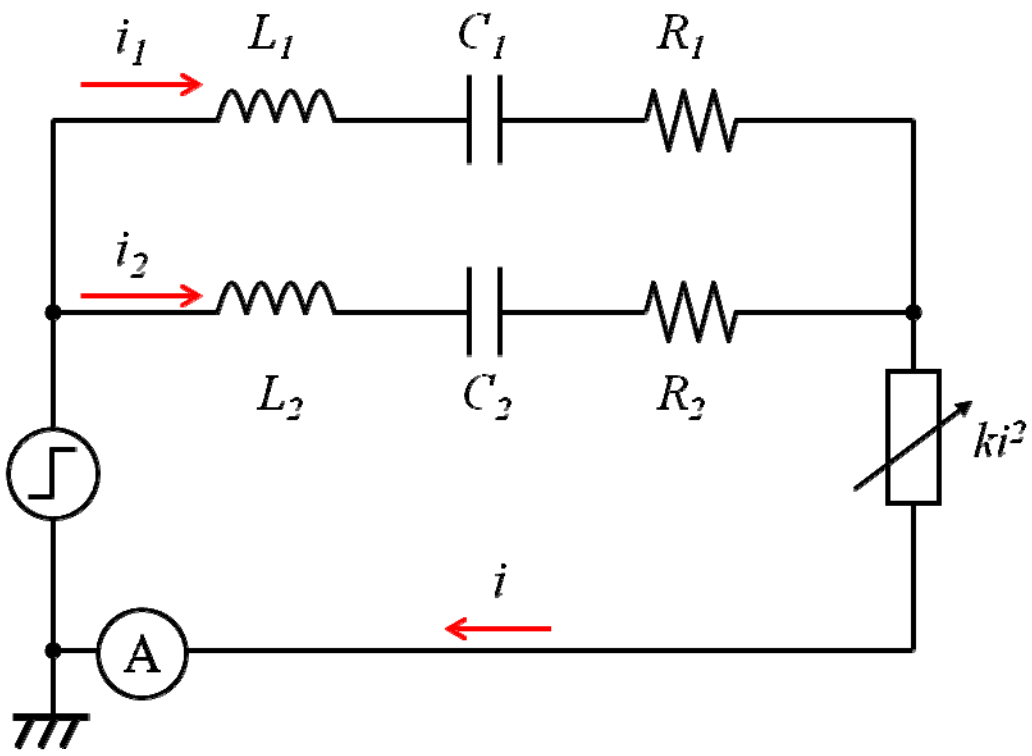


Fig. 3.7 Deformed CM Leakage Current

The relationship between them shows as below:

$$L_1{}' = L_1 = \frac{1}{3}L_{31} + L_{31} \tag{3.11}$$

$$L_2{}' = L_2 - L_1{}' = \frac{1}{3}L_{32} \tag{3.12}$$

$$C_1{}' = C_1 = 3C_{31} \tag{3.13}$$

$$C_2{}' = C_2 = 3C_{32} \tag{3.14}$$

$$R_1{}' = R_1 = \frac{1}{3}R_{31} \tag{3.15}$$

$$R_2{}' = R_2 = \frac{1}{3}R_{32}$$

(3.16)

The equivalent circuit of Fig. 9 is applied to calculate the parameters of two frequencies separately. The high frequency circuit parameter is performed with the subscript 1, and the low frequency circuit is performed with the subscript 2.

$$i_1(t) = \frac{E}{Z_1}e^{-\zeta_1\omega_1 t}\sin\omega_1 t$$

(3.17)

$$i_2(t) = \frac{E}{Z_2}e^{-\zeta_2\omega_2 t}\sin\omega_2 t$$

(3.18)

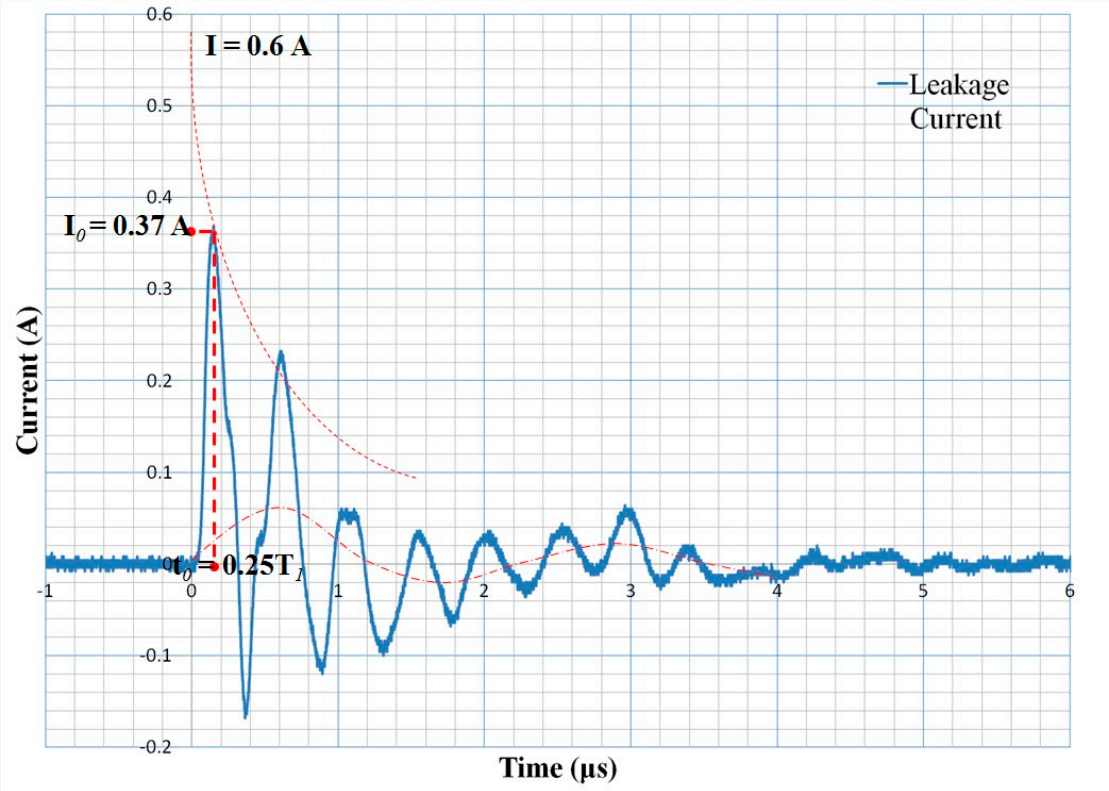


Fig. 3.8 Calculation of Leakage Current

There are two resonance frequencies in the system. So the parameter should be calculated separately. The high frequency circuit parameter is performed with the subscript 1, and the low frequency circuit is performed with the subscript 2. According to the result of FFT transform,

$$f_1 = 2.13\text{MHz}, \qquad T_1 = 0.47 \times 10^{-6}\text{s}, \qquad \omega_1 = 13.38 \times 10^6\text{rad/s} \tag{3.19}$$

$$f_2 = 425\text{KHz}, \qquad T_2 = 2.35 \times 10^{-6}\text{s}, \qquad \omega_2 = 2.67 \times 10^6\text{rad/s} \tag{3.20}$$

As shown as Fig. 3.8,

$$I = 0.6\ \text{A} \tag{3.21}$$

$$i_0 = 0.37\ \text{A} \tag{3.22}$$

$$t_0 = \frac{1}{4}T_1 = 0.118\ \mu\text{s} \tag{3.23}$$

$$\frac{1}{2}T_2 = 1.175\ \mu\text{s} \tag{3.24}$$

$$\sin(\omega_2 t_0) = \sin\left(\frac{t_0}{\frac{1}{2}T_2} \times \pi\right) = 0.31 \tag{3.25}$$

Because of the π style equivalent circuit, the parasitic capacitances are the same both of beginning and end of coil. Therefore, it can be supposed that

$$C_1 = C_2 \tag{3.26}$$

According to the equation (3.10),

$$\frac{1}{\omega_1 Z_1} = \frac{1}{\omega_2 Z_2}, \qquad \frac{\omega_1}{\omega_2} = \frac{Z_2}{Z_1} = \frac{I_1}{I_2} \tag{3.27}$$

$$I_1 = 5.01 I_2 \tag{3.28}$$

The leakage current which is shown as Fig. 3.8 can be drawn apart as two parts shown as Fig. 3.9.

Suppose,

$$i_2 \cong I_2 \tag{3.29}$$

$$i_0 = i_1 + \frac{1}{5.01} i_1 \times \sin(\omega_2 t_0)$$

(3.30)

$$i_1 = 0.35\text{A}$$

(3.31)

According to equation (3.10),

$$Z_1 = \frac{E}{I_1} = 112$$

(3.32)

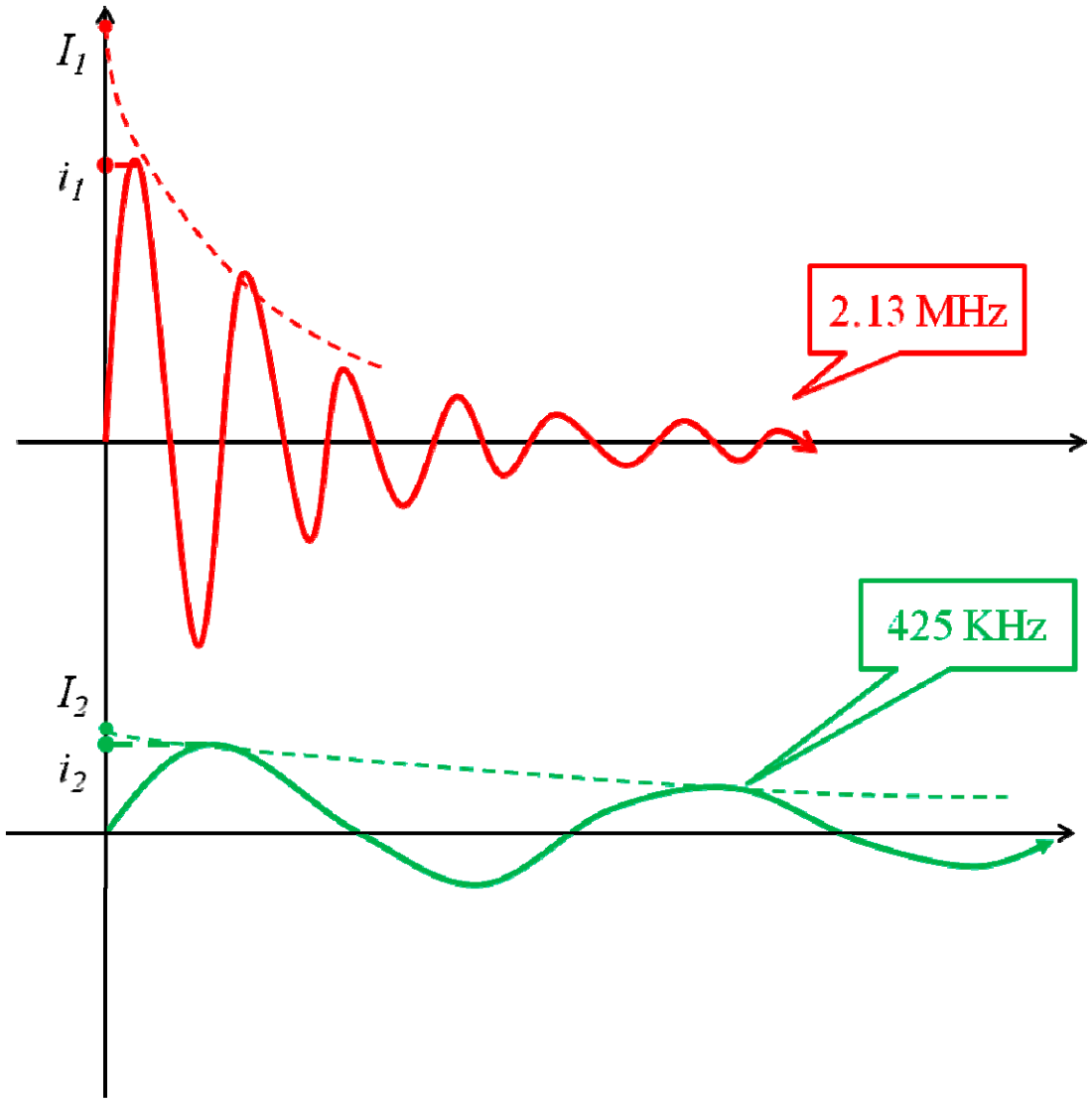


Fig. 3.9 Leakage Current deformation

ζ_a is the attenuation factor in the initial stage, and ζ_1 is the attenuation factor in the following stage, According to the waveform of leakage current,

$$\zeta_a = 0.23 \tag{3.33}$$

$$\zeta_1 = 0.8 \tag{3.34}$$

Suppose the non-linear resistance is $VR(t) = k \times i^2$ Ω. When the current is high, the non-linear resistance is much higher than the linear. Thus,

$$\zeta_a = \frac{R_1 + VR(t)}{2Z_1} \cong \frac{VR(t)}{2Z_1} \tag{3.35}$$

Further,

$$k = \frac{2Z_1\zeta_a}{{i_1}^2} \tag{3.36}$$

Finally,

$$k = 415, \quad R_1 = 8\,\Omega, \quad L_1 = 8.4\,\mu\text{H}, \quad C_1 = 667\,\text{pF} \tag{3.37}$$

By using the same method, the parameter of low frequency is

$$R_2 = 247\Omega, \quad L_2 = 210\mu\text{H}, \quad C_2 = 667\text{pF} \tag{3.38}$$

Substitute the equations (3.11) ~ (3.16). The parameters of equivalent circuit $\mathrm{L_{31}}$, $\mathrm{L_{32}}$, $\mathrm{C_{31}}$, $\mathrm{C_{32}}$, $\mathrm{R_{31}}$, $\mathrm{R_{32}}$ and *k* can be calculated.

3.3 PSIM Model and Simulation Result

Because of two resonance frequencies and the π style equivalent circuit, by introducing the values of parameter calculated to the PSIM model, and the model is shown as Fig. 3.10.

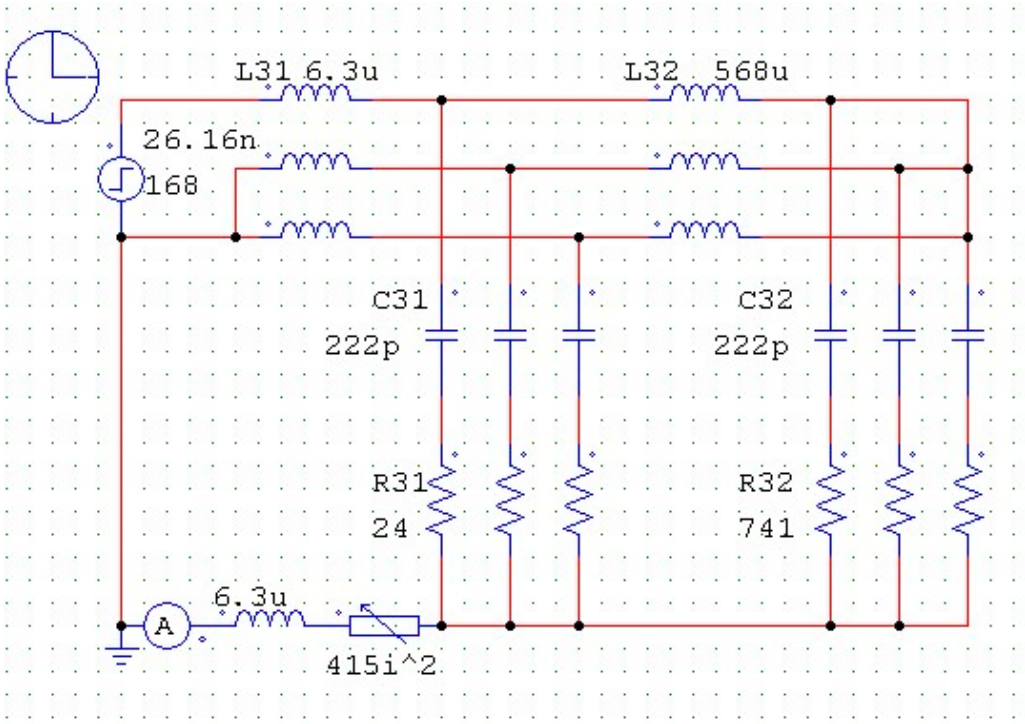


Fig. 3.10 PSIM Model with One Phase Switching First

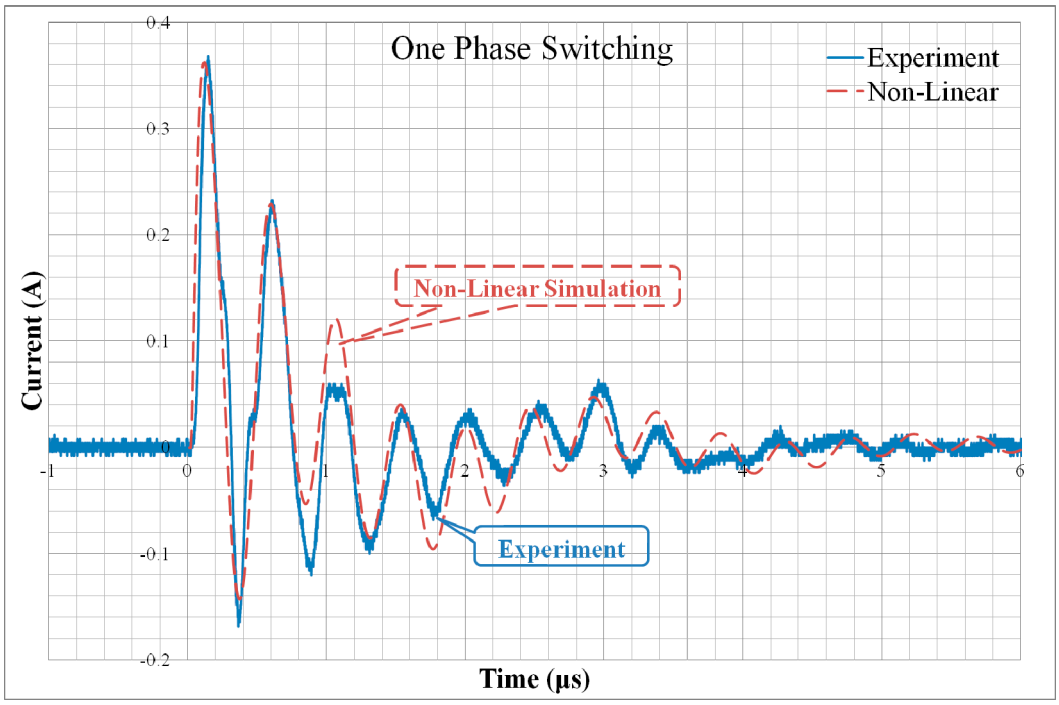


Fig. 3.11 Simulation Result with One Phase Switching First

The simulation result is shown as Fig. 3.11. The simulation result (red line) can quite well meet with the experiment waveform (blue line).

Substitute the parameter to the PISM equivalent circuit model, when two phases are switching at the same time. The model is shown as Fig. 3.12.

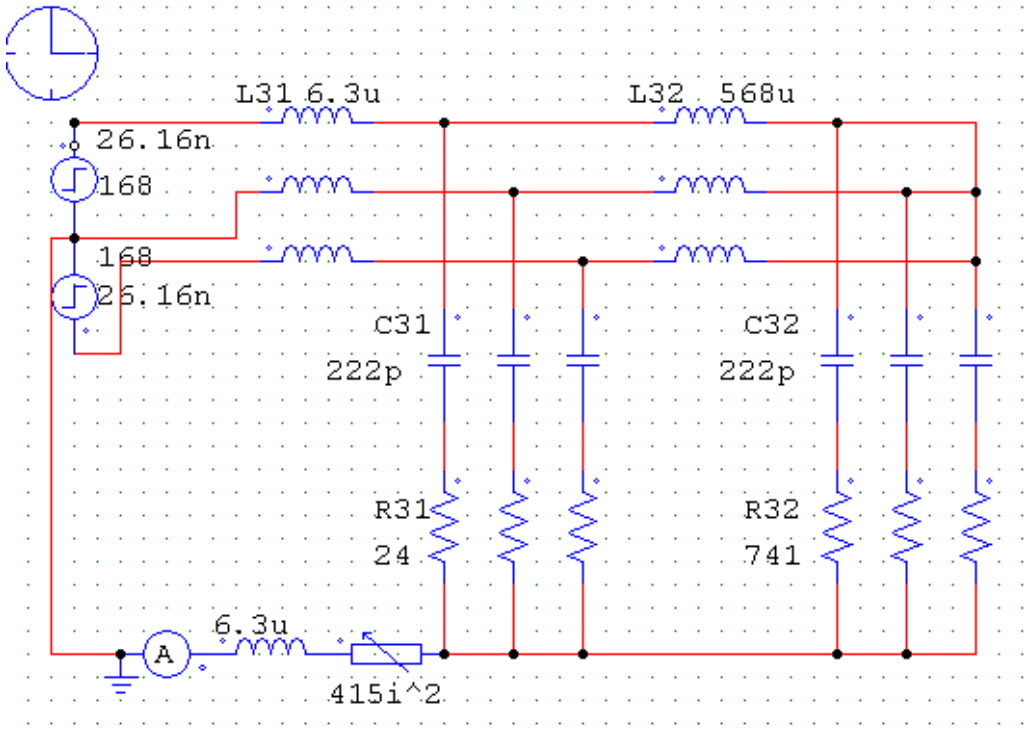


Fig. 3.12 PSIM Model with Two Phases Switching First

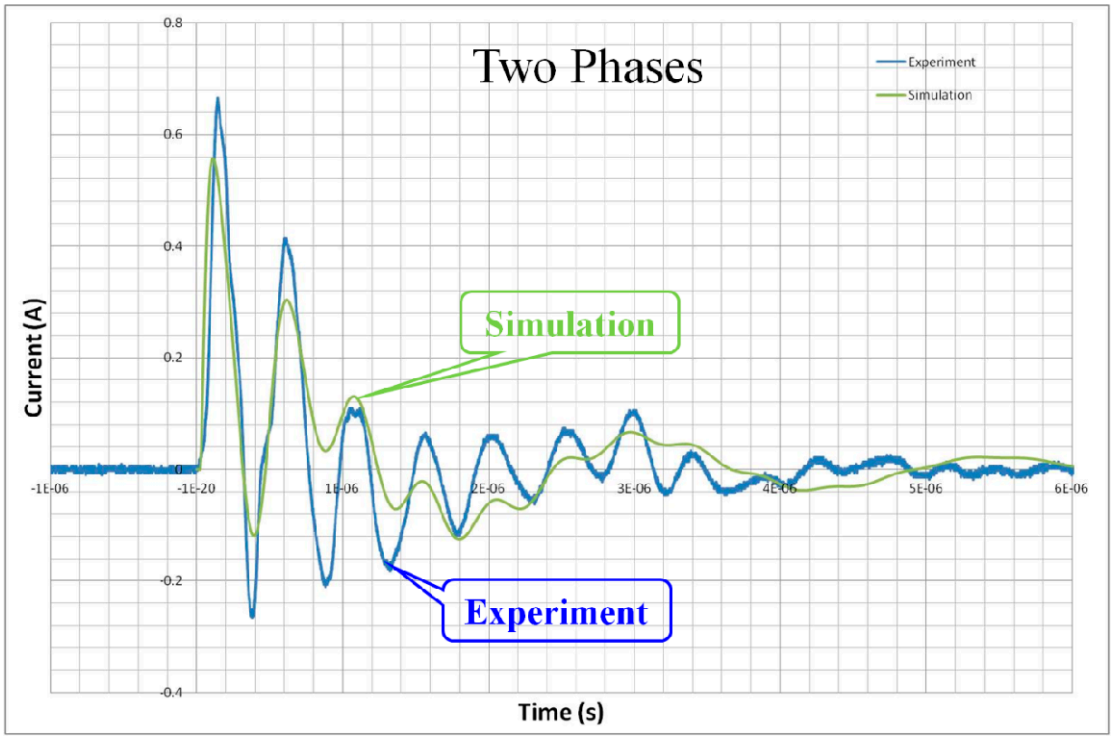


Fig. 3.13 Simulation Result of Two Phases Switching First

The simulation result is shown as Fig. 3.13, when two phases are switching at the same time. The simulation result (green line) cannot well meet with the experiment waveform (blue line).

The simulation result deviates from the experiment measure data. It means there are some problems in this equivalent circuit, especially the effect of the non-linear resistance. The rate of decay is determined by the value of resistance. Large resistance leads to high rate of decay. In order to verify the effect of non-linear resistance, an equivalent circuit without non-linear element needs to double confirm.

3.3.1 Linear equivalent circuit

Use the same method to calculate the parameter of equivalent circuit without non-linear resistance. The PSIM model is shown as Fig.3.14.

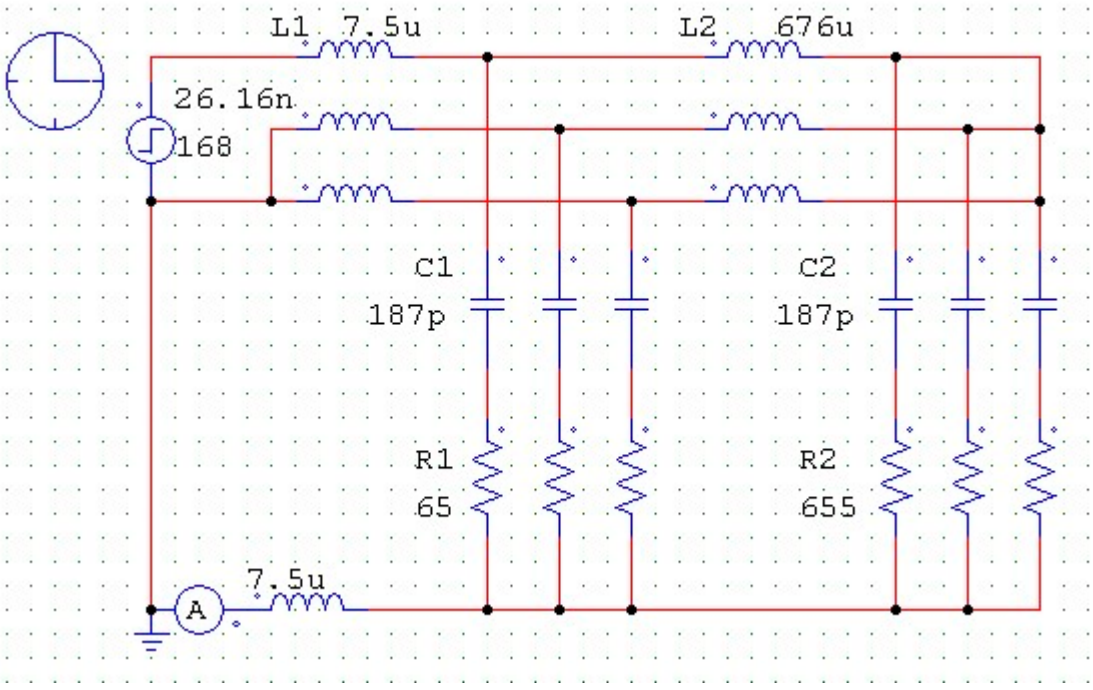


Fig. 3.14 Linear Equivalent Circuit Model

Fig. 3.15 shows the linear simulation result (green line) when only one phase is switching. The result also can quite well meet with the experiment waveform (blue

line) too. Fig 3.16 shows the simulation result when two phases of PWM inverter are switching at the same. The blue line is the experiment waveform, the green line is the simulation result of equivalent circuit without non-linear resistance, and the red line is the simulation result with non-linear resistance. Compared these results, it can be confirmed that comparing with linear resistant, the non-linear resistance can significantly increase the rate of current decay. When the simulation result could well meet the experiment waveform in only one phase switching mode, large non-linear resistance will lead to decay too fast. Contrarily, no non-linear resistance will lead to decay too slowly. According to these results, the non-linear resistance exactly exists in this PWM inverter-fed motor drive system. But it is not very large in the model shown as Fig. 3.10. The value of non-linear resistance should be recalculated.

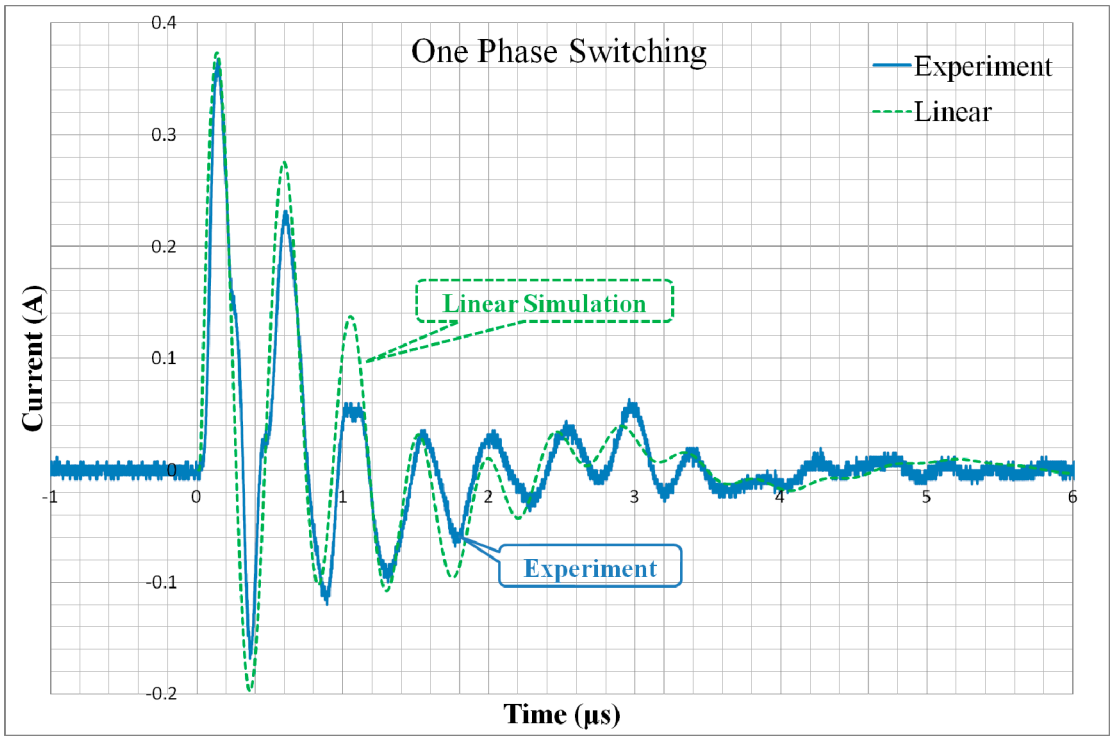


Fig. 3.15 Simulation Result in One Phase Switching

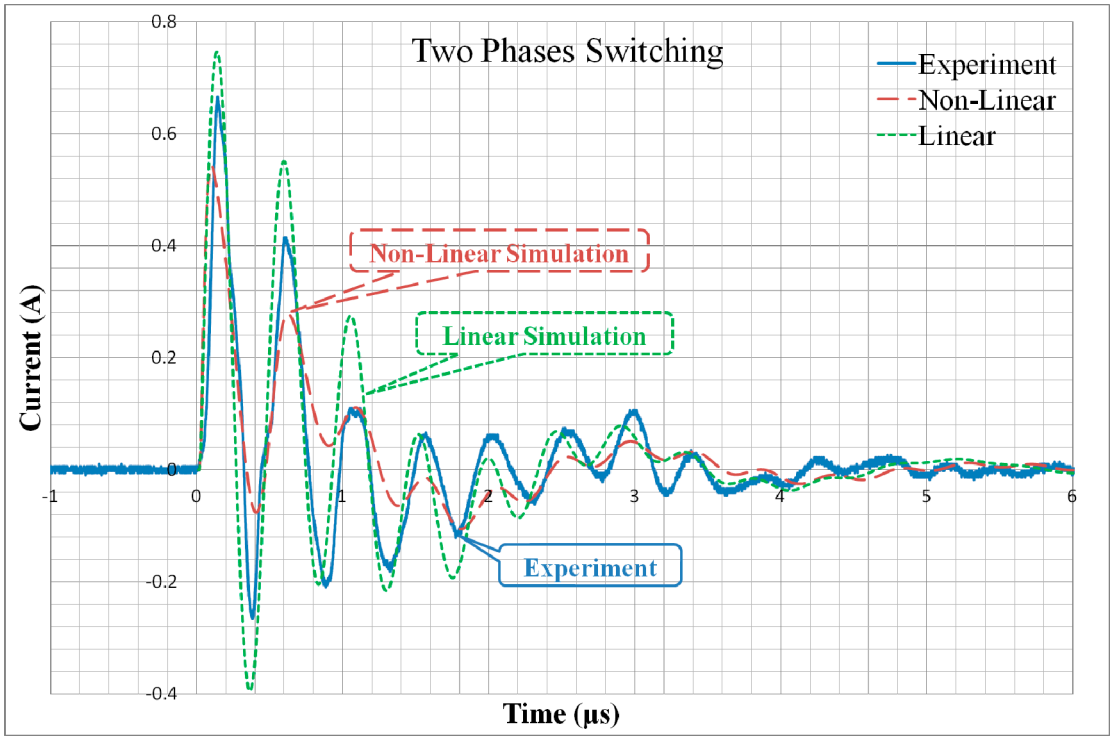


Fig. 3.16 Simulation Result in Two Phase Switching

3.3.2 Reconfirmation of Non-Linear Equivalent Circuit

The attenuation factor is ζ is speculated by the waveform of leakage current. It will lead to errors during the speculation. The non-linear resistance and linear resistance will change by changing the attenuation factor ζ. In the end, the new PSIM model is shown as Fig. 3.17. In this model, the appropriate value of non-linear resistance is confirmed. And the simulation result can meet well with experiment result, both in one phase switching and in two phases switching. These results are shown as Fig. 3.18 and Fig 3.29. The red line shows the simulation result, and the blue line shows the experiment waveform. But it is very difficult to calculate the suitable parameters. It will cost a lot of time to try the different parameter combinations. More efficiency method is necessary.

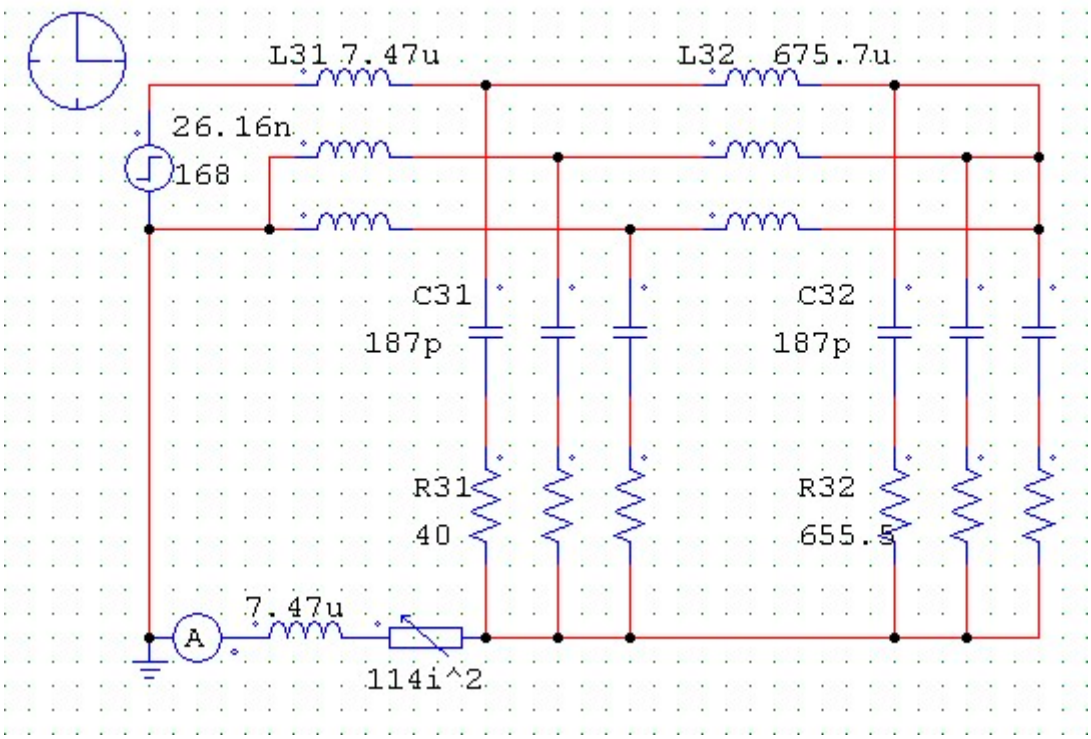


Fig. 3.17 Reconfirmed Equivalent Circuit with Non-Linear Resistance

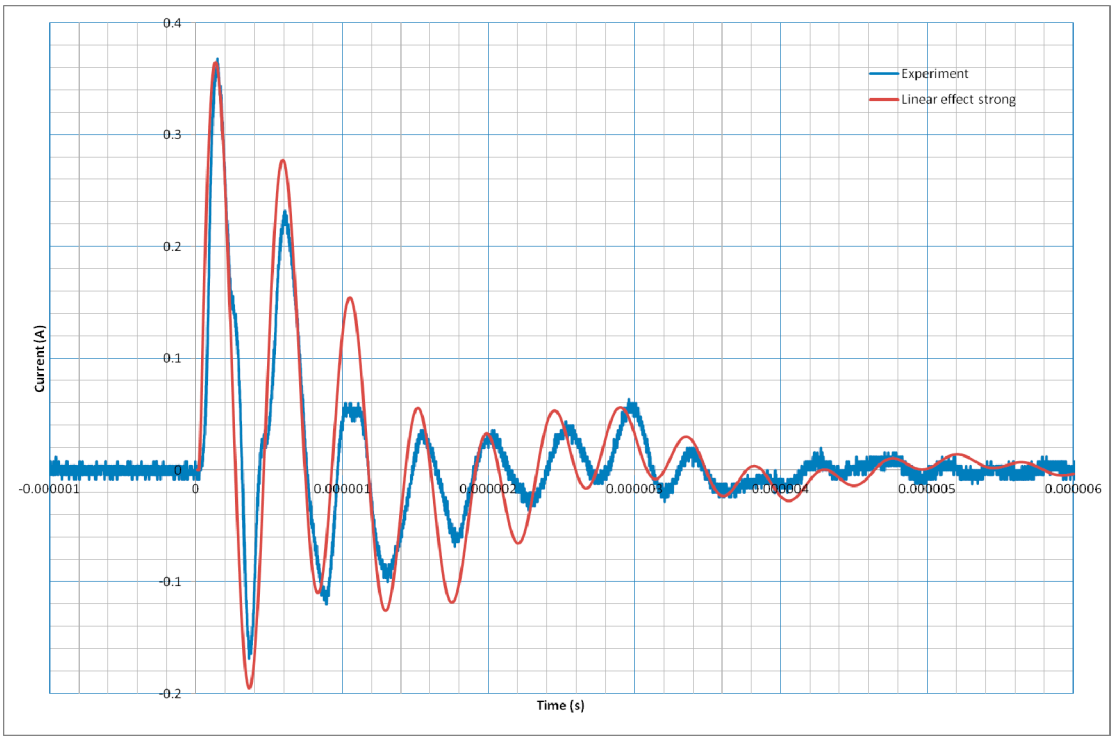


Fig. 3.18 Simulation Result in One Phase Switching Mode

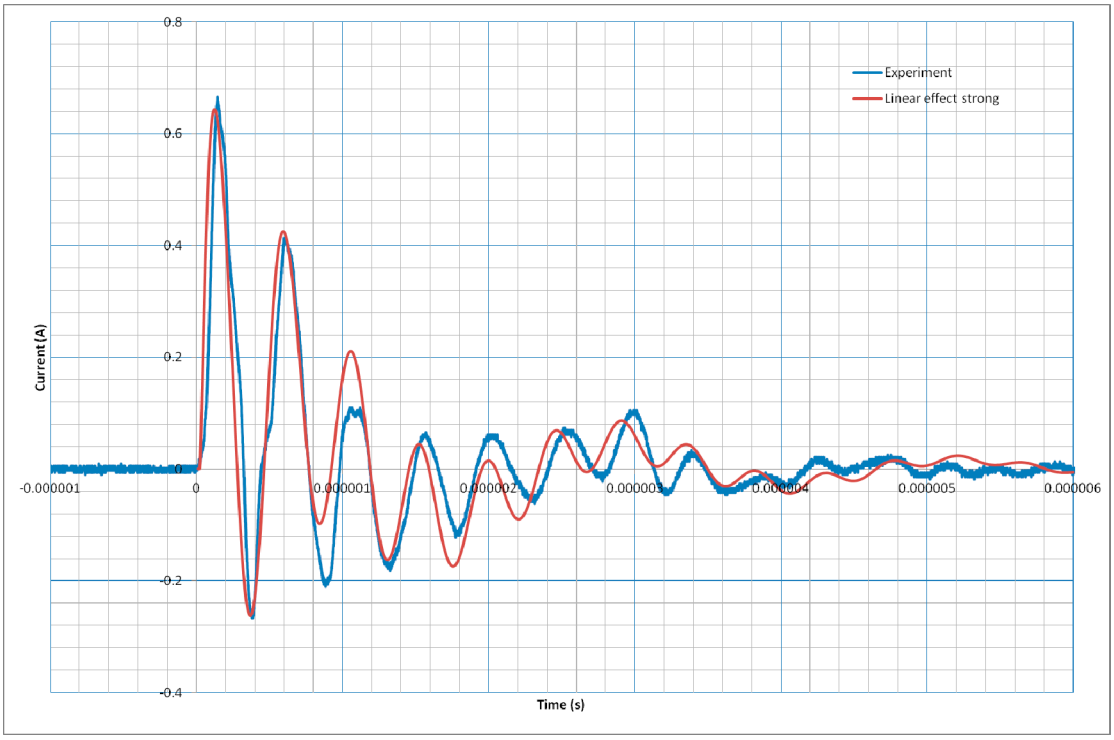


Fig. 3.19 Simulation Result in Two Phases Switching Mode

3.4 Necessity of Non-Linear Resistance about CM Equivalent Circuit

According to the results in Chapter 3.3, it can be confirmed that the introduction of non-linear resistance about CM equivalent circuit is necessary. Although the simulation results of equivalent circuit model with or without non-linear resistance both can meet well with the experiment data, when only one phase of PWM inverter is switching. But in order to simultaneously make sure the simulation result can meet well with experiment waveform when two phases of PWM inverter are switching at the same time, the introduction of non-linear resistance into the CM equivalent circuit model is necessary. The model without non-linear resistance cannot meet the both two situations. And the leakage current should be two times of the current when only one phase is switching. But the leakage current in two phases switching mode 668 mA is smaller than two times of the one in one phase switching mode 740 mA, though the resonant frequencies are identical.

3.5 Summary

In this chapter, firstly, the possibility and rationality of non-linear resistance existing in the CM equivalent circuit model is confirmed.

Secondly, based on the waveform of leakage current, the parameter calculation method is discussed. Accord to the waveform and the structure of interference conduction route, the parameters of equivalent circuit could be calculated. Transform the equivalent circuit and then calculate the parameters. All the known parameters are based on the waveform of leakage current. Because some of values are speculated, it may produce some errors, e.g., the value of current I, i_0, and the attenuation factor ζ. These errors will be corrected in Chapter 4 by using the optimization software modeFRONTIER. More accurate equivalent circuit model can be discussed.

Thirdly, considering two aspects, only one phase switching and two phases switching at the same, the effectiveness of the non-linear resistance is confirmed. Accurate equivalent circuit model has been certified.

Finally, by analyzing the linear model and non-linear model, the effectiveness and necessity of non-linear equivalent circuit is confirmed. This is because the leakage current of linear equivalent circuit should be two times of the leakage current when only one phase is switching, though the resonant frequencies are identical.

Chapter 4 Identification of Non-Liner Common-Mode Equivalent Circuit

4.1 Speculation Errors in Calculating the Parameters of Equivalent Circuit and Computer-Aided Optimization Software

4.1.1 Identification Errors in Calculating the Parameters of Equivalent Circuit

In Chapter 3, an equivalent circuit for PWM inverter-fed motor drive systems with non-linear resistance is proposed, and the parameters of the equivalent circuit can be calculated according to the waveform of the leakage current in the ground path. Therefore, the CM noise of PWM inverter-fed motor drive systems can use the mathematical models to represent. Thus the CM noise level of the system can be predicted, and the efficient and low-cost suppression circuit can be designed.

Fig. 4.1 shows the decreasing current of LCR series circuit. According to the calculation method in Chapter 3, some of the known numbers are subjectively predicted according to the waveform of the leakage current. It is complex process to calculate the parameters of the equivalent circuit. And these subjectively prediction may lead to some small errors. In the calculation process, the amplitude of current i_0 and the attenuation factor ζ are subjectively predicted. Because these parameters

cannot be directly measured by the measuring equipments, the small errors cannot be prevented. It is difficult to guarantee the high accuracy. Therefore, a kind of objective and accurate method is necessary to improve the accuracy and reduce the calculation error. In the next section, a parameter identification method is proposed by using an optimization software. Therefore, in order to simplify the calculation steps and improve the accuracy of the equivalent circuit parameters, it must rely on the computer. In this paper, a kind of computer-aided optimization software modeFRONTIER is introduced to decide the element of CM equivalent circuit objectively and improve the accuracy.

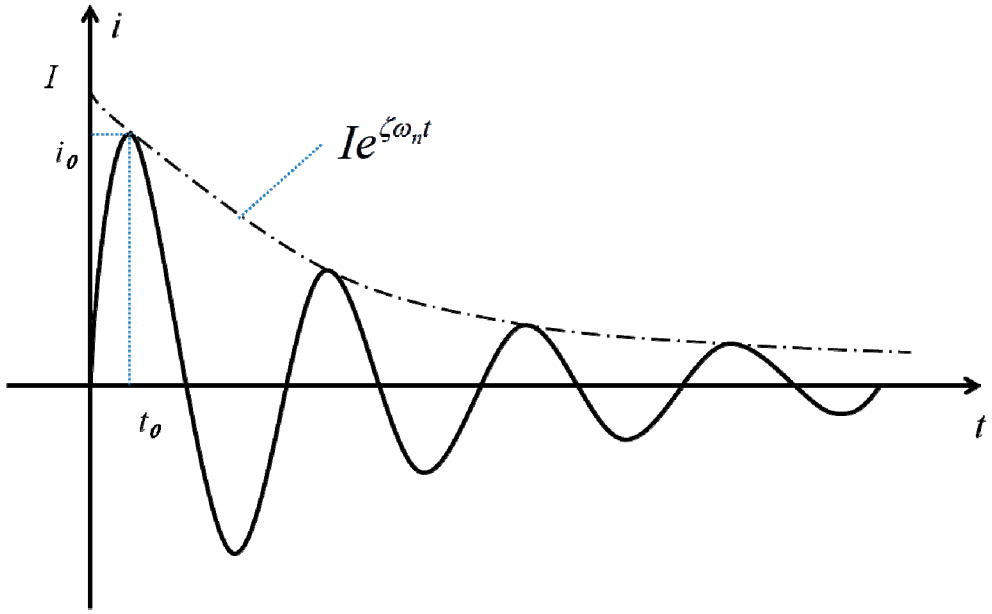


Fig. 4.1 Decreasing Current of LCR Series Circuit

4.1.2 Computer-Aided Optimization Software

In present years, following the rapid development of computer science, computer-aided software has been widely applied in various fields of scientific research. Reasonable and effective computer-aided software, can greatly improve the efficiency and accuracy of the results.

modeFRONTIER is a multi-objective optimization and design environment, written to allow easy coupling to almost any computer aided engineering (CAE) and computer aided design (CAD) tools, finite element structural analysis and

computational fluid dynamics software. The concept behind modeFRONTIER is shown as Fig. 4.2.

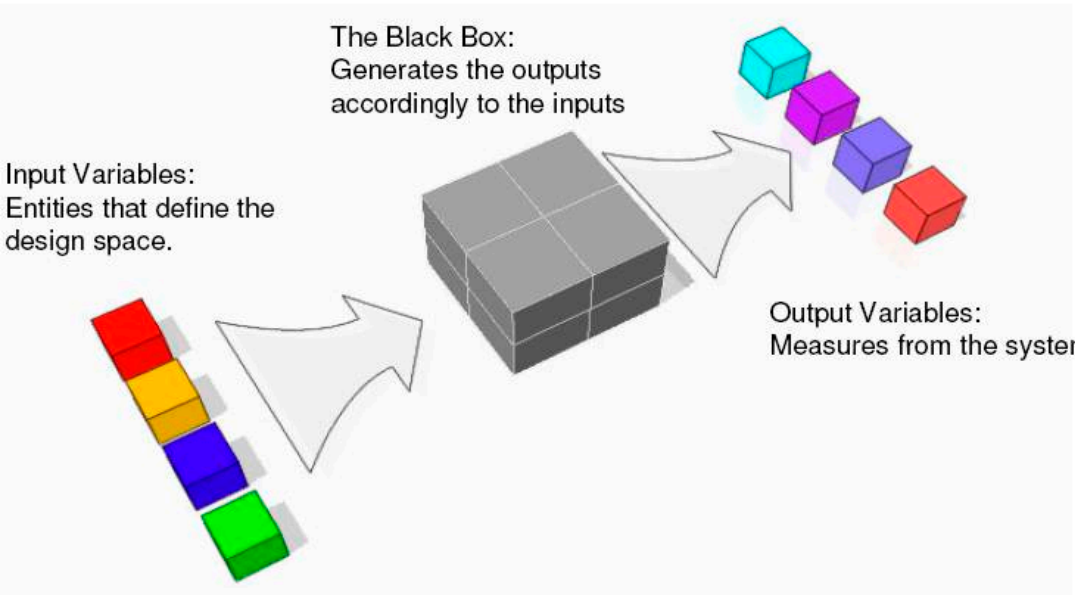


Fig. 4.2 Concept behind modeFRONTIER

Variables in Fig. 4.2 are the free parameters, i.e. the quantities that the designer can vary according to the number of variables in the equivalent circuit. Variables can be continuous variables and discrete variables. The black box can be a set of solvers that models and solves in a numerical manner the design problem (e.g. CAD/CAE tools), and a set of experiments that produces some data.

The working flow of modeFRONTIER is shown as Fig. 4.3. Input variables are the free parameters, e.g., R, C, L in the equivalent circuit. Software modeFRONTIER can be coupled with a lot of CAE tools, e.g., MATLAB, Excel, ProE. The different combination of input variables are taken in the CAE tools to get a group of output variables. These output variables will be compared with the desire value. This process will loop, until the simulation can meet with the desirable value.

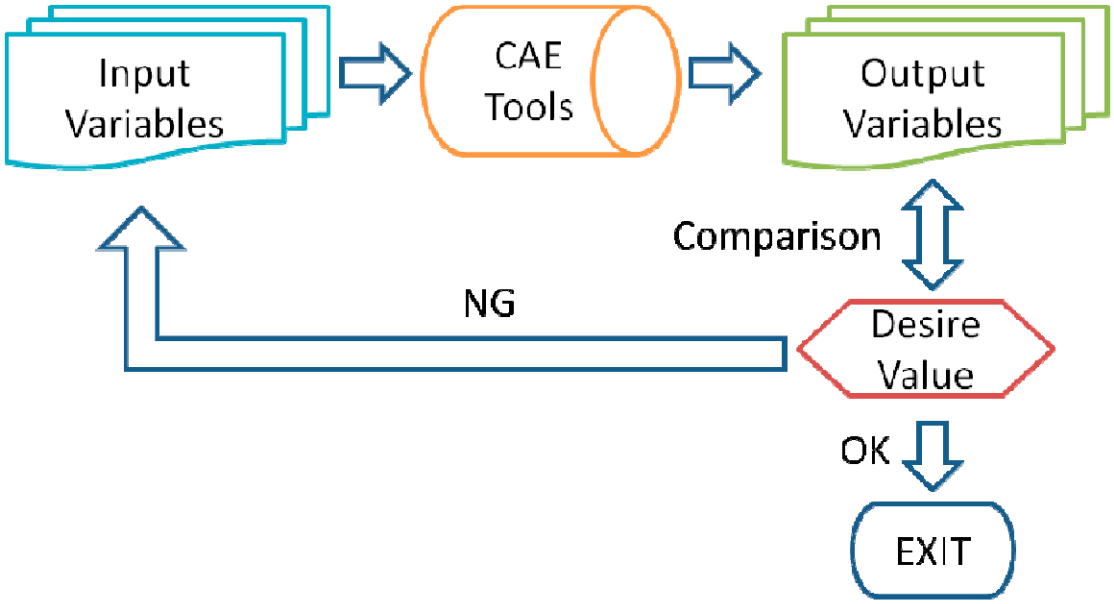


Fig. 4.3 Working Flow of modeFRONTIER

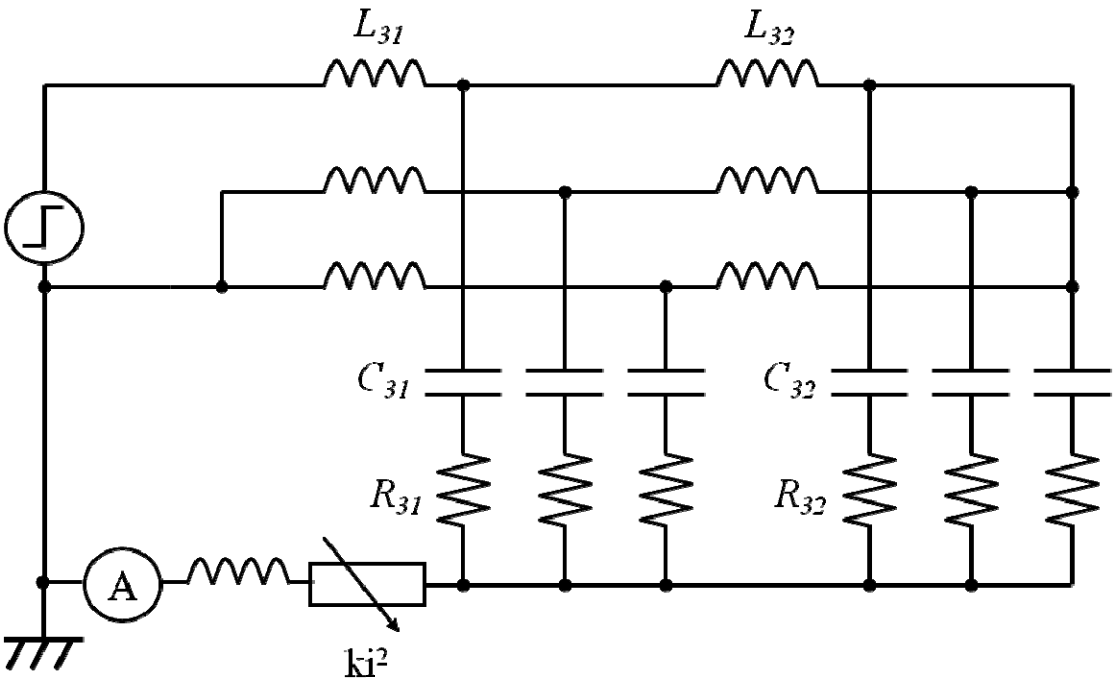


Fig. 4.4 CM Noise Equivalent Circuit of PWM Inverter-Fed Drive System

According to the conclusion in Chapter 2.3, the CM noise equivalent circuit of PWM inverter-fed drive system is shown as Fig. 4.4. And the equivalent circuit can be turned into the type shown as Fig. 4.5, further be turned into Fig. 4.6. The equivalent

circuit of Fig.4.5 is simple and easy understanding. And the equivalent circuit of Fig. 4.6 is beneficial to simply the MATLAB mathematical model which is necessary in the following simulation in modeFRONTIER.

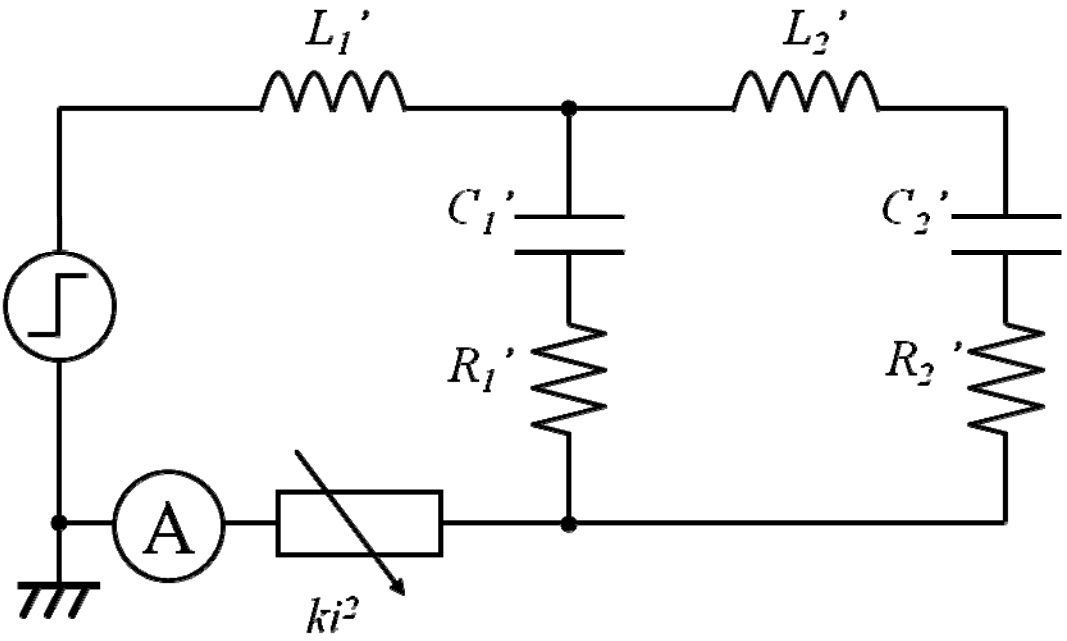


Fig. 4.5 Deformation of Equivalent Circuit

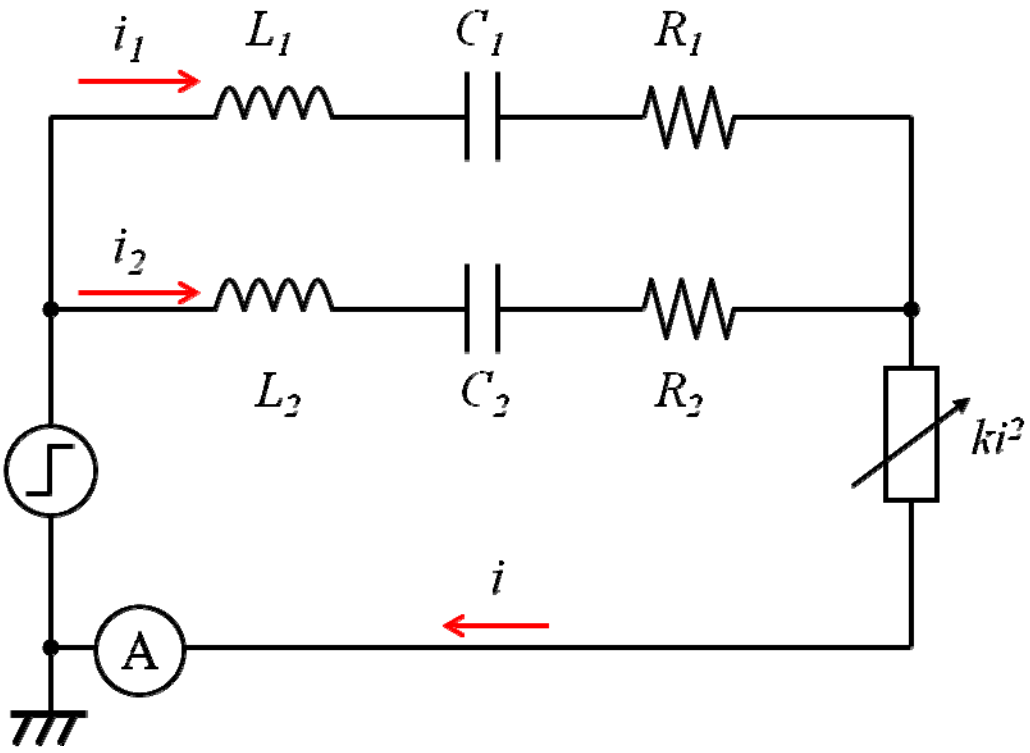


Fig. 4.6 Parallel Connection Equivalent Circuit

In this thesis, the input variables according to the equivalent circuit of Fig. 4.6 are L_1, L_2, C_1, C_2, R_1, R_2 and k. Because the equivalent circuit of motor is π style which is mentioned in Chapter 3.12, C_1 is almost equal to C_2. And the black box is made up of a MATLAB model and the other arithmetic block. The output variables are a lot of excel tables of the leakage current. By comparing the simulation tables with the experiment table of CM leakage current, the optimal parameters of the equivalent circuit can be simulated. The precision of the equivalent circuit can be dominated by setting the number of the output simulation tables. Assisted by high-performance computer, the equivalent circuit of sufficient precision can be obtained.

4.2 modeFRONTIER Simulation

The decay rate of leakage current is determined by the values of resistances in the equivalent circuit. Higher resistance leads to higher rate of decay. In order to confirm the effect of non-linear resistant, an equivalent circuit without non-linear element should be confirmed too. And, when only one phase of PWM inverter is switching the leakage current is different with the current when two phases of PWM inverter are switching at the same time. So the equivalent circuit should be double confirmed in these two situations.

4.2.1 Linear and Non-Linear MATLAB Models

According to the FFT transform result of the leakage current in Chapter 3.12, the resonance frequencies are 425 KHz and 2.13 MHz. The leakage current with the low resonance frequency 425 KHz almost does not pass through the current with the high resonance frequency 2.13 MHz. Similarly, the leakage current with the high resonance frequency 2.13 MHz almost does not pass through the current with the low resonance frequency 425 KHz. So the equivalent circuit shown as Fig. 4.6 can be considered as two LCR series circuits.

Fig. 4.7 shows a LCR series circuit with non-linear resistance. The loop current is i, the non-linear resistance is $k \times i^2$, a parameter about the current i, and k is unknown number.

$$v(t) = L\frac{di}{dt} + \frac{1}{C}\int i(t)dt + R \times i(t) + ki^2 \times i \tag{4.1}$$

Laplace transform is,

$$V(s) = LsI(s) + \frac{1}{C} \times \frac{1}{s} I(s) + R \times I(s) + kI(s)^3 \tag{4.2}$$

Therefore,

$$I(s) = (V(s) - kI(s)^3 - \frac{1}{C} \times \frac{1}{s} I(s) - R \times I(s)) \times \frac{1}{L} \times \frac{1}{s} \tag{4.3}$$

According to the formula (4.3), the MATLAB model of LCR series circuit with non-linear resistance can be shown as Fig. 4.8.

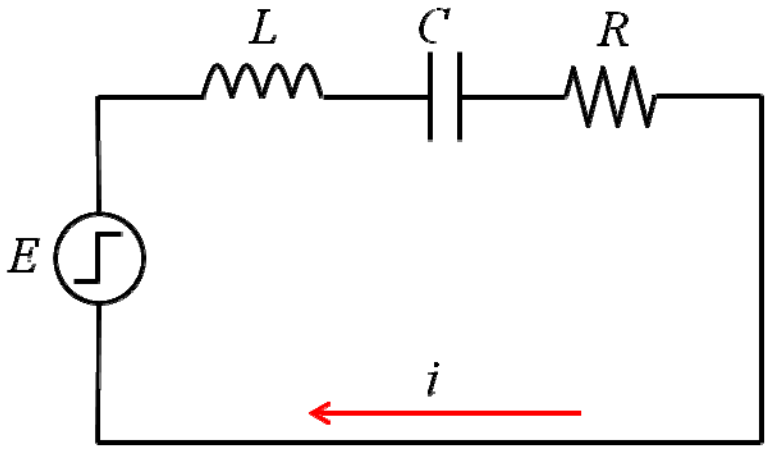


Fig. 4.7 LCR Series Circuit

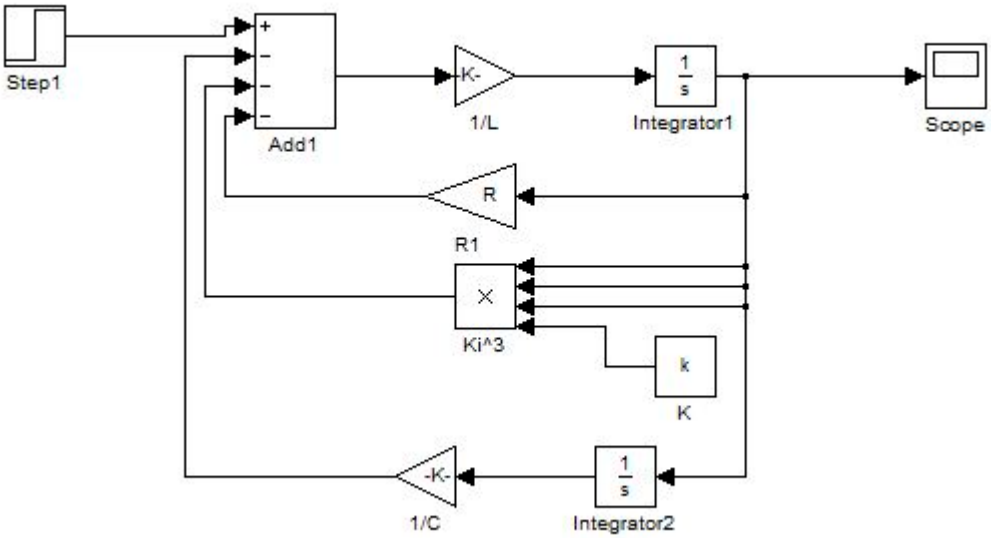


Fig. 4.8 MATLAB Model of LCR Series Circuit with Non-Linear Resistance

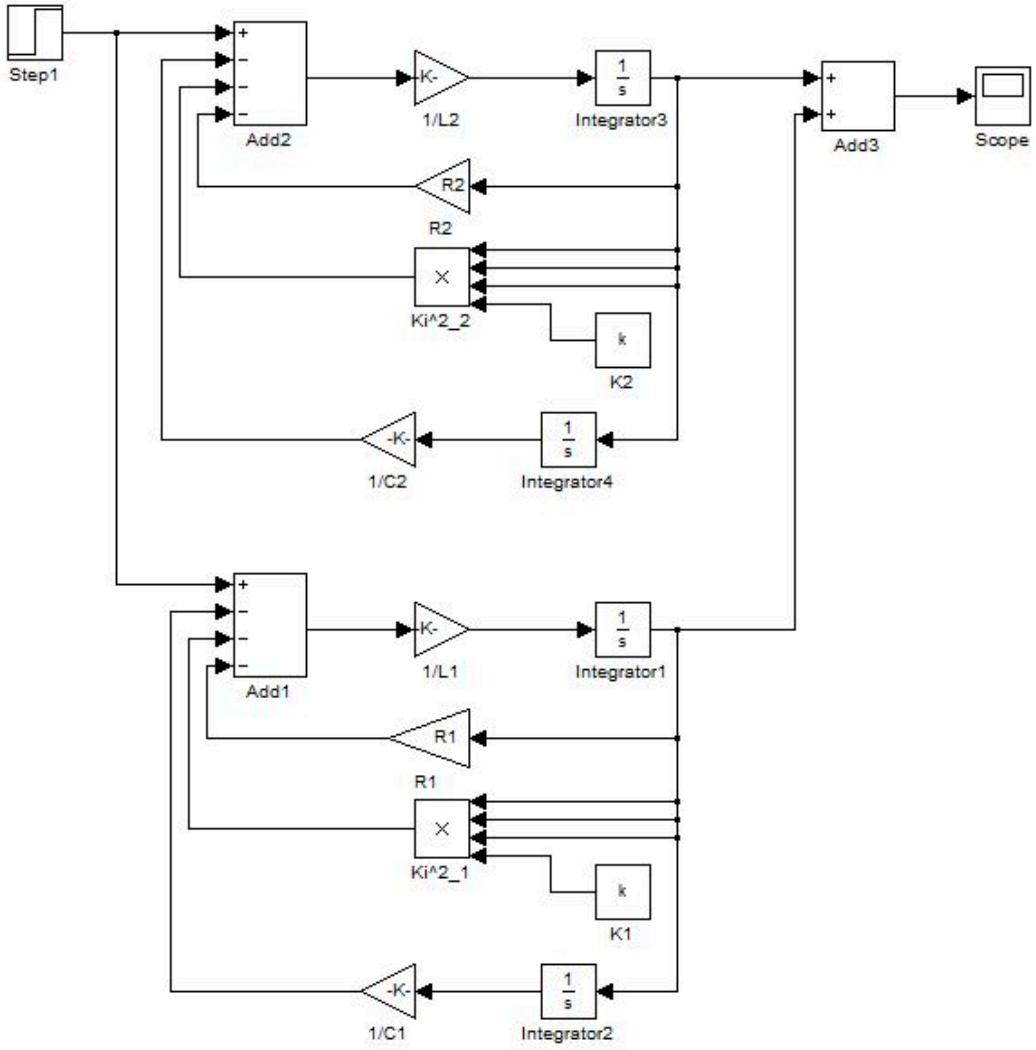


Fig. 4.9 MATLAB Model of Equivalent Circuit for PWM Inverter-Fed Drive System with Non-Linear Resistance

Therefore, the MATLAB model of equivalent circuit for PWM inverter-fed drive system with non-linear resistance can be shown as Fig. 4.9.

Based on the formula (4.3), the relationship of LCR series circuit without non-linear is

$$I(s) = (V(s) - \frac{1}{C} \times \frac{1}{s} I(s) - R \times I(s)) \times \frac{1}{L} \times \frac{1}{s} \tag{4.4}$$

Therefore, the MATLAB model of equivalent circuit for PWM inverter-fed drive system without non-linear resistance can be shown as Fig. 4.10.

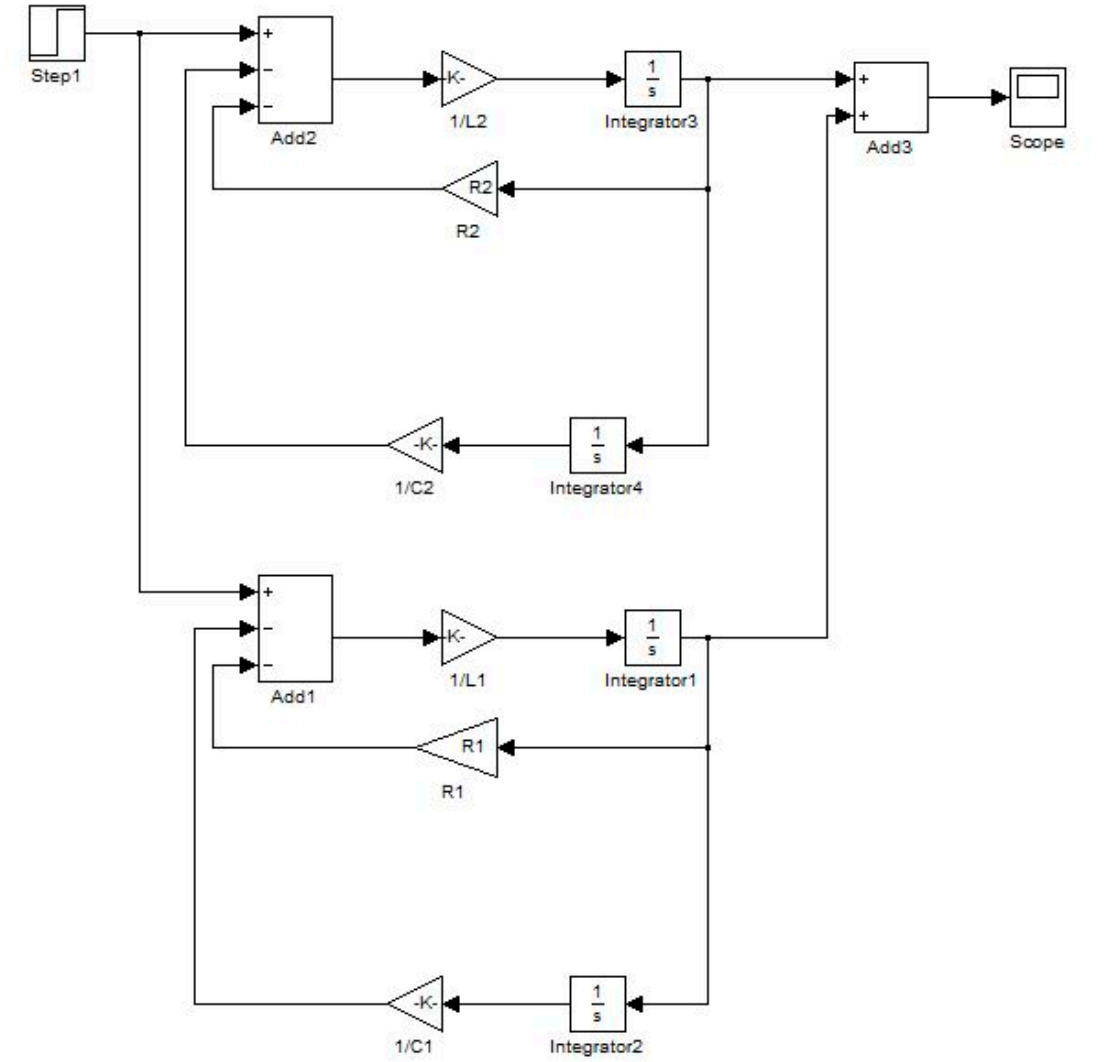


Fig. 4.10 MATLAB Model of Equivalent Circuit for PWM Inverter-Fed Drive System without Non-Linear Resistance

4.2.2 modeFRONTIER Model

In order to simulate the model in modeFRONTIER software, the MATLAB model should be transformed, shown as Fig. 4.11. The parameters of equivalent circuit should change into constant parameters, shown in the red blocks, and the output leakage current should change into a workspace, shown in the blue block.

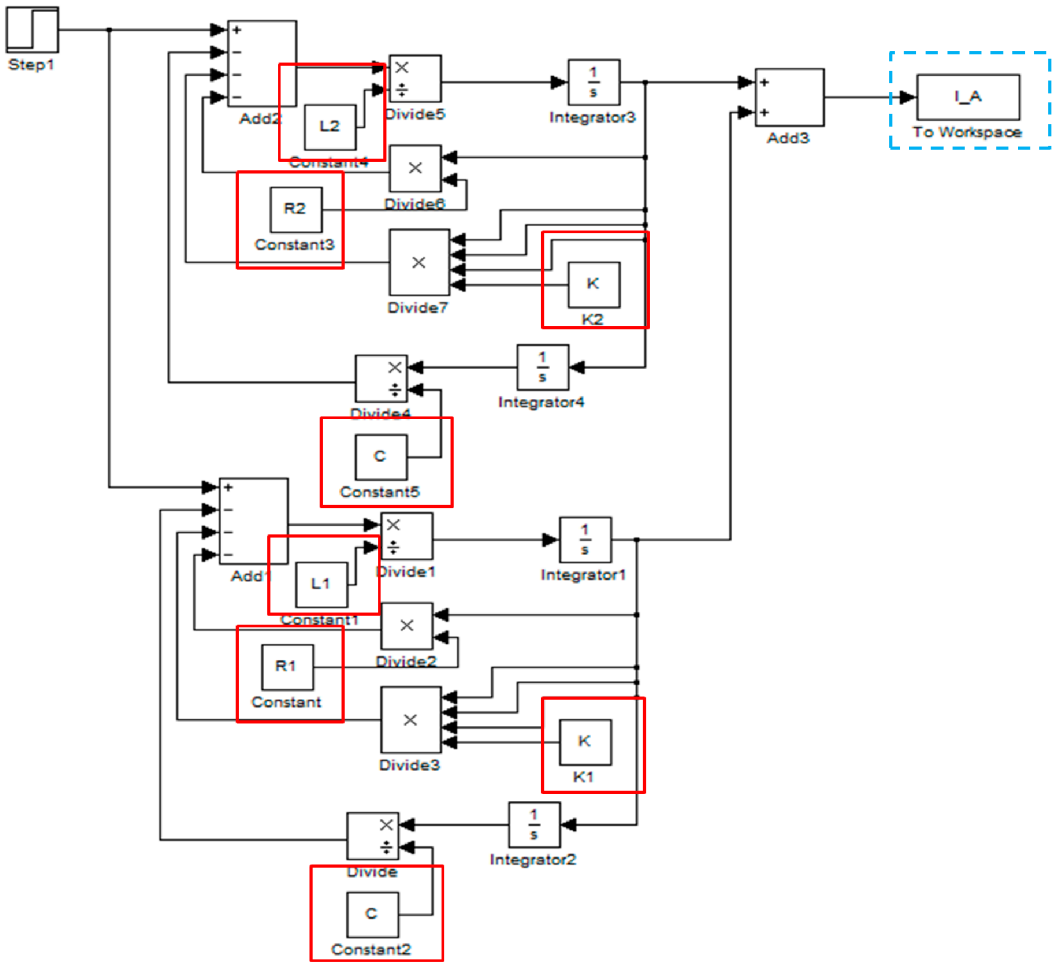


Fig. 4.11 MATLAB Model of Equivalent Circuit for PWM Inverter-Fed Drive System in modeFRONTIER

There are two modeFRONTIER models. The two simulation results will compare to the waveform of leakage current which is got from experiment. And when only one phase of PWM inverter is switching the waveform is different with the waveform when two phases are switching at the same time. Fig. 4.12 shows one modeFRONTIER model. In this situation, the simulation result just compare to the waveform in one phase switching or in two phases switching. The modules in the green line are the input variables. According to the resonance frequencies, the values of $L \times C$ can be determined, and the modules in the red line show this function. The modules in the purple line define the algorithm of simulation. The MATLAB model will import into the module in the yellow line. The output variables of leakage current

bring into the module in the green point line with the format of excel tables. The waveform data of experiment is in the modules in the yellow point line. The differences with the format of standard deviation between the simulation results and the experiment waveform will import into the module in the blue line. The modules in the blue point line are the function to calculate the smallest standard deviation. The module in the red point line will limit the range of standard deviation which can be accepted.

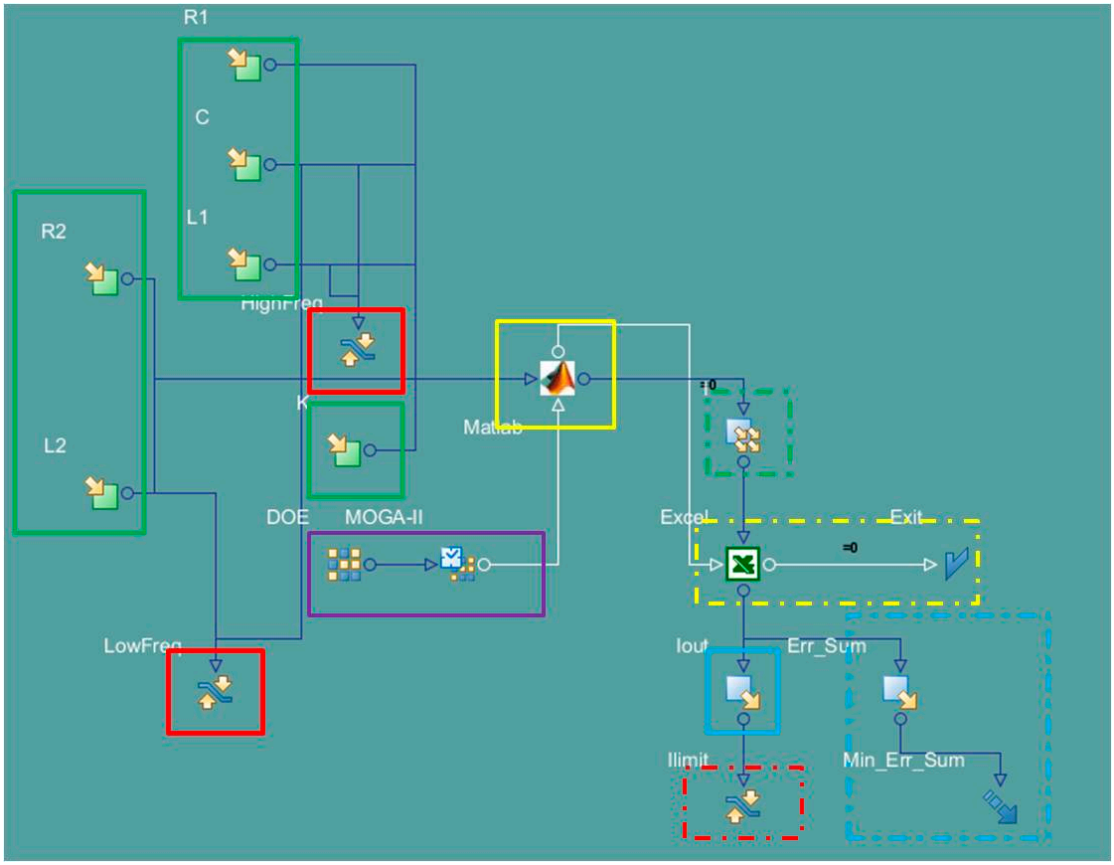


Fig. 4.12 modeFRONTIER Model in One Phase Switching

In addition, the range of the parameters in the equivalent circuit also can be configured. And all the simulations are completed in the same parameter ranges. The simulation result is shown as Fig. 4.13. The plots in the green line are the simulation results of L_1, L_2, C_1, C_2, R_1, R_2 and k. By ranking the errors between the simulation results and experiment data, the most accurate circuit parameters can be

received. The data shown in the red blocks is the optimization result. The table in the purple line shows the ranking table. The graph in the green line shows the distribution of the input variables. The vertical axis shows the standard deviation. Therefore the data at the bottom of the graph is the best value.

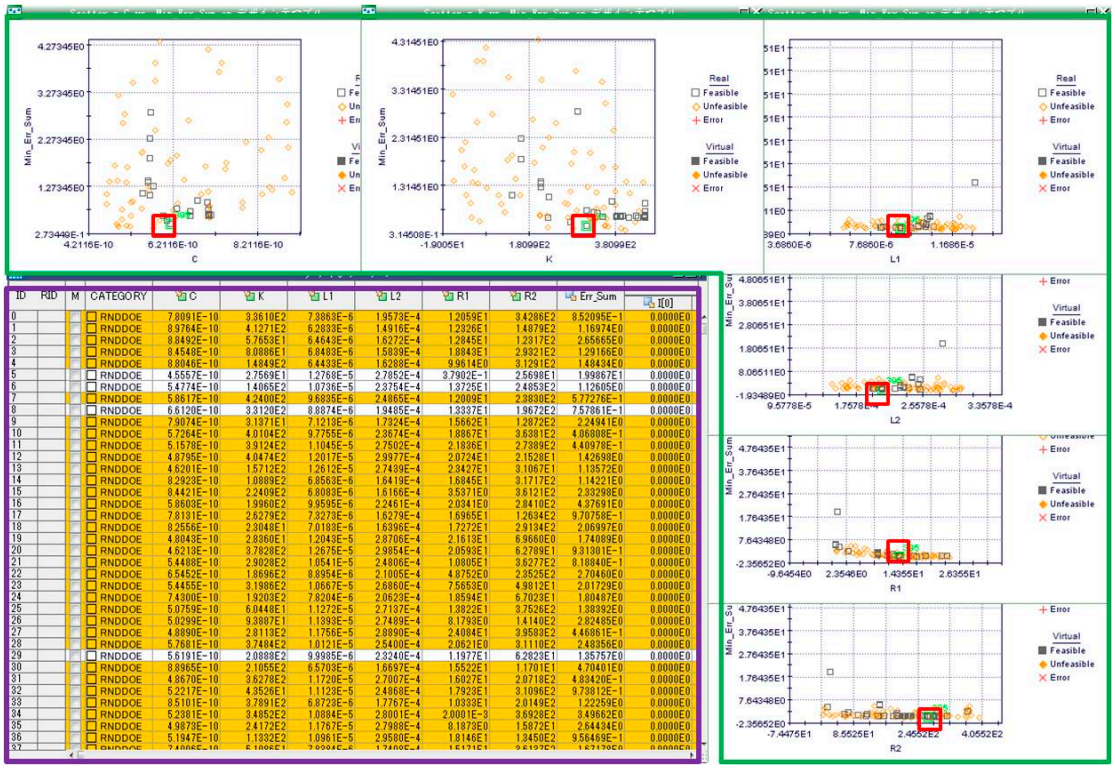


Fig. 4.13 modeFRONTIER Simulation Result

4.2.3 modeFRONTIER Simulation Result

Fig. 4.14 shows the non-linear equivalent circuit in PSIM software with the parameters got from the simulation of modeFRONTIER, when only one phase of PWM inverter is switching. The parameters are different with the calculation results in Chapter 3. The green line in Fig. 4.15 shows the simulation result in PSIM and the blue line shows the waveform of leakage current which is measured through the experiment. In this situation the simulation result can meet well with the experiment waveform. Use the same parameters to confirm the simulation result when two phases of PWM inverter are switching at the same time. The result is shown as Fig. 4.16. The simulation result cannot meet the experiment waveform well in two phases switching. The leakage current decays too fast.

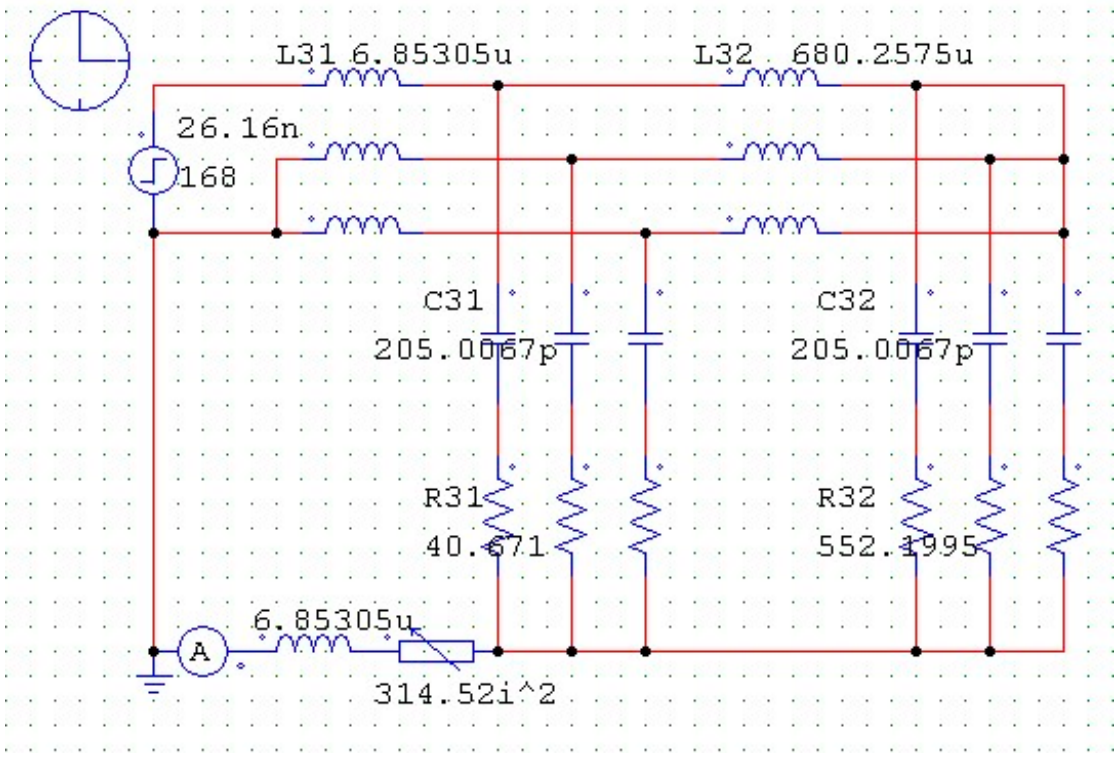


Fig. 4.14 Non-Linear PSIM Model in One Phase Switching with modeFRONTIER Optimization Parameters

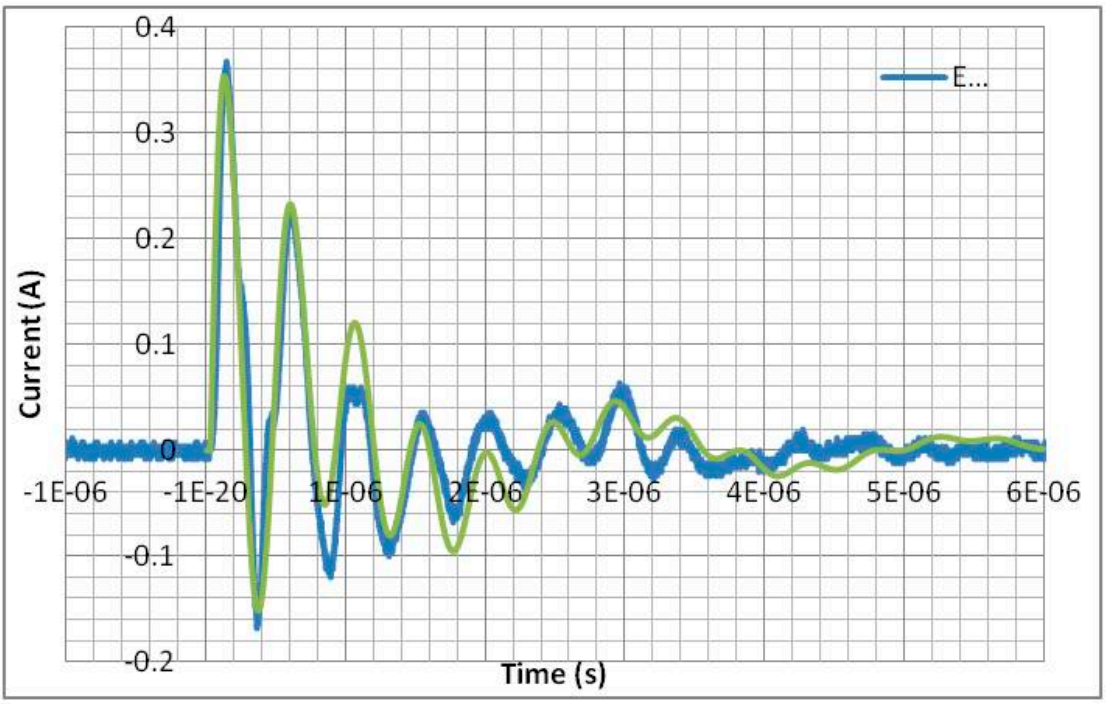


Fig. 4.15 Non-Linear Simulation Result in One Phase Switching with modeFRONTIER Optimization Parameter

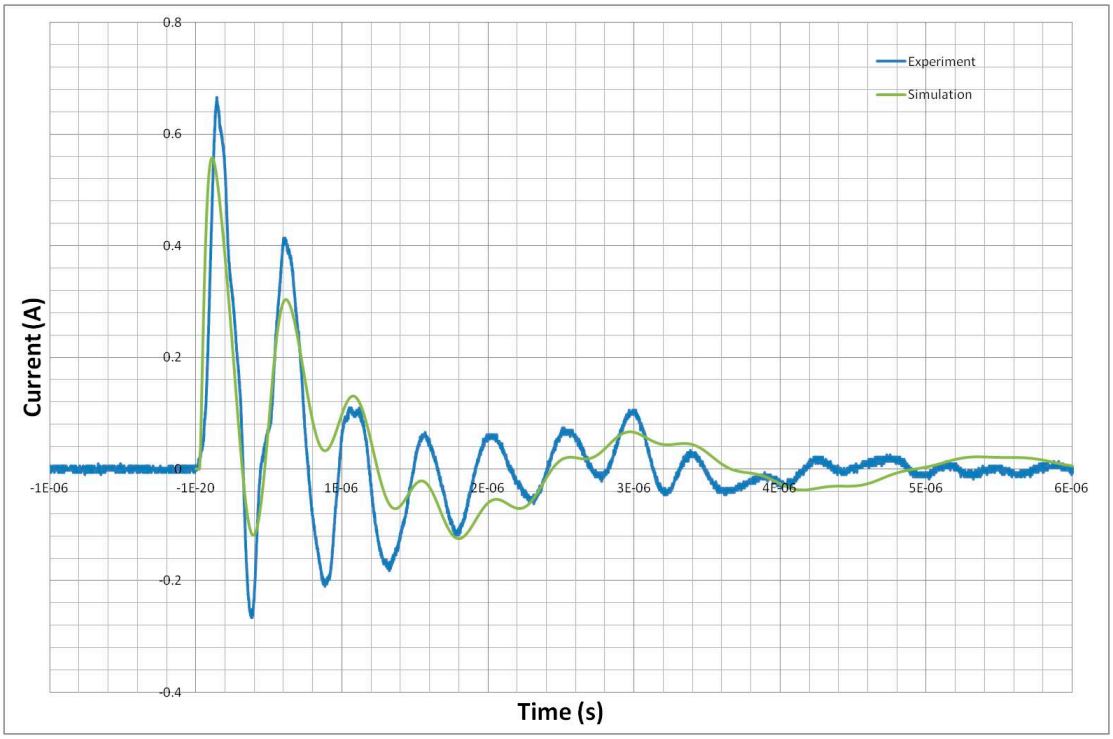


Fig. 4.16 Non-Linear Simulation Result in Two Phases Switching with modeFRONTIER Optimization One Phase Parameters

Fig. 4.17 shows the non-linear equivalent circuit in PSIM software with the parameters got from the simulation of modeFRONTIER, when two phases of PWM inverter are switching at the same. The parameters are also different with the calculation results in Chapter 3. The green line in Fig. 4.18 shows the simulation result in PSIM and the blue line shows the waveform of leakage current which is measured through the experiment. In this situation the simulation result can meet well with the experiment waveform. Use the same parameters to confirm the simulation result when only one phase of PWM inverter is switching. The result is shown as Fig. 4.19. The simulation result cannot meet the experiment waveform well in one phase switching. The leakage current decays too slowly. And the peak value of leakage current is also smaller than the experiment waveform.

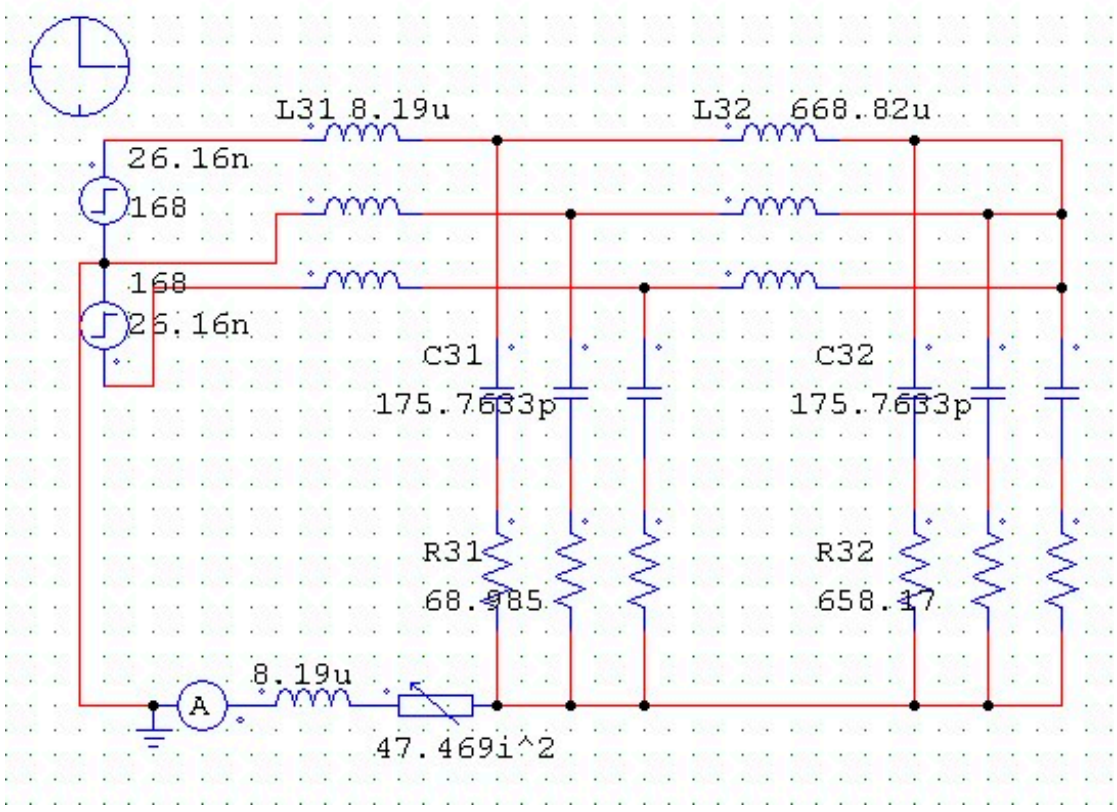


Fig. 4.17 Non-Linear PSIM Model in Two Phases Switching with modeFRONTIER Optimization Parameters

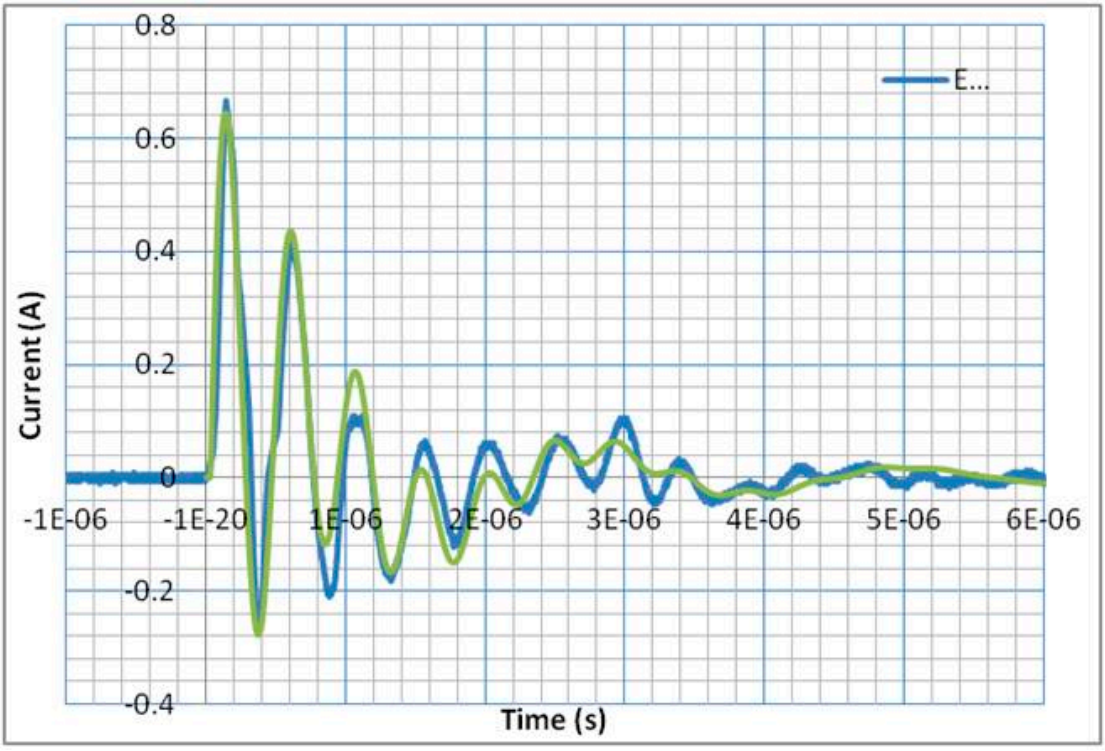


Fig. 4.18 Non-Linear Simulation Result in Two Phases Switching with modeFRONTIER Optimization Parameters

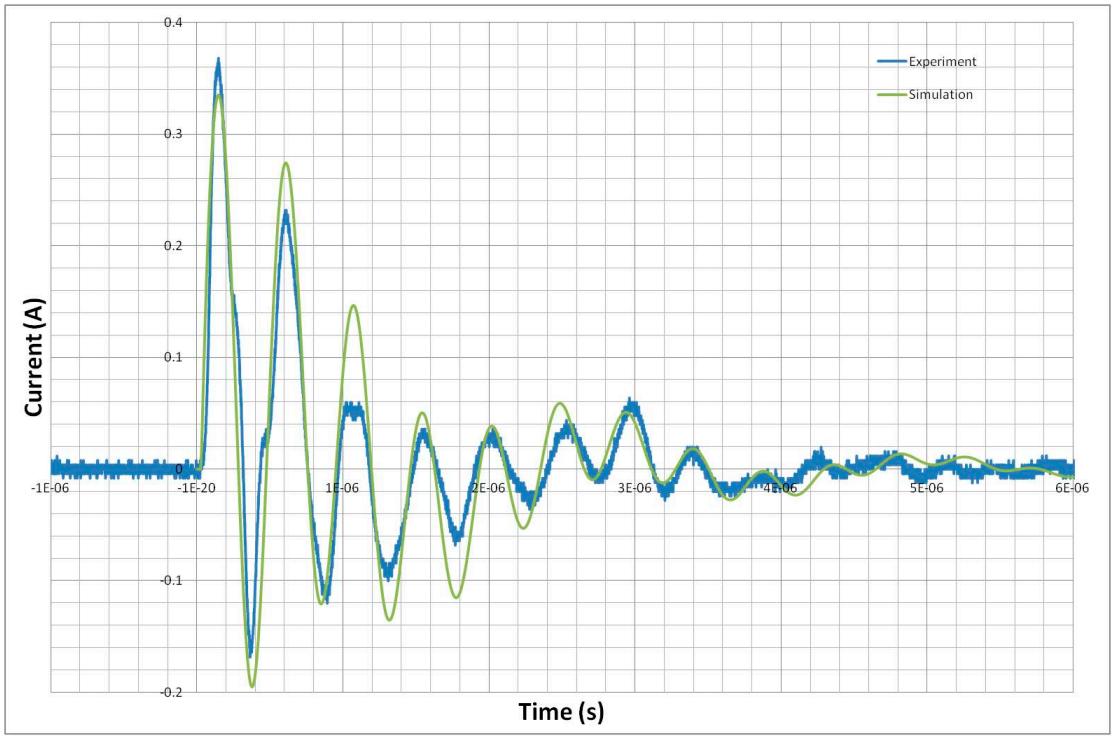


Fig. 4.19 Non-Linear Simulation Result in one Phase Switching with modeFRONTIER Optimization Two Phases Parameters

Fig. 4.20 shows the linear equivalent circuit in PSIM software with the parameters got from the simulation of modeFRONTIER, when only one phase of PWM inverter is switching. The parameters are different with the linear calculation results in Chapter 3. The green line in Fig. 4.21 shows the simulation result in PSIM and the blue line shows the waveform of leakage current which is measured through the experiment. In this situation the simulation result can meet well with the experiment waveform. Use the same parameters to confirm the simulation result when two phases of PWM inverter are switching at the same time. The result is shown as Fig. 4.22. The simulation result cannot meet the experiment waveform well in two phases switching. The leakage current decays too fast.

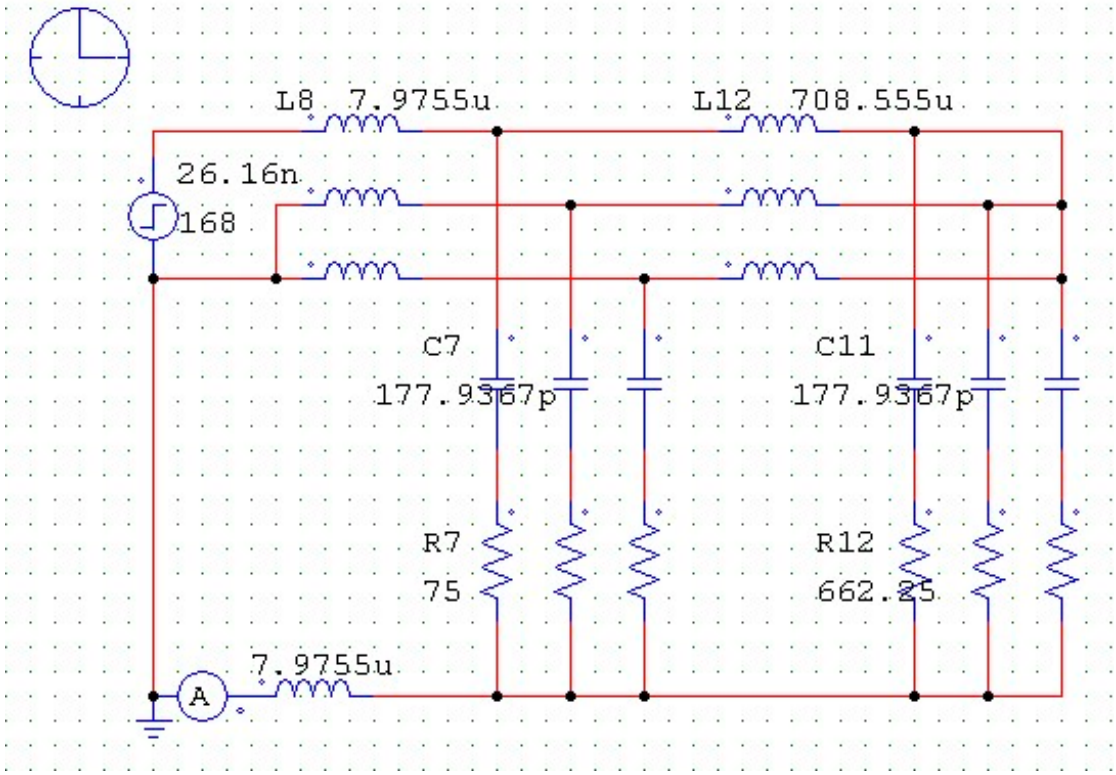


Fig. 4.20 Linear PSIM Model in One Phase Switching with modeFRONTIER Optimization Parameters

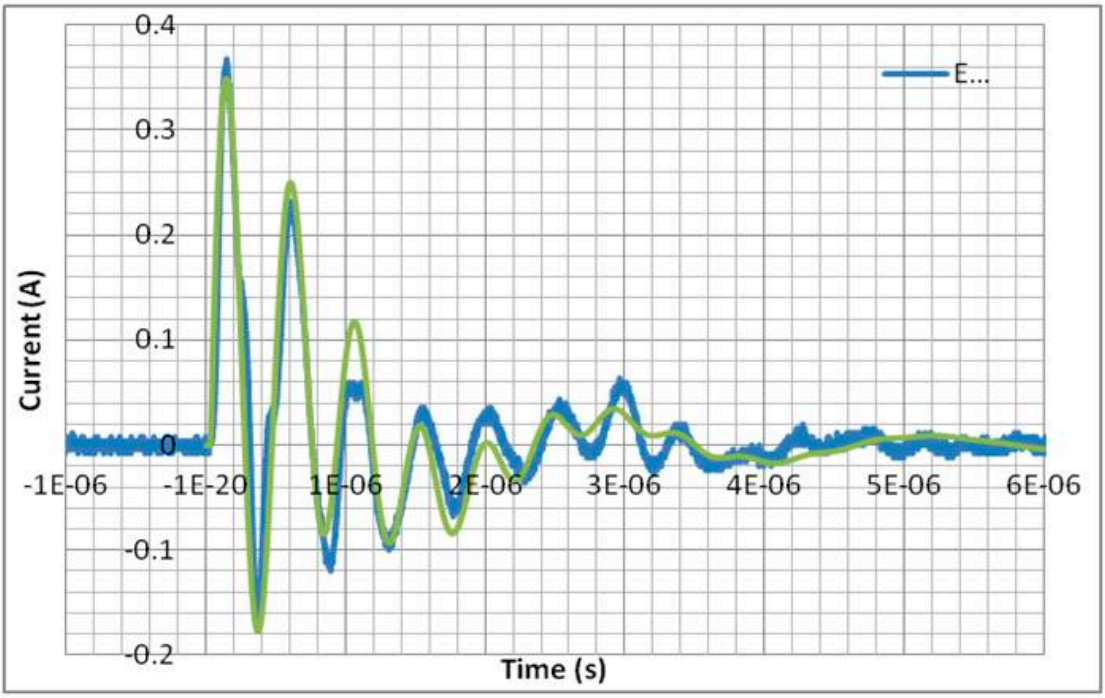


Fig. 4.21 Linear Simulation Result in One Phase Switching with modeFRONTIER Optimization Parameters

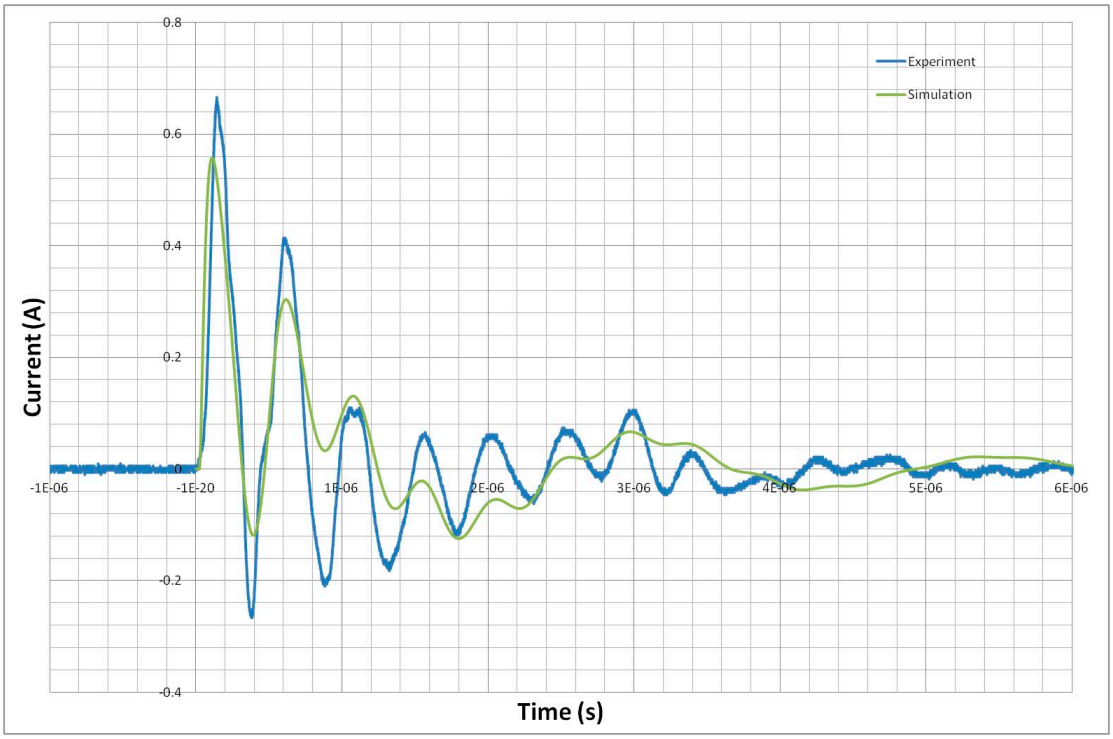


Fig. 4.22 Linear Simulation Result in Two Phases Switching with modeFRONTIER Optimization One Phase Parameters

Fig. 4.23 shows the linear equivalent circuit in PSIM software with the parameters got from the simulation of modeFRONTIER, when two phases of PWM inverter are switching at the same. The parameters are different with the linear calculation results in Chapter 3. The green line in Fig. 4.24 shows the simulation result in PSIM and the blue line shows the waveform of leakage current which is measured through the experiment. In this situation the simulation result can meet well with the experiment waveform. Use the same parameters to confirm the simulation result when only one phase of PWM inverter is switching. The result is shown as Fig. 4.25. The simulation result cannot meet the experiment waveform well in one phase switching. The leakage current decays too slowly.

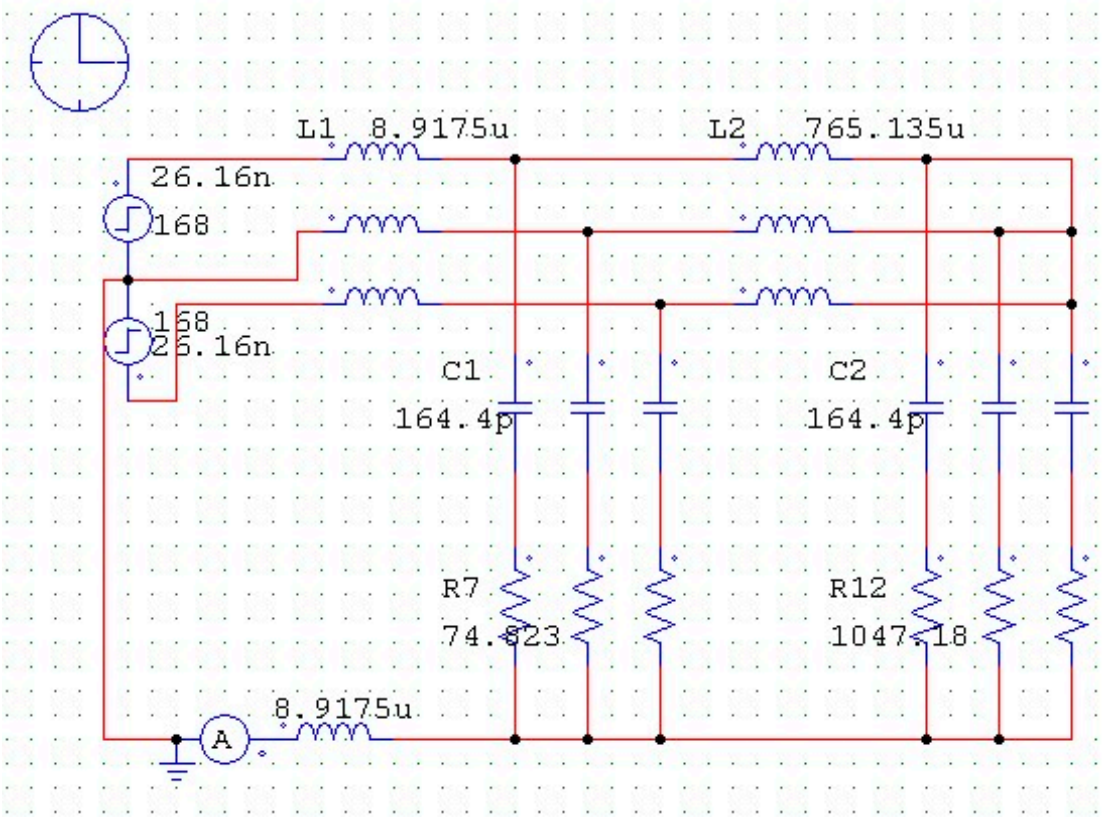


Fig. 4.23 Linear PSIM Model in Two Phases Switching with modeFRONTIER Optimization Parameter

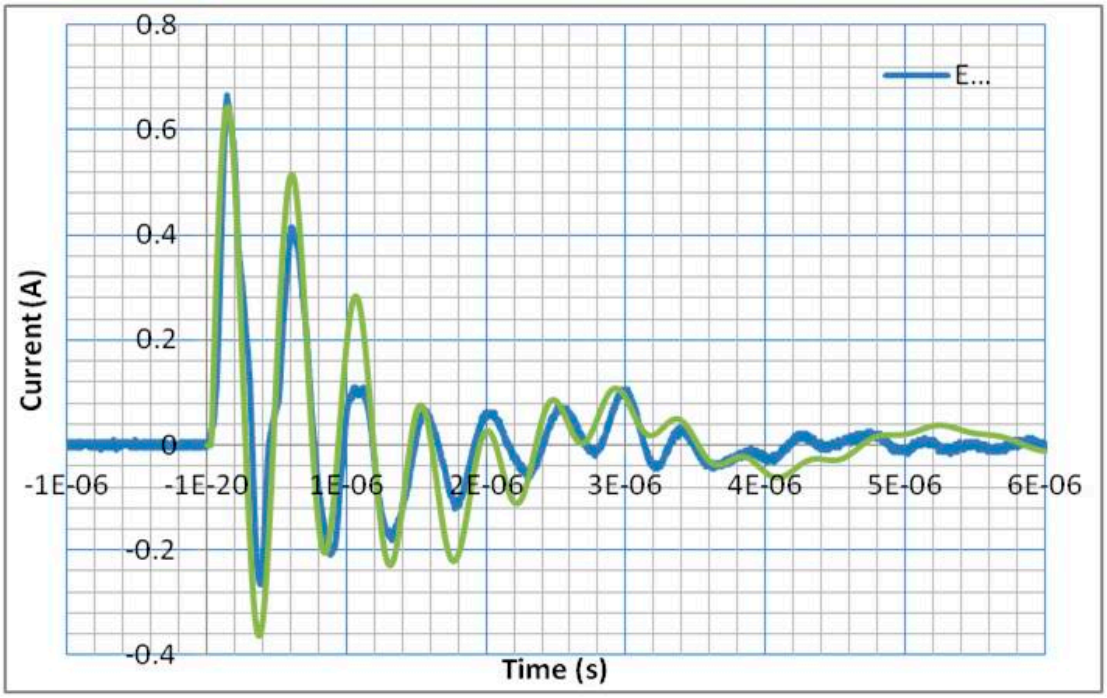


Fig. 4.24 Linear Simulation Result in Two Phases Switching with modeFRONTIER Optimization Parameter

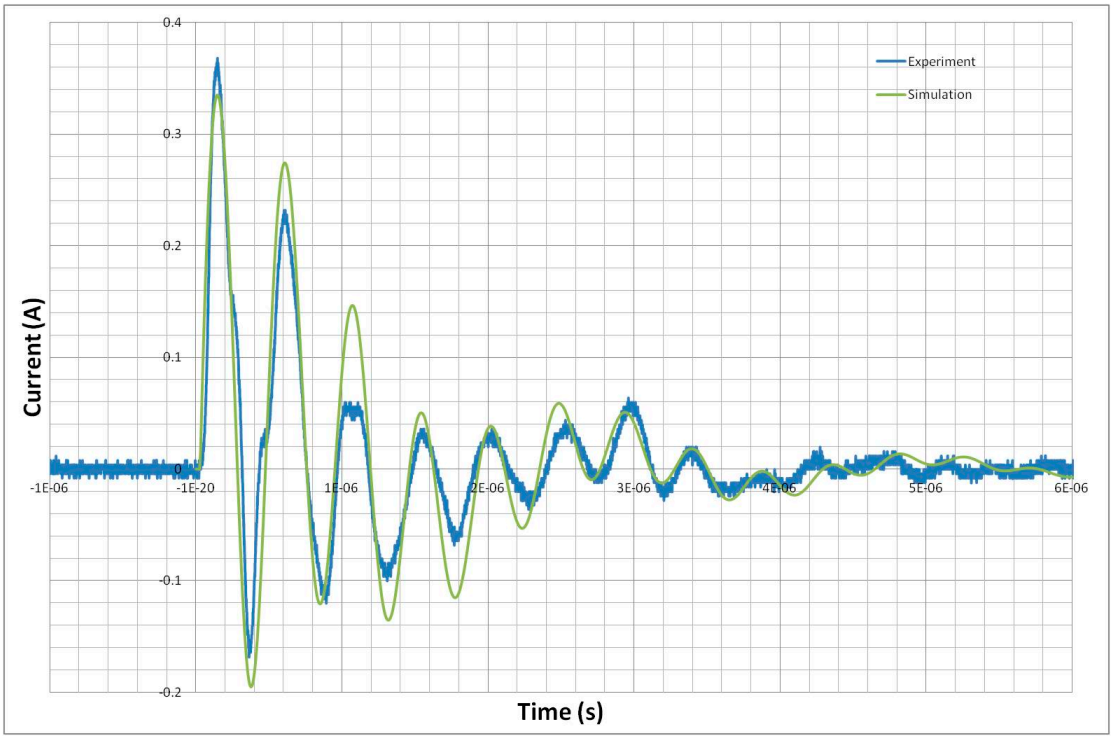


Fig. 4.25 Linear Simulation Result in one Phase Switching with modeFRONTIER Optimization Two Phases Parameters

When the parameters are simulated by only comparing the result with the waveform in one phase switching or in two phases switching, both linear equivalent circuit and non-linear equivalent can meet well with the experiment waveform of leakage current. But the same parameters cannot well meet the waveforms in the two situations of phase switching.

4.3 Identification of Linear Common-Mode Equivalent Circuit mode

4.3.1 New MATLAB Model for Simulation

The equivalent circuit shown in Fig. 4.5 is simple and easy understanding. But the equivalent circuit shown in Fig. 4.6 is beneficial to simply the MATLAB mathematical model. So it is applied in the modeFRONTIER simulation in Chapter 4.2. But the deformation of the equivalent circuit is depends on L_1 is much smaller than inductance L_2. On the other hand, it is supposed that C_1 is almost equal to C_2. But the parasitic capacitances still exist between the power semi-conductor devices and the heat-sinks. Even they are much smaller than the parasitic capacitance between the coil and the frame of AC motor. For improving the accuracy of the equivalent circuit, Fig. 4.5 will be applied in the following simulation.

Fig. 4.26 shows the modeFRONTIER model when only one phase of the PWM inverter is switching. The modules in the solid box are the input variables. Each input variable can be limited in a range to reduce the simulation time. According to resonance frequencies, the values of $L \times C$ can be limited in some acceptable range. By defining the suitable tolerance of resonance frequencies, the flexibility of simulation can be ensured. The modules in long broken box show this kind of function. The different combinations of the different input variables are introduced into the MATLAB model to simulate the leakage current separately. The MATLAB model for the modeFRONTIER simulation is shown as Fig. 4.27. One MATLAB simulation result of the leakage current will be written as a table. This table will be compared with the Excel table which is filled with the experiment leakage current waveform. Software modeFRONTIER will calculate the standard deviation between the simulation result and the experiment result. When the standard deviation becomes zero, software modeFRONTIER will stop the calculation. But it is almost impossible to get the 0 value of standard deviation, software modeFRONTIER will decide

another group of input variables to calculate the standard deviation again according to the result which has been calculated. The modules in the point broken box shows the function decide how to combine the next group of input variables. There are a lot of algorithm of optimization can be chosen, e.g., SIMPLEX algorithm, scheduler based on multi objective genetic algorithm. The modules in the short broken box show the function which makes sure the standard deviation as small as possible. The modules in point box limit the peak value of the leakage current will not far away from the experiment result.

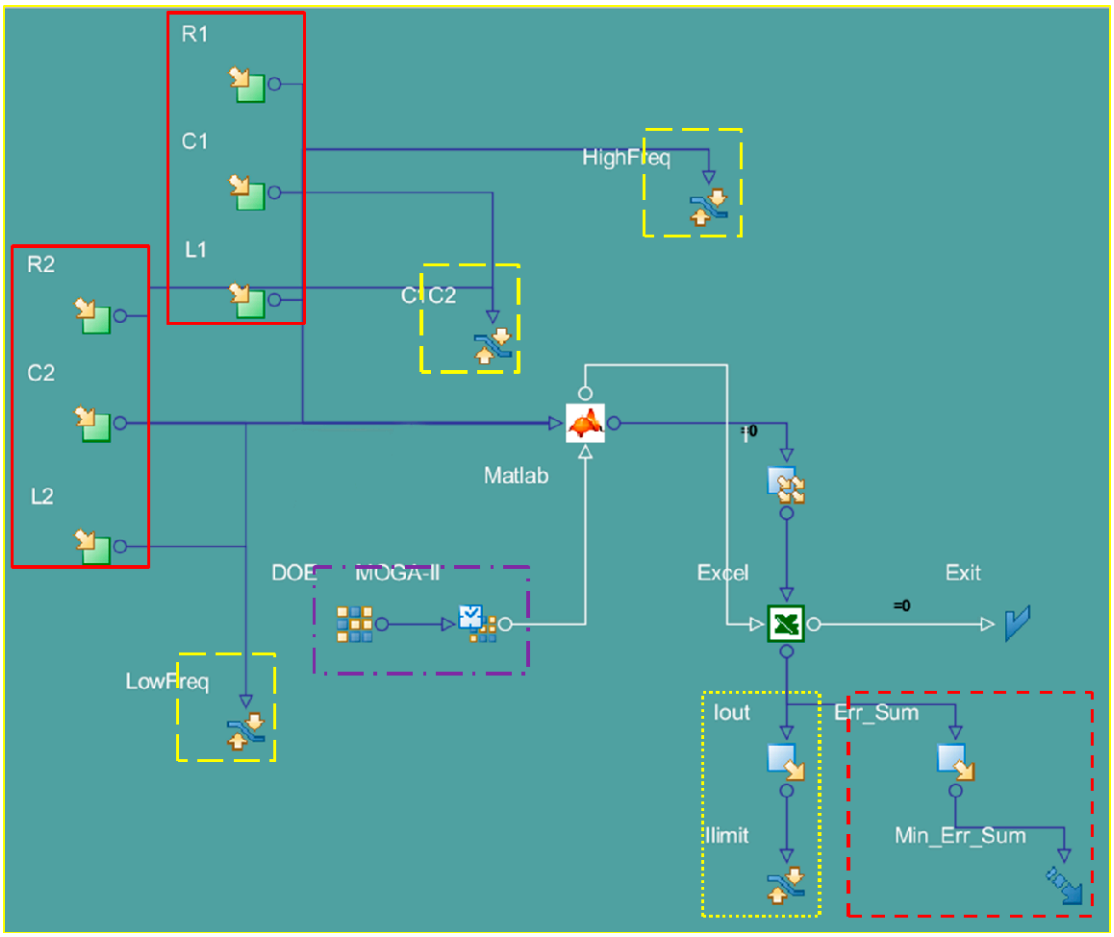


Fig. 4.26 Linear modeFRONTIER Simulation Model in One Phase Switching

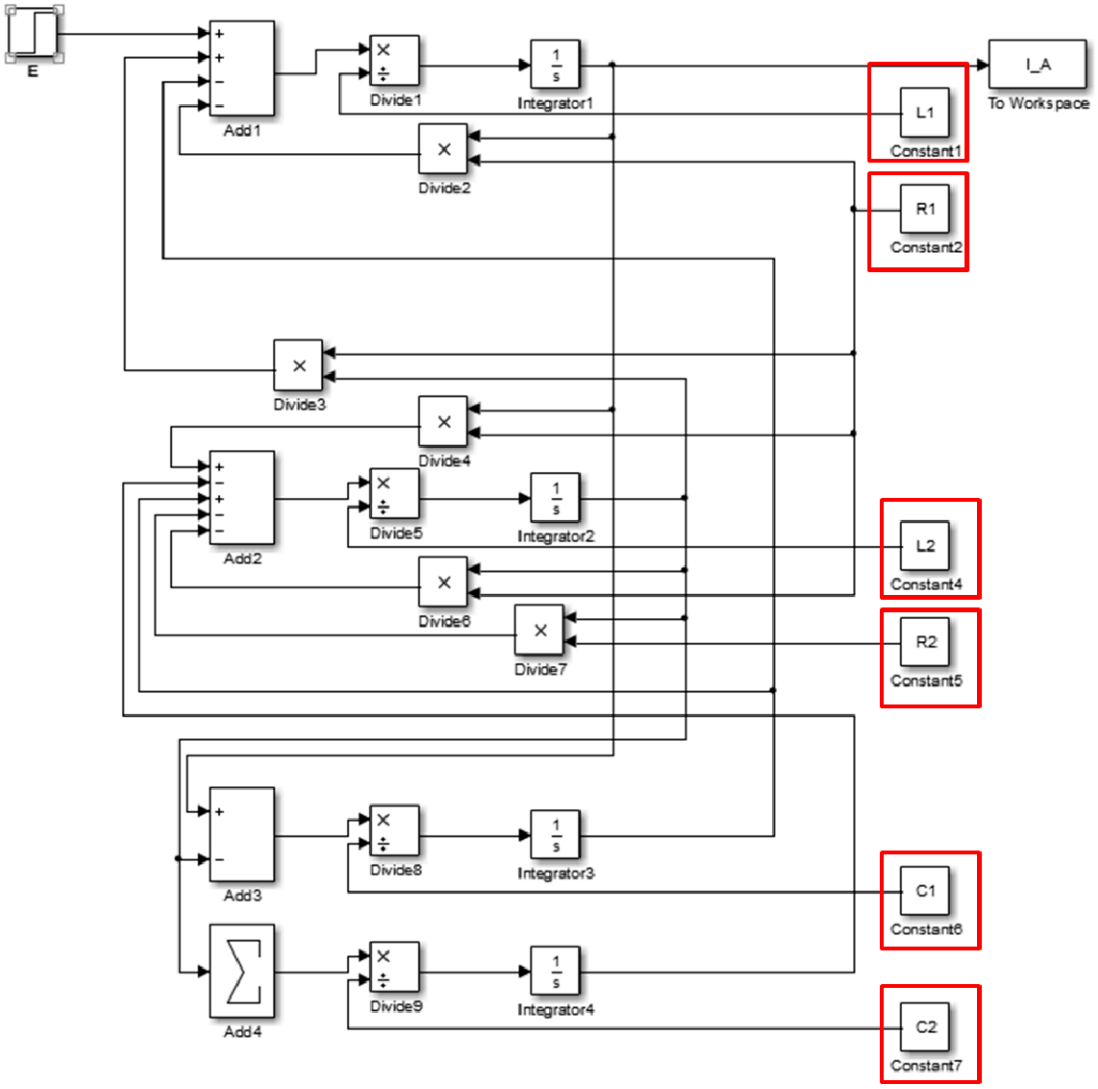


Fig. 4.27 Linear MATLAB Model for modeFRONTIER

4.3.2 Simulation Result of Leakage Current

In order to double check this equivalent circuit, the software PSIM simulator is applied to get the simulation result instead of the software MATLAB. The best modeFRONTIER simulation result is introduced into PSIM modeling. Fig. 4.28 shows the model of the equivalent circuit. Fig. 4.29 shows the simulation result when only one phase is switching. The simulation result (short broken line) can meet well with the experimental result (solid line). The computer aided optimization software

can help the researchers analyze the equivalent circuit of the system. And the simple equivalent circuit also can show the main characteristics of the inverter-fed motor system well.

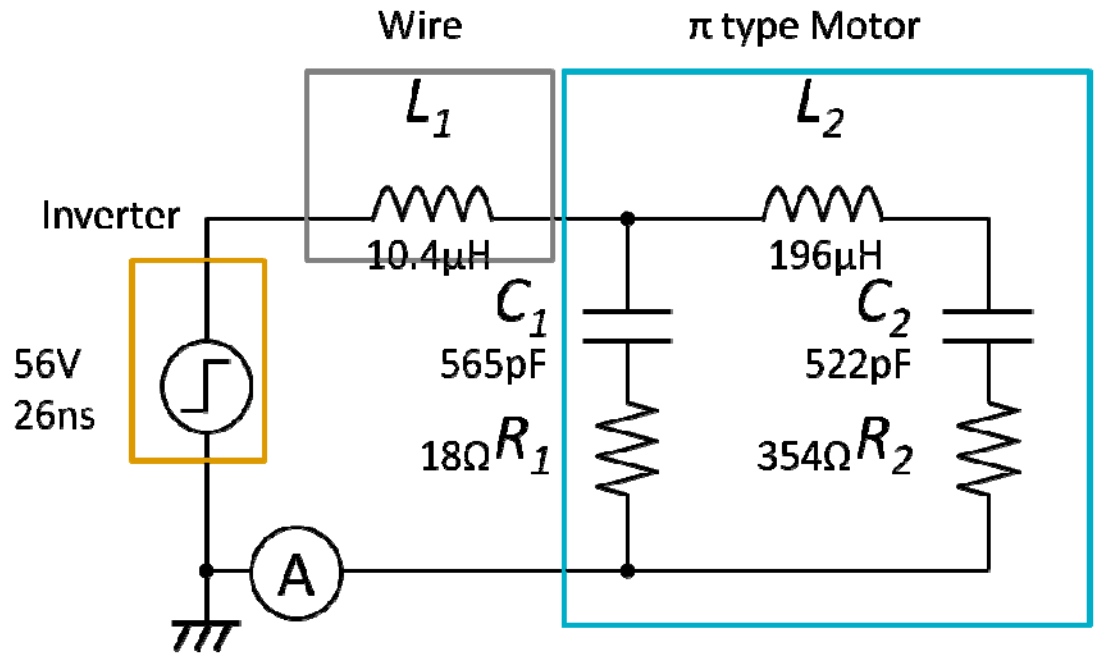


Fig. 4.28 Linear Model of One Phase Switching

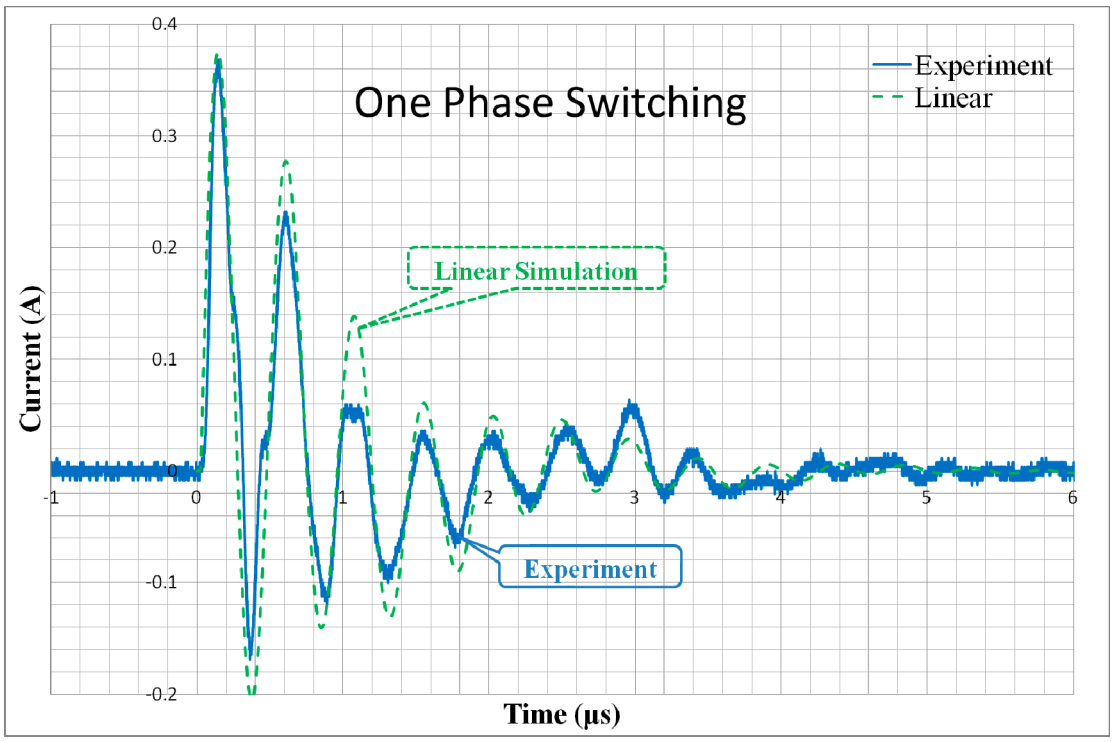


Fig. 4.29 PSIM Linear Simulation Result of One Phase Switching

4.3.3 Consideration of Proposed CM Equivalent Circuit

In order to confirm validity of the proposed CM equivalent circuit, some impedance measurements are performed, using an LCR Hi-Tester HIOKI 3535.

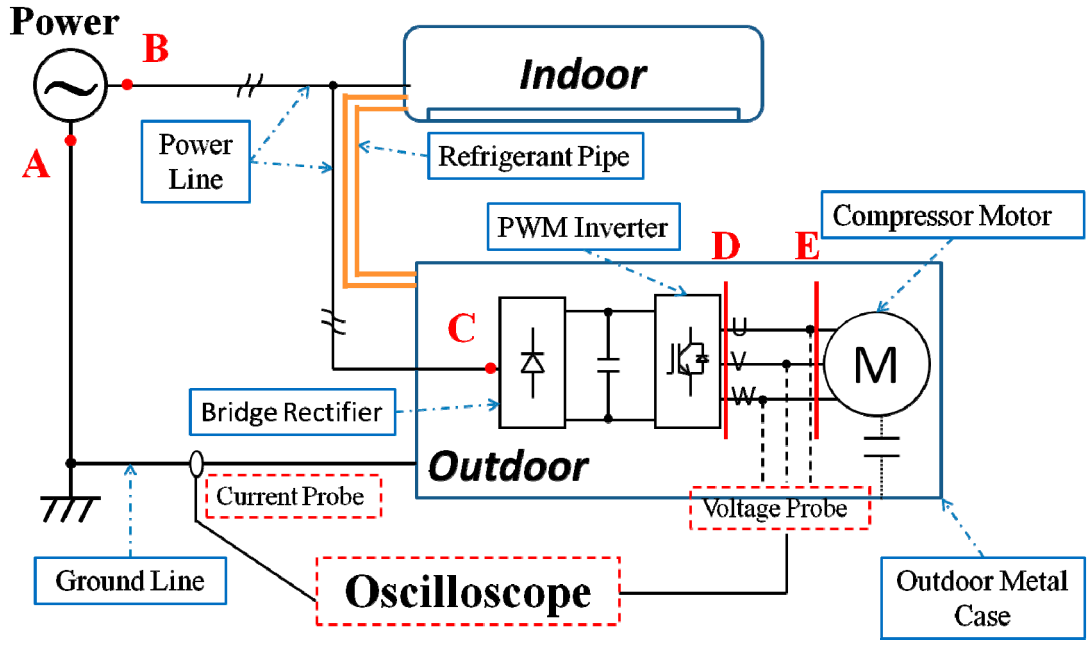


Fig. 4.30 Impedance Testing Connection

At D-point in Fig. 30, the motor windings is disconnected from the inverter and shorted, and the capacitance is measured between the shorted motor terminal (D-point) and the compressor metal case (F-point), in which the motor is installed. Since the measured capacitance varies with frequency, the measurement is performed at a frequency much lower than the first resonant frequency of 425 kHz. The measured capacitance value is 740 pF, and it is smaller than the corresponding value of $C_1 + C_2 = 1087$ pF, though order of two capacitances is closed. The reason is that the refrigerant and lubrication oil having higher permittivity exist between the motor windings and motor stator when the compressor is running. Therefore, it is impossible to measure the capacitance when the compressor is running. However, it is clear that $C_1 + C_2$ means the parasitic capacitance between the motor windings and motor stator.

On the other hand, it is important that the optimized capacitances of C_1 and C_2 are almost identical. C_1 and C_2 mean the parasitic capacitances around the input terminals and the neutral point of the motor windings, respectively. Because of symmetry of each motor winding from the input terminal and neutral point, the motor equivalent circuit consisting of C_1 ,C_2, and L_2 becomes almost symmetry. This shows validity of the motor model, which is represented by a π type circuit in the proposed CM equivalent circuit.

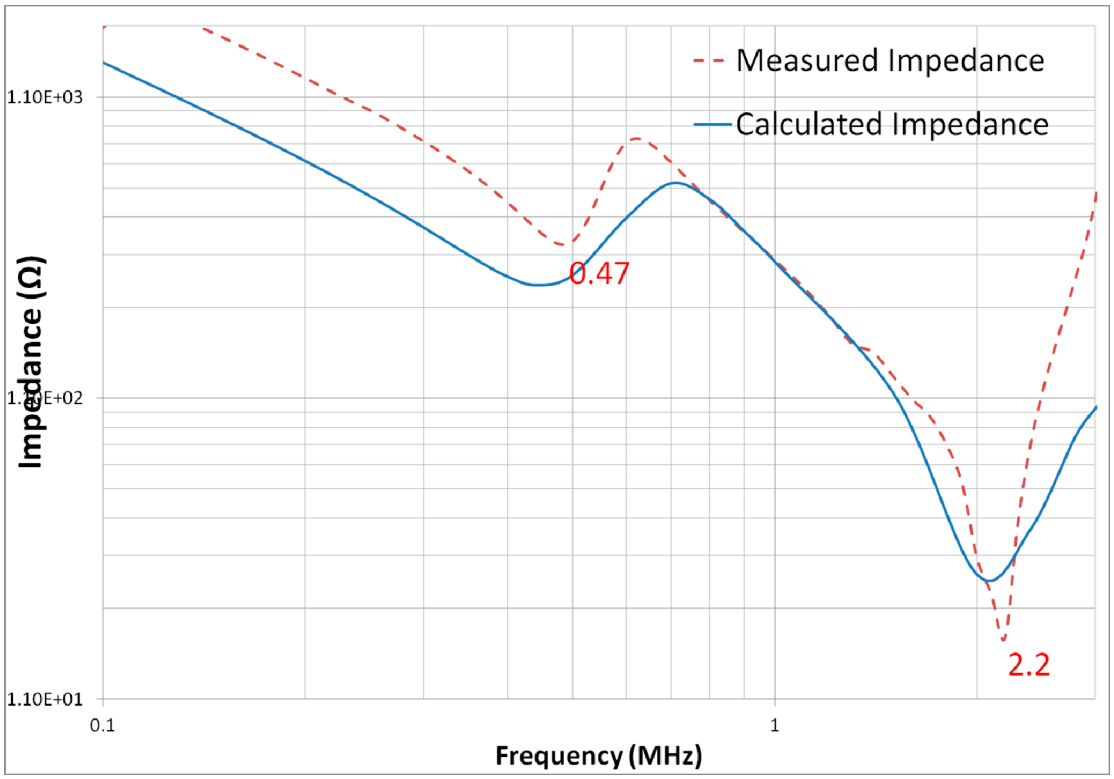


Fig. 4.31 Impedance Characteristics

At the switchboard corresponding A-point and B-point in Fig. 30, the terminals of the power cable and the grounding wire are shorted, and at E-point the power cable between the inverter and motor is shorted to the compressor metal case (F-point). The inductance between C-point and D-point is measured as 7.185 μH, which is smaller than L_1 of 10.4 μH. Considering the internal inductance inside of the switchboard, it is valid that L_1 represents the line inductance of the common-mode loop.

Similar to the previous measurement, the terminal of the power cable (B-point)

and the grounding wire (A-point) are shorted, and the impedance between C-point and D-point is measured with respect the frequency. The broken line in Fig. 4.31 shows the measured impedance characteristics, and the solid line means the characteristics calculated from the optimized equivalent circuit shown in Fig. 4.28. The calculated impedance is smaller than the measured impedance in a frequency range lower than the first resonant frequency because of the parasitic capacitance of $C_1 + C_2$ as mentioned above. Similarly, the calculated impedance is smaller than the measured impedance in a frequency range higher than the second resonant frequency because of the line inductance of L_1. However, the outline of the two characteristics is quite similar. This concludes that the proposed CM equivalent circuit can model the common-mode characteristics of the experimental system.

4.3.4 Limitation of Proposed Equivalent Circuit

As mentioned in section 3, the proposed equivalent circuit models only two major resonance phenomena. Therefore, other resonance phenomena in a frequency range higher than the second resonant frequency cannot be modeled by the proposed circuit. Then the frequency range adequate for using the proposed circuit is less than about 3 MHz.

On the other hand, the switching time of IGBTs used in the inverter is in a few hundred nanoseconds range. This restricts the frequency range of the inverter common-mode voltage as a noise source to several MHz. Therefore, the proposed simplified equivalent circuit can be practical in use and help to reduce the simulation effort.

4.4 Identification of Non-Linear Common-Mode Equivalent Circuit

In most cases, CM equivalent circuit can be modeled by only linear elements. In this system, non-linearity slightly appears as mentioned

4.4.1 Phase Switching Time Lag

When little time lag occurs for the switching, the phase angle that the peak value of the sinusoidal of the same frequency becomes small. Even if it is switching at the same time, it is caused by the fact that minute time lag occurs. To clarify this problem, the simulation below is carried out.

The modeling (Fig. 4.6) proposed in this paper is a transformation of Fig. 4.5. It is applied the modeling in Fig. 4.5 to run this simulation to explain this time lag problem. There is a step (2-level) component in PSIM. Vstep1 is the first step voltage and Vstep 2 is the second step voltage. Tstep is the the time of Vstep 1, and T_transsition is the rising time from Vstep 1 to Vstep 2. Fig. 4.32 shows a sample. If it is set the Vstep 1 as 0, the Tstep can be considered as a time lag. The time lag will affect the amplitude of the leakage current. Fig. 4.33 shows the modeling with no time lag. Fig. 4.34 shows the simulation result. At this time, the peak of leakage current is 0.74mA. A lot of simulations are carried out to confirm how long the time lag happens, the peak will decrease 10%. When the time lag is 81ns, the peak is almost 90% of the peak when the time lag is 0. This result is shown as Fig. 4.35. When the time lag is 81ns, the peak of leakage current will reduce 10%.

The experiment data in this experiment is confirmed and the result is shown as Fig. 4.36. The blue line is the U phase voltage and the green line is the W phase voltage. And the time lag between two phases is 25.4ns. When the time lag is 25.4ns, the simulation is carried out again. And the result is shown as Fig. 4.37. The peak of the leakage current is 739mA, almost 99.8% of the peak with no time lag. Therefore, in this experiment system the time lab problem can be neglected

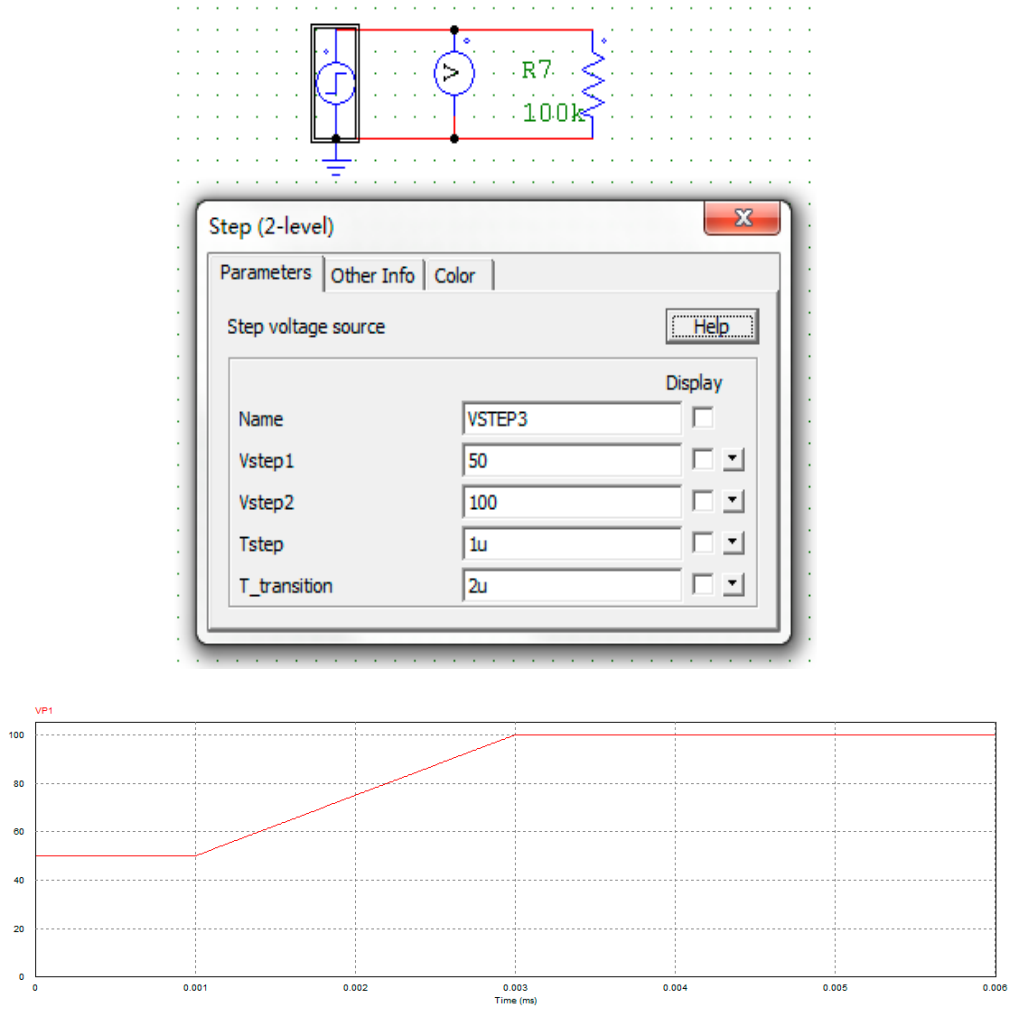


Fig. 4.32 Step (2-level) Component in PSIM

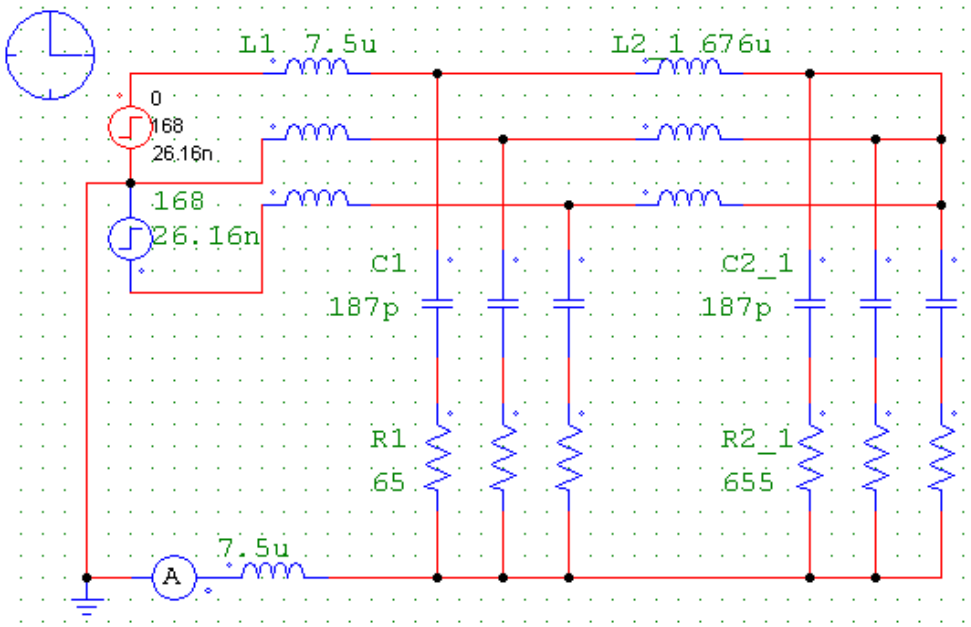


Fig. 4.33 Modeling with no Time Lag

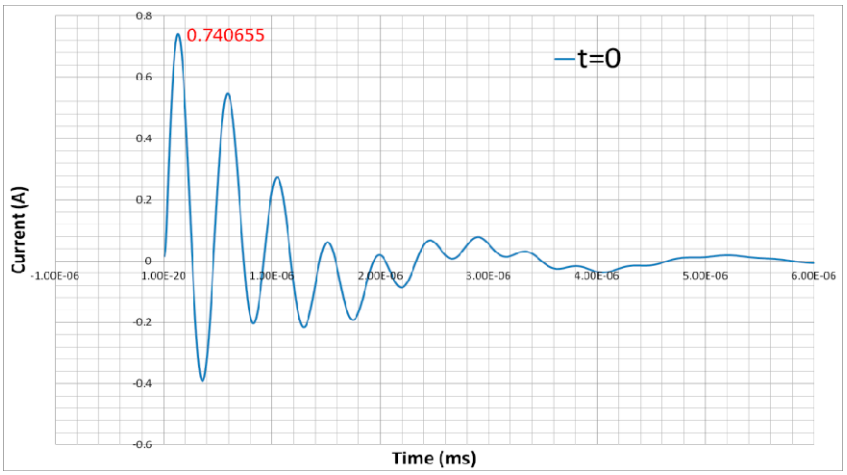


Fig. 4.34 Leakage Current with Time Lag 0

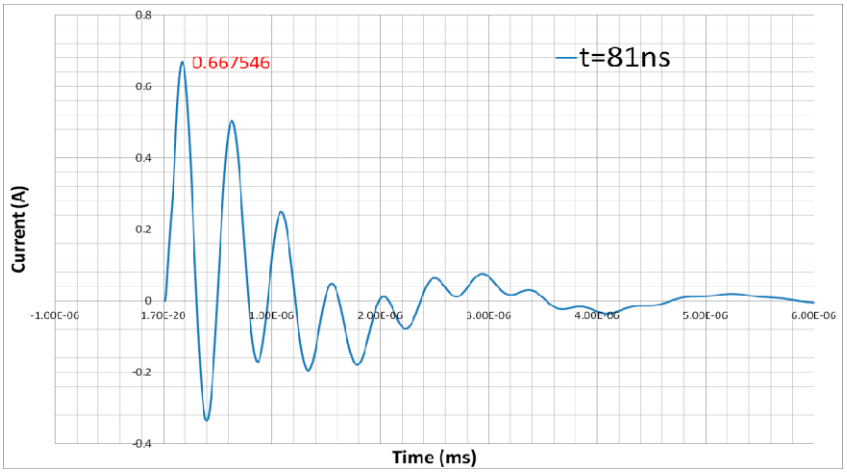


Fig. 4.35 Leakage Current with Time Lag 81ns

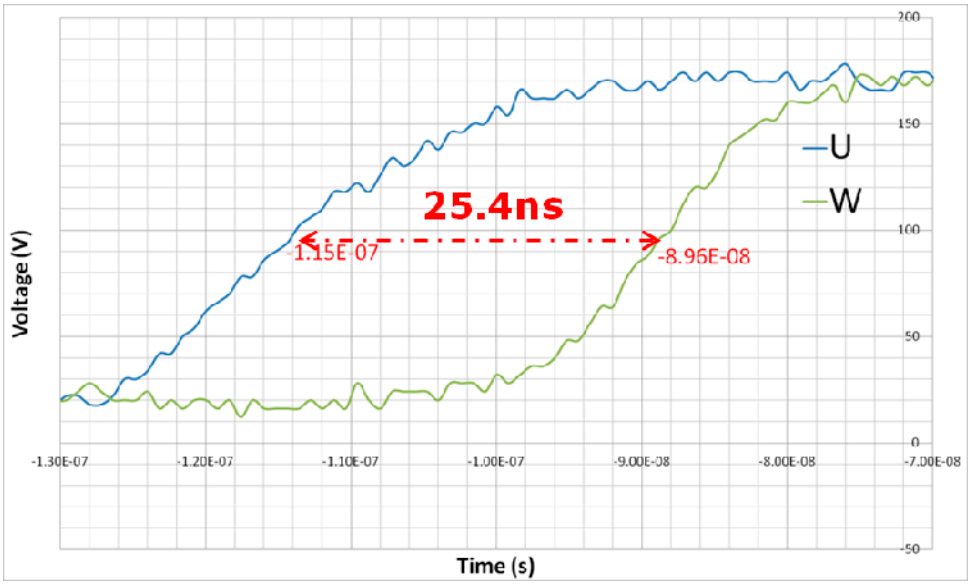


Fig. 4.36 Time Lag of Experiment Data

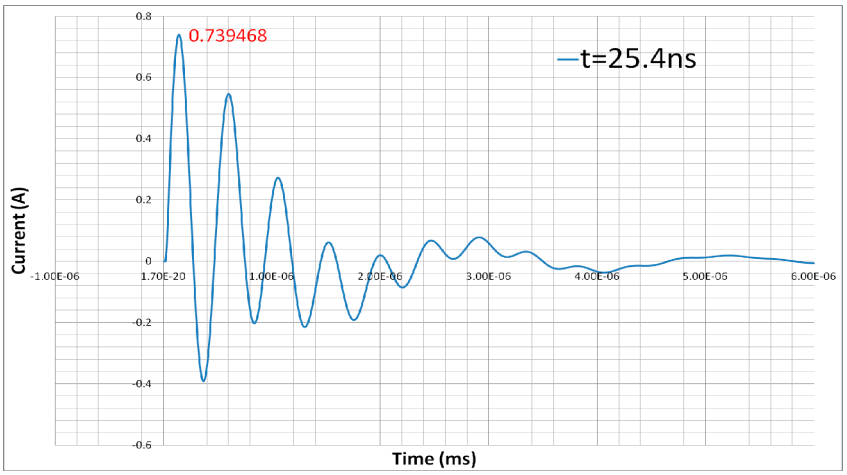


Fig. 4.37 Leakage Current with Time Lag 25.4ns

4.4.2 Non-linear CM Equivalent Circuit

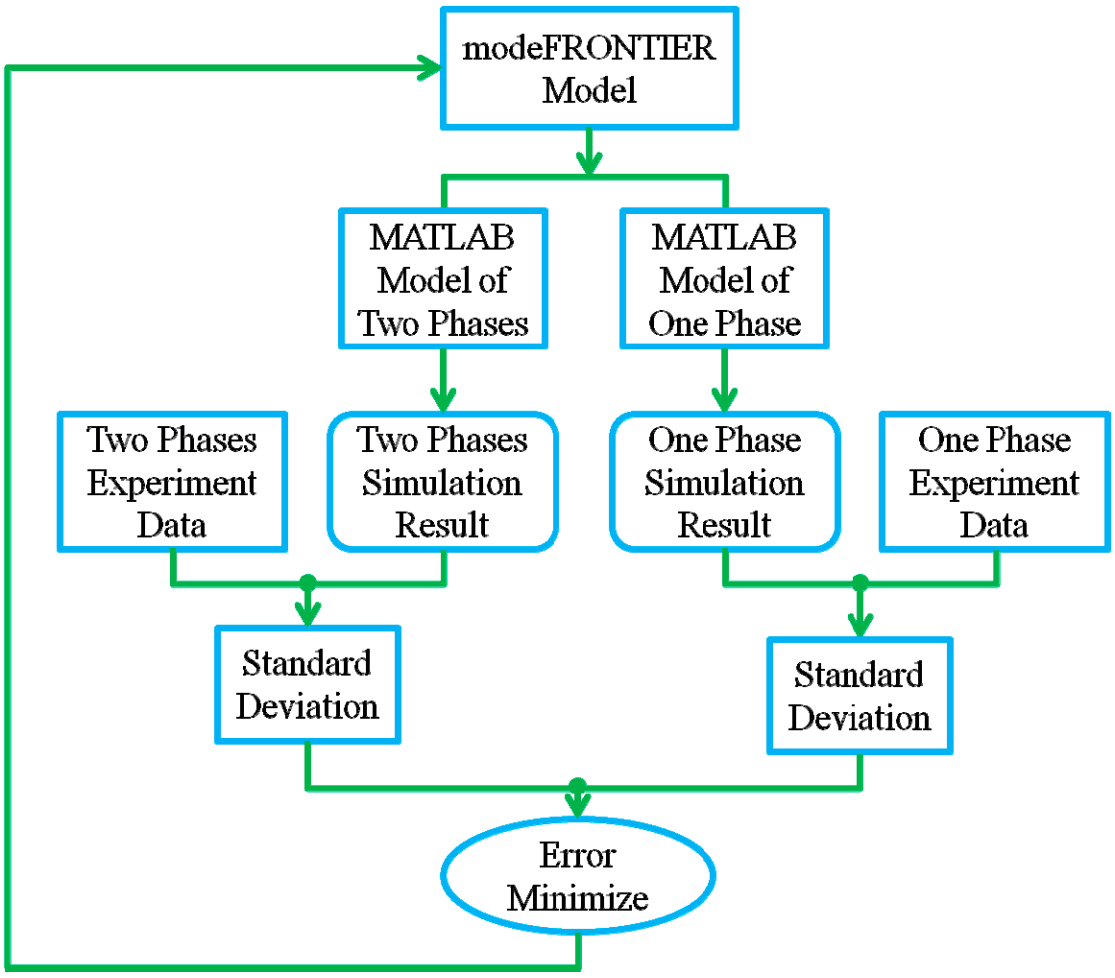


Fig. 4.38 Flow Chart for Both Cases

Fig. 4.38 shows the flow chart of the identification to make the simulation results meet well with the experimental results in both one-phase and two-phase switching cases. Two MATLAB models of the proposed non-linear equivalent circuit are built in both cases. By comparing the simulation results with the experimental results separately, two standard deviations are calculated and added. The modeFRONTIER determines the circuit parameters for the next calculation so that the total standard deviations are minimized. Finally, repetition of this calculation brings accurate circuit parameters of the proposed equivalent circuit including non-linear resistance. The modeFRONTIER model is shown as Fig. 3.39.

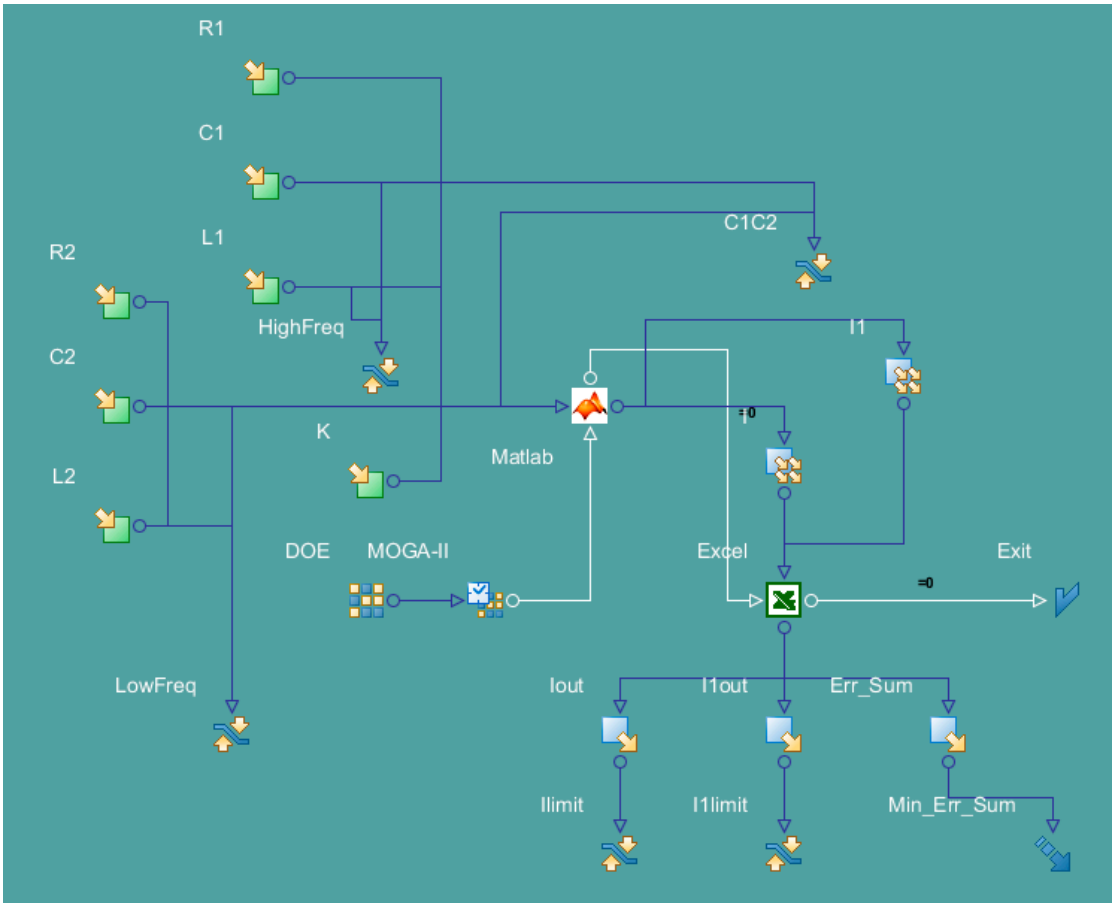


Fig. 4.39 Non-Linear modeFRONTIER Model for Both Cases

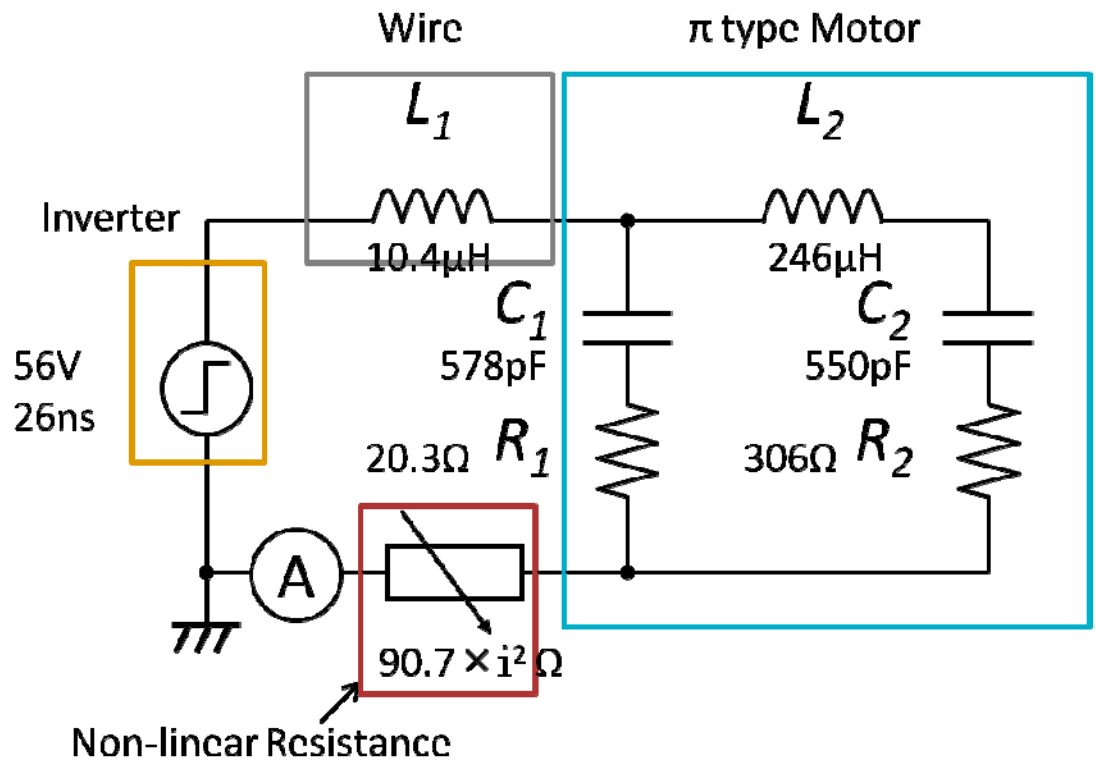


Fig. 4.40 Non-Linear Equivalent Circuit of Inverter-Fed Motor Drive System

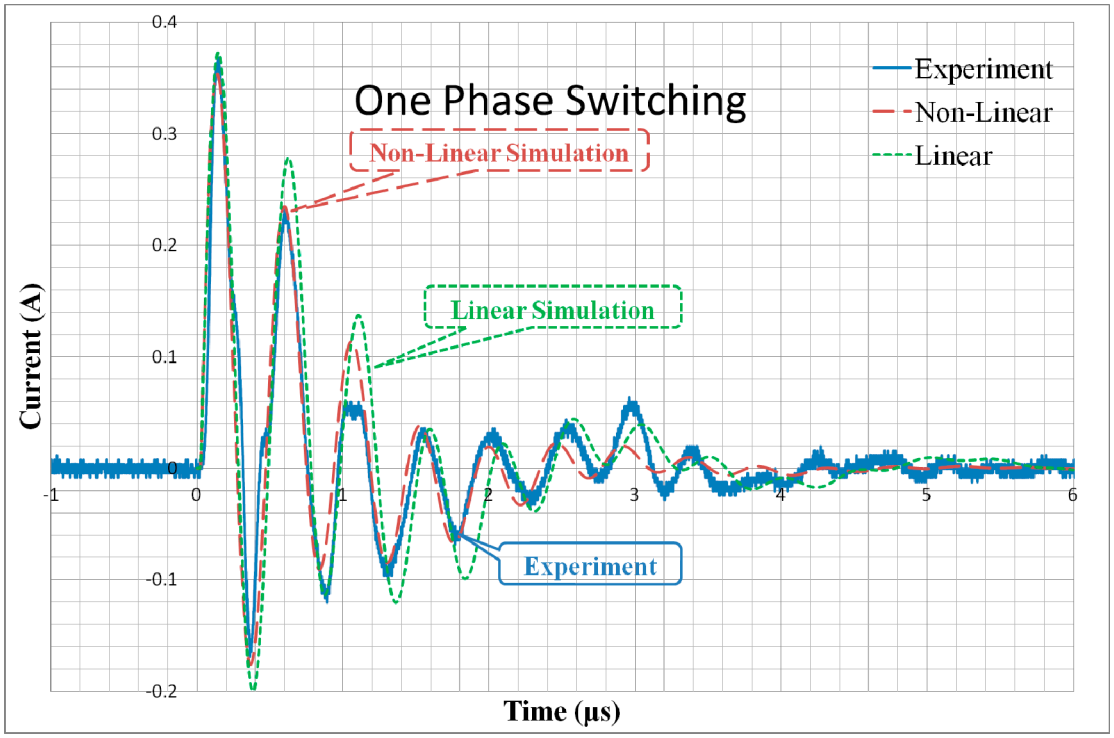


Fig. 4.41 Simulation Result of One Phase Switching

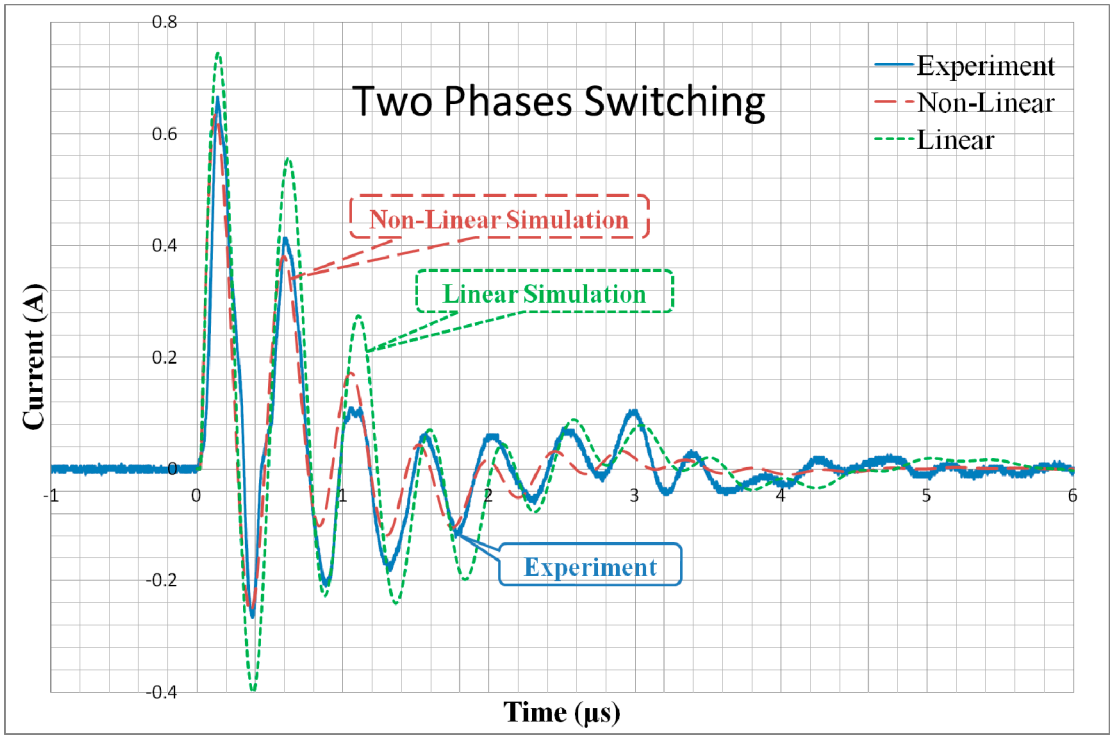


Fig. 4.42 Simulation Result of Two Phases Switching

Table 4-1 Standard Deviations between Simulation and Experiment

	Non-Linear (Fig. 4.40)	Linear (Fig.4.28)
One Phase Switching	7.736	12.040
Two Phases Switching	15.481	24.130

Fig. 4.40 shows the non-linear equivalent circuit, the parameters of which are identified by the proposed method. Fig. 4.41 and 4.42 show the simulation results of one-phase and two-phase switching, respectively. The solid lines show the experiment waveforms of leakage current. The long broken lines show the non-linear simulation results, applying the non-linear equivalent circuit shown in Fig. 4.40. The short broken lines show the linear simulation results, using the circuit parameters shown in Fig. 4.28. The non-linear simulation results can meet well with the experiment waveforms in both cases, compared with the linear simulation results.

Table 4.1 shows the standard deviations between the simulation and the

experimental waveforms. Regardless of switching phase number, the standard deviations of non-linear simulation are smaller than those of linear simulation. It means the introduction of non-linear resistance about CM equivalent circuit of inverter-fed drive motor system is effective.

Use the same method to verify the linear equivalent circuit. The result of motoFRONTIER is shown as Fig. 4.43. The effective data could not be found with linear equivalent circuit. It means the introduction of non-linear resistance about CM equivalent circuit of inverter-fed drive motor system is necessary.

This equivalent circuit provides the precise parameters and reduces the errors in Chapter 3.

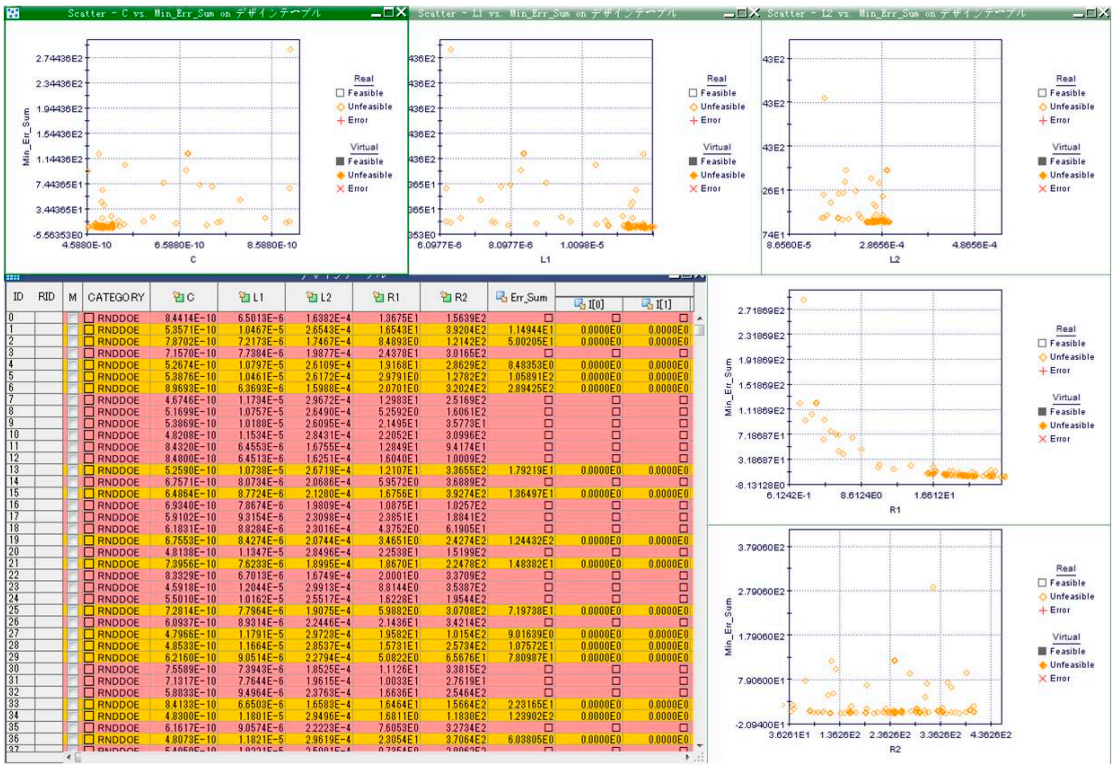


Fig. 4.43 modeFRONTIER Result of Linear Equivalent Circuit When Comparing to Experiment Waveform in Two Situations

4.5 Effect of Non-Linear Resistance about Common-Mode Equivalent Circuit for Inverter Drive System

4.5.1 Simulation for Verifying Non-Linear

In order to verify effect of the non-linear resistance in the equivalent circuit, do the following simulation. Fig. 4.44 shows a circuit with non-linear resistance.

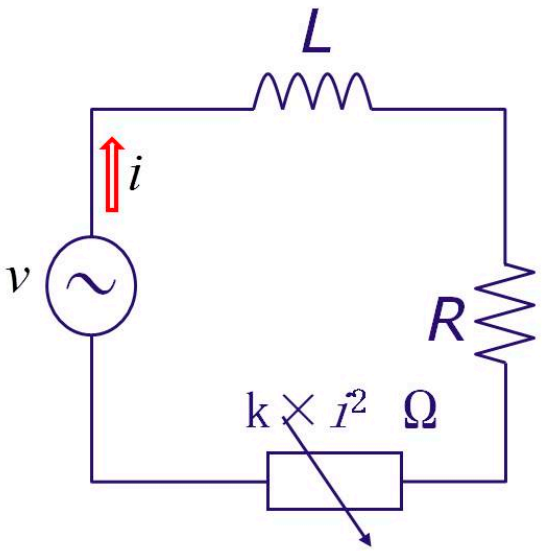


Fig. 4.44 Circuit with Non-Linear Resistance

There are two main resonance frequencies in the system, and the effect of high frequency is relatively high. So the input voltage *v* is sine signal, and the frequency is equal to the high resonance frequency of CM noise equivalent current. The parameter is configured as the high-frequency parameters of the equivalent circuit calculated in Chapter 4.4. The magnetic flux of circuit is

$$\Psi = \int v(t)dt \tag{4.5}$$

The MATLAB model of this circuit is shown as Fig. 4.45.

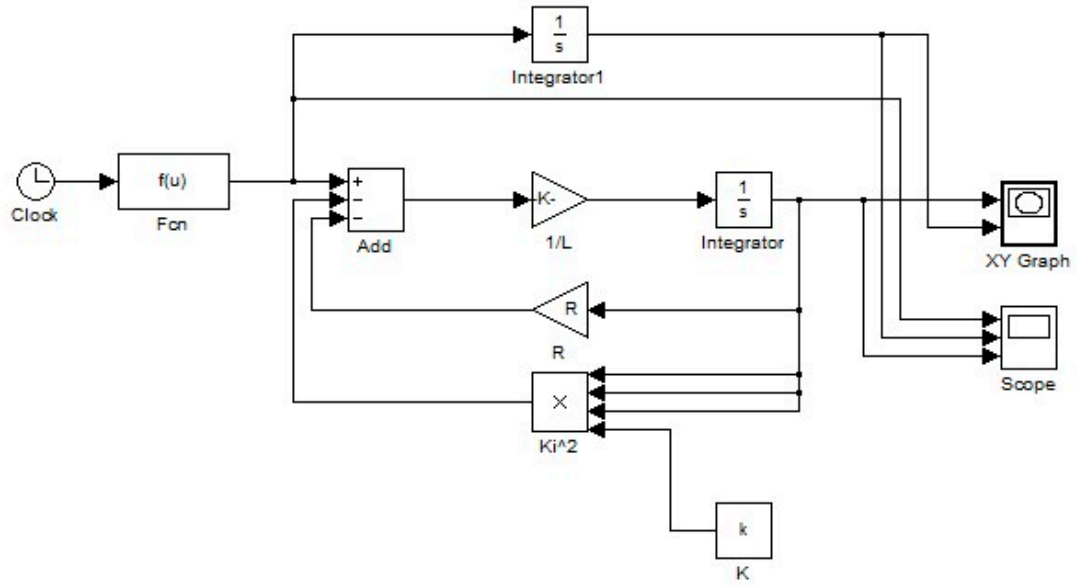


Fig. 4.45 MATLAB Model of Circuit

By adding the scope component, the waveform of the input voltage *v*, the loop current *i* can be monitored. the magnetic flux Ψ can be monitored by adding the XY graph component. The waveforms of *i*, *v* and Ψ are shown as Fig. 4.46.

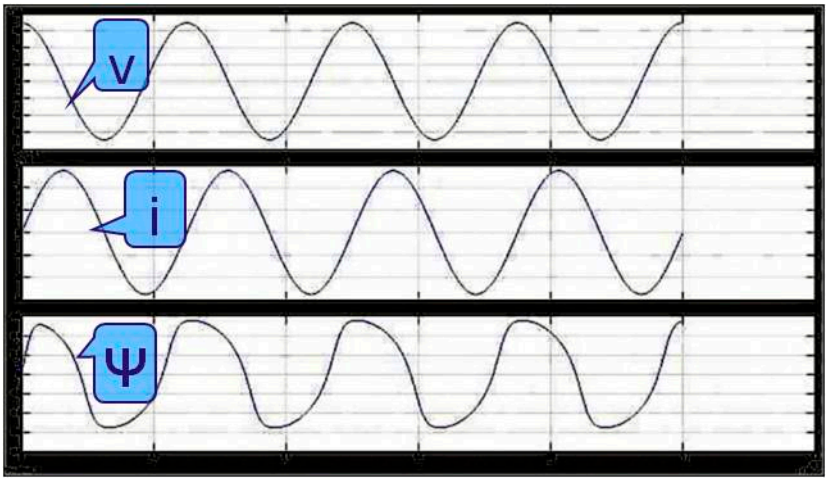


Fig. 4.46 Waveform of Voltage, Current and Magnetic Flux

Fig. 4.47 shows the relationship of current *i* and magnetic flux Ψ. The *x* axis is current, and the *y* axis is magnetic flux. The shape of the graph is similar to the B-H

curve of magnetic material. When the input voltage is low, the *i*-Ψ curve is shown as the red line. When the input voltage is high, the *i*-Ψ curve is shown as the blue line. The shape of the graph looks like the hysteresis phenomenon of magnetic material. When the input voltage is higher, the area of *i*-Ψ curve is lager.

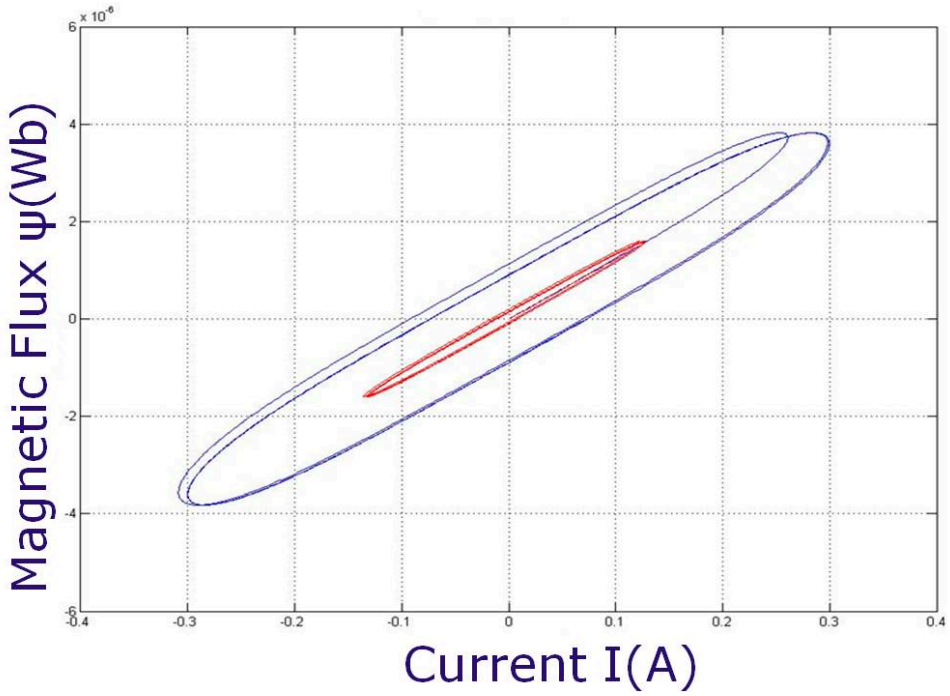


Fig. 4.47 *i*-Ψ Curve of Simulation

Table 4-2 List of Experiment for Effectiveness of Non-Linear

Name	Brand	Model
Air Conditioning	Toshiba	RAS-281A
Oscilloscope	Tektronix	MSO4034
Current Probe	Tektronix	TCP0150
Voltage Probe	Tektronix	P5205
Power Amplifier	YOKOGAWA	705810

4.5.2 Experiment for Verifying Non-Linear

The following experiment will verify the effect of non-linear resistance. The

high-frequency power amplifier is connected to the input port connector of ac motor and the metallic frame of air conditioner. Fig. 4.48 shows the connection diagram. Table 4-2 shows the list of equipments. An oscilloscope will be applied to measure the input voltage and the loop current.

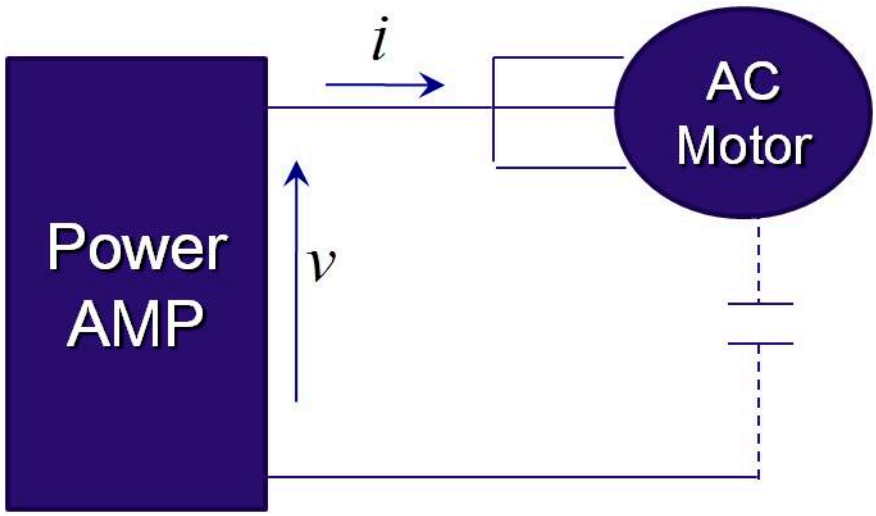


Fig. 4.48 Connection Diagram of Experiment

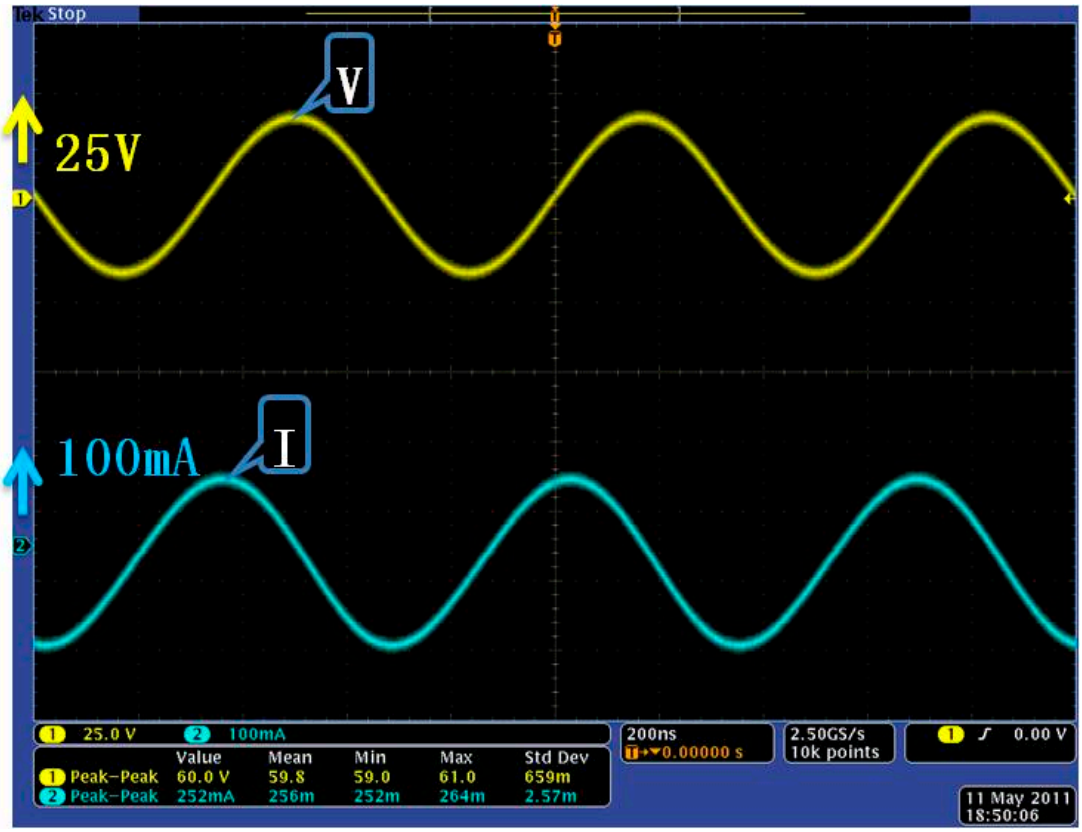


Fig. 4.49 Input Voltage at 60Vpp

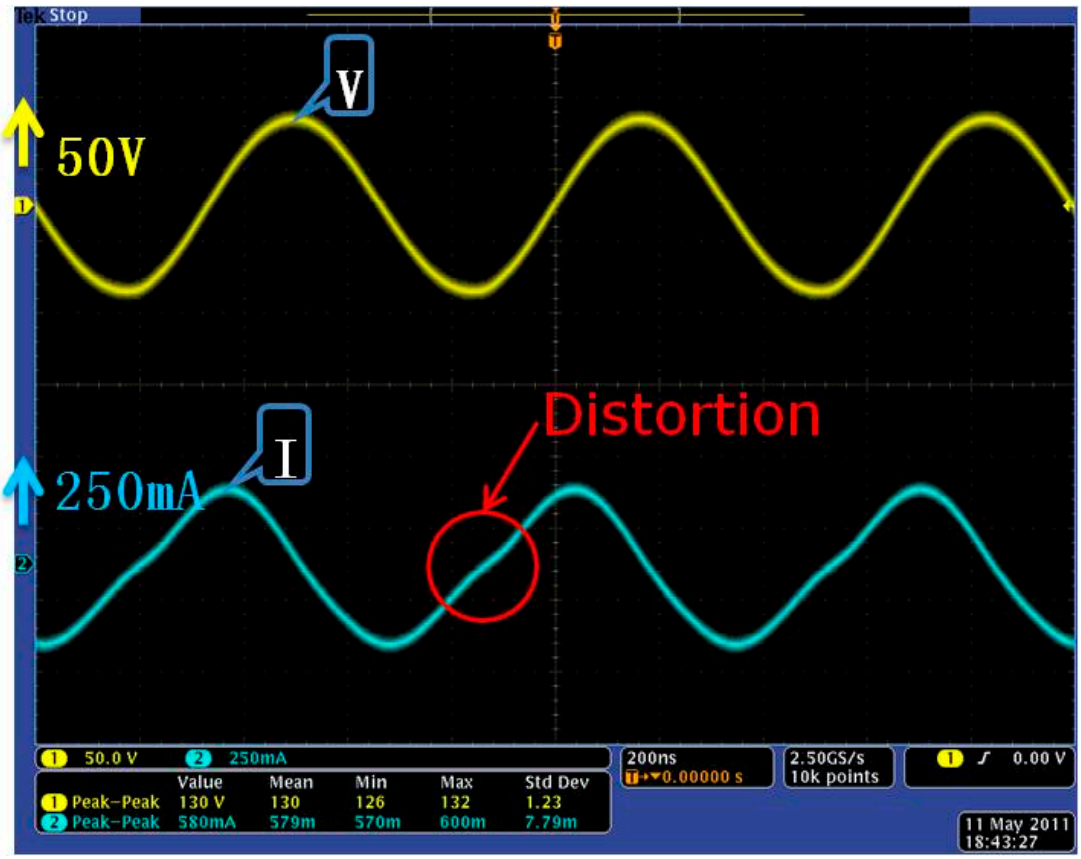


Fig. 4.50 Input Voltage at 130Vpp

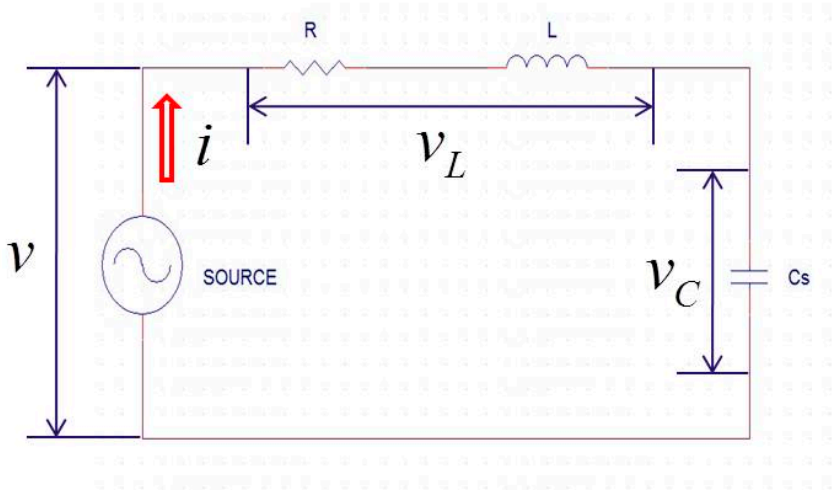


Fig. 4.51 Equivalent Circuit of Experiment

It is set the output voltage of the power amplifier as a sine signal with a frequency. The frequency is the same with the high resonance frequency of the equivalent circuit. Fig. 4.49 and Fig. 4.50 show the voltage and current waveforms.

The yellow line is the voltage waveform and the blue line is the current

waveform. When the input voltage is low as 60 Vpp, the current lags the voltage about 90 deg. When the input voltage is 130 Vpp, the current waveform becomes distorted softly. Compared the phase position of current waveform with the position when the input voltage is 60Vpp, the phase position lags more. The changing of input voltage will impact the phase position of current. It means there is non-linear effect in the system.

The equivalent circuit can be shown as Fig. 4.51.

In this equivalent circuit,

$$v_C = \frac{1}{C_s}\int i(t)dt \tag{4.6}$$

$$v_L = v - v_C \tag{4.7}$$

The magnetic flux Ψ is

$$\Psi = \int v_L(t)dt \tag{4.8}$$

In order to calculate the value of magnetic flux Ψ, the effect of parasitic capacitance in the system should be removed. LCR Hi-Tester can measure the parasitic capacitance of motor when the motor is not running. The connection of equipments is shown as Fig. 4.52.

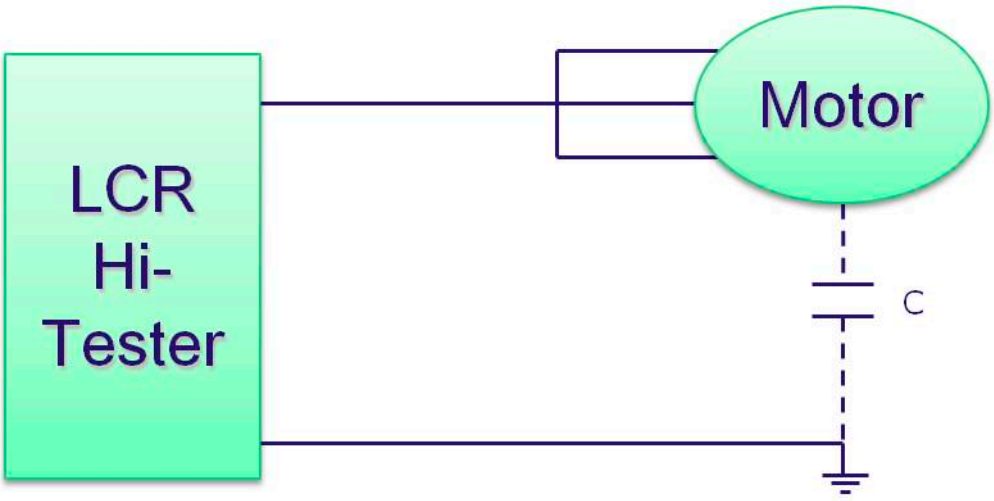


Fig. 4.52 Equipment Connection for Parasitic Capacitance Testing

The list of equipments is shown as Table 4-3.

Table 4-3 List of Equipments for Parasitic Capacitance

Name	Brand	Model
Air Conditioning	Toshiba	RAS-281A
LCR Hi-Tester	HIOKI	3535

When the motor is running, there is the mixture, which is made up by the lubrication oil and refrigerant, existing between the coil and the metallic frame of AC motor. Fig. 4.53 shows the parasitic capacitance in different frequency measured by LCR Hi-Tester.

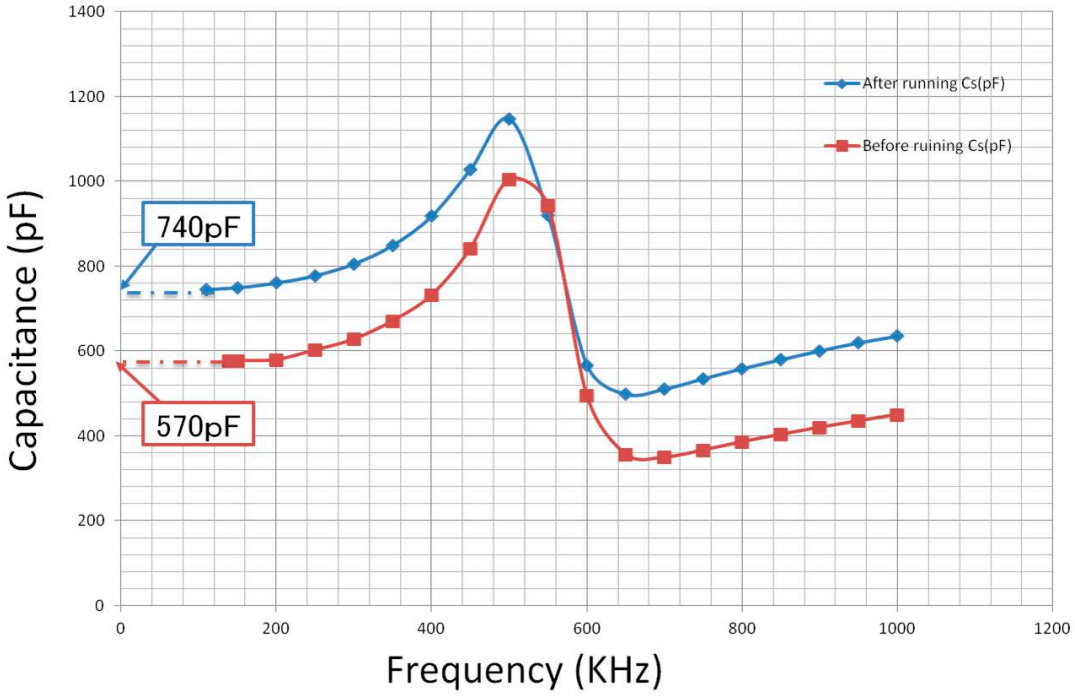


Fig. 4.53 Parasitic Capacitance in Different Frequency

The red line is the parasitic capacitance when the motor does not run for a long times, and the blue line the parasitic capacitance just after motor run. The capacitance of red line is smaller than the blue line.

Because of the limitation of LCR Hi-Tester, it is impossible to measure the parasitic capacitance directly when the frequency is 0. According to the capacitance

could be measured, the value when the frequency is 0, can be speculated. The parasitic is about 570 pF.

Only the capacitance of high-frequency circuit is needed in this experiment. And the Cs is the half of the capacitance measured. So the Cs is 285 pF.

According to the data of voltage, current, capacitance, and the formula (4.6), (4.7), (4.8), the magnetic flux Ψ can be calculated. Further, the i-Ψ curve is shown as Fig. 4.54. The blue line is the curve when the voltage is high, and the red line is the curve when the voltage is low. The shape of the graph looks like the hysteresis phenomenon of magnetic material. And the area of i-Ψ curve is lager, when the input voltage is higher.

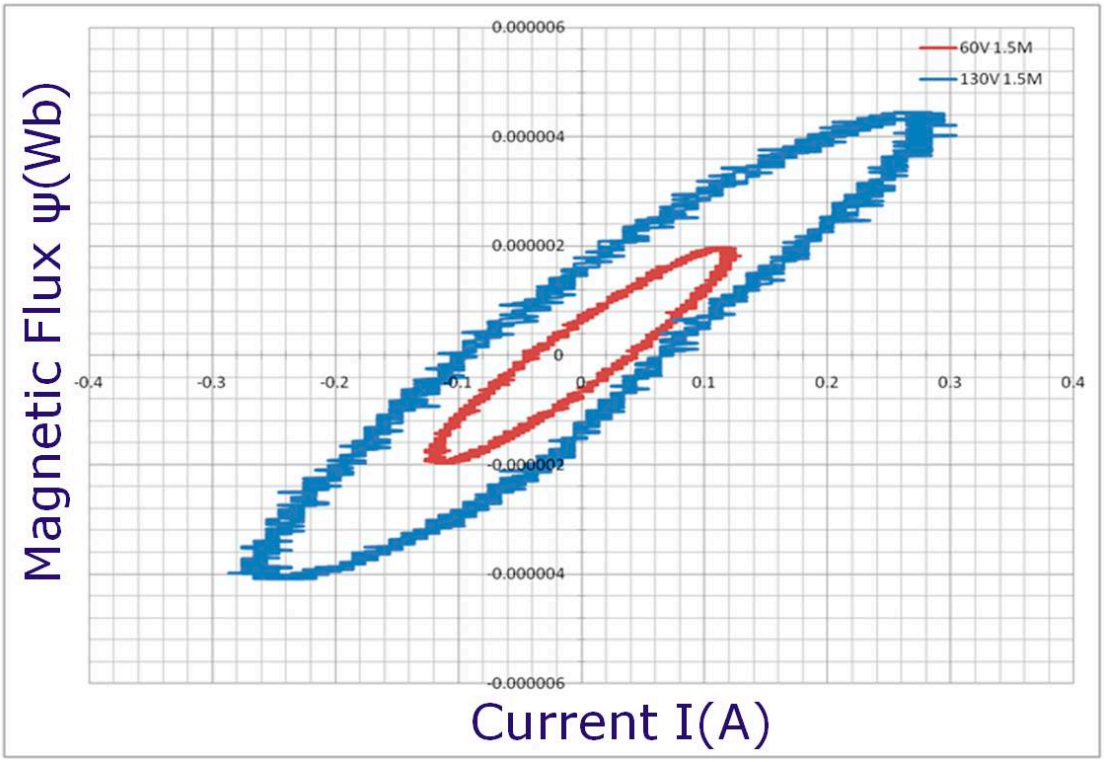


Fig. 4.54 i-Ψ Curve of Experiment

Fig. 4.54 is the i-Ψ curve of simulation and Fig. 5.11 is the i-Ψ curve of experiment. Both the two curves look like the hysteresis phenomenon of magnetic material. And the area of i-Ψ curve follows the input voltage changes. Therefore, it can confirm that the introduction of non-linear of CM equivalent circuit of inverter-fed drive motor system is effective.

4.5.3 Physical Meaning of Non-Linear

Because consider that the reason of non-linear happened is the magnetic saturation of the iron, the following experiment is carried out. Fig. 4.55 shows the connection. The component in Fig. 4.55 is the cover which is cut off from an air conditioner compressor. A signal generator and a power amplifier are connected to this cover, and then the voltage and current are measured by the oscilloscope. The list of Experiment is shown as Table 4-4. The frequency of the signal generator is configured as sine signal, and the frequency is the same with the high resonance frequency of equivalent circuit. When the current is 300mA, the waveform is shown as Fig. 4.56. The blue line is the input voltage, and the cyan blue line is the loop current. No matter how high the loop current is, there is no distortion happening. Tut this kind of distortion happened during the experiment in Chapter 4.3.2.

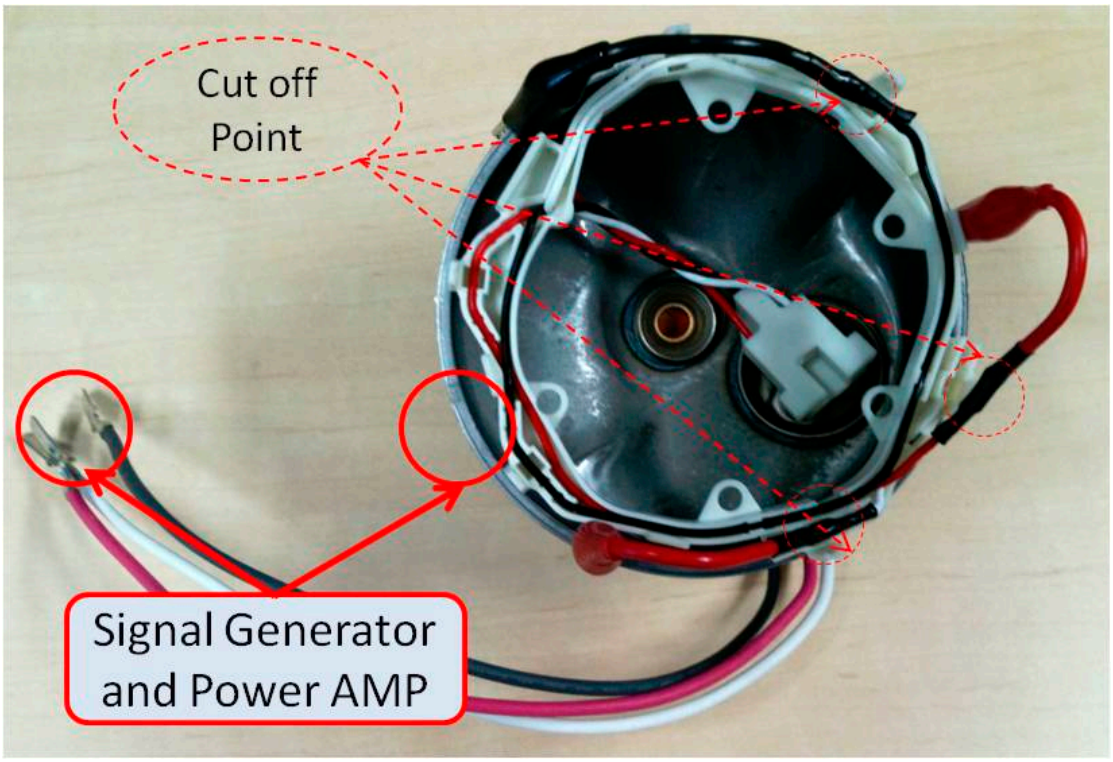


Fig. 4.55 Connection of Experiment for Verifying Non-Linear Physical Meaning

Table 4-4 List of Equipments for Verifying Non-Linear Physical Meaning

Name	Brand	Model
Cover of Compressor	Toshiba Air Conditioner	RAS-281A
Oscilloscope	Tektronix	MSO4034
Current Probe	Tektronix	TCP0150
Voltage Probe	Tektronix	P5205
Power Amplifier	YOKOGAWA	705810
Signal Generator	Tektronix	AFG 3252

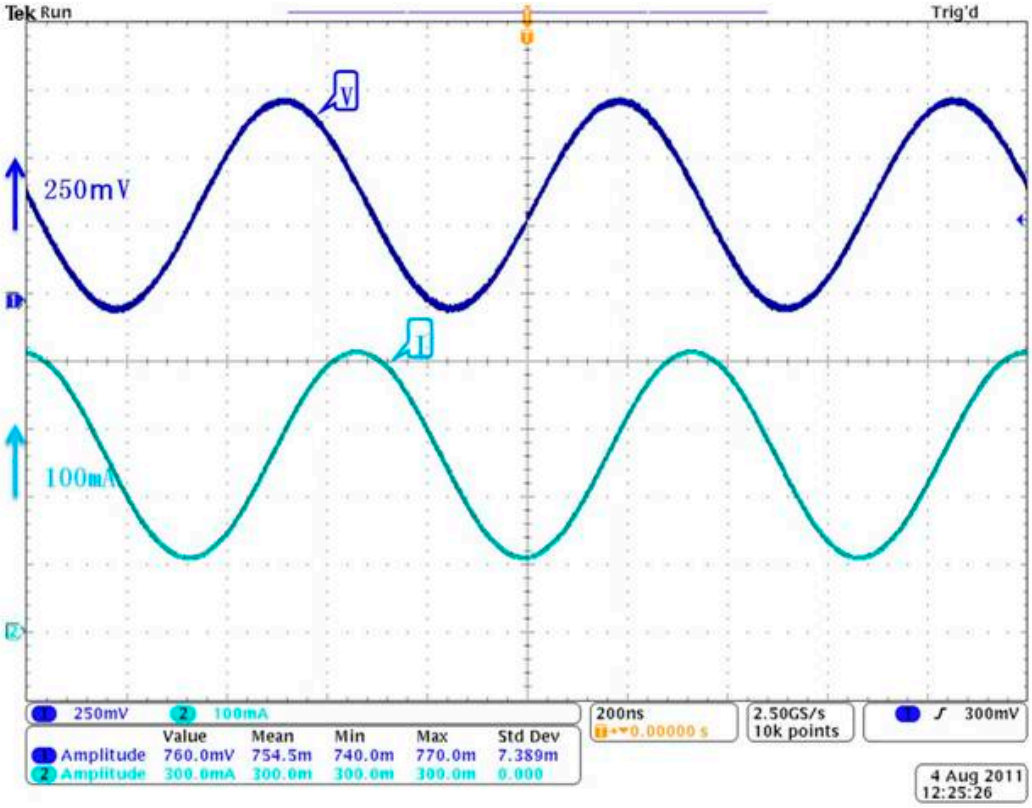


Fig. 4.56 Waveform for Verifying Non-Linear Physical Meaning

Because the parasitic capacitance does not exist in this experiment, the magnetic flux Ψ can be calculated directly according to the voltage and the current. The i-Ψ curve in different loop currents is shown as Fig. 4.57. The area of the i-Ψ curve becomes larger, following the increasing of the loop current. The area of i-Ψ curve means the energy loss of the circuit.

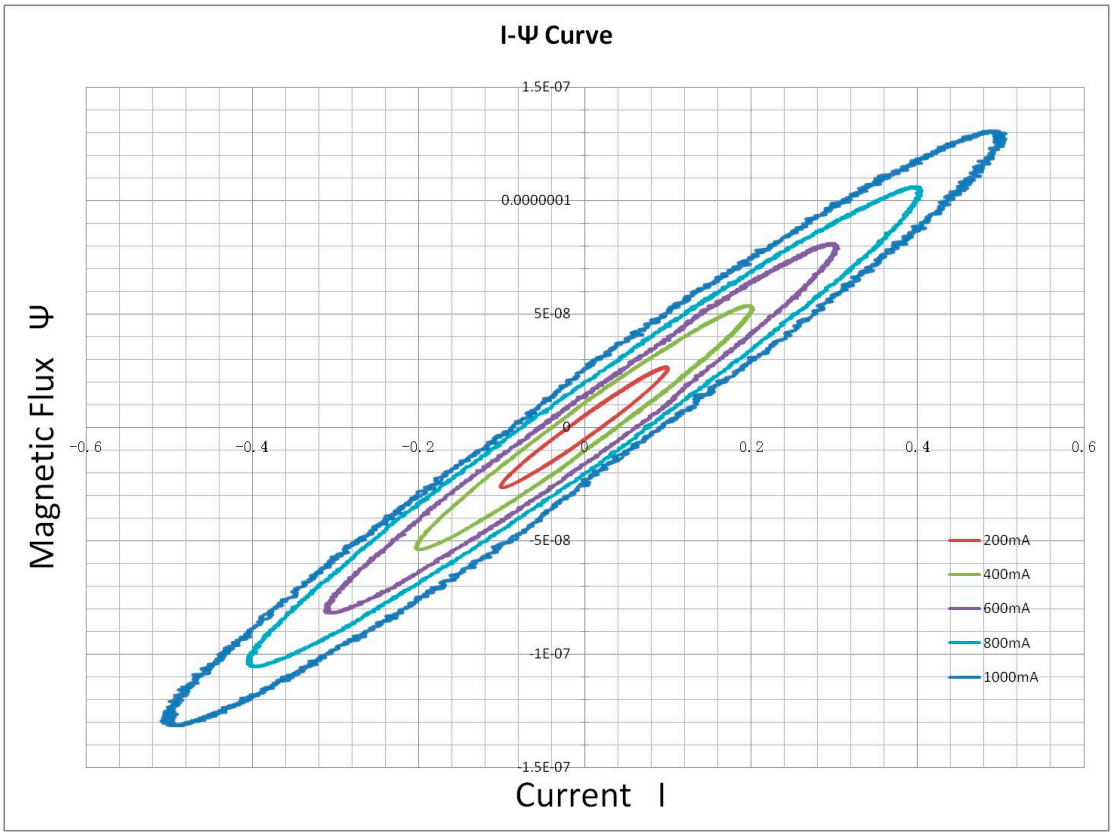


Fig. 4.57 *i*-Ψ Curves in Different Loop Currents

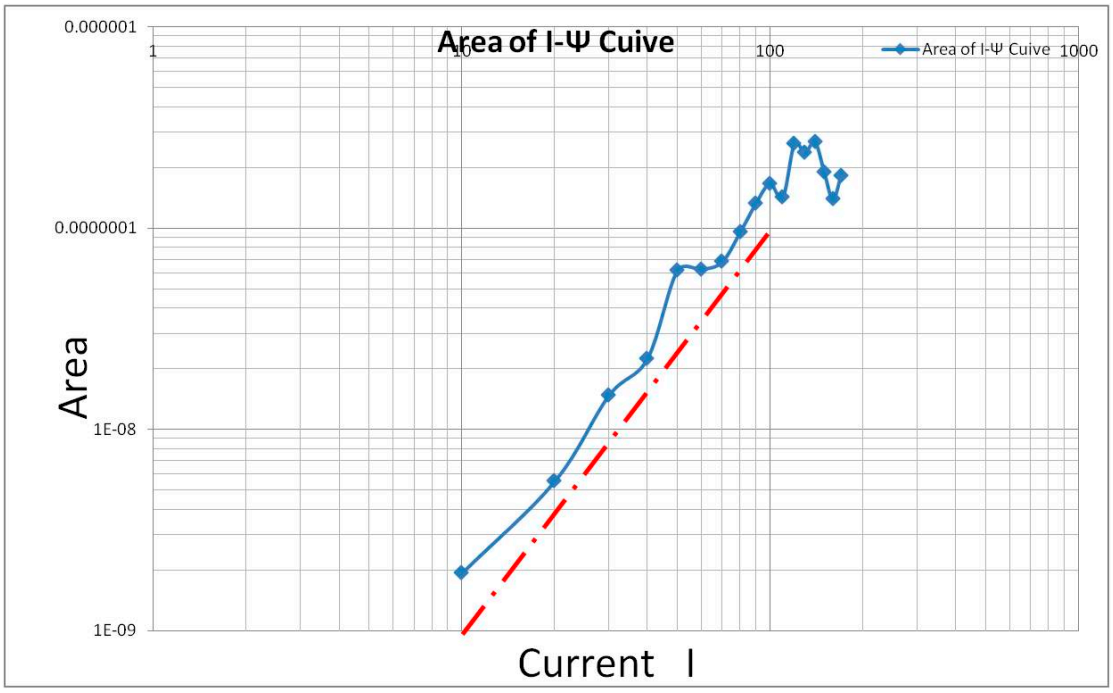


Fig. 4.58 Logarithm Relationship between Current *i* and Area of *i*-Ψ Curve

The logarithm relationship between the current i and the area of i-Ψ curve is shown as Fig. 4.58. The energy loss is the square of current. The red line in Fig. 4.58 shows the square of current relationship. The change trend of area is almost the same along the red line. It means there is no non-linear element in the cover of air conditioner compressor.

The physical meaning of non-linear needs further confirmation.

4.6 Summary

In Chapter 3, some of the known parameters are subjectively speculated according to the experiment waveform of the leakage current. It may lead to some small errors in calculating the parameters of the equivalent circuit. The optimization software modeFRONTIER is applied to improve the accuracy of the equivalent circuit parameters and reduce errors.

In order to verify the effect of non-linear resistant, an equivalent circuit without non-linear element is also confirmed. A linear MATLAB equivalent circuit model and a non-linear model are made up.

The two equivalent circuits are simulated in modeFRONTIER in two situations below. In situation one, the simulation result is just compared to the waveform in one phase switching or in two phases switching. In situation two, the simulation result is compared to the waveforms from one phase switching and from two phase switching at the same time. The linear equivalent circuit and non-linear equivalent circuit can meet well with the experiment data in situation one. Regardless of switching phase number, the standard deviations of non-linear simulation are smaller than those of linear simulation. Further, only the equivalent circuit with non-linear resistance can meet well in situation both cases (one phase switching and two phases switching). So the introduction of non-linear resistance about CM equivalent circuit of inverter-fed drive motor system is effective and necessary.

The effect of the non-linear in the equivalent circuit is verified, by do another group of experiment and simulation. The changing of input voltage will impact the phase position of current shown as Fig. 4.49 and Fig. 4.50. It means there is non-linear effect in the system. Both the simulation i-Ψ curve and experiment curve look like the hysteresis phenomenon of magnetic material. And the area of i-Ψ curve is lager, when the input voltage is higher. So the introduction of non-linear about CM equivalent circuit for inverter-fed drive motor system is effective.

A probable method of verifying the physical meaning of non-linear element is proposed. And this method is applied to analyze the cover of air conditioner

compressor. Unfortunately, there is no non-linear element exist in the cover of air conditioner compressor. The physical meaning of non-linear element needs further confirm.

Chapter 5 Estimation of Stray Capacitance and Permittivity between Compressor Motor Windings and Stator in Operation

5.1 Development of Refrigerant

Destruction of the ozone layer is one serious environmental problem in the modern global scale. According to the data from United Nations Environment Programme (UNEP), the ultraviolet (UV) from the sun to the ground will increase approximately 2% when the ozone decreases 1%, which have been reported. By the amount of ultraviolet light increases, ① damage to the health of mankind, ② damage and adverse effects to plants and marine life, ③ greenhouse effect, are considered. The history of the refrigerant can be divided into three stages. In the first stage, NH3, HC, CO2 are applied as refrigerant. But some of them are toxic, and some combustible, a bit inefficient. In the second stage, chlorofluorocarbon (CFC) and hydrochlorofluorocarbon (HCFC) are applied as main refrigerant. But these refrigerants will damage the ozone layer. The ozone damage coefficient of CFC is 0.5~1.0, and the coefficient of HCFC is 0.02~0.1. In the third stage, hydrofluorocarbon (HFC) will replace CFC and HCFC to be the main refrigerant, because the ozone damage coefficient of HFC is 0. However, HFC is due to have an impact on global warming, and it will be replaced by hydrocarbon (HC) which is almost no impact on global warming [34]-[37][44].

5.2 Air Conditioner

5.2.1 Structure of Air Conditioner

Air conditioner is a control system that can regulate temperature, humidity and air freshness. The basic principle is that the compressor controls the refrigerant to give rise to the evaporation or condensation of the ambient air, in order to achieve the purpose of the change in temperature and humidity. Fig. 5.1 shows the air conditioner system [45].

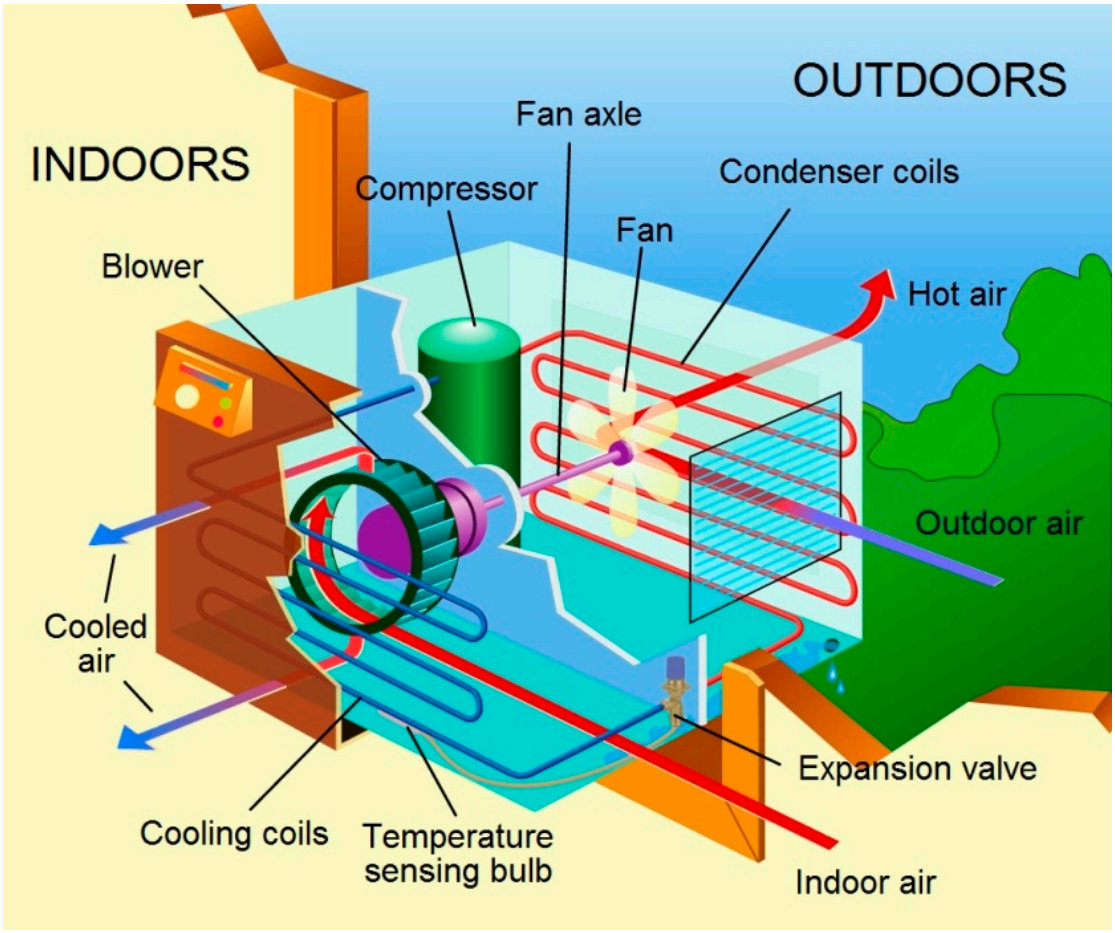


Fig. 5.1 Air Conditioner System

5.2.2 Compressor of Air Conditioner

Fig. 5.2 shows a section plan of compressor. In order to reduce the friction resistance and prevent the wear between institutions parts, the lubrication oil is applied. Compressor motor is stored in the compressor vessel and has a structure for cooling the motor windings directly by the refrigerant. Thus motor compressor will take excellent cooling, and this structure has been greatly contributes to miniaturization of the motor.

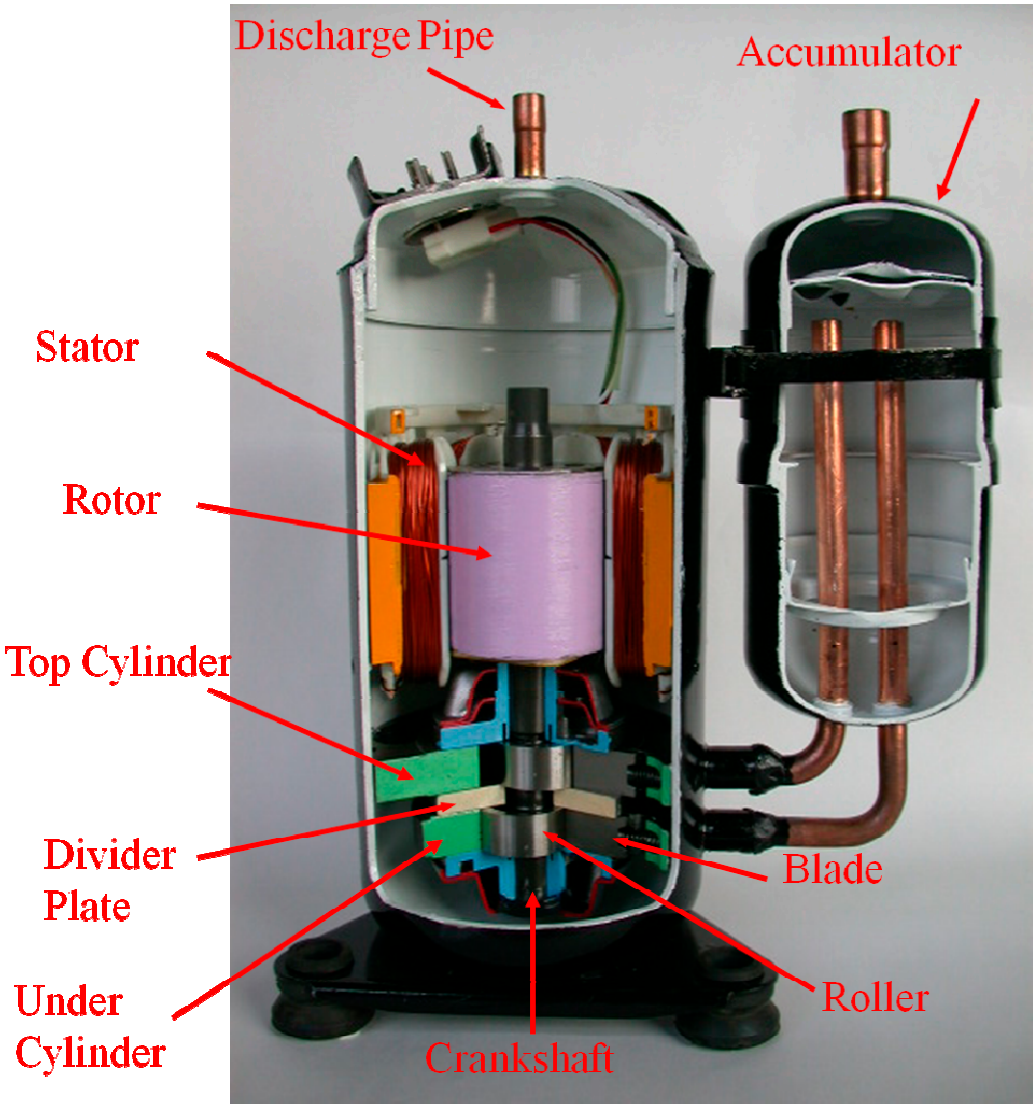


Fig. 5.2 Section Plan of Compressor

When the motor of compressor is running, the oil will mix with the refrigerant. Because the permittivity of this mixture is usually larger than the air, when the motor is running the parasitic capacitance is larger than the capacitance when the motor is filled nothing but only the air. When these power semiconductor devices do high-speed switching, because of the switching time is quite short, *dv/dt* and *di/dt* become considerable [3]. It means the high-amplitude and high-frequency leakage current will occur. This kind of leakage current goes through the parasitic capacitances, and then backtracks to the power supply system to affect the other equipments in the same power supply system. However, these latest of refrigerant tends relatively large dielectric constant. The increase in the dielectric constant leads to an increase in high-frequency leakage current. This will take more serious EMI problems [37][42][46][47].

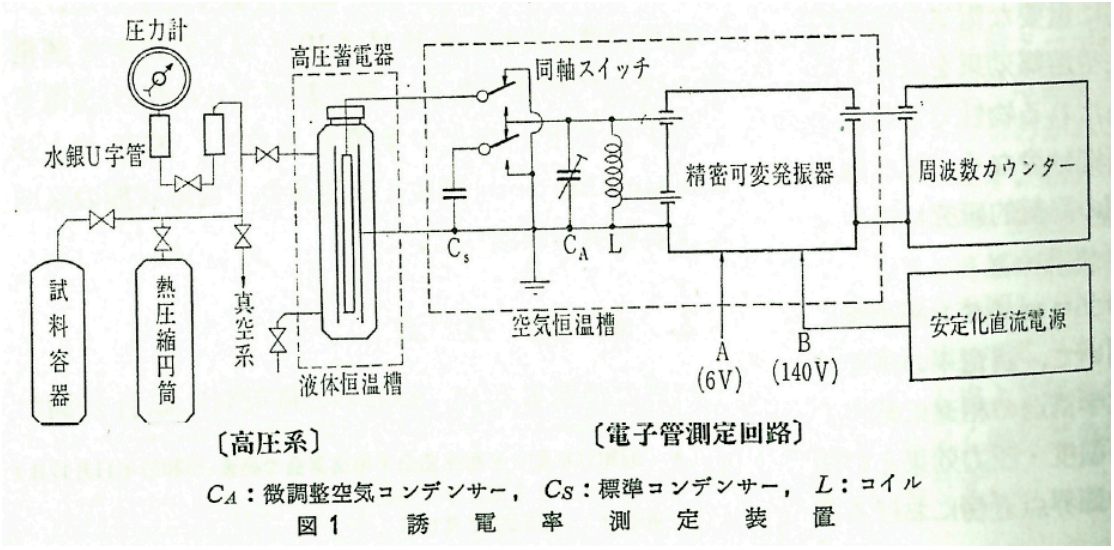


Fig. 5.3 Measurement Method One

Previously, there are several reports which have shown the methods of evaluation and measurement of the dielectric constant of the refrigerant and lubricating oil [38]-[41]. Fig. 5.3 shows a measurement method by applying a resonant frequency counter to measure the resonant frequency of sample to estimate the capacitance. Fig. 5.4 shows a measurement method by applying a small capacitance senor to connect to

the LCR tester to measure the capacitance directly. These methods can accurately measure the physical properties of the refrigerant and the lubricating oil by using a container or sensors for experiments. It is difficult to completely reproduce the refrigerant and the lubricating oil situation which exist between the windings and stator when the compressor is in operation. Therefore, it is difficult to be applied in the EMI study.

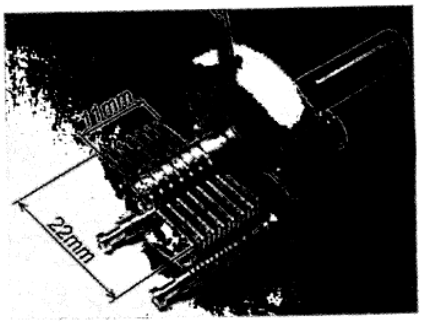


Fig.1 Variable condenser type sensor

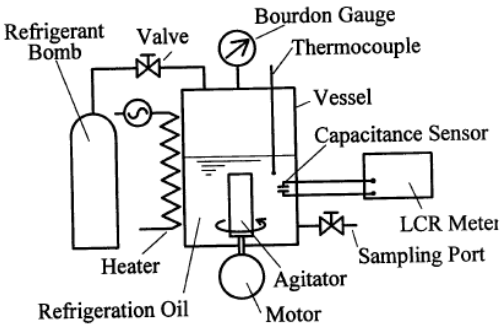


Fig.2 Experimental setup

Fig. 5.4 Measurement Method Two

In this research, by applying the method to identify the parasitic parameters according to the waveform of the high-frequency leakage current which is flowing through the ground line at the time of the inverter air conditioner in operation. Basing on the parasitic parameters of the high-frequency common-mode equivalent circuit, the parasitic capacitance between the coil and the frame of compressor motor can be estimated. And this kind of method has been proved that will provide sufficient accuracy in the motor research when it is working in the air [18][48][49]. By this method, it is possible to obtain a stray capacitance that reflects the situation of the refrigerant and the lubricating oil present between the motor windings and stator core when the compressor is running.

5.3 Predict about Permittivity

According to the research in Chapter 4, the high-frequency CM equivalent circuit of this compressor motor is shown as Fig. 5.5.

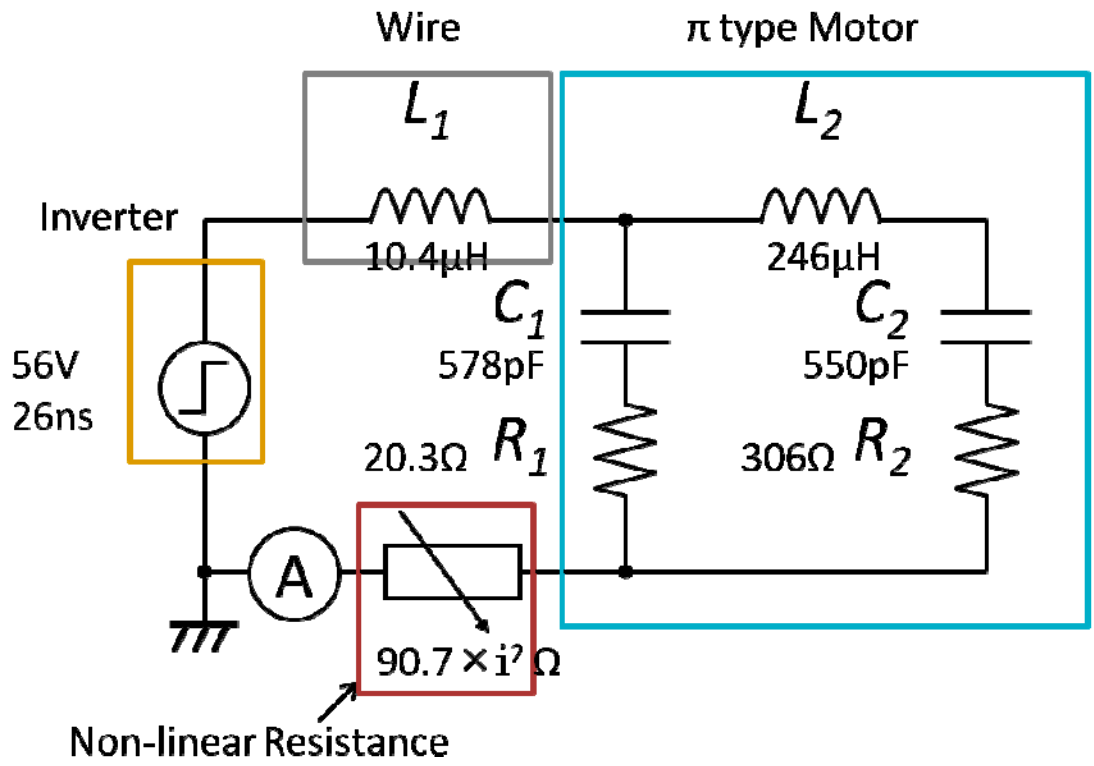


Fig. 5.5 High-Frequency CM Equivalent Circuit

To actually determine the dielectric constant of the refrigerant and the lubricating oil existing between the motor windings and the stator core during operation, and the capacitance measurements is carried out when there is no refrigerant and lubricating oil in the compressor. Fig. 5.6 shows the equipment connection. To measure the CM capacitance characteristic, the paint of the compressor case is peeled, and the three-phase input terminals are shorted together. These two points are connected to the LCR Hi-Tester to measure the parasitic capacitance of compressor motor with only air. Fig. 5.7 shows the measurement results of the motor stray capacitance, when the refrigerant and the lubricating oil are not encapsulated in the compressor.

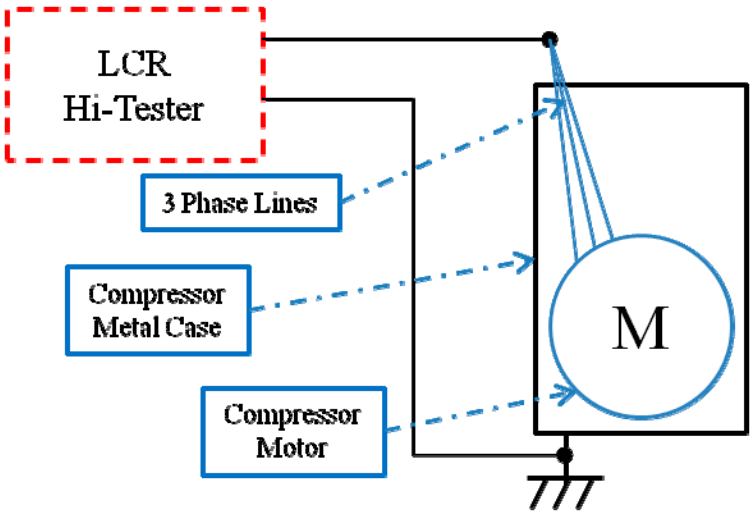


Fig. 5.6 Impedance Test of Compressor Motor without Refrigerant and Lubricaing Oil

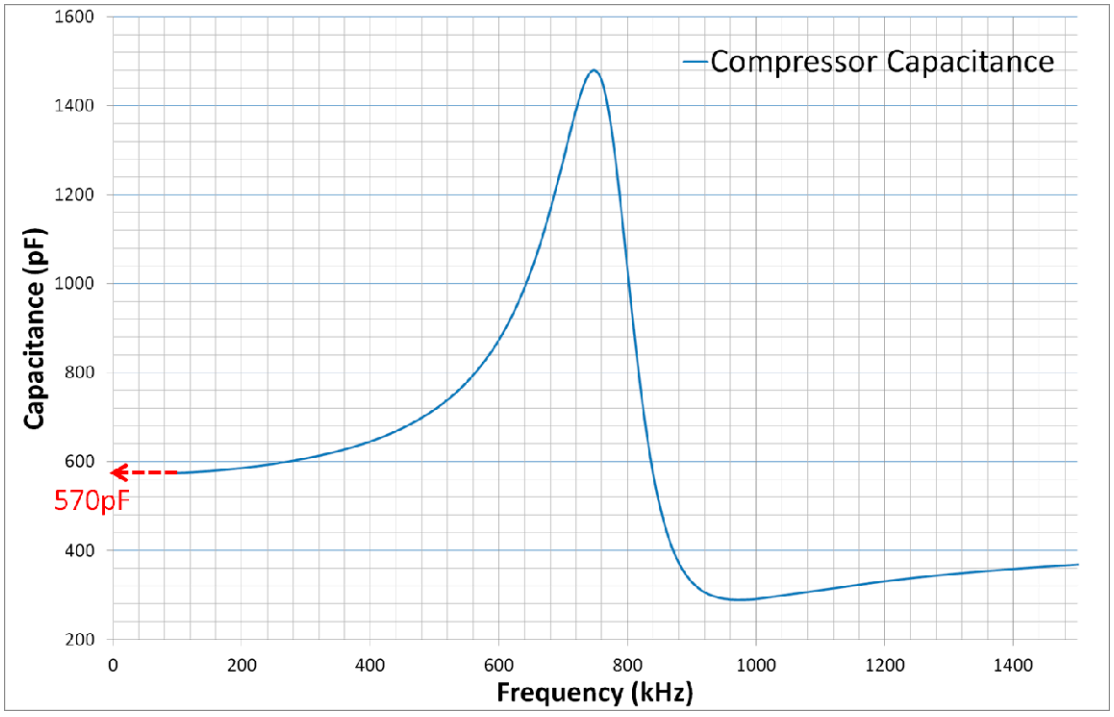


Fig. 5.7 Capacitance of Compressor without Refrigerant and Lubricating Oil

For the resonance phenomena of the winding, measured values of the capacitance greatly changes with frequency. Therefore, the true measurement is the capacitance of sufficiently low frequency without influence of the resonance phenomenon. As a result, the stray capacitance of the compressor motor when the

refrigerant and the lubricating oil are not encapsulated is 570 pF.

Meanwhile, Fig. 5.5 shows that the capacitance of sufficiently low frequency of the equivalent circuit can be determined as 578 + 550 = 1128 pF. Fig. 5.5 shows an equivalent circuit that it is obtained by identifying the high-frequency leakage current waveforms during compressor operation. Therefore, the parasitic capacitance is presented between the windings stator during the compressor in operation. Thus, by taking the ratio of the stray capacitance when the refrigerant and the lubricating oil is not encapsulated, the dielectric constant of the refrigerant and the lubricating oil in the compressor can be estimated as 1.98. Since the motor windings are widely distributed in the compressor chamber, wherein the resulting dielectric constant is not a local number, it is considered to represent the average value of the entire periphery between the winding and frame of the AC motor.

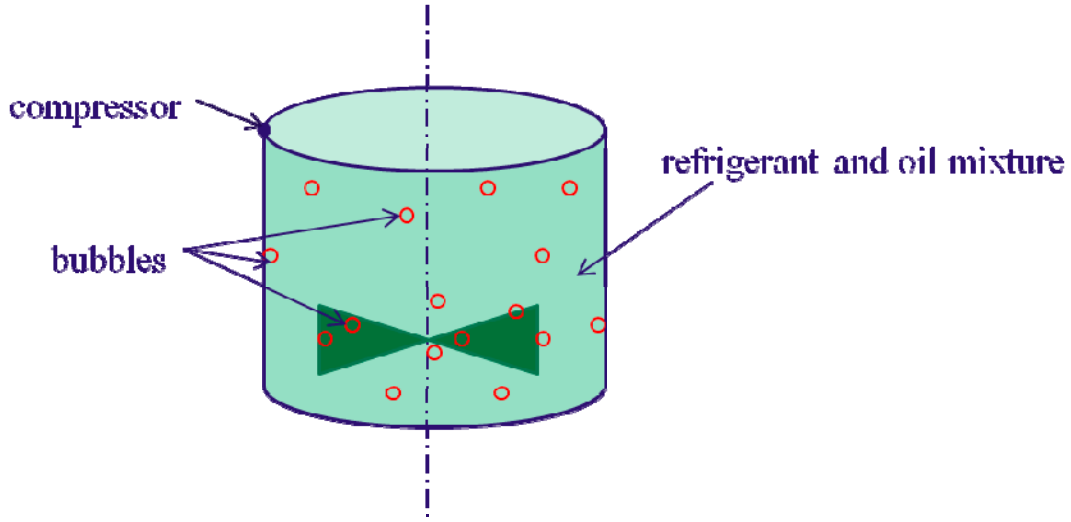


Fig. 5.8 Compressor with Refrigerant and Lubricating Oil in Operation

Thus, that the average dielectric constant of the refrigerant and the lubricating oil that exists between the motor windings and stator core is measured, which is difficult to measure before, and it is estimated by applying a high-frequency equivalent circuit. Although this estimate general refrigerant and lubricant mixture is smaller than the relative permittivity [33], this is due to the generation of bubbles. However, since it is

not possible to observe the internal state in this experimental apparatus, and this confirmation is the future work.

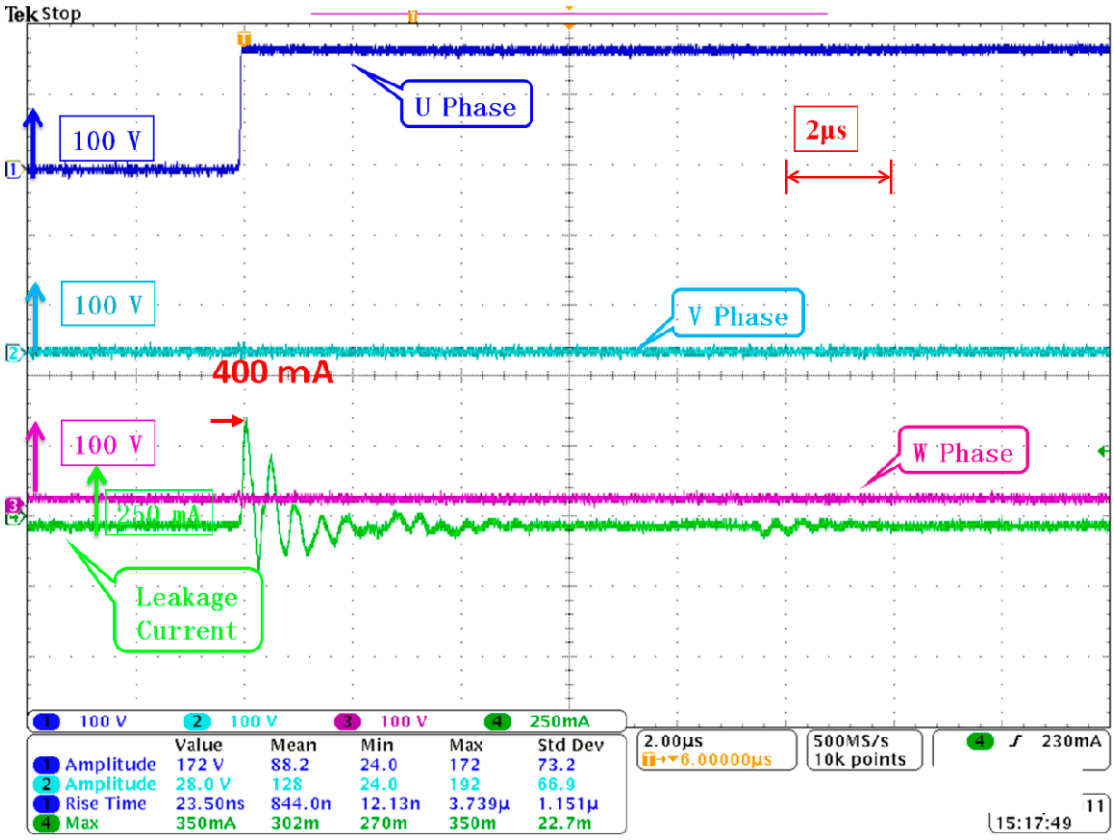


Fig. 5.9 Leakage Current Waveform of One Phase Switching at Compressor Just Running

Fig. 5.8 shows the picture when the compressor is running with refrigerant and lubricating oil. At this moment the bubbles will appear. It is difficult to duplicate the situation under compressor running according to the researches before. Fig. 5.9 shows the picture of leakage current when the compressor is just running. At this moment, the leakage current is 400 mA. It is a little higher than the current 370 mA which is applied to calculate in this research before. This is because the situation of refrigerant and lubrication oil mixture in the compressor is changing as time going on. Therefore, it is helpful to duplicate the situation instantaneously when the motor is running.

Fig. 5.10 shows the picture that the parasitic capacitance between compressor

windings and stator. The blue line is the parasitic capacitance and the red the line is the temperature at that moment. Temperature will affect the capacitance. And as time going on, the capacitance will increase. That is why the leakage current in Fig. 5.9 will higher than the current 370 mA after over 1 hour running.

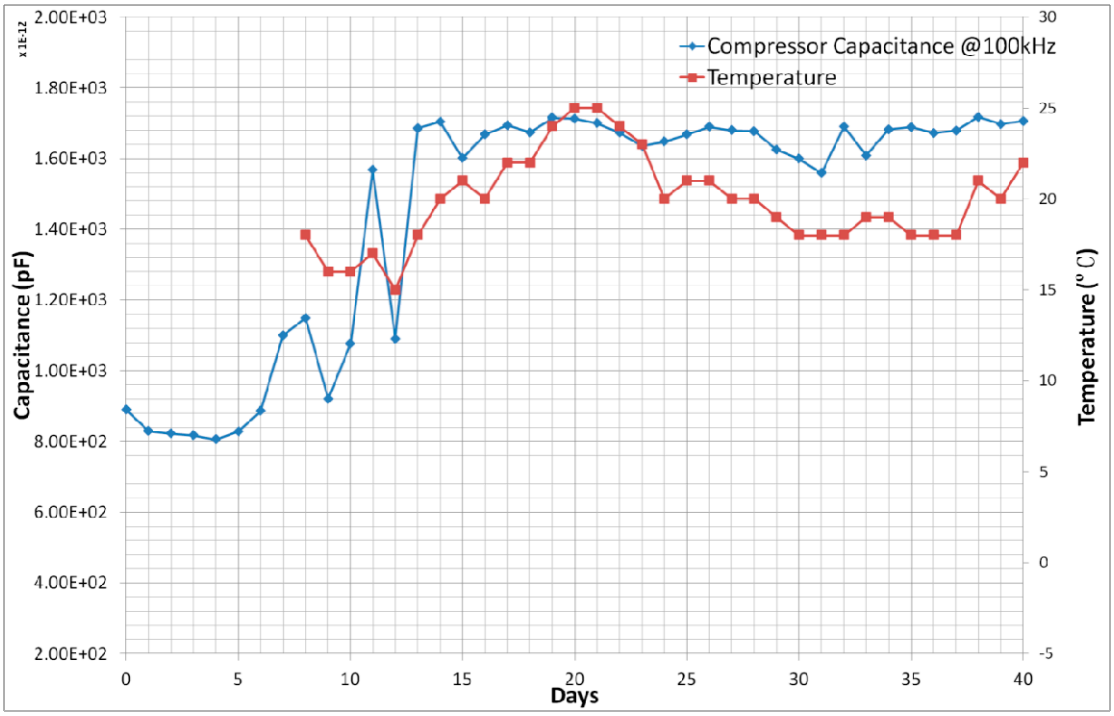


Fig. 5.10 Parasitic Capacitance between Compressor Motor Windings and Stator as Time Going on

5.4 Summary

HFC is widely applied as the permittivity, instead of CFC and HCFC, in order to protecting the environment. But the permittivity of mixture with HFC and oil is larger than the permittivity of HCFC and oil. And higher parasitic capacitance is more conductive to the leakage current conduction. Therefore, the research about the permittivity of refrigerant is important and necessary.

In the past, it is difficult to measure the parasitic capacitance of motor when the motor is running. In Chapter 5, a high-precision equivalent circuit makes it become possible and easy. And the parasitic capacitance can be speculated, when the motor does not run for a long time. So the permittivity of mixture which is made up the lubrication oil and refrigerant can be accurately predicted for the first time.

The proposed method has the following features.

(1) It does not require special laboratory equipment and sensors.

(2) It is possible to estimate the stray capacitance when the compressor is in operating state.

(3) It can be estimated only in a short period of time according to waveform data.

(4) It is helpful to duplicate the situation instantaneously when the motor is running.

Stray capacitance has been estimated by the proposed method. It can provide useful information to EMI studies with the inverter air conditioner inverter in operation. Furthermore, since it can be estimated from the short-time waveform data immediately in operation, it is considered to be available also to elucidate the volume relationship between the fast changes in capacitance with the conditions of the compressor are operating.

Chapter 6 Research and Design System for EMI Problem

6.1 Novel EMI Design System and Experiment Equipment

6.1.1 Novel EMI Design System

In the past, the designer designs the product, the product is assembled, then measure the EMI noise. If the test result could not fill the EMI standard, the product will be design again. The procedure is shown as Fig. 6.1 left part. This kind of design flow will waste long time and lead to high cost.

This research will improve the design process like this. After the design, the EMI noise can be simulated through the computer-aided software. According to the experiment test result to built the equivalent circuit and calculate the parameters through some method. It is shown as Fig. 6.1 right part.

The complex model can represent the circuit well, but it will increase the simulation time. How to get the appropriate model is important. And the Power electronics devices have many parts. In order to predict the EMI noise, it must be known the model of every part. So it is need to build a parts library. According to the system connection diagram, the separate parts models can be connected to a system equivalent circuit. Then according to this system equivalent circuit it can be got the simulation result to predict the EMI noise level. this research will focus on these two points, how to build the optimized equivalent circuit and calculate the parameters by

computer-aided software and how to connect parts models together as a system equivalent circuit. It is shown as Fig. 6.2.

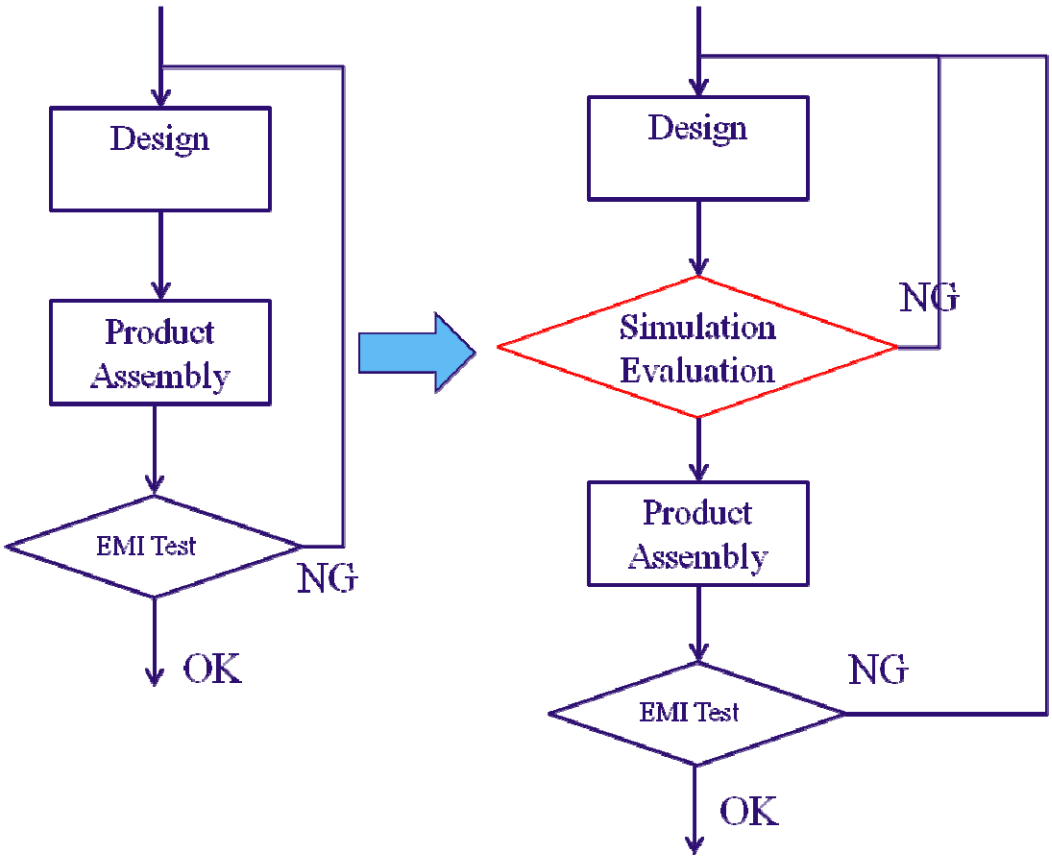


Fig. 6.1 Improvement of EMI Design Flow

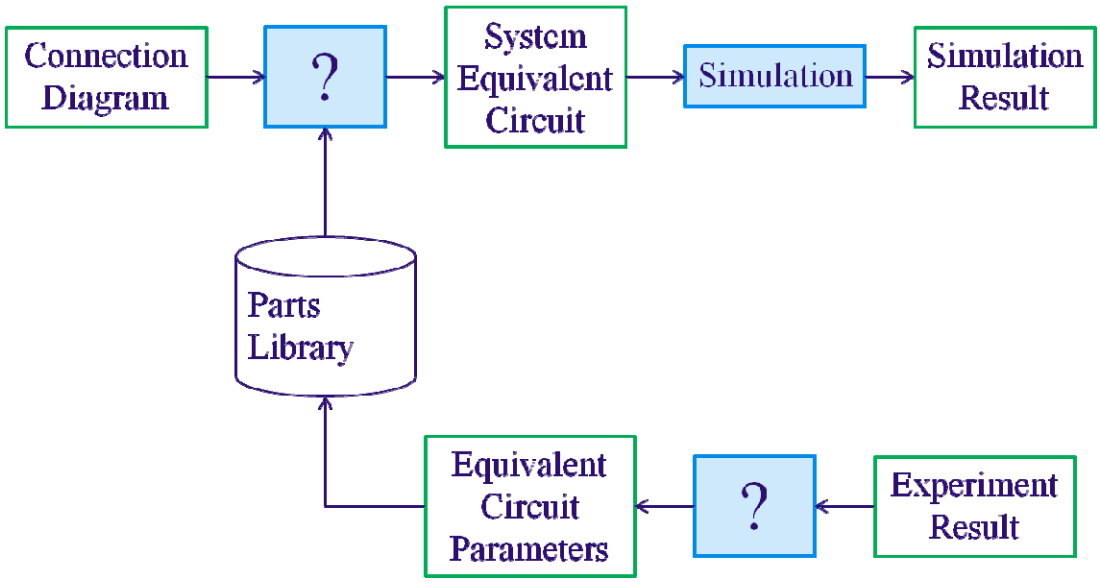


Fig. 6.2 Research Flow Chart

6.1.2 Experiment Equipment

Toshiba air conditioner ROA-AP1405H and the oscilloscope with high accuracy are adopted to analyze the CM leakage current. The list of experiment equipments are shown as Table 6-1.

Table 6-1 List of Equipments

Name	Brand	Model
Air Conditioner	Toshiba	ROA-AP1405H
Oscilloscope	Tektronix	MSO4034
Current Probe	Tektronix	TCP0150
Voltage Probe	Tektronix	P5205
LISN	DK	KNW-341F
Signal Analyzer	Agilent Technologies	N9010A
Attenuator	Agilent Technologies	8495A
LCR Hi-Tester	HIOKI	3535

6.1.3 Connection of equipments

Air conditioner is composed by indoor section and outdoor section. Indoor section is connected to the power supply in the laboratory. An oscilloscope (Tektronix MSO4034) is adopted to measure the CM leakage current in the ground line of the system. The leakage current is measured with the current probe (Tektronix TCP0150). And the phase voltage of the inverter can be measured with the voltage probe (Tektronix P5205). In order to analyze the EMI noise, signal analyzer (Agilent

Technologies EXA Signal Analyzer N9010A), attenuator (Agilent Technologies 8495A Attenuator/70dB) and LISN (DK KNW-341F) are applied. The connection of experimental equipment including an inverter air conditioner is shown as Fig. 6.3. The air conditioner picture for experiment is shown as Fig. 6.4. And according to the instruction of LISN, the equivalent circuit of LINS can be shown as Fig. 6.5.

In Chapter 4, the CM equivalent circuit is discussed in the time domain. The model is built according to the leakage current. In this chapter, the CM equivalent circuit will be discussed in the frequency domain. For the standard of CM EMI noise, the test frequency range is form 150 kHz to 30 MHz. All this data can be measured by applying the signal analyzer. The equivalent circuit will be calculated by comparing the impedance with the experiment data which is measured by LCR hi-tester (HIOKI 3535). Before the discussing of equivalent circuit, the effect of EMI is confirmed firstly.

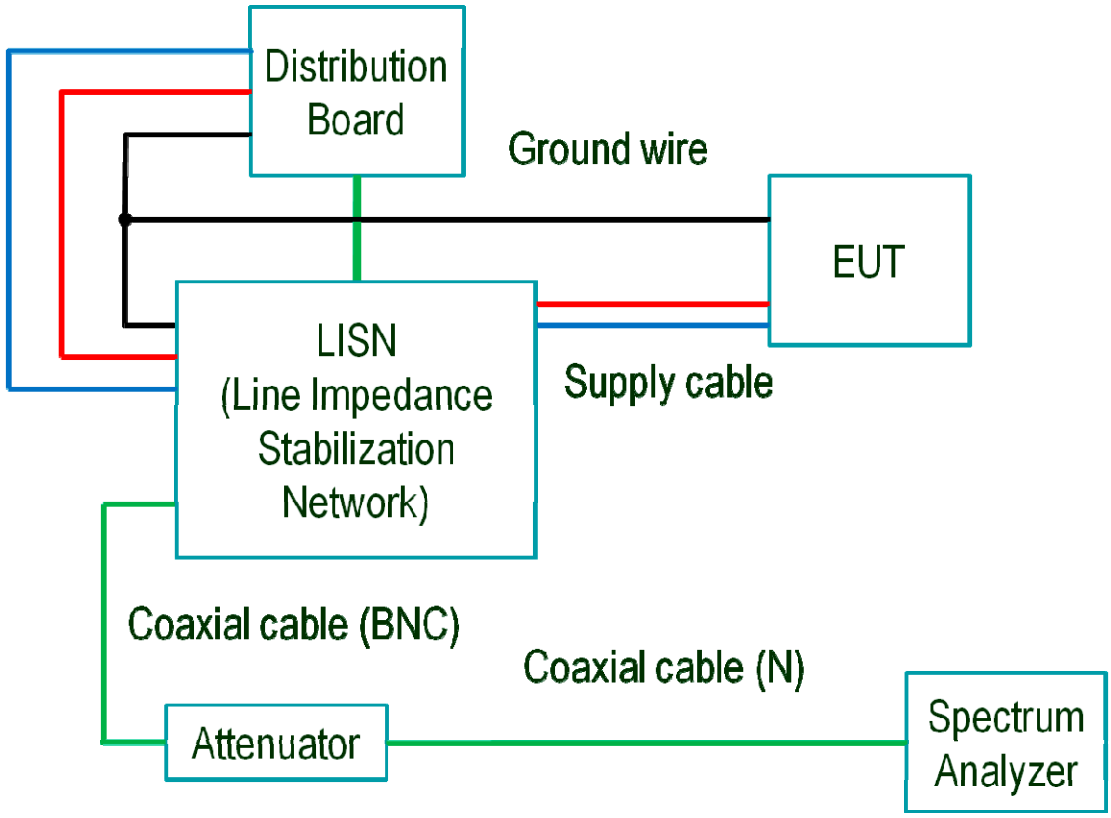


Fig. 6.3 Connection Diagram of Experiment for EMI Noise Level



Fig. 6.4 Air Conditioner Picture for Experiment

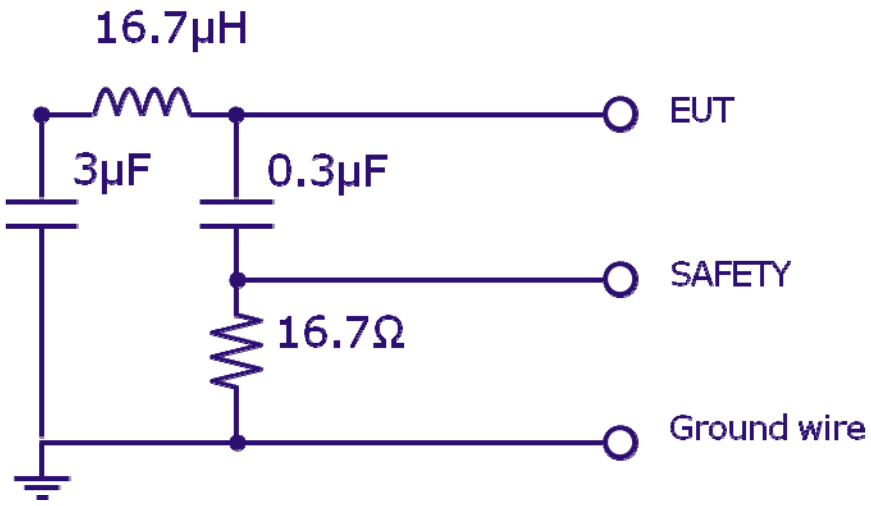


Fig. 6.5 Equivalent Circuit of LISN

6.2 Effect of EMI Filters

The air conditioner is divided into two main parts, outdoor part and indoor part. These two parts is connect through the power cables and pipe which is used for refrigerant and lubrication oil flowing. And there are three main noise sources, the inverter for compressor motor, the inverter for outdoor fan and the inverter for indoor fan.

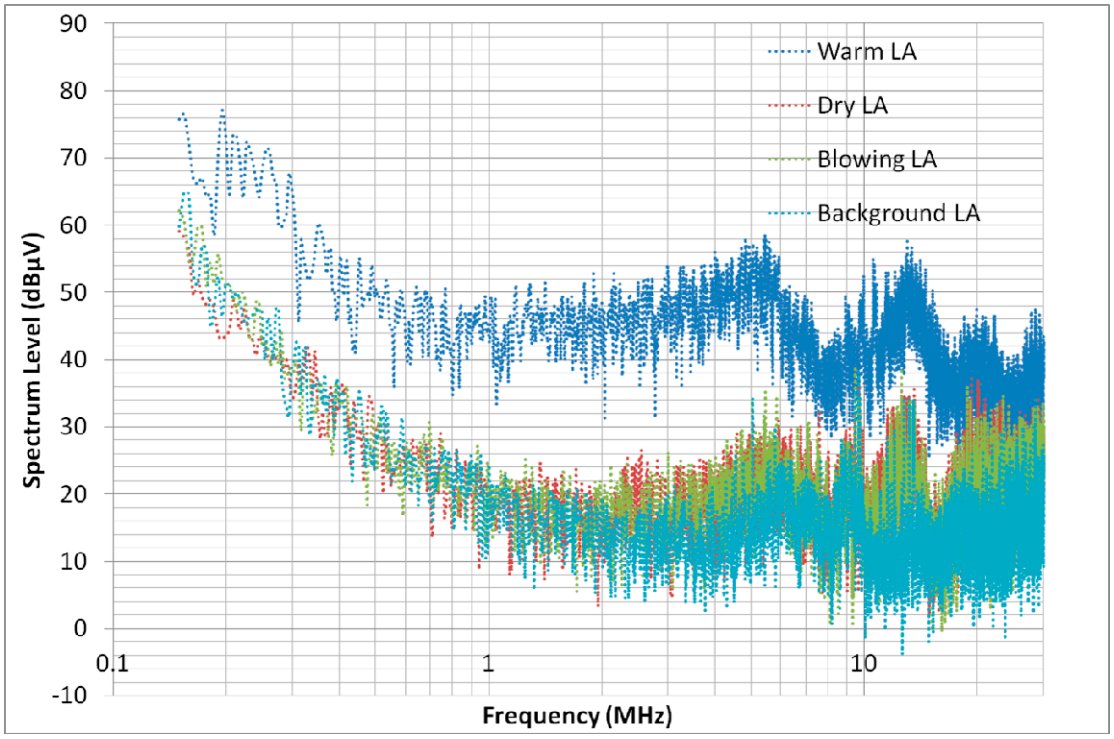


Fig. 6.6 E Noise Level of Every Running mode

There are four operation modes, warming mode, cooling mode, blowing mode and drying mode. Fig. 6.6 shows the noise level of each mode, and it has been confirmed that the noise level of warming mode is the same with cooling mode in Chapter 2. The blue point line is noise level of warming mode. The red point line shows the noise of drying mode. The green point line is the noise of blowing mode. And the cyan point line is the background noise. At this moment, all EMI filters are acting. When the air conditioner is working as warming mode, the noise comes to the peak. This is because the compressor motor is running, and the motor system is the

major EMI noise source. On the other hand, when the air conditioner is running as the drying mode and blowing mode, the noise level is quite close to the background noise. It means the EMI filter is effective.

6.2.1 Outdoor Part of Air Conditioner

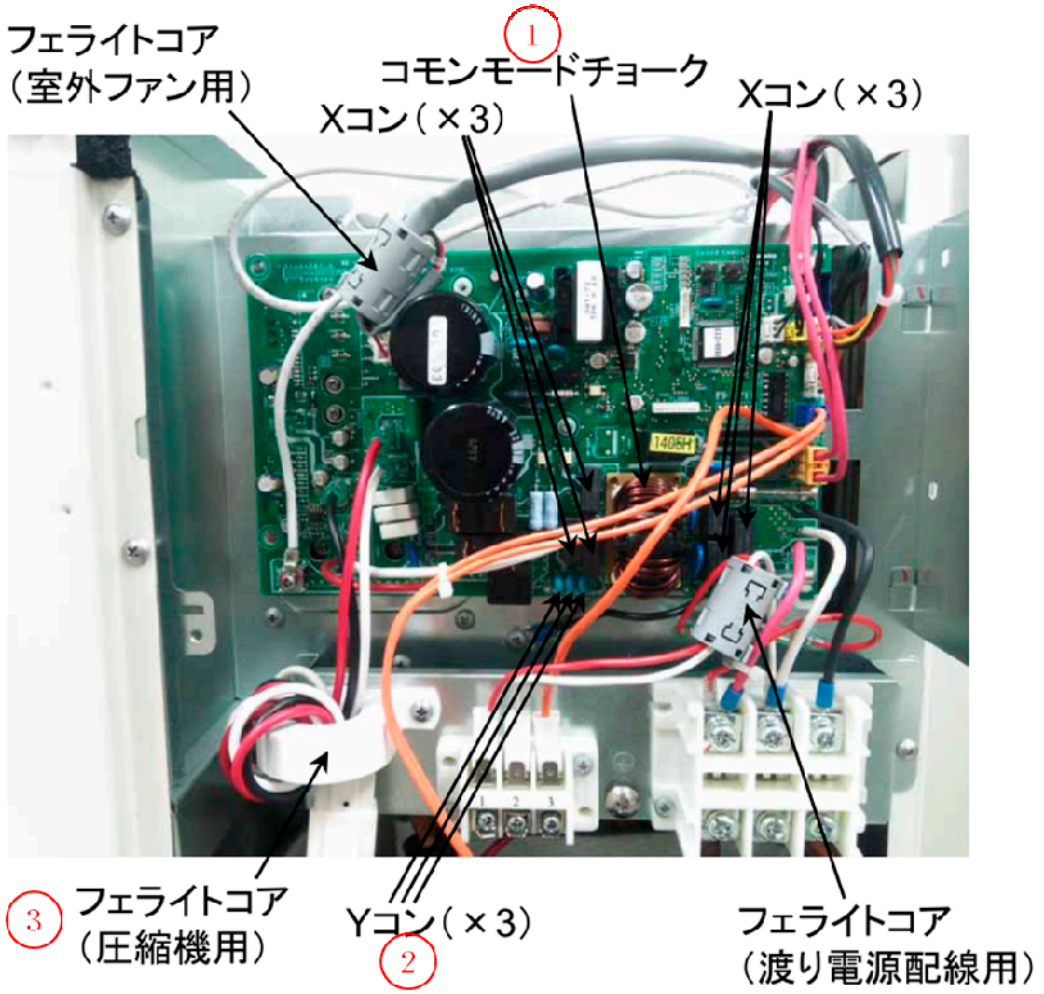


Fig. 6.7 EMI Filter Of Outdoor Part

The outdoor circuit board is shown as Fig. 6.7. There are three kinds of EMI noise filter, common-mode choke, Y capacitance and ferrite core. The EMI filters are taken away in proper order (as shown the red number in Fig. 6.7) to clarify the effect of everyone.

The common-mode choke is most important EMI filter and taken away first. The noise level is shown as orange point line Fig. 6.8. By comparing the noise level with

all EMI filter, it can be confirmed that the common-mode choke is effective in the low frequency range until 5 MHz. Then the Y capacitance is taken away. And the red point line in Fig. 6.8 shows the noise. By comparing the noise level with the noise without common-mode choke, it can be confirmed that the Y capacitance is effective in the frequency range between 5 MHz to 10 MHz. Finally, the ferrite core on the power cables is taken away, which is used for the compressor motor power serving. And the noise level at this moment is shown as green point line in Fig. 6.8. By comparing the noise level with the noise without common-mode choke and Y capacitance, it can be confirmed that, the ferrite core on the power cables of compressor motor is effective in the frequency range over 10 MHz.

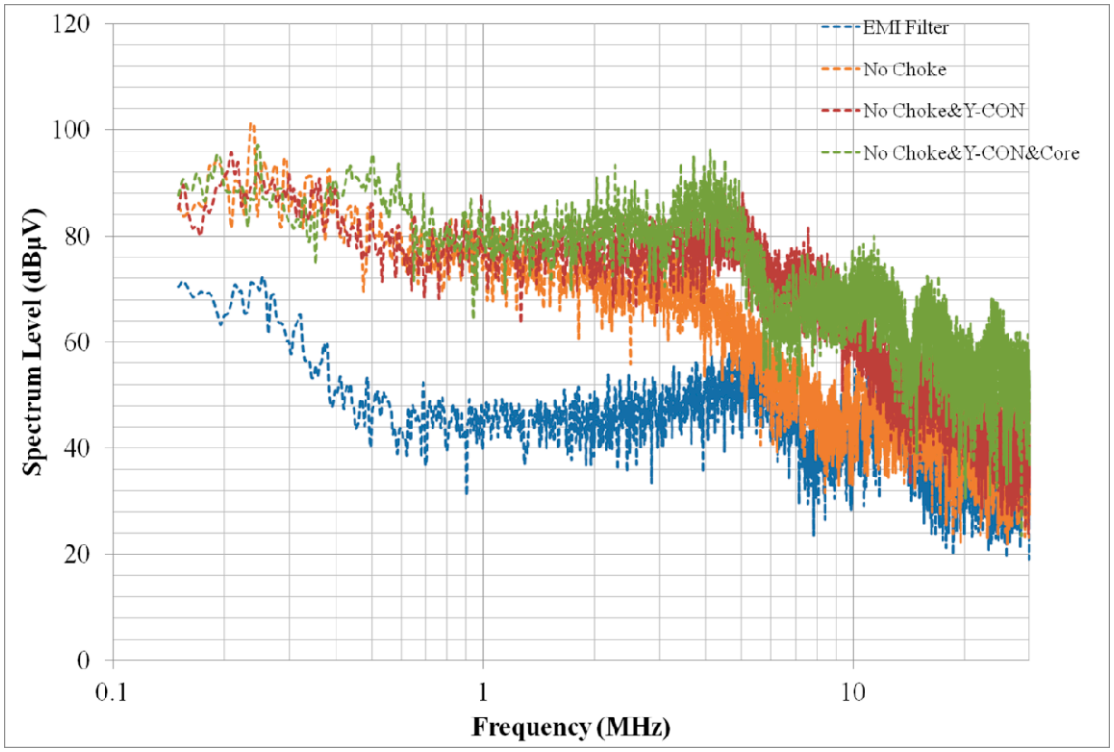


Fig. 6.8 Noise Level of Every Running mode

And then, the ferrite core on the power cable is taken away, which is used for outdoor fan power serving. The noise level is shown as Fig. 6.9, when the air conditioner is running as the blowing mode. At this moment, only the fan is running. The blue line shows the noise with the ferrite core, and the red line shows the noise

without the ferrite core. It means that the ferrite core on the power cables of outdoor fan is effective in the frequency range over 10 MHz.

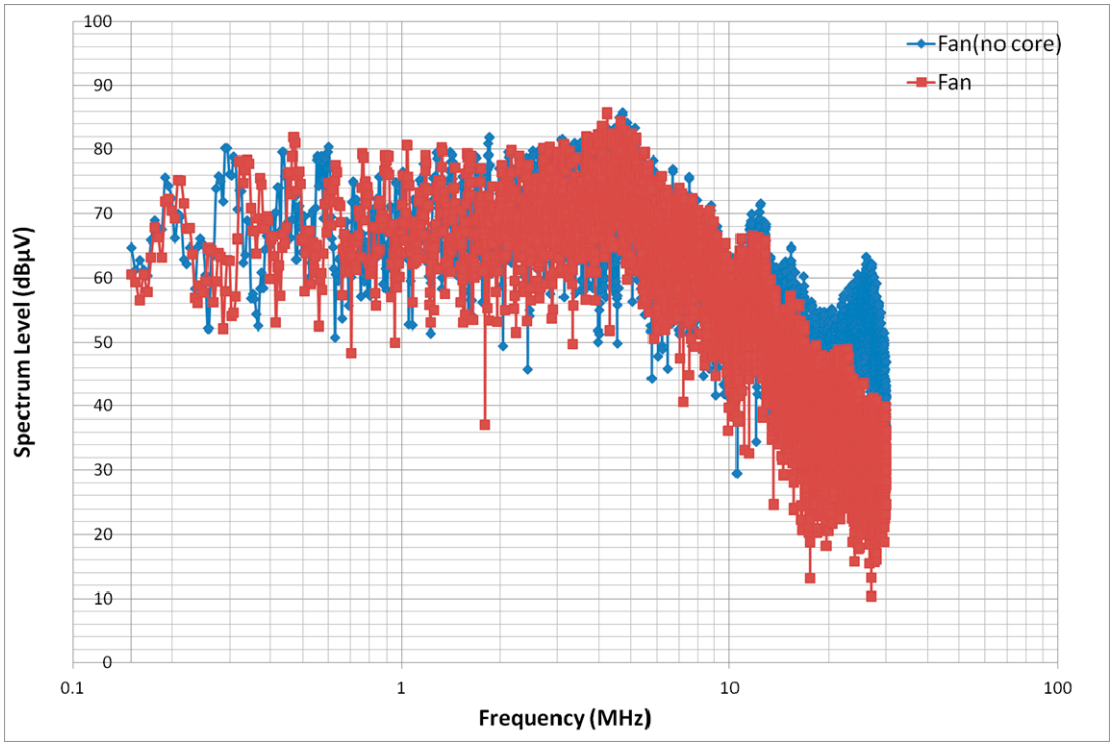


Fig. 6.9 Noise Level about Outdoor Fan Ferrite Core

6.2.2 Outdoor Leakage Current of Air Conditioner

Chapter 4 shows a method to estimate the equivalent circuit according to the leakage current of ground line. So the leakage current in this system is measure by an oscilloscope. Fig. 6.10 shows the leakage current when the compressor motor is running. Fig. 6.11 shows the leakage current when only the fan is running. The red line shows the current when two phases of outdoor fan inverter is switching at the same time. And the blue line shows the current when only on phase in switching. This phenomenon has not happened in the motor inverter because of the fed method. When the motor is running, the leakage current comes to 1.75 A. When only one phase of outdoor fan inverter is running, the leakage current comes to 0.344 A and 0.174A. Therefore, the system of outdoor fan part is linear.

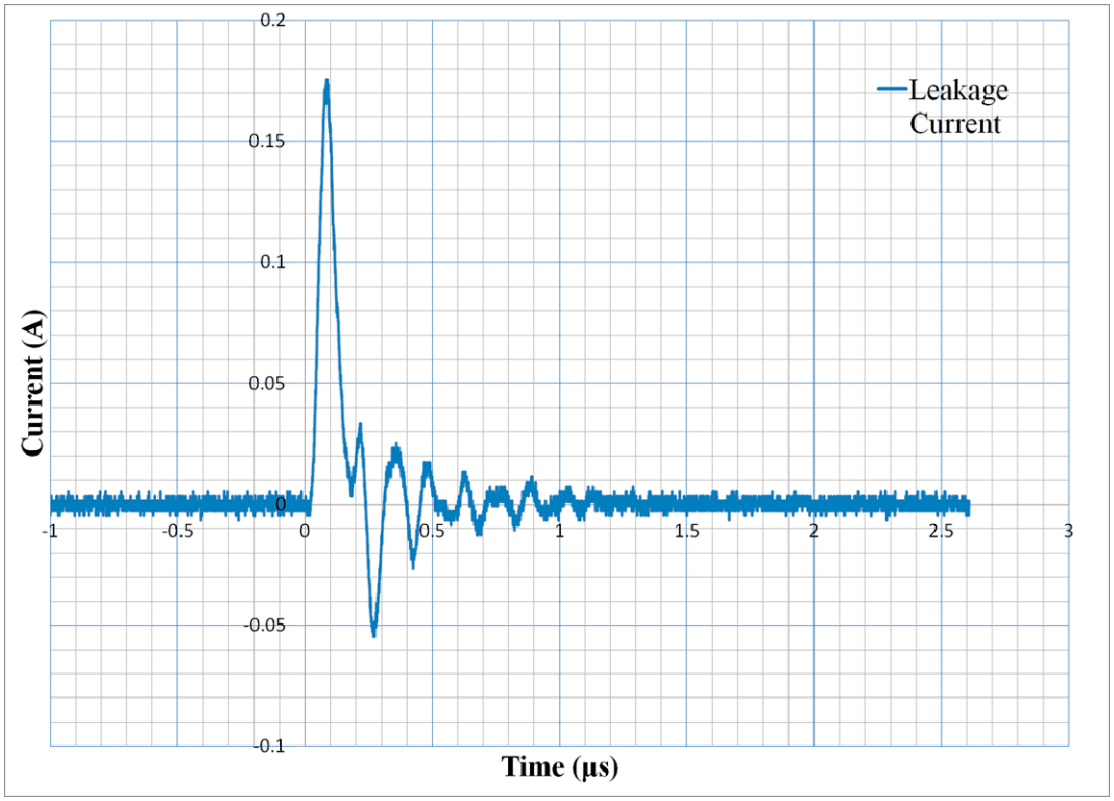


Fig. 6.10 Leakage Current of Warming Mode

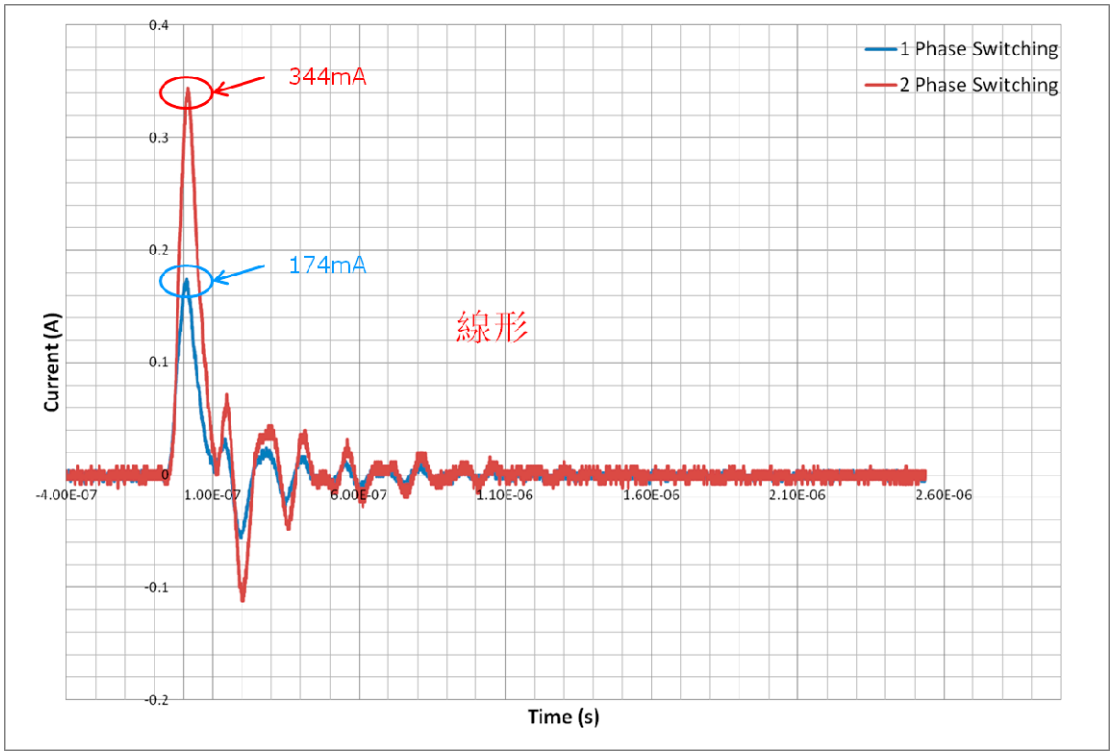


Fig. 6.11 Leakage Current of Blowing Mode

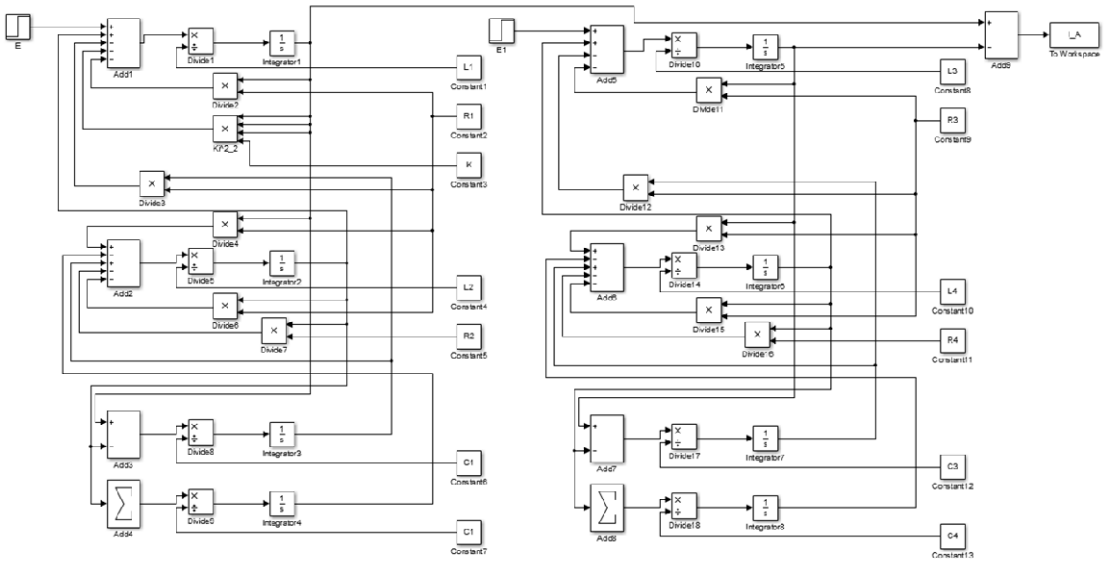


Fig. 6.12 MATLAB Model for modeFRONTIER

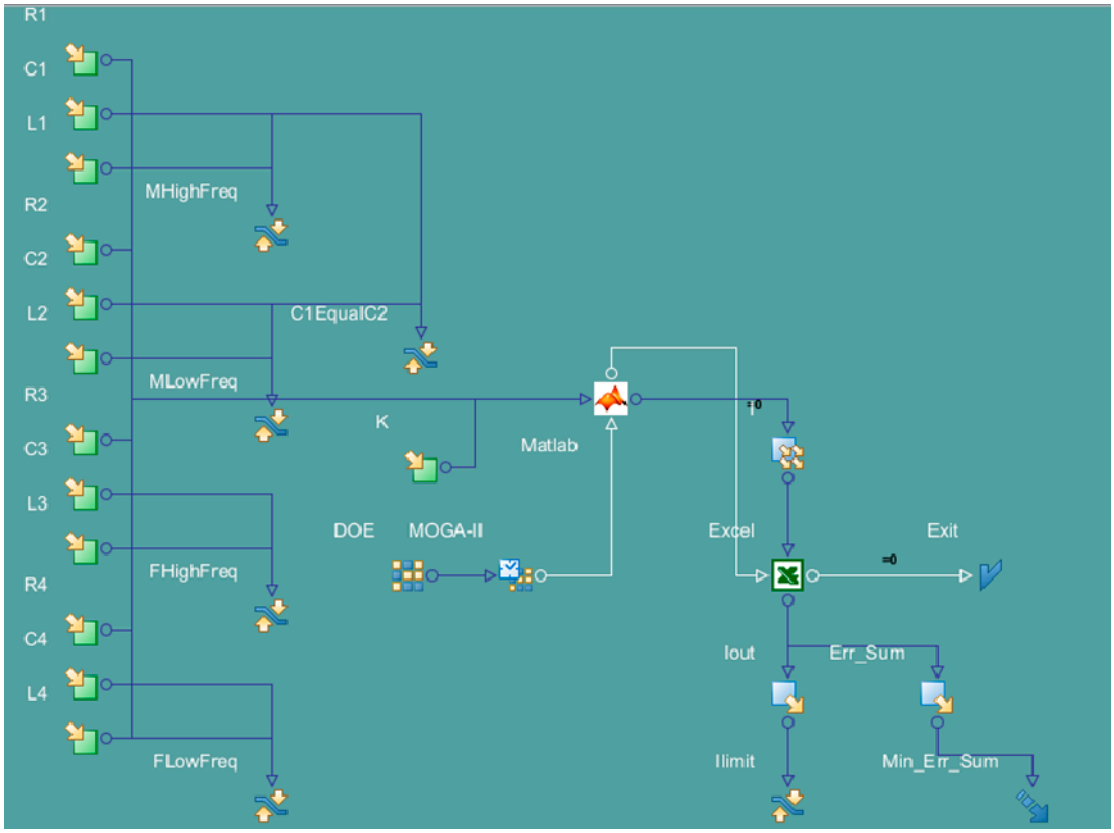


Fig. 6.13 Outdoor modeFRONTIER Model

The leakage current from outdoor fan is smaller than the leakage current from compressor motor. But it cannot be neglected. The method mentioned in Chapter 4 is

applied again. Fig. 6.12 shows the MATLAB model for modeFRONTIER simulation. Fig. 6.13 shows the modeFRONTIER model.

But the simulation is negative. This is because the input variables number of this model is 6 more than the one in Chapter 4. Even if every variable is calculate 1000 times. The total number of calculation will increase 1000^6 times. Therefore, the cost will very considerable when the simulation is completed. This is not economy method. Finally the traditional method is applied to calculate the equivalent circuit by measuring the impedance. Before measuring the impedance, the indoor EMI filter is discussed.

6.2.3 Indoor Part of Air Conditioner

The indoor circuit board is shown as Fig. 6.14. There are also three kinds of EMI noise filter, common-mode choke, Y capacitance and ferrite core. The EMI filters are taken away in proper order as same as outdoor experiment to clarify the effect of everyone.

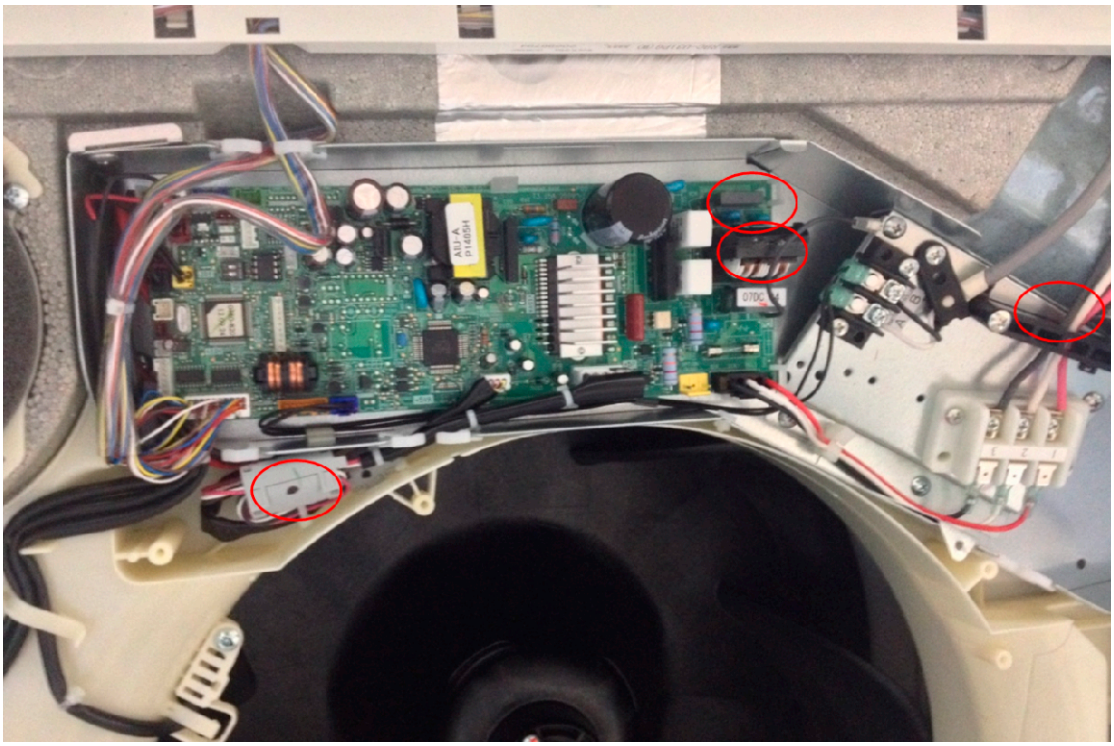


Fig. 6.14 EMI Filter Of Indoor Part

The common-mode choke is taken away first. The noise level is shown as blue point line in Fig. 6.15. By comparing the noise level with indoor EMI filter as shown as red line in Fig. 6.15, it can be confirmed that the common-mode choke is effective in the low frequency range until 5 MHz. Then the Y capacitance is taken away. And the green point line in Fig. 6.16 shows the noise. By comparing the noise level with the noise without only common-mode choke as shown as the red line in Fig. 6.16, it can be confirmed that the Y capacitance is effective in the frequency range between 1 MHz to 10 MHz. Thirdly, the ferrite core on the input power cables is taken away, which is connected with outdoor part. And the noise level at this moment is shown as purple point line in Fig. 6.17. By comparing the noise level with the noise without common-mode choke and Y capacitance, it can be confirmed that, the ferrite core on the power cables of compressor motor is effective in the frequency range over 10 MHz.

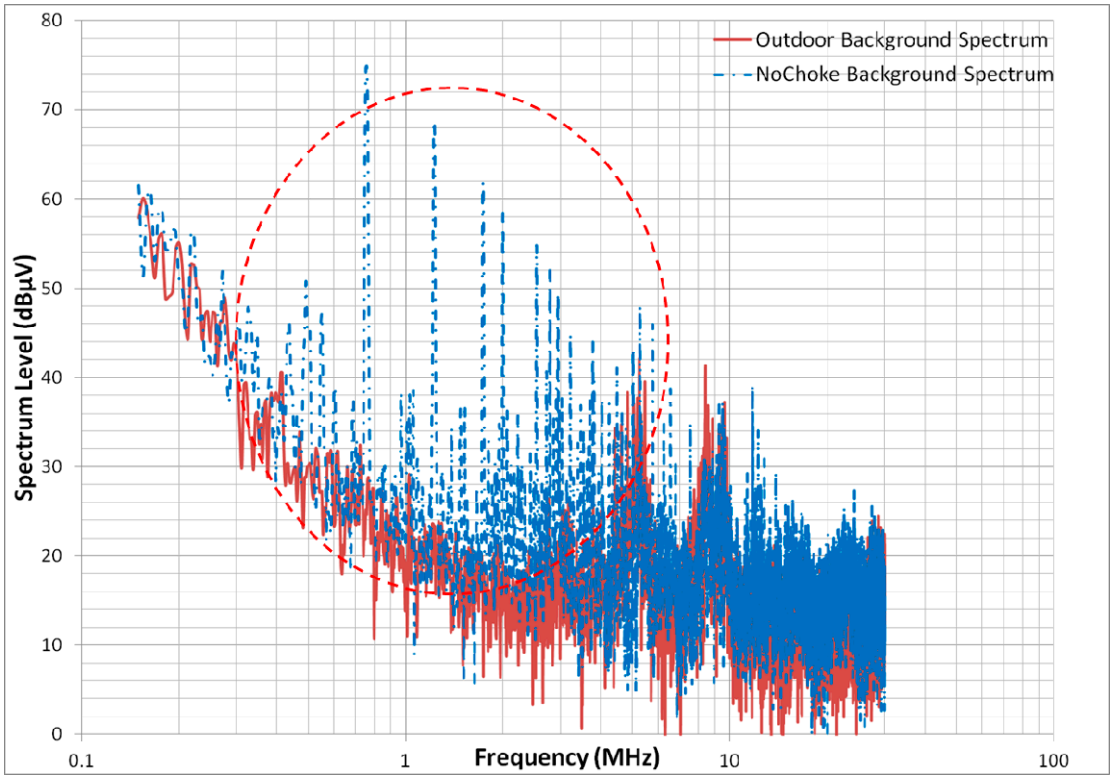


Fig. 6.15 Effect of Indoor CM Choke

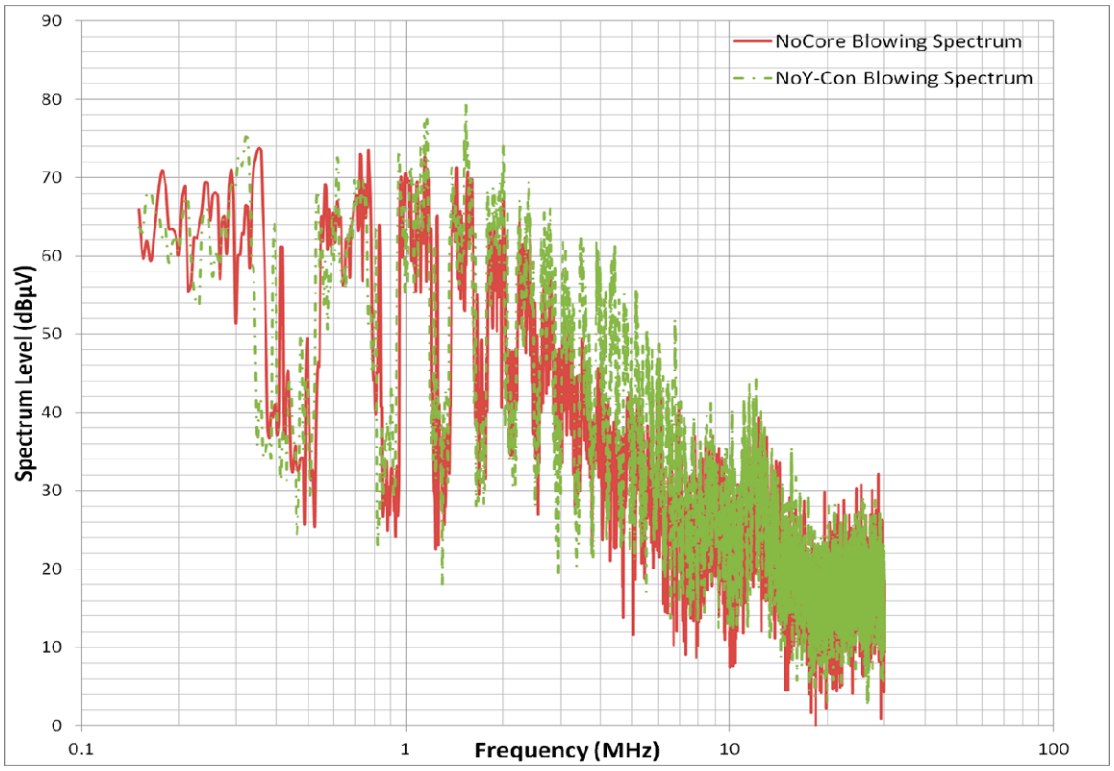


Fig. 6.16 Effect of Indoor Y Capacitance

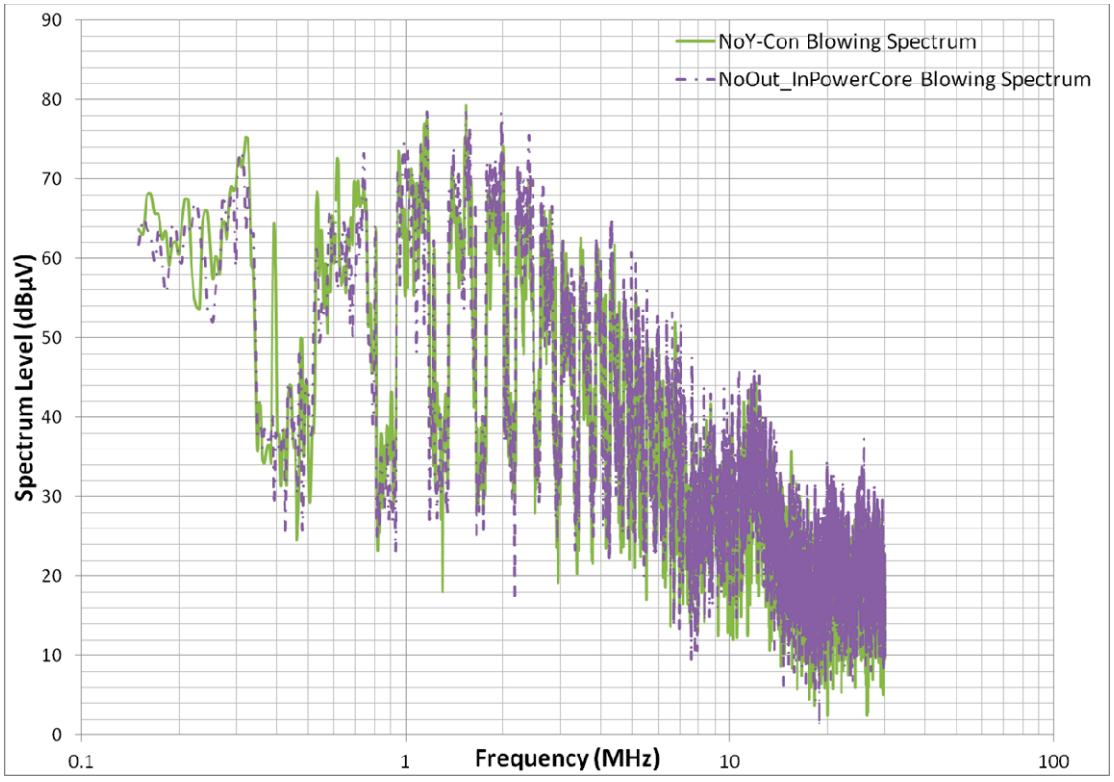


Fig. 6.17 Effect of Indoor Ferrite Core on Power Cables

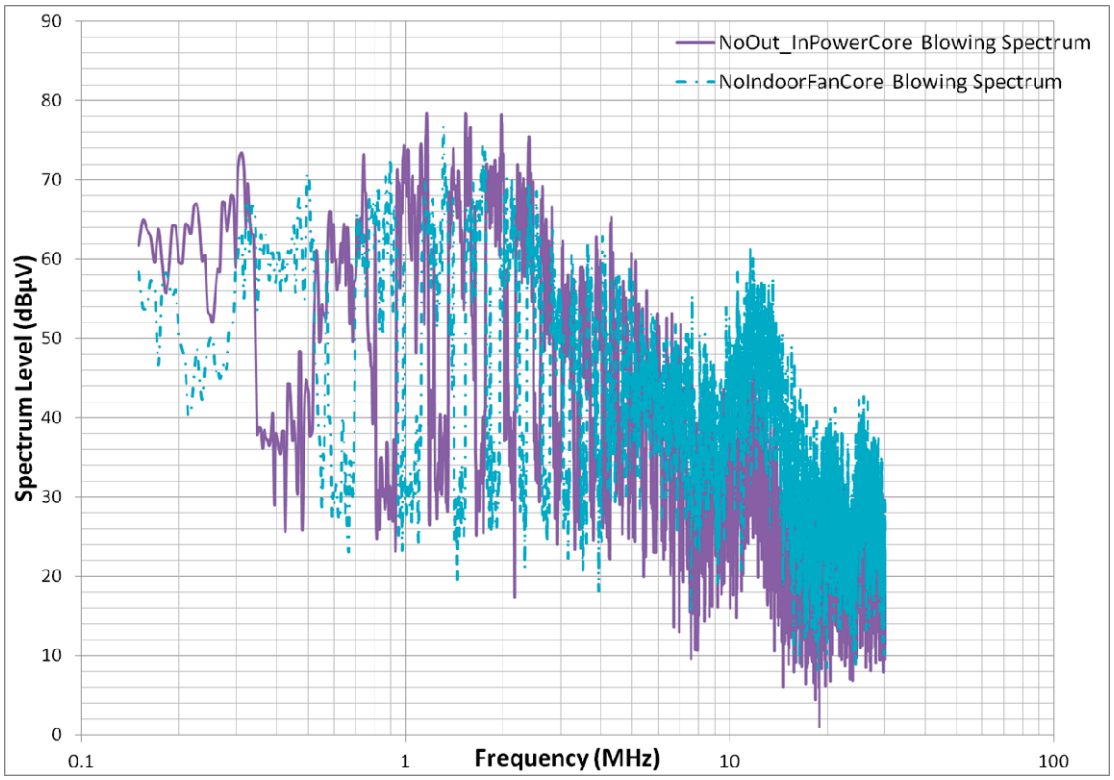


Fig. 6.18 Effect of Indoor Ferrite Core on Fan Cables

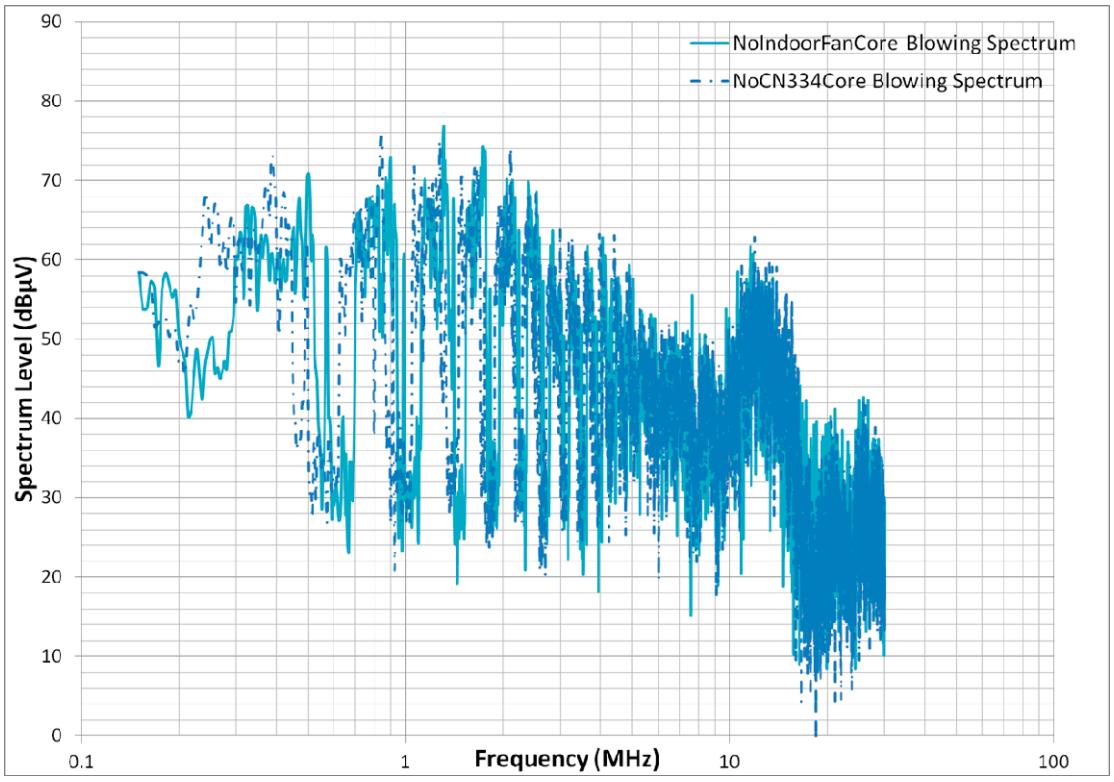


Fig. 6.19 Effect of Indoor Ferrite Core on Control Signal Cables

Fourthly, the ferrite core on indoor fan power cables is taken away, which is used for indoor fan power serving. And the noise level at this moment is shown as cyan point line in Fig. 6.18. By comparing the noise level with the noise without common-mode choke, Y capacitance and ferrite core on power cables, it can be confirmed that, the ferrite core is effective in the frequency range over 10 MHz. Finally, the ferrite core on control signal cables is taken away. The noise is shown as blue point line in Fig. 6.19. By comparing the noise level with the data before, it can be confirmed that the noise is almost the same. Therefore, there is almost no noise comes from the control signal cable. This ferrite core can be canceled for cost down from the perspective of EMI noise.

6.2.4 Noise Sources of Air Conditioner System

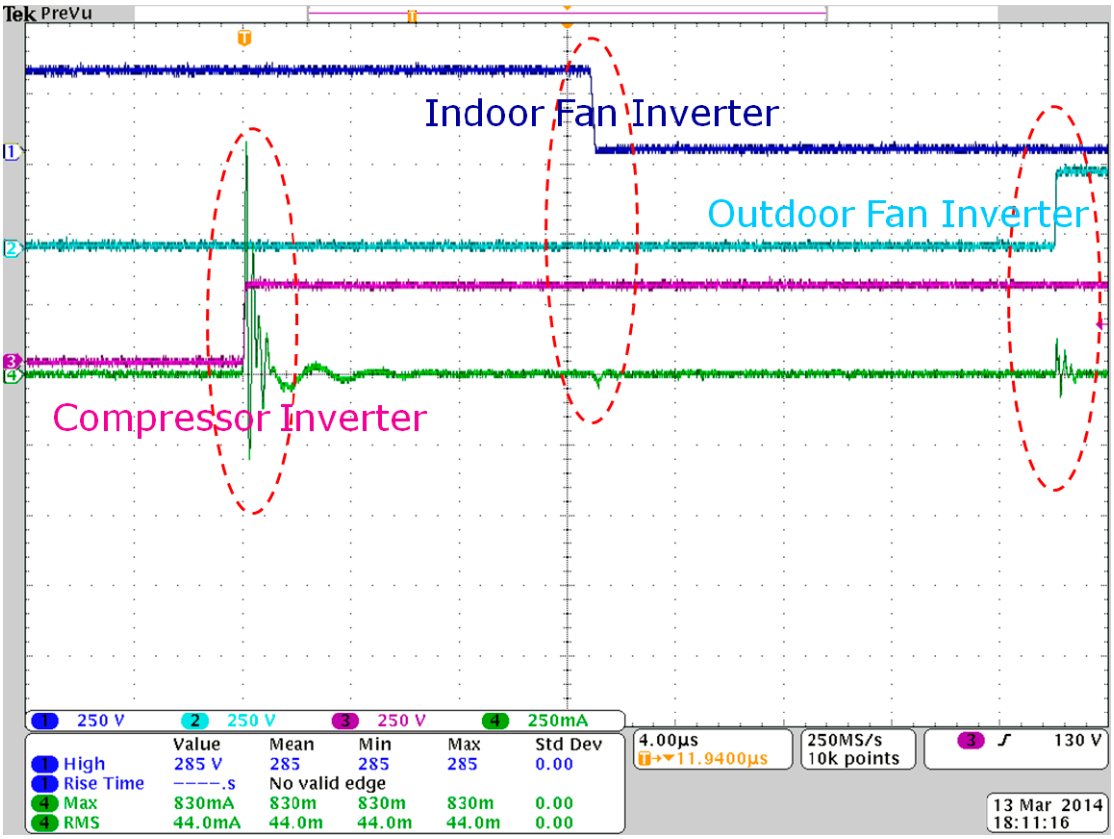


Fig. 6.20 Different Noise Sources of Air Conditioner System

Before the construction of system equivalent, the CM EMI noise sources are

discussed. There are three main noise sources in this air conditioner system. The most serious noise source is the PWM inverter which is used for compressor motor driving. The other noise source is the inverter for outdoor fan driving. Another noise source is the inverter for indoor fan driving. When the inverter is running as a very fast switching, because of the switching time is quite short, *dv/dt* and *di/dt* become considerable, the high-amplitude and high-frequency leakage current will occur. And the leakage current noise level shows the impact of EMI. The green line in Fig. 6.20 shows the leakage current on the ground line. The blue line shows the inverter voltage for indoor fan. The cyan line shows the inverter voltage for outdoor fan. The magenta line shows the inverter voltage for compressor motor. When the inverters are switching, the leakage current happened. The leakage current comes to the peak when the motor inverter is switching, then the outdoor fan inverter. When the indoor fan inverter is switching, the leakage current basically unchanged.

Therefore, it can be confirmed that the inverter of compressor motor is the most serious noise source, then the outdoor fan inverter. There is almost no leakage current from the indoor fan inverter.

6.3 Equivalent Circuit of Every Part According to the Impedance Characteristics

Before the calculation, the accuracy of LCR hi-tester is confirmed and Table 6-2 shows the result. Frequencies 100 kHz, 1 MHz and 5 MHz are chosen to verify the accuracy by measuring the same sample. According to Table 6-2, the accuracy is enough and the test system is stable.

Table 6-2 Accuracy of LCR Hi-Tester

Freq. (MHz)	Z (Ω)	Cs (pF)	Θ (°)	Ls (μH)
5	83.08	388.0	-80.9	2.611
5	83.09	387.9	-80.9	2.612
5	83.09	387.9	-80.9	2.612
5	83.10	387.9	-80.9	2.612
5	83.09	387.9	-80.9	2.612
Freq. (MHz)	Z (Ω)	Cs (pF)	Θ (°)	Ls (μH)
1	573.9	292.1	-71.7	86.72
1	573.9	292.1	-71.7	86.72
1	573.9	292.1	-71.7	86.71
1	573.9	292.1	-71.7	86.72
1	573.9	292.1	-71.7	86.72

Freq. (kHz)	Z (kΩ)	Cs (pF)	Θ (°)	Ls (mH)
100	2.770	574.6	-89.6	4.409
100	2.768	574.9	-89.6	4.406
100	2.767	575.3	-89.6	4.403
100	2.773	574.0	-89.6	4.413
100	2.771	574.3	-89.6	4.410

6.3.1 Structure of Air Conditioner System

Fig. 6.21 shows the structure of this air conditioner system. There are two main parts, outdoor part and indoor part. These two parts is connect through the power cables and pipe which is used for refrigerant and lubrication oil flowing. And the

power cables are quite closed with the pipes. There are three main noise sources, compressor motor inverter, outdoor fan inverter and indoor fan inverter. So the main noise routes are three, the compressor motor part, outdoor fan part and indoor fan part.

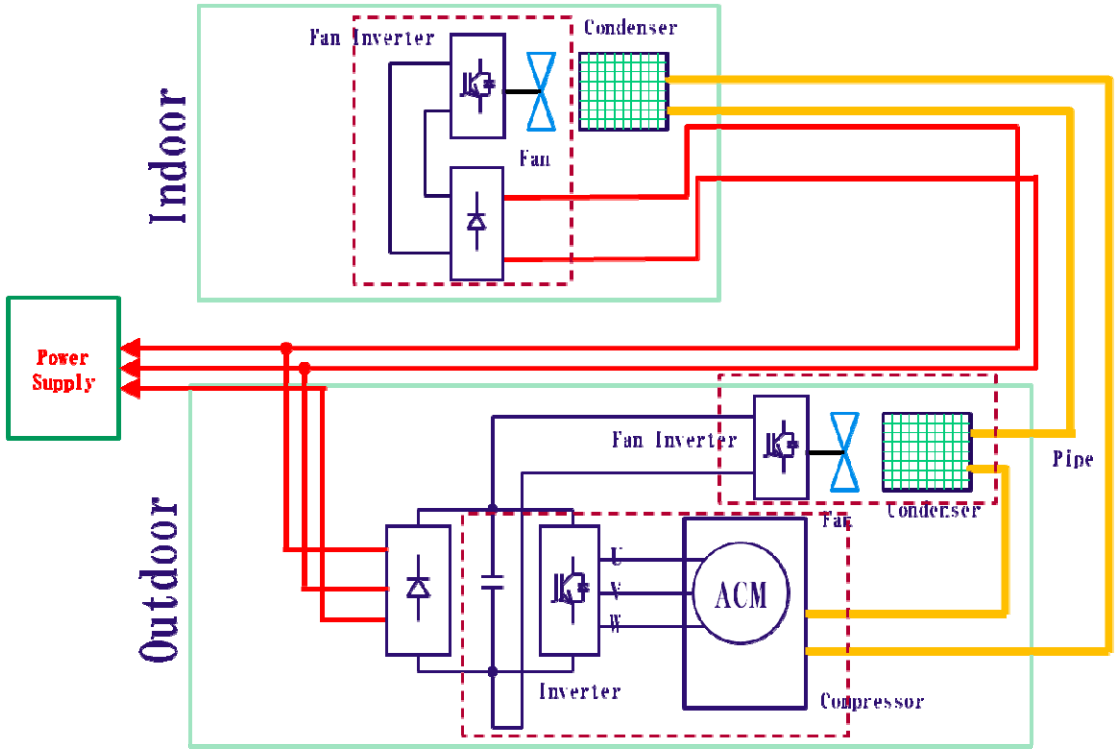


Fig. 6.21 Structure of Air Conditioner System

6.3.2 Equivalent Circuit of Every Part

Fig. 6.22 shows the equipment connection. To measure the CM capacitance characteristic, the three-phase input terminals are shorted together. This point and the metal case of air conditioner are connected to the LCR Hi-Tester to measure the impedance of compressor motor. Blue line in Fig. 6.23 shows the impedance of compressor motor. Because the frequency range of CM noise is from 150 kHz to 30 MHz, five constant points are determined to calculate the equivalent circuit. Fig. 6.24 shows the equivalent. The impedance characteristic is shown as the red point line in Fig. 6.23. The red is quite close to the blue line. Therefore, the equivalent circuit is

effective and right.

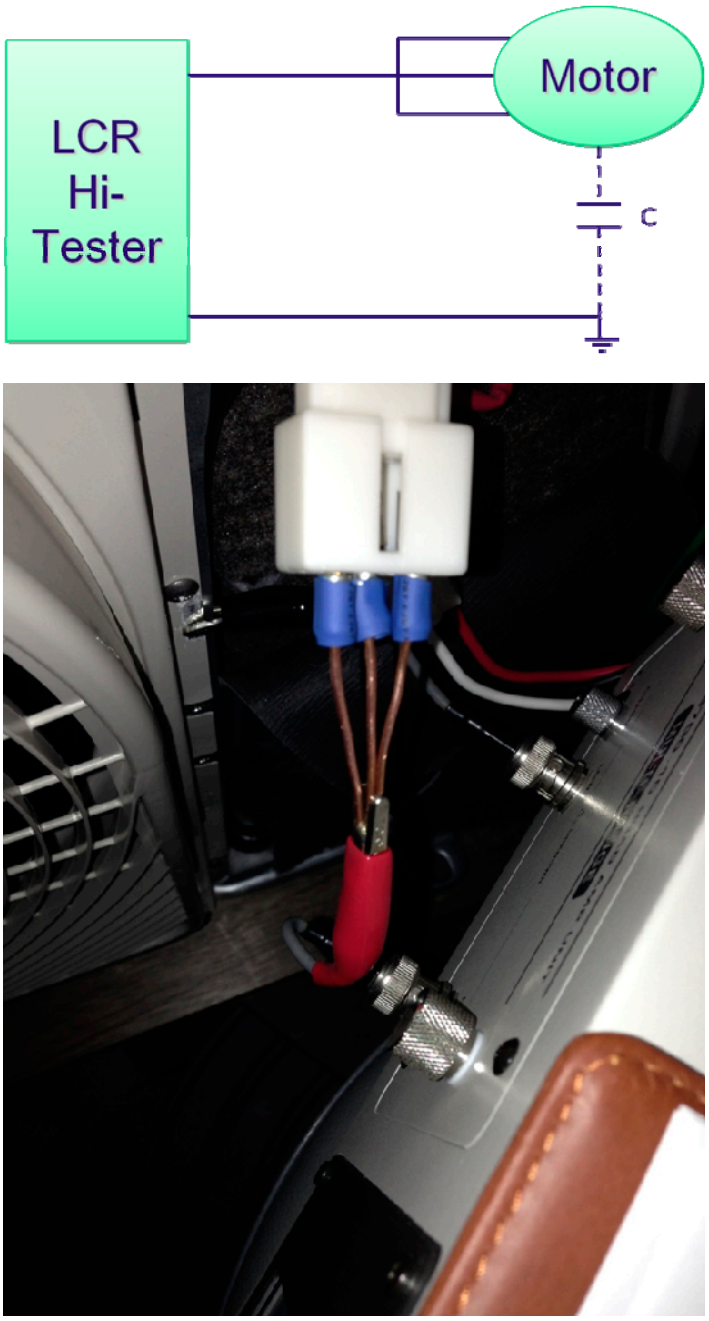


Fig. 6.22 Connection of Compressor Impedance Measurement

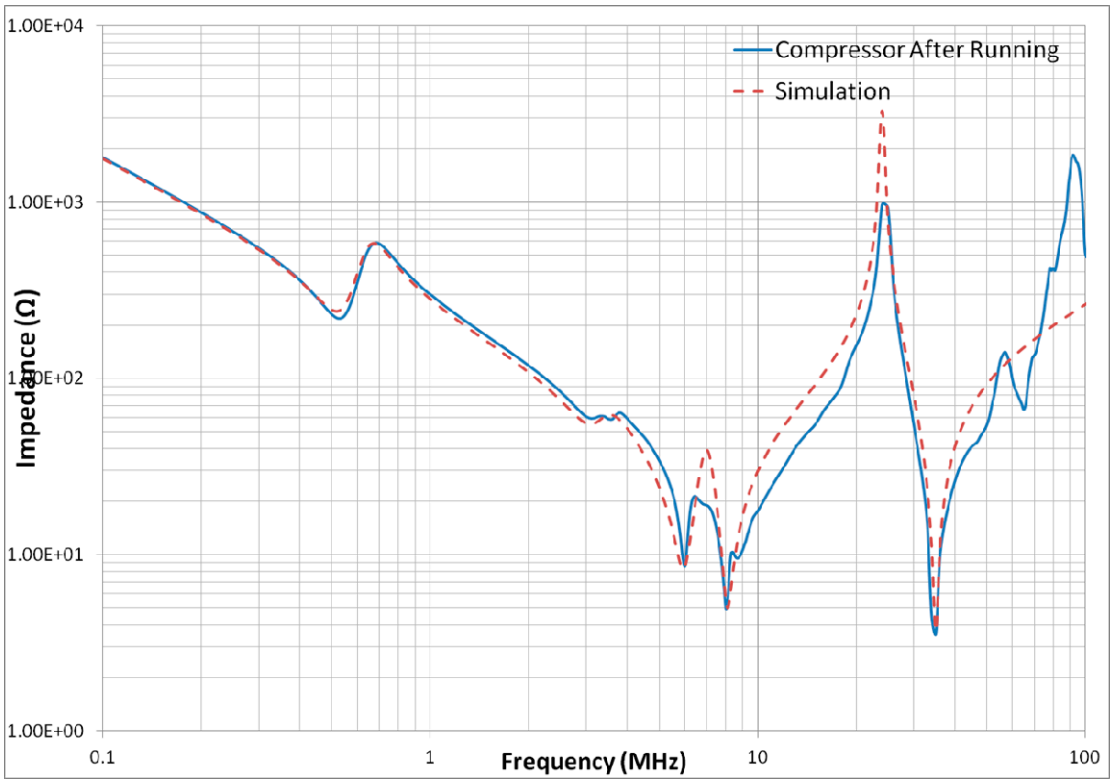


Fig. 6.23 Impedance Calculation of Compressor Motor

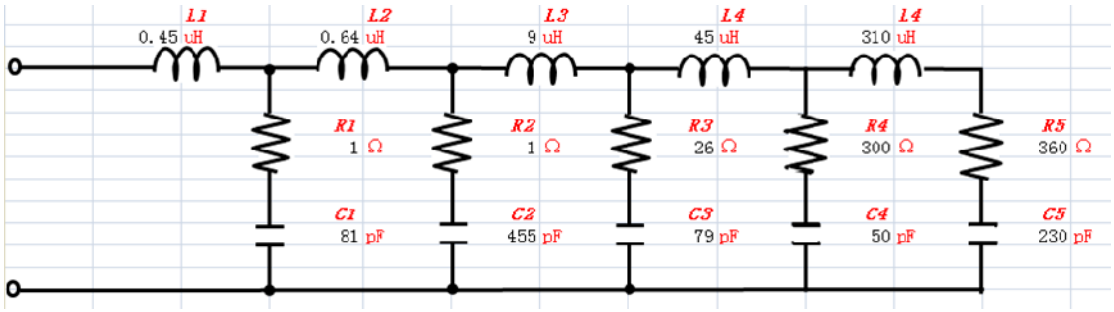


Fig. 6.24 Equivalent Circuit of Compressor Motor

By applying the same method, the equivalent circuit of outdoor fan is calculated. To measure the CM capacitance characteristic, the three-phase input terminals are shorted together. This point and the metal case of air conditioner are connected to the LCR Hi-Tester to measure the impedance. Blue line in Fig. 6.25 shows the impedance of outdoor fan. Fig. 6.26 shows the equivalent. The impedance characteristic is shown as the red point line in Fig. 6.25. The red is quite close to the blue line. Therefore, the

equivalent circuit is effective.

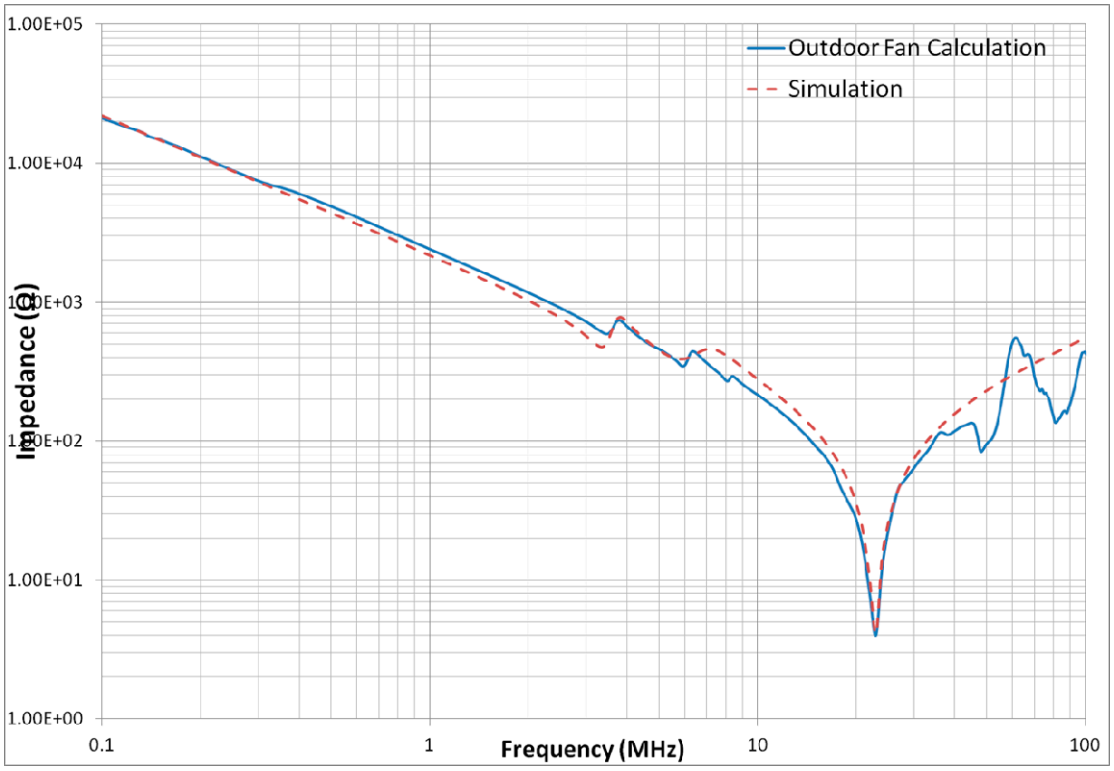


Fig. 6.25 Impedance Calculation of Outdoor Fan

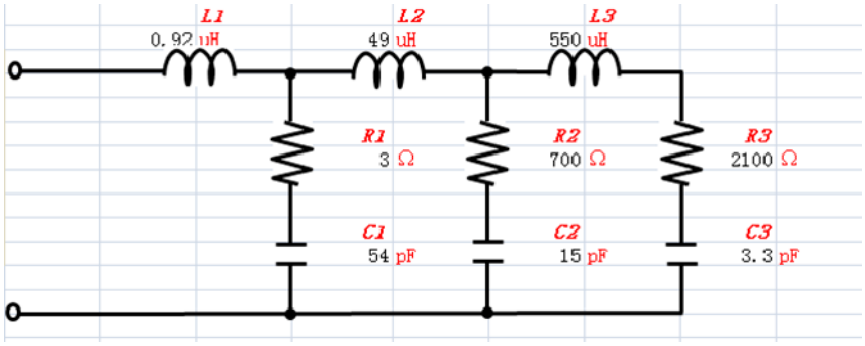


Fig. 6.26 Equivalent Circuit of Outdoor Fan

Blue line in Fig. 6.27 shows the impedance of indoor fan. Fig. 6.28 shows the equivalent. The impedance characteristic is shown as the red point line in Fig. 6.27. The red is quite close to the blue line. Therefore, the equivalent circuit is effective.

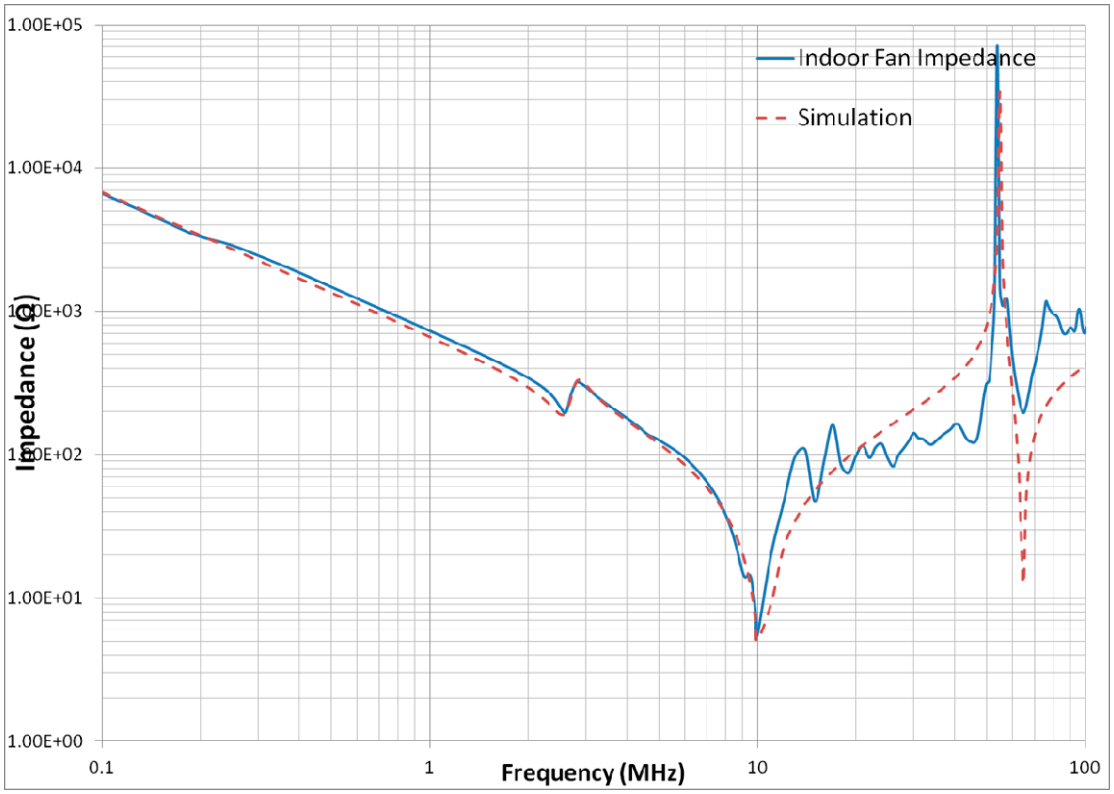


Fig. 6.27 Impedance Calculation of Indoor Fan

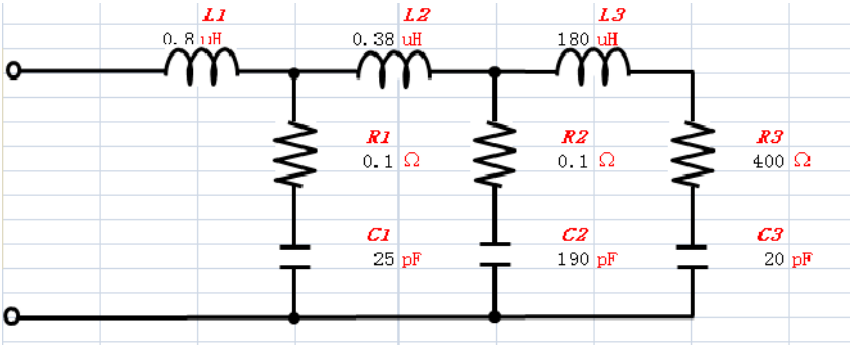


Fig. 6.28 Equivalent Circuit of Indoor Fan

There are long power cables and pipes between the indoor part and outdoor part. Because of the length is sizable, the equivalent circuit for this part is necessary. Two kinds of equivalent circuits are applied to calculation to make sure the equivalent circuit is precise. Fig. 6.29 shows these two equivalent circuits. C_1 and C_2 are the parasitic capacitances between the power cables and pipes. Theses capacitances are

distributed throughout, and they are considered to concentrate in the beginning and the end. R_2 is resistance of power cables. R_1 and R_2 are the parasitic resistances between the cables and the pipes. The inductances of power cables L_1, L_2 and L_3 are considered as three parts, and they are separated by the parasitic capacitances. At the beginning, the cables and the pipes are shorted separately, after that these two points are connected to the LCR hi-tester. At the end, the cables and pipes are considered as two situations. The cables are opened to the pipes and shorted, as shown as Fig. 6.29

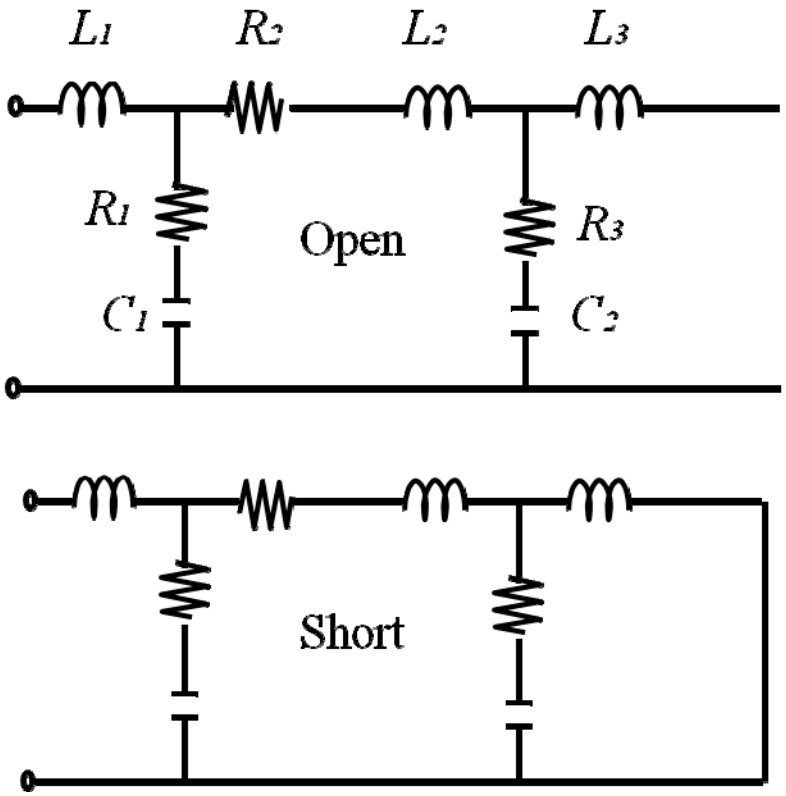


Fig. 6.29 Equivalent Circuit of Pipe Part

Fig. 6.30 shows the connection pictures of experiment when the cables and the pipes are opened. There are three cables, and the black one is the signal line between the indoor part and outdoor part to control the air conditioner. The red line and white line are the power cables. The CM leakage current is flowing in these two lines,

therefore the parasitic capacitances between these two lines and two pipes are considered. At the end, two pipes are shorted. Blue line in Fig. 6.31 and Fig. 6.32 shows the measured impedance of pipe part. Fig. 6.33 shows the equivalent circuit of pipe part in the case of short. The same equivalent circuit is considered as two situations, therefore this equivalent is trustworthy.

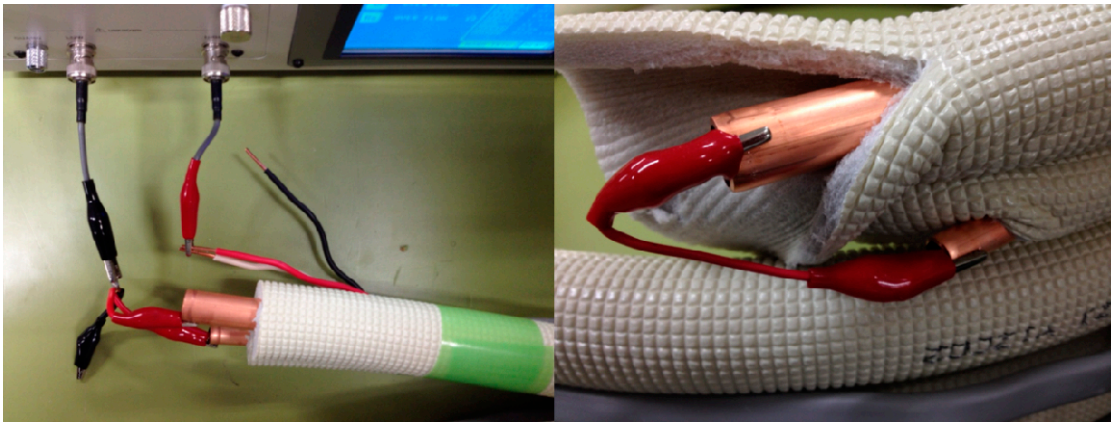


Fig. 6.30 Equivalent Connection of Pipe Part

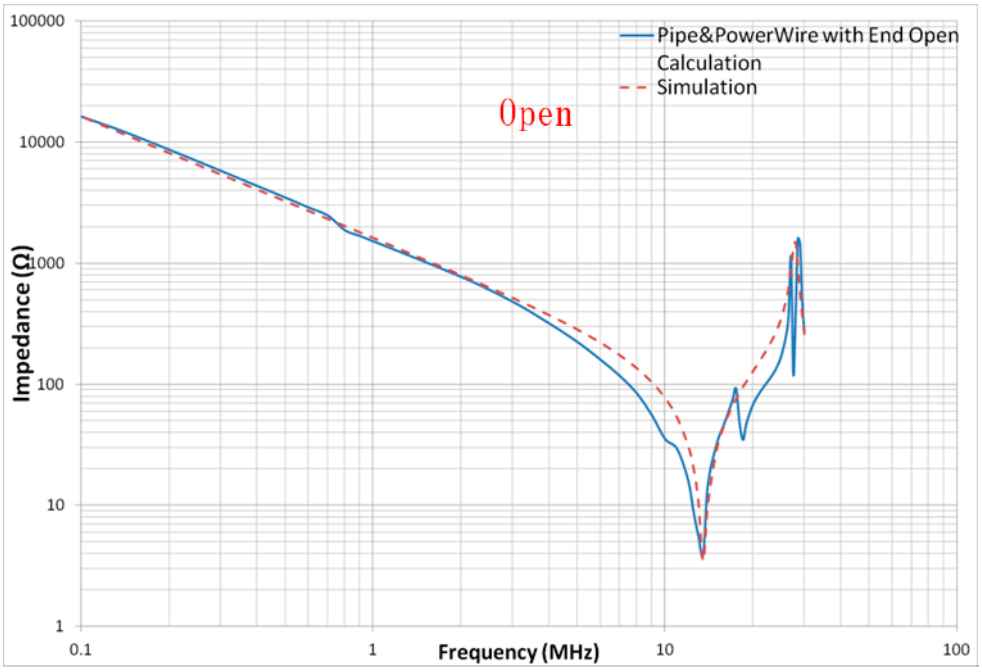


Fig. 6.31 Impedance of Pipe Part in the Case of Open

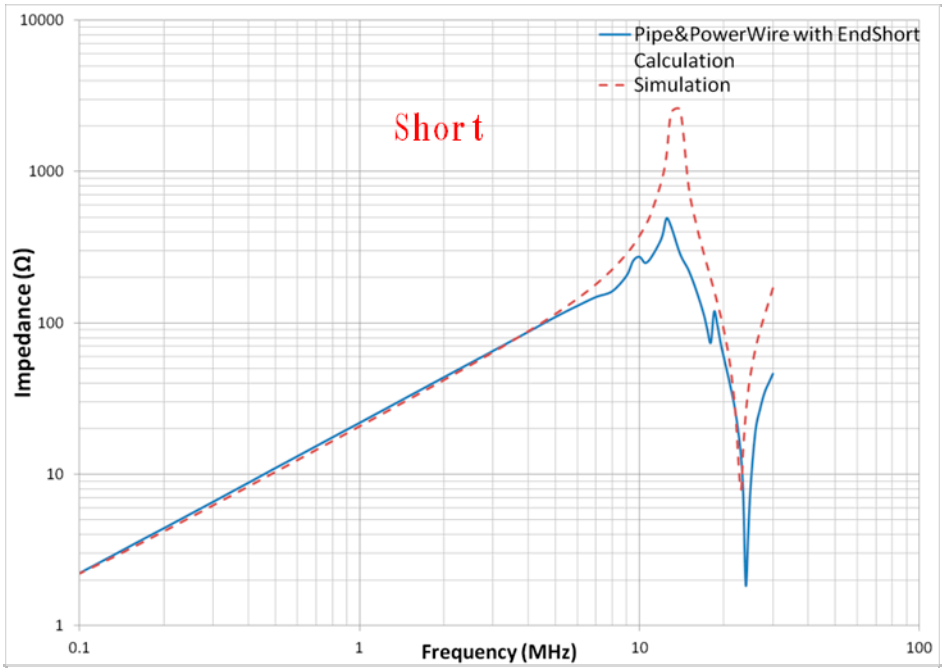


Fig. 6.32 Impedance of Pipe Part in the Case of Short

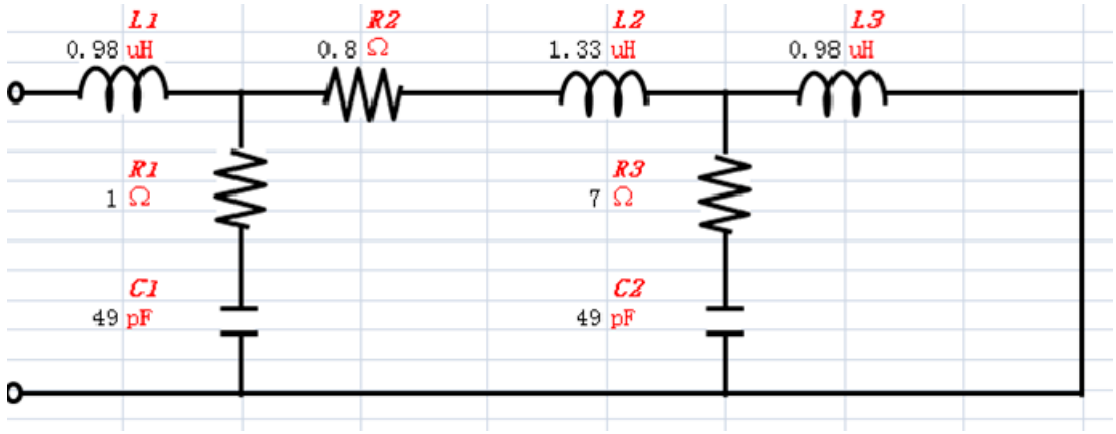


Fig. 6.33 Equivalent Circuit of Pipe Part in the Case of Short

All the other lines in this system are considered as inductances according to the length. 1 m line is considered as 0.1 μH.

6.4 Equivalent Circuit of Air Conditioner System

6.4.1 Simulation Result without EMI Filters

Fig. 6.21 shows the structure of air conditioner system. There are three main noise sources. And the main noise routes is considered as four, compressor motor part, outdoor fan part, indoor fan part and pipe part. The CM model of air conditioner is shown as Fig. 6.34. Fig. According to the equivalent circuits of every part which are calculated in Chapter 6.3 and LISN part, the equivalent circuit without EMI filters is shown as Fig. 6.35. Fig. 6.36 shows the simulation result. The blue line is the experiment waveform and the red line is the simulation. The simulation result without EMI filters can meet with experiment waveform on the resonant frequencies. And the amplitude of noise is almost the same.

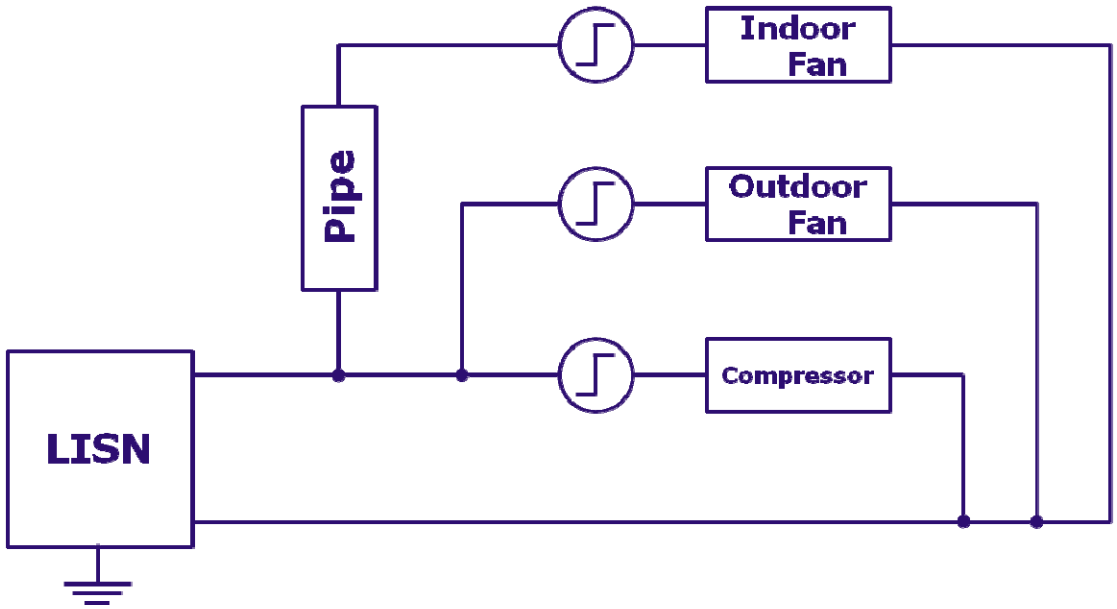


Fig. 6.34 CM Model of Air Conditioner

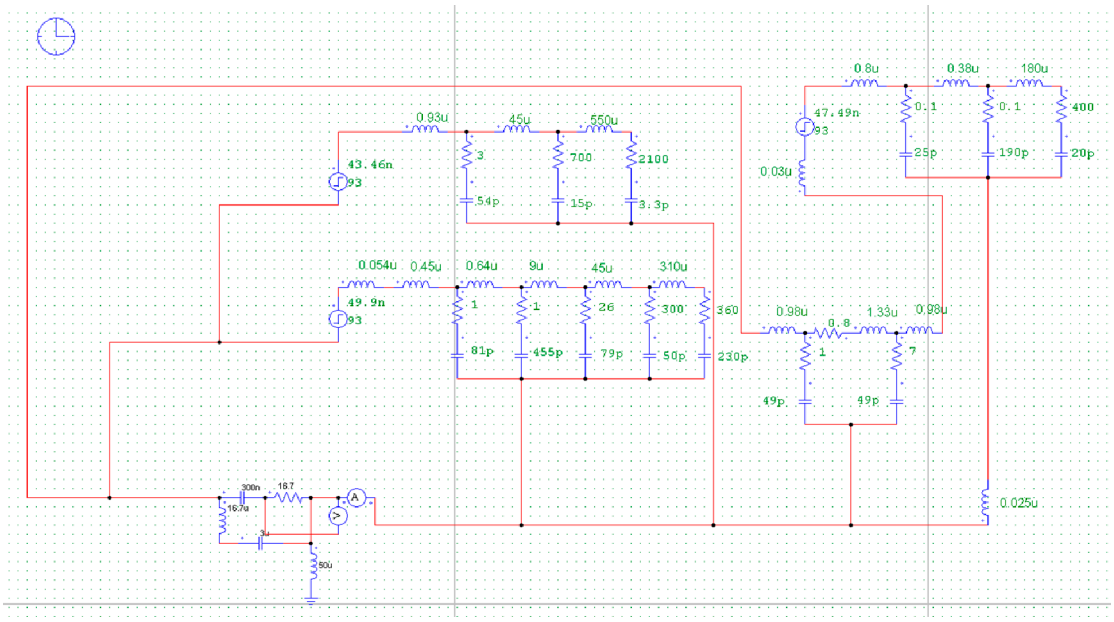


Fig. 6.35 Equivalent Circuit without EMI Filters

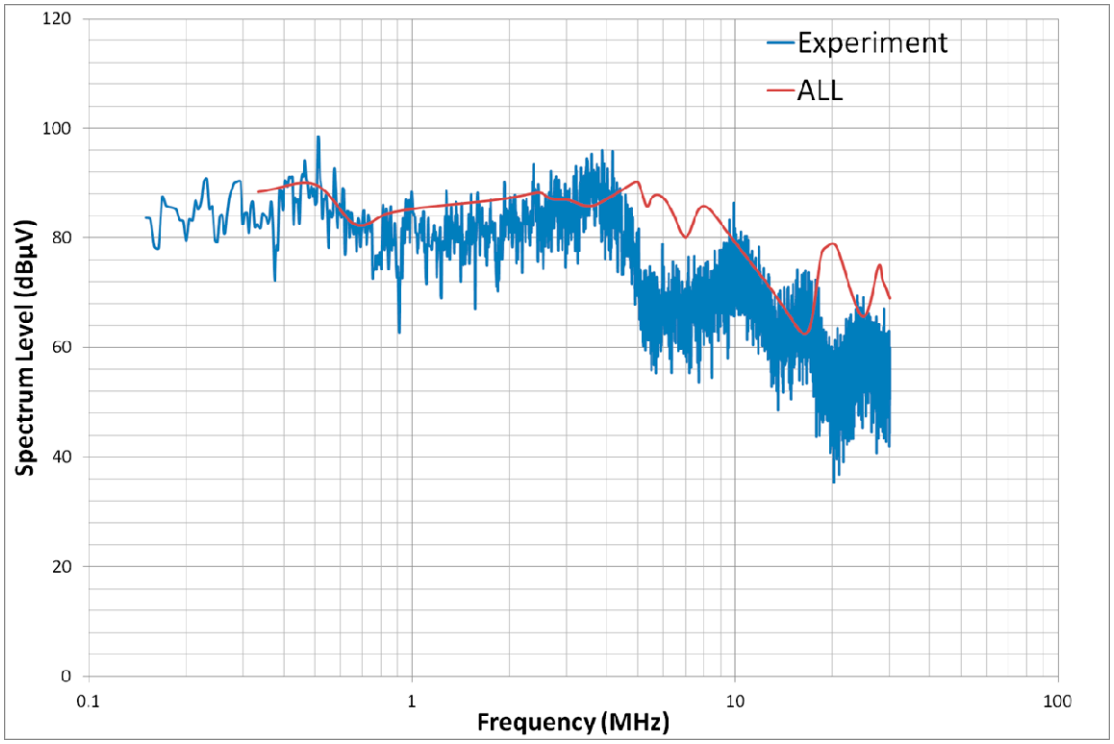


Fig. 6.36 Simulation Result without EMI filters

6.4.2 Simulation Result with EMI Filters

The EMI filters in this air conditioner system can be considered as three kinds, common-mode choke, Y capacitances and ferrite core. For further confirming effectiveness of this equivalent circuit, EMI filters are imported into this equivalent. The input terminals and output terminals of common-mode choke are shorted for impedance measurement, as shown as Fig. 6.37. Two shorted terminals are connected to LCR hi-tester. Fig. 6.38 and Fig. 6.40 show the result. The blue line is the experiment measurement result of impedance, and the red line is the simulation result of equivalent circuit.

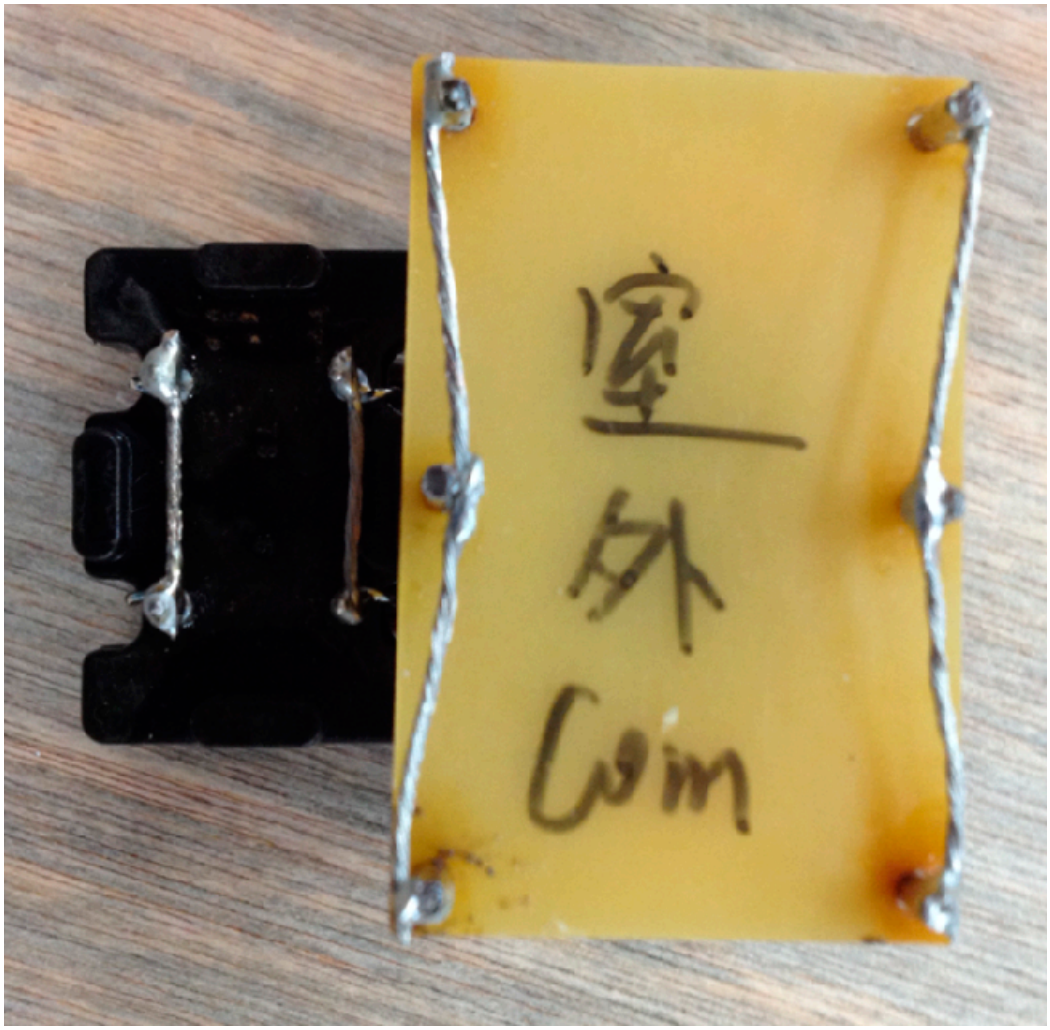


Fig. 6.37 Impedance Measurement of Common-Mode Choke

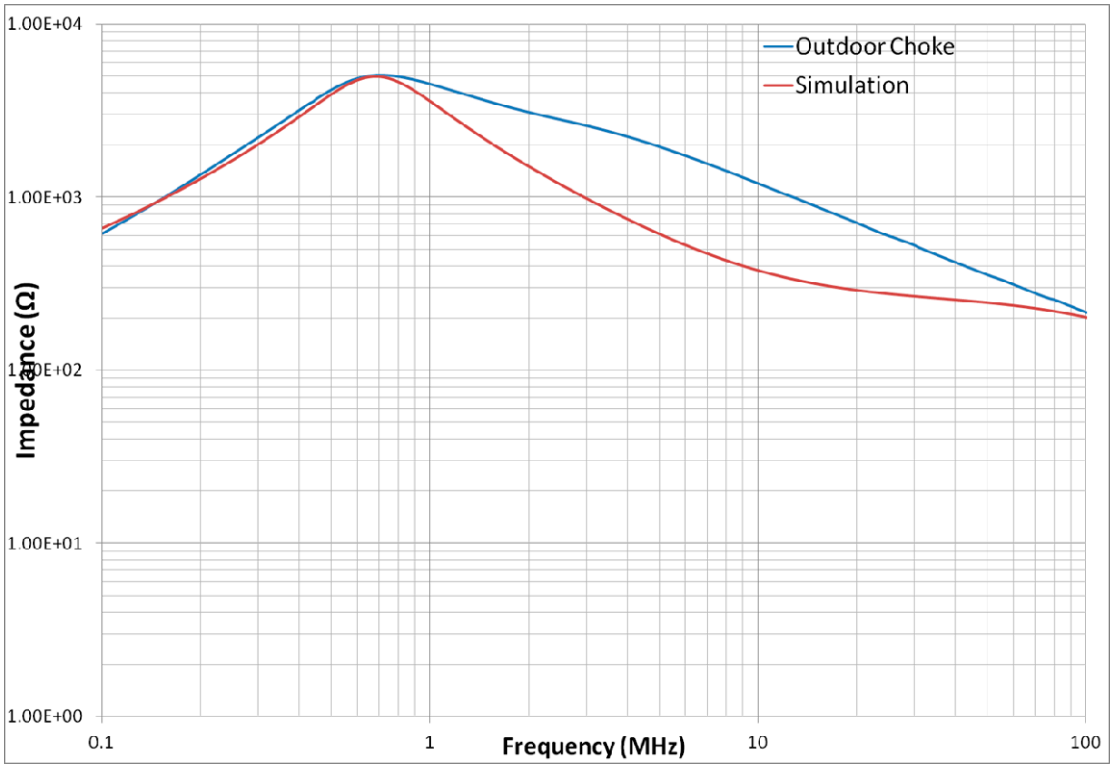


Fig. 6.38 Impedance of Outdoor Common-Mode Choke

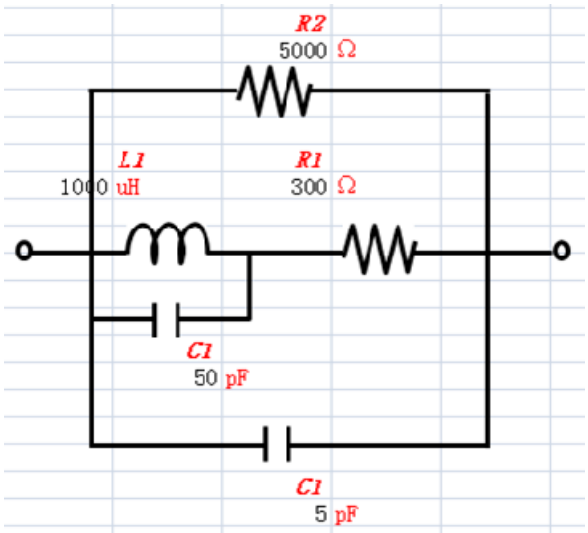


Fig. 6.39 Equivalent of Outdoor Common-Mode Choke

Fig. 6.39 shows the equivalent circuit of outdoor's common-mode choke. And Fig. 6.41 shows the equivalent circuit of indoor's common-mode choke. The red lines

Fig. 6.38 and Fig. 6.40 show the impedance simulation result of equivalent circuits. The simulation result can meet with experiment measurement impedance on resonant frequency. The equivalent circuit is effective.

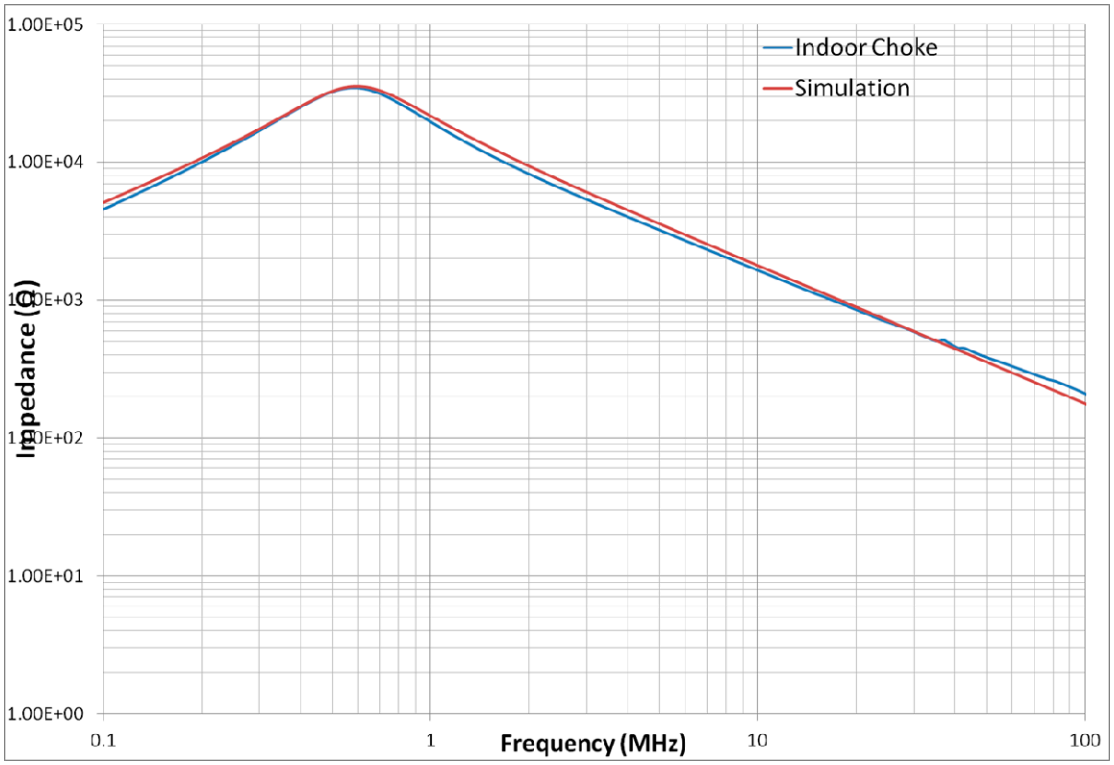


Fig. 6.40 Impedance of Indoor Common-Mode Choke

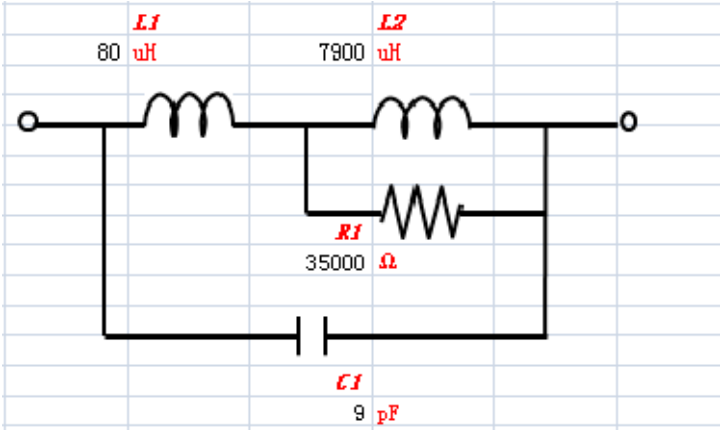


Fig. 6.41 Equivalent of Indoor Common-Mode Choke

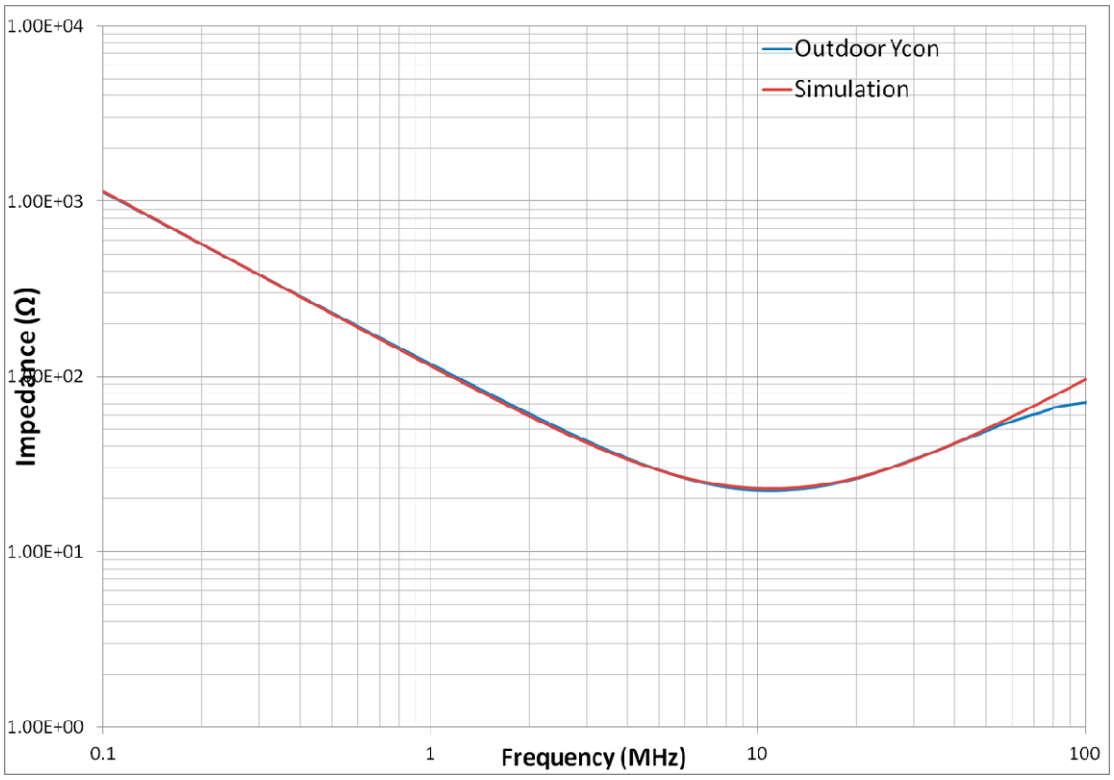


Fig. 6.42 Impedance of Outdoor Y Capacitance

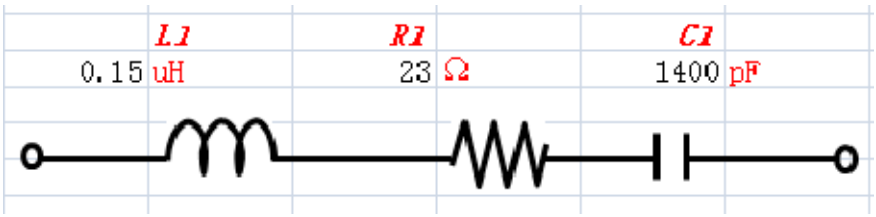


Fig. 6.43 Equivalent of Outdoor Y Capacitance

The red lines in Fig. 6.42 and Fig. 6.44 show the equivalent circuit impedance of Y capacitance outdoor and indoor. The blue lines show the experiment measurement impedance. The impedance waveform of simulation can meet well with the experiment measurement impedance. The equivalent circuits of outdoor and indoor Y capacitances are effective.

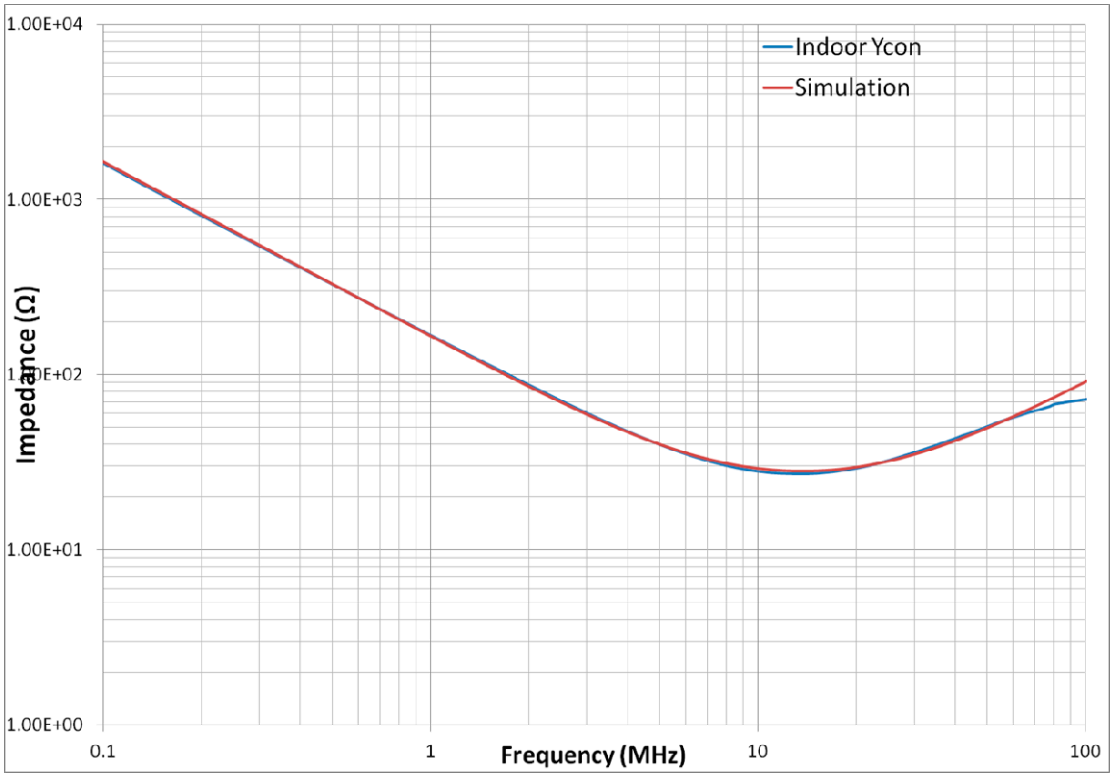


Fig. 6.44 Impedance of Indoor Y Capacitance

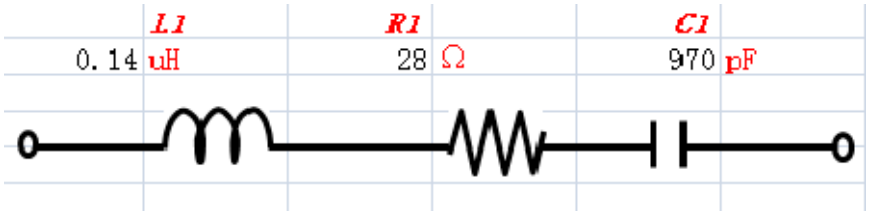


Fig. 6.45 Equivalent of Indoor Y Capacitance

The equivalent circuits are imported into the equivalent circuit in Fig. 6.35. Fig. 6.46 shows the equivalent circuit with EMI filters. Fig. 6.47 shows the result. The blue line is the experiment waveform without EMI filters, and the red line is the simulation result. The simulation result with EMI filters can meet with experiment waveform on the resonant frequencies. And the amplitude of noise is almost the same. The equivalent circuit of this air conditioner system is effective.

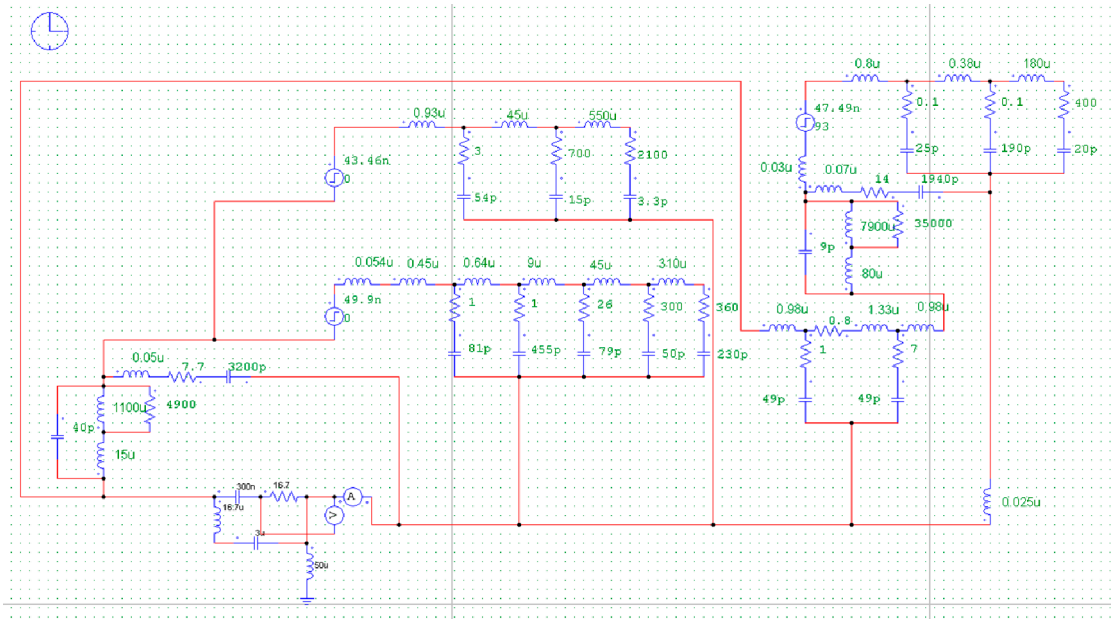


Fig. 6.46 Equivalent Circuit with EMI Filters

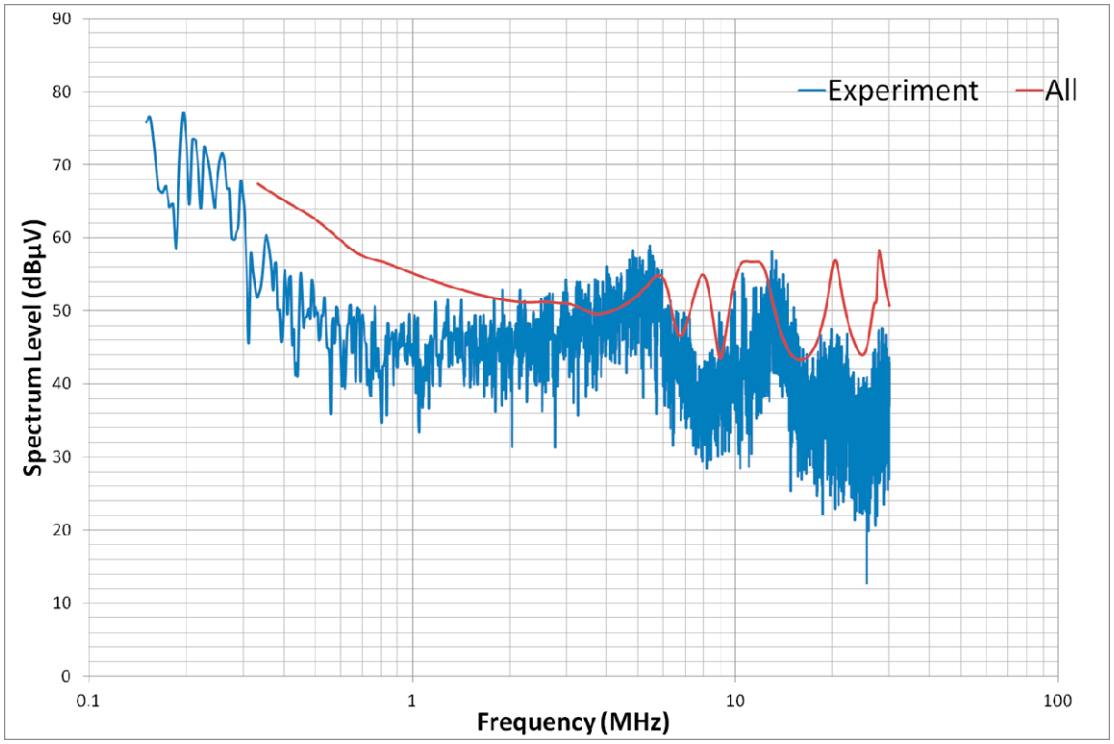


Fig. 6.47 Simulation Result with EMI Filters

6.5 Summary

In Chapter 6, for improving the EMI design system from after assembling to before assembling as shown as Fig. 6.1. CM Equivalent circuits of every part are speculated according to the impedance experiment waveform. This is because the method mentioned in Chapter 4 makes the model of this system too complex. The simulation cost is not ideal. According to the leakage current, the compressor motor part is the main noise source. The noise level is more serious than outdoor fan part and indoor fan part.

Before the calculation of equivalent circuit, the effectiveness of common-mode choke, Y capacitance and ferrite core are confirmed. It can be confirmed that the common-mode choke is effective in the low frequency range until 5 MHz. The Y capacitance is effective in the frequency range between 1 MHz to 10 MHz. And the ferrite core on cables is effective in the frequency range over 10 MHz.

The equivalent circuits of four parts, compressor motor part, outdoor fan part, indoor fan part and pipe part, are calculated separately. The impedance of equivalent circuit can meet well with the experiment impedance.

According to the structure of air conditioner system, the equivalent circuit of system without EMI filters is constructed. The simulation result without EMI filters can meet with experiment waveform on the resonant frequencies. And the amplitude of noise is almost the same.

The equivalent circuits of EMI filters, common-mode chokes and Y capacitances are calculated separately. The impedance of equivalent circuit can meet well with the experiment impedance. These equivalent circuits are imported into the equivalent circuit in Chapter 6.41. The simulation result with EMI filters can also meet with experiment waveform on the resonant frequencies. And the amplitude of noise is almost the same.

The effectiveness of the proposed equivalent circuit is verified, by comparing the simulation result with the experiment waveform by considering two situations with EMI filters and without EMI filters. But in high frequency range over 10 MHz, the

simulation results a little depart from the experiment results. And the resonant frequencies are a little different. This is because the impedance of compressor motor when the motor is running is a little different with the impedance of measurement. And the ferrite core on cables is effective in the frequency range over 10 MHz. The equivalent circuits of ferrite core are not included in, therefore the noise level of equivalent circuit with EMI filters is a litter higher than experiment waveform in the range over 10 MHz. According to the other research, there is light non-linear phenomenon in outdoor common-mode choke. It means the linear equivalent circuit is not enough. All these problems will be discussed in the future work.

Chapter 7 Conclusions and Future Work

7.1 Conclusions

The major conclusions of this dissertation are summarized as follows.

First, the constitution of PWM inverter-fed motor drive system and the impact factors of CM noise are confirmed. Shorter rising time of the PWM inverter phase switching will result in higher leakage current. And when two phases of PWM inverter is switching at the same time, the leakage current reaches to the maximum.

Second, the possibility and rationality of non-linear resistance existing in the CM equivalent circuit model is confirmed. A calculation method for the parameter of equivalent circuit is derived according to the waveform of leakage current. Considering two aspects, only one phase switching and two phases switching, the effectiveness and necessity of non-linear equivalent circuit has been confirmed. A simple π type CM equivalent circuit of inverter-fed motor drive system is proposed. Validity and physical meaning of the proposed equivalent circuit are confirmed by some simulations and experiments.

Third, in order to improve the accuracy of the equivalent circuit parameters and reduce errors, the optimization software modeFRONTIER is applied. Identify non-liner CM equivalent circuit, and then get the conclusion that the introduction of non-linear resistance about CM equivalent circuit of inverter-fed drive motor system is efficiency and necessary. Do another group of experiment and simulation to verify the effect of the non-linear in the equivalent circuit. Then confirm that the

introduction of non-linear is efficiency again. It is shown that introduction of a non-linear resistance into the proposed simple equivalent circuit can improve accuracy of the simulation for analyzing the common-mode circuit causing conductive EMI.

Fourthly, this thesis proposes a method to estimate the stray capacitance between compressor motor windings and stator in operation, and the permittivity of refrigerant and lubricant oil mixture in this area. By applying this method, the complex experiment equipments and sensors are unnecessary. The estimation about the stray capacitance between the motor windings and stator in operation becomes possible according to the equivalent circuit of the inverter air conditioner by analyzing the high frequency leakage current of ground line. Further, the permittivity of refrigerant and lubricant oil mixture can be calculated by comparing the stray capacitance of equivalent circuit in operation with the stray capacitance of the compressor without refrigerant and lubricant oil. It is meaningful to discuss and solve the problem of EMI noise. And it is helpful to duplicate the situation instantaneously when the compressor is running.

Finally, a design procedure for EMI problem is proposed. The EMI noise can be predicted and the EMI filter can be designed from after assembling to before assembling. Before the calculation of equivalent circuit, the effectiveness of common-mode choke, Y capacitance and ferrite core are confirmed. The equivalent circuits of every part and EMI filters are calculated separately. According to the structure of air conditioner system, the equivalent circuits of system are constructed, by considering two situations with EMI filters and without EMI filters. The effectiveness of the proposed equivalent circuit is verified, by comparing the simulation result with the experiment waveform.

7.2 Future Work

7.2.1 Physical Meaning of Non-Linear

Although a probable method of verifying the physical meaning of non-linear element is proposed. And this method is applied to analyze the cover of air conditioner compressor. Unfortunately, there is no non-linear element exist in the cover of air conditioner compressor. The physical meaning of non-linear element needs further confirm.

7.2.2 CM Equivalent Circuit in Frequency Domain

In high frequency range over 10 MHz, the simulation results are a little depart from the experiment results. And the resonant frequencies are a little different. This is because of a little difference in compressor motor equivalent circuit and outdoor common-mode equivalent circuit. And the introduction of ferrite core equivalent circuit [50][51] is also necessary in high frequency range over 10 MHz. All these problems will be discussed in the future work.

7.2.3 EMI Suppression Method

The purpose of study is designing an efficiency and low-cost EMI suppression system. Although there have been many achievements in reducing the CM conducted EMI noise [52]-[62], suppression of CM interference still needs to improve. A simple and accurate equivalent circuit is not only beneficial to the prediction of EMI, but also conducive to the design of filter. Therefore a new EMI suppression method needs further investigation.

The following research will propose a new active filter by applying the current mirror circuit in the future, shown as Fig. 7.1. The I_{ref} is equal to I_{c2} . First, CM current is detected and injected into current mirror circuit as I_{ref}. Then the reverse current I_{c2} is injected into ground loop, thereby the CM current finally becomes 0.

The future research will focus on how to supply the power to current mirror circuit.

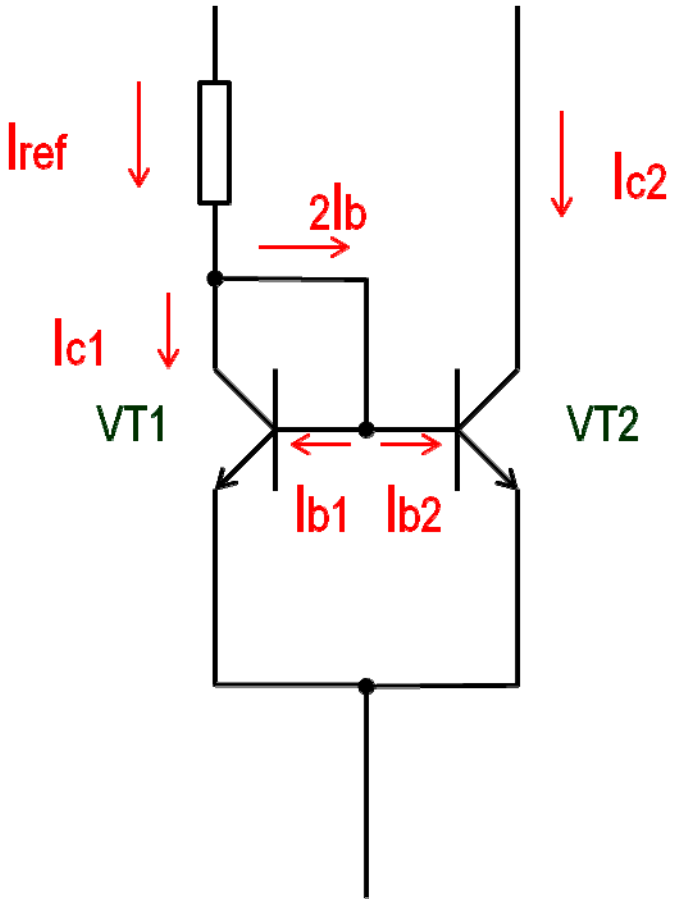


Fig. 7.1 Current Mirror Circuit

REFERENCES

[1]. J. L. Norman Violette, D. R. J. White. M. F. Violette, Electromagnetic Compatibility Handbook, 1987.

[2]. D.A. Weston, Electromagnetic Compatibility: Principles and Applications, Ed Marcel Dekker, New York, 2001

[3]. G. Skibinski, R. Kerkman, D. Schlegel, "EMI Emissions of Modern PWM AC Drives", IEEE Industry Applications, Vol. 5, No. 2, pp.47-81, 1999.

[4]. S. Chen, T.A. Lipo, D. Fitzgerald, "Source of Induction Motor Bearing Currents Caused by PWM Inverters", IEEE Transactions on Energy Conversion, Vol. 11, No. 1, pp. 25-32, 1996.

[5]. N. Aoki, K. Sotoh, A. Nabae, "Damping Circuit to Suppress Motor Terminal Over-Voltage and Ringing in PWM Inverter-Fed AC Motor Drive Systems with Long Motor Leads", IEEE Transactions on Industry Applications, Vol. 35, No. 5, pp 1014-1020, 1999

[6]. A. Noboru, "Damping Circuit to Suppress Motor Tterminal Over-Voltage and Ringing in PWM Inverter-Fed AC Motor Drive Systems with Long Motor Leads", IEEE Transactions on Industry Applications, Vol. 35, No. 5, pp 1014-1020, 1999.

[7]. Y. Murai, T. Kubota, Y. Kawase, "Leakage Current Reduction for A High-Frequency Carrier Inverter Feeding an Induction Machine", IEEE Transactions on Industry Applications, Vol. 28, pp 858-863, 1992.

[8]. J. M. Erdman, R. J. Kerkman, D. W. Schlegel, G. L. Skibinski et al. "Effect of PWM Inverters on AC Motor Bearing Currents and Shaft Voltages", IEEE Transactions on Industry Applications, Vol. 32, pp 250-259, 1996.

[9]. L. Ferrer, J. Balcells, D. Gonzalez, J. Gago, M. Lamich, "Modeling of Differential Mode Conducted EMI Generated by Switched Power Inverters", Industrial Electronics Society, IECON '03, The 29th Annual Conference of the IEEE, Vol. 3, pp 2312-2315, Nov. 2003.

[10]. X. D. Huang, E. Pepa, J. S. Lai, S. T. Chen, T. W. Nehl, "Three-Phase Inverter Differential Mode EMI Modeling and Prediction in Frequency Domain", Industry Applications Conference, 38th IAS Annual Meeting, Vol. 3, pp 2048-2055, Oct. 2003.

[11]. G. T. Chern, J. J. Shieh, C. H. Chao, W. Chuang, "Reducing Differential-Mode EMI and Low-Frequency Common-Mode Voltage in Switching-Mode Power Converters", Electrical Machines and Systems (ICEMS), Beijing, China, Aug. 2011.

[12]. H. L. Chen, Z. M. Qian, "Modeling and Characterization of Parasitic Inductive Coupling Effects on Differential-Mode EMI Performance of a Boost Converter", IEEE Transactions on Electromagnetic Compatibility, Vol. 53, No. 4, pp 1072-1080, Nov. 2011.

[13]. R. J. Kerkman, G. L. Skibinski, D. W. Schlegel, "Voltage Harmonics Generated by

Voltage-Fed Inverters Using PWM Natural Sampling", IEEE Transactions on Industry Applications, Vol. 3, No. 3, pp 297-301, 1988.

[14]. H. F. Ma, D. G. Xu, X. Y. Chen et al. "Research of Voltage Reflection of PWM Inverter-Fed Induction Motor with Long Motor Leads", Proceedings of the CSEE, Vol. 21, No. 11, pp 109-113, 2001. (In Chinese).

[15]. H. F. Ma, D. G. Xu, X. Y. Chen et al. "A Novel Common-Mode Sinusoidal Inverter Output Filter with Variable Inductor", Power Conversion Conference, Osaka, Japan, pp 710-715, 2002.

[16]. X. Y. Chen, B. Yan, D. G. Xu et al. "Fuzzy Optimization of Inverter Output Filter in Motor Drive System", Proceedings of the CSEE, Vol. 23, No. 8, pp 134-138, 2003. (In Chinese).

[17]. N. Idir, R. Bausiere, J.J. Franchaud, "Active Gate Voltage Control of Turn-on di/dt and Turn-off dv/dt in Insulated Gate Transistors", IEEE Transactions on Power Electronics, Vol. 21, No. 4, pp. 849-855, 2006.

[18]. S. Ogasawara and H. Akagi, "Modeling and Damping of High-Frequency Leakage Currents in PWM Inverter-Fed AC Motor Drive Systems", IEEE Transactions on Industry Applications, Vol. 32, No. 5, pp 1103-1114, Sep./Oct. 1996.

[19]. H. Akagi and T. oe, "A Specific Filter for Eliminating High-Frequency Leakage Current from the Grounded Heat Sink in a Motor Drive with An Active Front End", IEEE Transactions on Industry Applications, Vol. 23, No. 2, pp 763-770, Mar. 2008.

[20]. R. Li, S. Gokani, J, Clare, "Conducted Electromagnetic Emission in Induction Motor Drive Systems I: Time Domain Analysis and Identification of Dominant Modes", IEEE Transactions on Power Electronics, Vol. 13, No. 4, pp 757-767, 1998.

[21]. R. Li, S. Gokani, J, Clare, "Conducted Electromagnetic Emission in Induction Motor Drive Systems II: Frequency Domain Modes", IEEE Transactions on Power Electronics, Vol. 13, No. 4, pp 768-776, 1998.

[22]. H. Akagi, T. Shimizu, "Attenuation of Conducted EMI Emissions from An Inverter-Driven Motor", IEEE Transactions on Power Electronics. Vol. 23, No. 1, pp. 282-290, 2008.

[23]. H. Zhu, J. S. Lai, A. R. Hefner, "Modeling Based Examination of Conducted EMI Emissions form Hard and Soft Switching PWM Inverters", IEEE Transactions on Industry Applications, Vol. 40, No. 5, pp 1383-1393, 2005.

[24]. J. Meng, W. M. Ma, "Power Converters EMI Analysis Including IGBT Nonlinear Switching Transient Model", IEEE Transactions on Industry Electronics, Vol. 53, No. 5, pp 1577-1583, 2006.

[25]. D. Cochrane, D. Y. Chen, "Passive Cancellation of Common-mode Noise in Power Electronic Circuits", IEEE Transactions on Power Electronics, Vol. 18, No. 3, pp 756-763, 2003.

[26]. J. Roudet, J. L. Schanen, P. Loizelet, "EMI Study of A Three Phase Inverter-Fed Motor Drives", Industry Applications Conference, 39th IAS Annual Meeting, Conference Record of

the 2004 IEEE, Vol. 4, pp 2657-2664, 2004.

[27]. C. X. Mao, W. B. Li, J. M. Lu et al. “Study of the Common-Mode Voltage in A High-Voltage ASD’s System”, Proceedings of the CSEE, Vol. 23, No. 9, pp 57-62, 2003. (In Chinese)

[28]. J. Meng, W. M. Ma, L. Zhang, Q. J. Pan, Z. H. Zhao, “High Frequency Model of Conducted EMI for PWM Variable-Speed Drive Systems”, Proceedings of the CSEE, Vol. 28, No. 15, pp 141-146, May 2008. (In Chinese).

[29]. Y. Koyama, M. Tanaka, H. Akagi, “Modeling and Analysis for Simulation of Common-Mode Noises Produced by an Inverter-Driven Air Conditioner”, IEEE Transactions on Industry Applications, Vol. 47, No. 5, pp 2166-2174, Sep./Oct. 2011.

[30]. X. Gong, I. Josifovic, J.A. Ferreira, “Modeling and Reduction of Conducted EMI in SiC JFET Motor Drives with Insulated Metal Substrate”, IEEE Transactions on Power Electronics, Vol. 28, pp. 3138-3146, 2012.

[31]. T. Kato, Y. Otomo, K. harada, Y. Ishihara, “Modeling and Simulation of A Power Electronic Converter for EMC”, Power Conversion Conference 2002, Osaka, Vol. 2, pp. 541-546, Apr. 2-5 2002

[32]. B. Basavaraja, D.V.S.S. Siva Sarma, “Modeling and Simulation of dv/dt Filters for AC Drives with Fast Switching Transients”, Power India Conference 2006, New Delhi, 2006.

[33]. J. Genoulza, C. Jettanasen, F. Costa, C. Vollaire, “Modeling of Common Mode Conducted Noise Emissions in PWM Inverter-Fed AC Motor Drive Systems”, Power Electronics and Applications, EPE 2007, pp. 1-10, Sep. 2-5 2007.

[34]. Environmental Effects of Ozone Depletion and Its Interactions with Climate Change: 2002 Assessment, http://www.unep.org (Sep. 2014).

[35]. S. Devotta, A. V. Waghmare, N. N. Sawant, B. M. Domkundwar, “Alternatives to HCFC-22 for Air-Conditioners”, Applied Thermal Engineering, Vol. 21, No. 6, pp 703-715, 2001.

[36]. http://jpca.jp/mrecologist/vol_62/ (Apr. 2015).

[37]. H. Arakawa, H. Kanazawa, J. Takuma,“RAS-405BD High-Performance Room Air Conditioner with New Refrigerant”, Toshiba Review, Vol. 53, No. 10, pp 57-61, Oct. 1998. (In Japanese)

[38]. N. Nakazawa, M. Kawamura, A. Sekiya, K. Ootake, R. Tamai, Y. Kurokawa, J. Murata, “Liquid Dielectric Constants of Fluorinated Ethers, Fluorinated Ketone and Fluorinated Alcohol”, Trans. of the JSRAE, Vol. 18, No. 3, 2001, pp. 263-271. (In Japanese)

[39]. M. Fukuta, T. Yanagisawa, Y. Ogi, J. Tanaka, “Measurement of Concentration of Refrigerant in Refrigeration Oil by Capacitance Sensor”, Trans. Of the JSRAE, Vol. 16, No. 3, pp. 239-248, 1999. (In Japanese)

[40]. H. Kashiwagi, N. Harada, Y. Tanaka, H. Kuboda, T. Makita, “Dielectric Constants of Refrigerants R113, R114, R114B2, R115, R116, and R124”, Trans. of the JSRAE, Vol. 1, No. 1, pp. 29-36, 1984. (In Japanese)

[41]. T. Makita, H. Kubota, Y. Tanaka, H. Kashiwagi, “Dielectric Constants of Refrigerants R12, R13, R22 and R23”, JSRAE 52 (596), pp. 543-551, 1977. (In Japanese)

[42]. R. Kondo, Y. Koyama, M. Tanaka, H. Akagi, “Conducted-EMI Emissions Analysis and EMI-Filter Optimization for an Inverter-Driven Air Conditioner”, Journal of the JIPE, Vol. 38, pp. 58-64, 2012. (In Japanese)

[43]. J. Fukuda, “Study on Analysis and Reduction for EMI Generated by Power Electronic Equipment”, Master Thesis, Hokkaido University, 2011.

[44]. http://www.norimura.ecnet.jp/gasu.html (Apr. 2015)

[45]. http://en.wikipedia.org/wiki/File:Air_conditioning_unit-en.svg

[46]. M. Morimoto, “Reduction of High Frequency Leakage Current form PWM Inverter-Motor System at the Integrated Grounding System”, APEC ’06, Twenty-First Annual IEEE, pp. 191-194, Mar. 2006.

[47]. P. Sarikprueck, P. Lumyong, “A Study of Phase to Ground Leakage Current in 3-Phase Induction Motor Fed by Switching Voltage Source”, ICEMS 2009, pp. 1-4, Nov. 15-18 2009.

[48]. A. Kempski, R. Smolenski, Ryszard, Strzelecki, “Common Mode Current Paths and Their Modeling in PWM Inverter-Fed Drives”, Power Electronics Specialists Conference 2002, PESC, IEEE 33rd Annual, Vol. 3, pp. 1551-1556, Feb. 2002.

[49]. J. Genoulaz, C. Jettanasen, F. Costa, C. Vollaire, “Modeling of Common Mode Conducted Noise Emissions in PWM Inverter-Fed Motor Drive Systems”, Power Electronics and Applications, 2007 European Conference, EPE 2007, pp. 1-10, Sep. 2-5 2007.

[50]. H.L. Chen, Z.M. Qian, Z.H. Zeng, C. Wolf, “Modeling of Parasitic Inductive Couplings in a PI-shaped Common Mode EMI Filters”, IEEE Transactions on Electromagnetic Compatibility, Vol. 50, No. 1, pp. 71-79, 2008.

[51]. J.L. Kotny, T. Duquesne, N. Idir, “EMI Filter Design Using High Frequency Models of the Passive Components”, Signal Propagation on Interconnects (SPI), 2001 15th IEEE Workshop, Naples, pp. 143-146, May 8-11 2011.

[52]. Y. S. Lai, “Investigations into the Effects of PWM Technique on Common-Mode Voltage for Inverter-Controlled Induction Motor Drives”, IEEE Engineering Society, New York, USA, Vol.1, pp 35-40, 2005.

[53]. P. Caldeire, R. Liu, “Comparison of EMI Performance of PWM and Resonant Power Converters”, IEEE PESC’93 Record, Seattle, USA, pp 134-140, 1993.

[54]. G. Oriti, T. A. Lipo, “A New Space Vector Modulation Strategy for Common-Mode Voltage Reduction”, IEEE Transactions on Power Electronics, Vol. 23, No. 4, pp 1541-1546, 2007.

[55]. S. Ogasawara, H. Akagi, “An Active Circuit for Cancellation of Common-Mode Voltage Generated by A PWM Inverter”. IEEE Transactions on Power Electronics, Vol. 5, No. 13, pp 835-841, 1998.

[56]. S. Ogasawara, H. Akagi, “Circuit Configurations and Performance of the Active

Common-Mode Voltage Generated by Voltage Source PWM Inverter", IEEE Industry Applications, Rome, Italy, pp 1482-1488, 2000.

[57]. I. Takahashi, A. Ogata, H. Kanazawa, A. Hiruma, "Active EMI Filter for Switching Noise of High Frequency Inverter", Power Conversion Conference Nagaoka 1997, Vol.1 pp. 331-334, Aug. 3-6 1997.

[58]. J.L. Kotny, T. Duquesne, N. Idir, "Modeling and Design of the EMI Filter for DC-DC SiC-Converter", Power Electronics, Electrical Drives, Automation and Motion (SPEEDAM) Symposium, Ischia, pp. 1195-1200, Jun. 18-20 2014.

[59]. A. Hiruma, Y. Shindo, "Reduction in EMI Noise of an Electric Compressor for Hybrid Electric Vehicles", Denso Technical Review, Vol. 16, pp 62-67, 2011. (In Japanese)

[60]. H. Akagi, H. Hasegawa, T. Doumoto, "Design and Performance of Passive EMI Filter for Use with a Voltage-Source PWM Inverter Having Sinusoidal Output Voltage and Zero Common-Mode Voltage", IEEE Transaction on Power Electronics, Vol. 19, pp. 1069-1076, 2004.

[61]. X.F. Wu, D.H. Xu, Y.J. Zhang, CH. Yi, "Integrated EMI Filter Design with Flexible PCB Structure", Power Electronics Specialists Conference PESC 2008, Rhodes, pp. 1613-1617, Jun. 15-19 2008.

[62]. H. Akagi, T. Doumoto, "A Passive EMI Filter for Preventing High-Frequency Leakage Current from Flowing through the Grounded Inverter Heat Sink of an Adjustable-Speed Motor Drive System", IEEE Transactions on Industry Applications, Vol. 41, No. 5, pp. 1215-1223, 2005.

RESEARCH ACHIEVEMENTS

1. Y.Z.Y. Tang, J. Fukuda, O. Satoshi, M. Takemoto, “Introduction of Non-linear Resistance into Common-mode equivalent circuit of Inverter Driver System,” 2011 National Convention Record of the IEE Japan, vol. 4, No. 4-037, pp. 70-71, 2011. (In Japanese).

2. Y.Z.Y. Tang, J. Fukuda, O. Satoshi, M. Takemoto, “Introduction of Non-linear Resistance into Common-mode equivalent circuit of Inverter Driver System,” 2011 National Convention Record of the IEE Japan, vol. 4, No. 4-037, pp. 70-71, 2011. (In Japanese).

3. Y.Z.Y. Tang, S. Ogasawara, T. Masatsugu, “Non-Linear Common-Mode Equivalent Circuit for Inverter-Fed Motor Drive Systems”, ECCE Asia Downunder (ECCE Asia), pp. 278 - 284, 2013.

4. T. Tokiwa, M. Kanamori, T. Endo, M. Iida, S. Ogasawara, Y.Z.Y. Tang, “Consideration for the Propagation Path of Conductive Noise in Air Conditioners”, IPEC-Hiroshima (ECCE Asia), pp. 2977-2982. 2014.

5. Y.Z.Y. Tang, S. Ogasawara, M. Takemoto, M. Kanamori, M. Iida, T. Endo, “Estimation of Stray Capacitance and Permittivity between Compressor Motor Windings and Stator in Operation”, Trans. of the JSRAE, Vol. 32, No. 3, Advanced Publication, published online on May 31, 2015. (Published Decision)

6. Y.Z.Y. Tang, S. Ogasawara, M. Takemoto, T. Tokiwa, M. Kanamori, “Parameter Identification of Simplified Common-Mode Equivalent Circuit for Inverter-Fed Motor Drive Systems by Applying Computer Aided Optimization Software”, IEEJ Transactions on Electrical and Electronic Engineering (TEEE) D, Vol.11, No.2, Mar. 2016. (Published Decision)

ACKNOWLEDGEMENT

I would first like to express my deep and sincere appreciation to my advisor, Dr. S. Ogasawara and Dr. M. Takemoto, both of whom helped me tremendously during the course of this thesis. It is my valued opportunity to learn the rigorous attitude toward research and presentation from them. Their suggestions were a source of guidance to me and without their timely help this research project would have taken a far longer time to finish. Their broad visions, keep insight on the technical issues and creative thinking have greatly inspired me. I would also like to especially thank Dr. H. Igarashi for taking the busy time to check my thesis.

I would also like to acknowledge the teachers and staff of Graduate School of Information Science and Technology, and the Japanese teachers of International Student Center Hokkaido University, for their great help and teaching.

I am grateful to receive numerous encouragement help and guidance. I have been a great pleasure to work with so many talented colleagues in the Electric Energy Conversion Laboratory. And thank all of them for their great help and meaningful discussions.

I am especially indebted to my abroad student friends in Hokkaido University. It was my great pleasure to know them.

My deepest gratitude I sent to my parents, Mr. Shaogang Tang and Mrs. Sulan Wang, for their countless love, care and sacrifice. I greatly value my parents' vision when they encourage me to study abroad and appreciate their great support.